

UCL-University College London

Institute of Ophthalmology

Faculty of Brain Sciences

Development and Molecular Properties of the Rodent Inner
Blood-Retinal-Barrier

By

Ewa Cecylia Kubala

*Thesis submitted to University College London for the degree of
Doctor of Philosophy*

2016

Declaration

I, Ewa Cecylia Kubala confirm that the work presented in this thesis is my own. Where information has been derived from other sources, I confirm that this has been indicated in the thesis. Also, the current thesis does not exceed the maximum limit of 100,000 words.

Acknowledgements

I would like to thank my supervisor Prof. David Shima for giving me the opportunity to work on this challenging but exciting project. I am grateful for his patience and encouragement during my studies.

I also thank to my second supervisor Dr. Eric Ng for his guidance, support and stimulating discussions.

My special appreciation goes to my past and present colleagues in the TVR lab and the Institute of Ophthalmology, especially Laura, Meihua, Raúl, Brett, Vivian, Richard, and Joanna. Thank you for all the good time that we had!

I am deeply thankful to Lucy Ensum, for her support and help with my “polienglish” and good word always when I needed it.

I am deeply thankful to my family, who have always believed in me and gave a support.

Abstract

Background: The blood-retinal barrier (BRB) and blood-brain barrier (BBB) protect, respectively, retina and brain from substances circulating in the blood that may affect the homeostatic regulation of the delicate and intricate neural microenvironment. Postnatal development of the murine vasculature in the retina affords the opportunity to explore mechanisms of BRB formation through use of tracers and pharmacological manipulation, and may provide information that is useful in understanding disorders characterised by BRB dysfunction, such as diabetic retinopathy.

Methods: To examine the onset of barrier function during post-natal vascular development, we modified a previously described in-vivo tracer assay (Poor, 2006). Fluorescent lysyl-dextran were injected in the intraperitoneal cavity at different stages of development, which after two hours led to consistent filling of the retinal vasculature with tracer. Animals were perfused and the retinas flat mounted and the leakage of tracer from the vasculature was evaluated by epifluorescence microscopy and image analysis. Phosphoproteomic analyses of the retina at early - P5 and later - P15 stage of development was performed in order to determine a key players in retina development. The role of VEGF-A and MLC signalling pathways in BRB formation was accomplished through immunostaining, Western blot and pharmacological blockade.

Results: 3kD fluorescent dextran freely extravasated from the retinal vasculature at post-natal day 5 (P5), but levels decreased at P8 and a complete barrier to the tracer was present by P10. Similar results were obtained with a larger tracer, 70 kD dextran, and a cross-linkable biotin (NHS-biotin). During the P9-P10 transition period, endothelial cell adhesion protein Claudin-5 showed a distinct accumulation at cell-cell junctions. Use of the cross-linkable tracer demonstrated that leakage prior to P10 occurred at the growing vascular front, but not in the more mature, central retinal regions. Pharmacological blockade of VEGF-A signalling, which is active at the growing vascular front, hastened barrier formation, suggesting that the BRB can only form following completion of the superficial vascular plexus and the concomitant down-

regulation of VEGF-A levels. Phosphoproteomics studies showed an increase of phosphorylation of various molecules implicated in VEGF-A signalling and cytoskeletal contraction in the pre-barrier period. Acquisition of BRB function was accompanied by a decrease in endothelial phospho-PAK and phospho-MLC, which is consistent with decreased VEGF-A signalling. Use of an MLCK inhibitor also hastened barrier function, suggesting a critical need to regulate the actomyosin cytoskeleton during formation of the BRB.

Conclusion: Our findings provide a framework for the continued investigation of the inter- and intra-cellular changes required for BRB formation, and will hopefully yield insight into developing therapies to repair the barrier during neurovascular retinal disease.

Contents

Declaration	2
Acknowledgements.....	3
Abstract	4
List of figures.....	10
List of tables.....	15
List of abbreviations.....	16
Chapter 1. Introduction.....	19
Retina development.....	19
Blood Brain and Blood Retinal Barriers.....	24
Differences between BBB and BRB.....	27
Endothelial cells	28
Vascular permeability	29
Diseases that are characterised by BRB dysfunction.....	30
Junction structure - formation and function	33
VEGF-A controls EC growth and permeability	38
VEGF receptors	40
Cytoskeleton compartments in the endothelial cells.....	42
The link between the Rho GTP-ase pathway and endothelial barrier function	43
Hypothesis and aims of the PhD project.....	46
Chapter 2. Materials and Methods	49
Reagents	49
In-vivo experiments.....	49
Retina dissection.....	49

Immunofluorescence staining of the whole mount retina tissue and cryostat section	50
Leakage assay in the retina with NHS- Biotin.....	55
Dextran – blood concentration measurement.....	56
Leakage assay in the retina with 3kD fixable dextran.....	56
Leakage assay in the retina with 70kD fixable dextran	57
VEGF-A triggered leakage assay in the retina.....	57
VEGFR1 and VEGFR2 in-vivo staining.....	58
VEGFR2 blocking antibody injection.....	58
Leakage assay after PIK injection	59
Protein techniques	59
Protein extraction from the retina for western blot	59
Protein concentration determination.....	60
SDS-PAGE (sodium dodecyl sulfate polyacrylamide gel electrophoresis)	60
Western-blot.....	61
Phosphoproteomic	62
Tissue culture	67
MVEC isolation.....	67
Immunostaining of cells cultured on dishes and filters.....	69
TEER measurement	70
Flux measurement.....	71
Capillaries isolation.....	71
VEGF-A treatment on the retina capillaries.....	72
Protein extraction from the retina capillaries.....	72
Retina capillaries immunostaining	72
Morphology.....	73
Light microscopy.....	73

Chapter 3. Onset of Blood Retinal Barrier function.....	75
Demonstration of poor BRB function at early stages of murine development	76
BRB formation based on 3kDa dextran leakage assay	84
BRB formation based on 70kD dextran leakage assay.....	86
BRB formation based on an NHS-biotin tracer assay	92
Junction protein localisation in the retina	94
Macrophage activation during BRB development	99
Onset of Blood Retinal Barrier function – conclusions and discussion	103
Chapter 4. The role of VEGF-A during Blood Retina Barrier development.....	105
Does VEGF-A expression reduce barrier function prior to P10?.....	105
VEGF-A localisation in the developing retina by in situ hybridisation	105
Identification and localisation of VEGF-A in the retina at different stages of BRB development	106
VEGFR2 blocking antibody injection.....	112
VEGF-A induced Blood Retina Barrier breakdown	114
VEGFR1 and VEGFR2 localisation in the retina	117
VEGFR1 and VEGFR2 polarity.....	120
The role of VEGF during Blood Retina Barrier development – discussion	125
Chapter 5. Phosphoproteomic comparison of P5 and P15 retinas	126
Phosphoproteomic study of P5 and P15 retina protein extracts.....	126
Pathways regulated by protein phosphorylation between P5 and P15	132
Adherens junction interaction	132
VEGF-A signalling.....	139
Rho GTP-ases	144
Phosphoproteomic analysis of P5 and P15 retina – conclusion.....	153
Chapter 6.....	155
The role of the cytoskeletal remodelling during BRB development.....	155

PAK, MLC and MLCK in the retina at different stages of postnatal retinal development.....	156
Immunostaining and localisation of PAK-P and MLC-P in the retina	160
Actin filament organisation in the vasculature	164
BRB functions after blocking MLCK.....	167
PIK peptide and its function.	167
The effect of PIK on permeability of P6 retinal vasculature	168
The role of cytoskeletal regulation during BRB development – discussion and summary	171
Chapter 7.....	174
Developing an in vitro model for studying BRB properties.....	174
Characteristic of the primary rat brain endothelial cells	174
Flux assay – barrier properties of the PRBEC.....	179
Permeability of PRBEC after VEGF-A treatment.....	182
Primary rat brain endothelial cell isolation and experimentation – discussion and conclusion	189
Capillary isolation.....	190
Characteristics of obtained retina capillaries.....	191
Exploring PAK and MLC activity in the retinal capillary fragments at P5 and P15, and after VEGF-A treatment.....	193
Ex-vivo model for studying BRB properties - discussion and conclusion	194
Chapter 8. Final discussion	197
References.....	206

List of figures

Figure 1. Schematic of the approximate time course of retinal vascularisation in a C57Bl/6 mouse.....	22
Figure 2. Schematic showing the time point for neuronal cells development in the retina.....	23
Figure 3. Electron micrograph on the retinal capillary.	26
Figure 4. Schematic structure of microvascular endothelial cells.....	27
Figure 5. Schematic of structures mediating paracellular and transcellular permeability (JU, 2013).....	30
Figure 6. Endothelial cell junctions.	36
Figure 7. Schematic illustrating VEGFR activation.	41
Figure 8. Schematic representation of the Ras proteins.	44
Figure 9. The control of actin-myosin contraction in endothelium.	45
Figure 10. The procedure of retina flat mounting.	50
Figure 11. 2° Antibody control staining (part1).....	54
Figure 12. 2° Antibody control staining (part2).....	55
Figure 13. Schematic representations of the MVEC post isolation treatment.	69
Figure 14. Morphological assessment of vascular development in the retina. ...	76
Figure 15. Blood cell leakage at the periphery of growing vasculature.	77
Figure 16. P5 flat mounted retina after 4kD dextran injection.....	79
Figure 17. P5 and P15 flat mounted retina after 4kD dextran injection.....	80
Figure 18. P5 and P15 retina after 3kD dextran injection.....	81
Figure 19. Measurement of the optimal time point for 3kD dextran leakage assay on P5 retina.....	83
Figure 20. 3kD dextran plasma concentration at the P5, P10, and P15.	84
Figure 21. BRB formation based on the 3kD dextran permeability assay.	85
Figure 22. P5 and P10 skin tissue fragment 2h after 3kD dextran injection.....	86
Figure 23. 3kD dextran and 70kD dextran plasma concentration at P5.....	87
Figure 24. P5- flat mounted retina 4 hours after 70 kD dextran IP injection.	88
Figure 25. Leakage of the 70kD dextran at P5 retina.	89

Figure 26. 70kD dextran plasma concentration at P5, P10 and P15 post-natal stage of development.	90
Figure 27. Time point for BRB formation based on the 70kD dextran tracer.....	91
Figure 28. The reactivity of NHS-biotin.	92
Figure 29. The permeability study of retina vasculature using NHS-biotin.	93
Figure 30. Claudin-5 localisation in the retina at P5.....	95
Figure 31. The localisation of Claudin-5 in the retina at P7 and P16.....	96
Figure 32. ZO-1 localisation in the P5 retina.	98
Figure 33. VE-Cadherin localisation in the P5 retina.....	99
Figure 34. P5 whole mount retina stained with IBA-1 and Lectin.	101
Figure 35. IBA-1 localisation in the retina at P5 and P15.....	102
Figure 36 Superficial and intermediate plexus at P10.....	104
Figure 37. VEGF mRNA expression in the retina.....	106
Figure 38. VEGF-A localisation in the P5 retina.....	108
Figure 39. VEGF-A staining at P5 and P15.....	109
Figure 40. VEGF-A staining at different stages of retina development.....	110
Figure 41. VEGF-A and GFAP staining in the periphery of P5 retina.....	111
Figure 42. VEGFR2 blocking antibody effects on BRB function at P6.....	113
Figure 43. Schematic illustration of the in vivo VEGF-A permeability study.....	114
Figure 44. Permeability study after VEGF-A intravitreal injection at P15 C57BL6.	115
Figure 45. Permeability study after VEGF-A intravitreal injection at P15.....	116
Figure 46. VEGFR2 immunostaining at P5 and P15 retina.....	119
Figure 47. VEGFR1 immunostaining at P5 and P15 retina.....	120
Figure 48. VEGFR1, VEGFR2 and DC101 cardiac infusion.....	122
Figure 49. Fragment of the skin after DC101 cardiac infusion and perfusion...	123
Figure 50. VEGFR1, VEGFR2 and DC101 staining without the permeabilisation step.....	124
Figure 51. Phosphopeptides identified in the P5 and P15 samples.....	127
Figure 52. Changes in phosphorylation of AJ proteins between P5 and P20 retina.	135
Figure 53. Changes in phosphorylation of α -catenin proteins between P5 and P20 retina.	136

Figure 54. Changes in phosphorylation of δ -catenin between P5 and P20 retina.	137
Figure 55. Changes in phosphorylation state of ZO-1 protein between P5 and P20 retina.	138
Figure 56. Changes in phosphorylation state of ZO-2 and ZO-3 protein between P5 and P20 retina.	139
Figure 57. Changes in phosphorylation of tyrosine protein kinase Src and Focal adhesion kinase.....	140
Figure 58. Changes in phosphorylation of Akt-1 in the retina between P5 – P20.	141
Figure 59. Changes in phosphorylation of MAPK in the retina between P5 – P20.	142
Figure 60. Changes in phosphorylation of PKC isoforms in the retina between P5 – P20.	144
Figure 61. Schematic illustrating Rho GTP-ase activity.....	145
Figure 62. Changes in phosphorylation of selected GAPs in the retina between P5 – P20.....	146
Figure 63. Changes in phosphorylation of selected GAPs in the retina between P5 – P20 (part2).....	147
Figure 64. Changes in phosphorylation of ARHGEFs in the retina between P5 – P20.....	148
Figure 65. Changes in phosphorylation of ARHGEFs in the retina between P5 – P20 (part2).....	149
Figure 66. The phosphorylation of MLC at different stages of retina development.....	150
Figure 67. The phosphorylation of MLCK at different stages of retina development.....	152
Figure 68. Changes in phosphorylation of p21-activated kinases (PAKs) at different stages of retina development.	153
Figure 69. Western blotting data showing the differences in expression of MLCK, PAK-P, MLC-P and PAK at P5 and P15.....	158
Figure 70. The differences in MLC-P and PAK-P expression between P5 and P15.	159

Figure 71. MLC-P immunostaining in the retina at P6 and P15.	160
Figure 72. MLC-P staining in the P5 and P15 retina.	161
Figure 73. PAK-P localisation in the retina at P5 and P15 (retina section).	162
Figure 74. PAK-P localisation in the retina at P5 and P15 (retina flat mount)..	163
Figure 75. Phalloidin staining of P5 retina.	165
Figure 76. Phalloidin staining of P5 and P15 retina.....	166
Figure 77 Schematic model of PIK action.....	168
Figure 78. The effect of PIK on BRB function.....	170
Figure 79. Potential mechanism involved in increased permeability at early stage of development.	173
Figure 80. Schematic comparison of in-vivo microvessels and primary endothelial cells seeded on transwells.....	176
Figure 81. PRBEC on 2 nd day after isolation and after 2 weeks in culture.	177
Figure 82. PRBEC stained with Occludin, VE-cadherin, VW-factor and CLaudin-5.	178
Figure 83. The effect of VEGF-A on VE-cadherin localization in PRBEC.	179
Figure 84. Flux assay on PRBEC of a different TEER values.	181
Figure 85. Flux assay on PRBEC and passaged PRBEC.	182
Figure 86. Permeability of the PRBEC after apical and basolateral VEGF-A treatment.	184
Figure 87. Permeability of the PRBEC after apical and basolateral VEGF-A treatment.	185
Figure 88. Optimisation of puromycin selection step.	187
Figure 89. Optimisation of the plating density of PRBEC cells.	188
Figure 90. Optimisation of collagenase/dispase digestion step.....	189
Figure 91. Cortical capillaries. Adapted from (Cristante, 2013).	190
Figure 92. Topographic picture of the capillaries isolated from the retina.....	191
Figure 93. Capillaries from P15 retina, stained with anti Claudin5 antibody...192	
Figure 94 Capillaries from P15 retina stained with Phalloidin and anti VE-cadherin antibody.	192
Figure 95. MLC-P, and PAK-P at P5 and P15 retina capillaries.....	193
Figure 96. MLC-P and PAK-P level after VEGF-A treatment on capillaries.	194

Figure 97. Proposed mechanism that is involved in increase permeability of EC
prior to P10.....202

List of tables

Table 1. Proteins involved in EC junction complex.....	37
Table 2. Primary antibodies and conditions used in immunofluorescent retina staining.....	52
Table 3. Secondary antibodies used in immunofluorescence staining of retina.	53
Table 4. Separating gel.....	60
Table 5. Stacking gel.....	60
Table 6. Primary antibodies and conditions used in Western blotting.....	62
Table 7. Secondary antibodies used in Western blotting.....	62
Table 8. Primary antibodies and conditions used in immunofluorescent PRBEC staining.....	70
Table 9. Secondary antibodies used in immunofluorescence staining of PRBEC.....	70
Table 10. Primary antibodies and conditions used in immunofluorescent capillary staining.....	73
Table 11. Secondary antibodies used in immunofluorescence staining of capillaries.....	73
Table 12. Proteins that are differentially phosphorylated between P5 and P15.....	128
Table 13. Composition of the Halt Protease and Phosphatase Inhibitor Cocktail.....	157

List of abbreviations

AJ - Adherens junction
AMD - age-related macular degeneration
BBB - Blood-Brain Barrier
bFGF - Basic fibroblast growth factor
BRB - Blood Retinal Barrier
DR - Diabetic retinopathy
EC - Endothelial cells
EPC - Endothelial progenitor cell
ESAM - Endothelial cell selective adhesion molecule
FA - Fluorescein angiography
FAK - Focal adhesion kinase
GAP - Rho GTP-ase activating protein
GCL - ganglion cell layer
GEF - Rho guanine nucleotide exchange factors
GJ - gap junctions
HGF - Hepatocyte growth factor
iBRB - inner Blood Retinal Barrier
IGF - Insulin like growth factor
IL-8 - interleukin-8
INL - Inner nuclear layer
JAM - Junctional adhesion molecules
JMD - Juxtamembrane domain
MAPK - Mitogen-activated protein kinase
MLC - Myosin II regulatory light chain
MLCK - Myosin light chain kinase
MLCP - Myosin light-chain phosphatase
oBRB - ouret Blood Retinal Barrier
OCT - Optical coherence tomography
OF - Ocular fluorophotometry

OPL - Outer plexiform layer
PAK - p21-activated kinase
PDGF - Platelet derived growth factor
PDGFR- α - Platelet derived growth factor α
PECAM - Platelet endothelial cell adhesion molecule
PKA - Protein kinase A
PKC - Protein kinase C
PlGF - Placental growth factor
PMVEC - Primary Microvascular Endothelial Cells
PRBEC - Primary rat brain endothelial cells
ROCK - serine/threonine protein kinase
ROP - Retinopathy of prematurity
RPE - Retinal pigment epithelium
RTK - Receptor tyrosine kinase
Src - Tyrosine protein kinase Src
TE - Transendothelial channels
TEER - Transendothelial electrical resistance
TGF- β - Transforming growth factor -beta
TJ - Tight junction
TMA - Thrombotic microangiopathy
TMD - Transmembrane domain
TNF - Tumour necrosis factor
VEGF-A - Vascular endothelial growth factor A
VEGFR1 - Vascular endothelial growth receptor 1
VEGFR2 - Vascular endothelial growth receptor 2
VEGFR3 - Vascular endothelial growth receptor 3
VPF - Vascular permeability factor
VVO - Vesiculo-vacuolar organelles
vWF - von Willebrand Factor
ZO-1 - Zona occludens 1
ZO-2 - Zona occludens 2
ZO-3 - Zona occludens 3

Introduction

Chapter 1.

Introduction

Retina development

The retina is one of the most energetically demanding of any other tissue in the body (Wong-Riley, 2010). Such high metabolic activity requires proper nutrition and oxygen supply. This is why careful regulation of blood supply is an essential characteristic of the mammalian retina. Retina neuronal cells have different demands and requirements for blood supply. These have been met by the evolution of two vascular routes – inherent intra-retinal vessels, which supply the inner two-thirds of the retina, while the choroidal circulation supplies the photoreceptors in the outer one-third of the retina. Interestingly, the fovea, which is the area in the retina composed of highly packed cones, remains avascular. This is a very interesting feature that shows compromise between two conflicting requirements in the retina, sufficient blood supply and a minimally obscured light path. In order to provide the highest visual acuity in the retinas, the fovea remained an avascular area in the retina (Kur, 2012).

During vascularisation in the rodent retina two processes take place, vasculogenesis and angiogenesis. The term vasculogenesis describes the de novo formation of vessels from vascular endothelial precursor cells - angioblasts. Angiogenesis is the process of growth of new capillaries from pre-existing blood vessels. There is no clear distinction between the end of vasculogenesis and the beginning of angiogenesis in retina vascular development, however, a widely held view is that the primary vascular development across the inner surface of the retina occurs by vasculogenesis,

whereas the establishment of the secondary network in the inner plexiform layer occurs by angiogenesis (Fruttiger, 2002).

In contrast to vasculogenesis, angioblasts are not implicated in the angiogenesis process. Angiogenesis involves highly complex biochemical and cellular processes requiring different types of cells, cytokines and growth factors that stimulate new blood vessel growth, such as vascular endothelial growth factor (VEGF-A), basic fibroblast growth factor (bFGF), hepatocyte growth factor (HGF), insulin like growth factor (IGF), placental growth factor (PlGF), platelet derived growth factor (PDGF), transforming growth factor -beta (TGF- β), tumour necrosis factor (TNF), and interleukin-8 (IL-8) (Penn, 2008, Stewart, 2012)

Retinal astrocytes play a significant role during the vascularisation process. The process of primary vascular growth in the retina is associated with astrocyte migration from the optic nerve head, moving as a proliferating population of cells which spread across the inner surface of the retina, creating a template for the developing retinal vasculature. This process begins at embryonic day 19 (E19) and the astrocyte network is fully developed at birth. Astrocytes express PDGFR- α and invade developing retina travelling on top of PDGF-A, expressing ganglion cells (RGC) (Figure 1-B) (Sapieha, 2012).

Retina vascular development arises postnatally and over very brief 3 weeks period. Growth of the vessels in the retina is highly organised and occurs in a characteristic and uniform fashion. Shortly after birth, at P0, the superficial plexus starts forming within ganglion cell layer (GCL). EC emerge from the optic nerve and spread towards the periphery of the retina. Sprouting vessels align with astrocytes fibres and are stabilised by R-cadherin mediated cell - cell adhesion between endothelium and astrocytes (Sapieha, 2012).

Expanding vascular front takes place is two-step process, which starts with the vessels sprouting followed by vessel anastomosis. Vessel sprouting and formation of tip cell protrusion is stimulated by the gradient of VEGF-A, tip cell fusion and new vessel loop formation is promoted by macrophages, also called microglia (Mackenzie, 2012, Fantin, 2010, Tata, 2015).

Hierarchical tree of superficial plexus layer is fully laid out at P10. Between around P8 and P12 of postnatal development EC dive deeper in the retina and

form the deep plexus near outer plexiform layer (OPL). The last stage of retina vascular development, the intermediate plexus formation, takes place between P14 and P20 at the inner edge of inner nuclear layer (INL) (Figure 1-A) (Milde, 2013, Dorrell, 2006).

The retina is a complex, multi-layered sheet of neural tissue. The layers of the retina, starting from its inner side are: internal limiting membrane, nerve fibre layer (ganglion cell axons), ganglion cell layer, inner plexiform layer (connections of the ganglion cells with amacrine and bipolar cells), inner nuclear layer (bipolar, amacrine, and horizontal cell bodies), outer plexiform layer (connections of the bipolar and horizontal cells with the photoreceptors), outer nuclear layer (photoreceptor cell nuclei), external limiting membrane, photoreceptor layer, retina pigment epithelium. Retinal neuronal cell development starts at the embryonic stage and all neuronal cells are developed by postnatal day 10 (P10) (Vaughan, 1995, Goldman, 2014).

The figure 2 represents the time points of neuronal development in the retina.

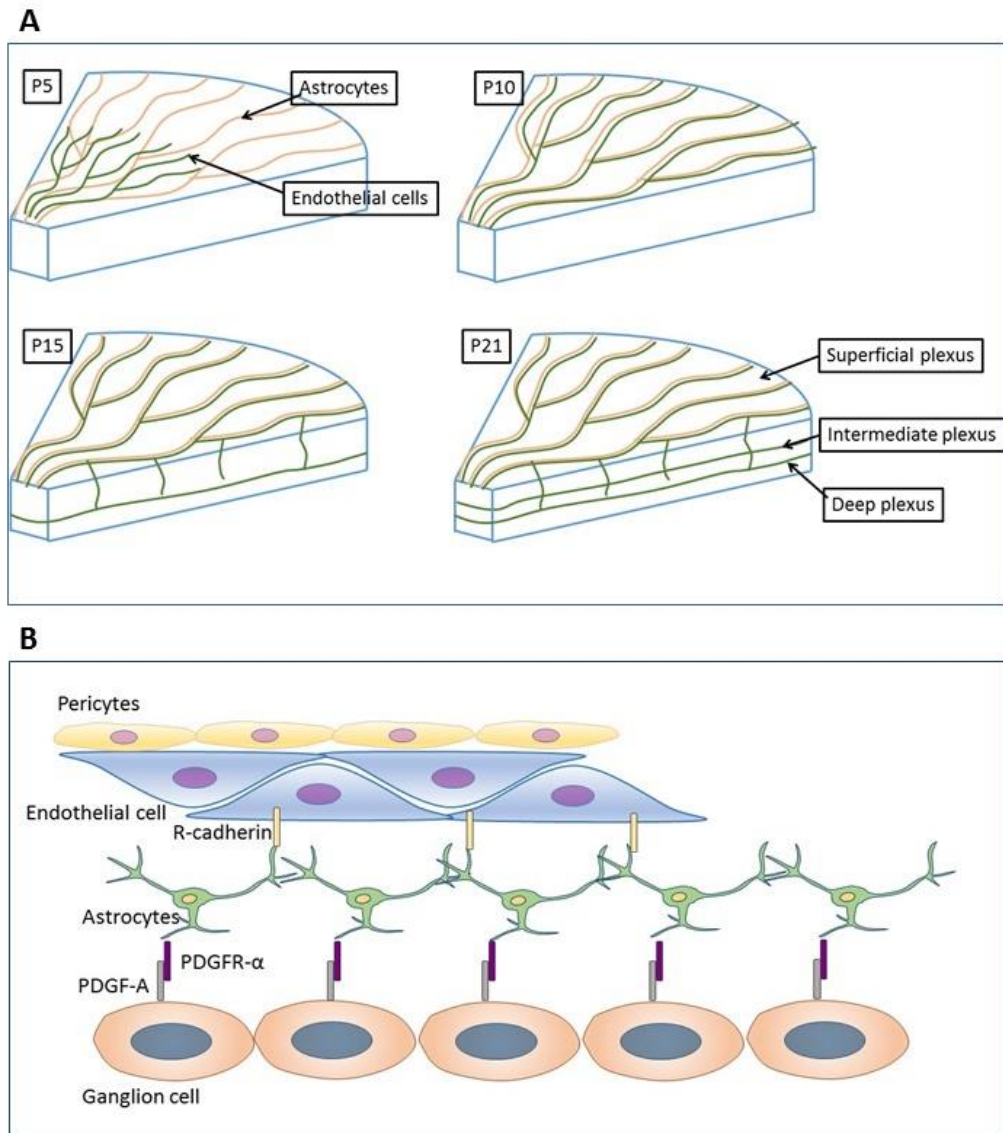


Figure 1. Schematic of the approximate time course of retinal vascularisation in a C57Bl/6 mouse.

A-The astrocytic template (green) is fully formed at birth. The superficial plexus grows between birth and P10, the deep plexus forms approximately between P8 and P12, whereas the intermediate plexus forms around P14-P20.

B- Astrocytes emerge in the retina from the optic nerve, and express PDGFR- α and invade the developing retina from the optic nerve head, ahead of the vascular front. They travel on top of PDGF-A expressing RGCs. Nascent endothelial cells supported by pericytes, follow the astrocytic template and form R-cadherin junctions with proximal astrocytes (Sapieha, 2012).

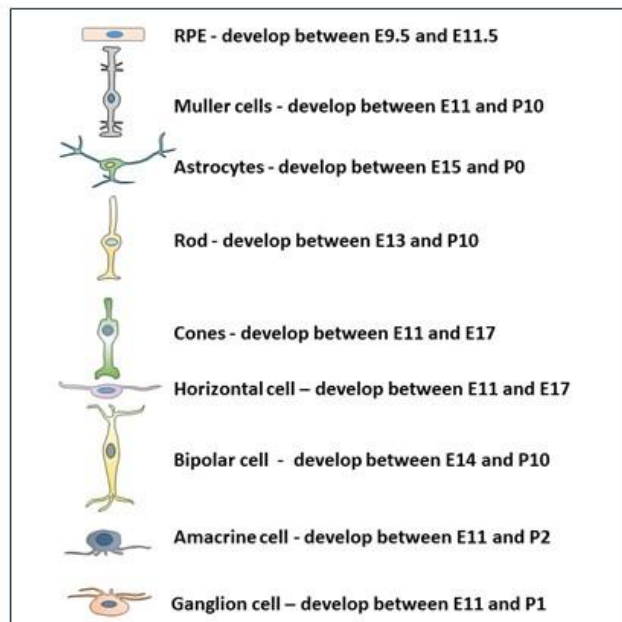
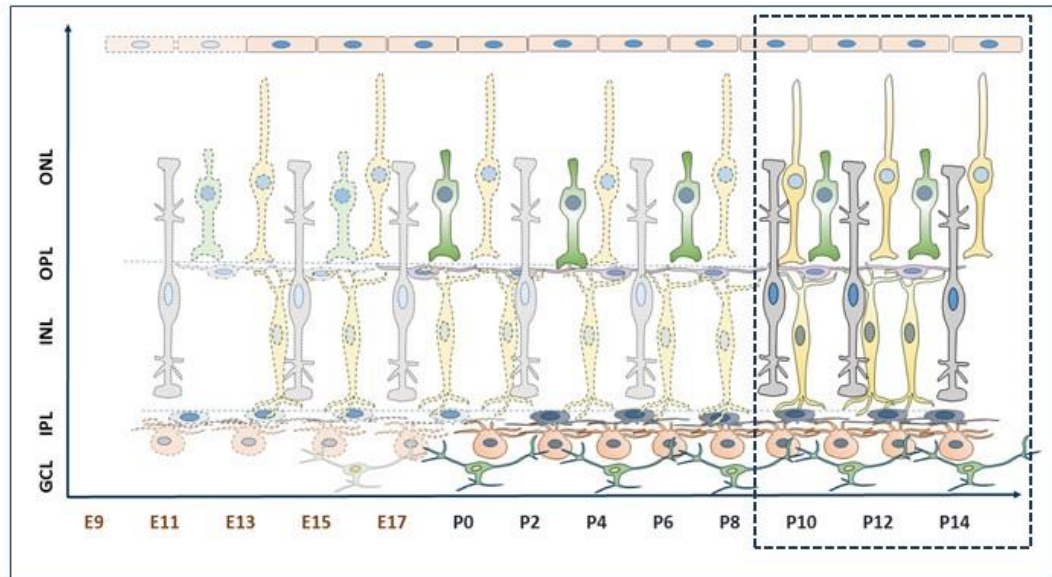


Figure 2. Schematic showing the time point for neuronal cells development in the retina.

RPE starts developing at Embryonal day 9.5 (E9.5) and is fully formed at E11.5 (Raymond, 1995). Muller cells begin to differentiate at E11 and are formed by postnatal day 10 (P10) (Bhattacharjee, 1975). Astrocytes starts forming at E15 and are fully formed at birth (P0) (Dorrell, 2002). Rod cells start to develop at E13, and are formed in the retina at P10. Cone cells are forming between E11 and E17. Horizontal cells starts forming at E11, and by E17 are already developed. Bipolar cells are forming between E14 and P10, Amacrine cells between E11 and P2 and ganglion cells between E11 and P1. Figure was developed based on Bassett *et al.* and Morgan *et al.* (Morgan, 2007, Bassett, 2012)

Blood Brain and Blood Retinal Barriers

The human brain is comprised of ~100 billion neurons and consumes about 15-20W of power. It is the most energy consuming organ in our body, but since it does not have the capacity to store energy, requires a constant blood supply, that is maintained via the vasculature (Wong, 2013).

Paul Ehrlich first reported that some substances injected into the circulation do not enter the brain (Carvey, 2009). Today we know that the interface between the vascular system and neuronal environment in the brain is composed of specialised vascular endothelial cells (EC) which form the Blood-Brain Barrier (BBB). This barrier is selective, ensuring protection of the neuronal tissue from potentially disruptive substances or foreign objects that could enter from the circulation, whilst still allowing critical blood-tissue exchange. The BBB is beneficial, for this reason, but also disadvantageous, because it is often a roadblock for drug entry into the brain parenchyma, thereby impeding treatment of many central nervous system diseases.

The retina shares similar energy and metabolism properties with the brain. It functions as a camera that detects light and converts it into an electro-chemical signal that, via the optic nerve transmits to the brain. The retina is a complex, multi layered sheet of neural tissue. In order to maintain its normal visual function, there is a specialised neuronal micro environment in the retina, which requires careful control of ionic, amino acid and other blood components—this in turn requires a highly regulated blood supply. This environment in the retina, is in part, maintained by the Blood Retinal Barrier (BRB), which is believed to share many if not most properties of the BBB (Radhika, 2011).

The BRB consists of two spatially distinct layers of cells: the retinal pigment epithelium, that sit above the choriocapillaris (outer barrier), and the retinal vascular endothelium (inner barrier) (Qaum, 2001). This unique, dual vascular supply provides oxygen and nutrients to the highly metabolically active neural retina. These distinct vascular beds differ in their properties and functions. The highly fenestrated and permeable choriocapillaris layer is located under the retina and Bruch's membrane, and provides a blood supply to the outer plexiform layer, outer nuclear layer, photoreceptors, and retinal pigment

epithelium. The capillaries sprouting from the central retinal artery provide oxygen and nutrients to the inner retina, whereas the outer retina is completely avascular (Vaughan, 1995, Klaassen, 2013).

The endothelial cells that line the inner vascular wall are the first to encounter circulating blood elements, separating them from the extravascular tissues (Figure 3). The vascular endothelium acts as a selective barrier for blood-tissue exchange of fluids, nutrients, metabolic waste, and prevents pathogens and harmful materials from entering the tissue (Yuan, 2010). Large molecules including peptides, recombinant proteins, monoclonal antibodies, RNA interference-based drugs and gene therapies, are restricted from crossing the BBB/BRB and the basis of the barrier is believed to be due to the fortification of cell-cell contacts (Qaum, 2001, Radhika, 2011).

Endothelial cells are not the sole component of blood vessels, they are surrounded and supported on the abluminal side by mural cells – pericytes or smooth muscle cells (Figure 4) (Penn, 2008, Bergers, 2005).

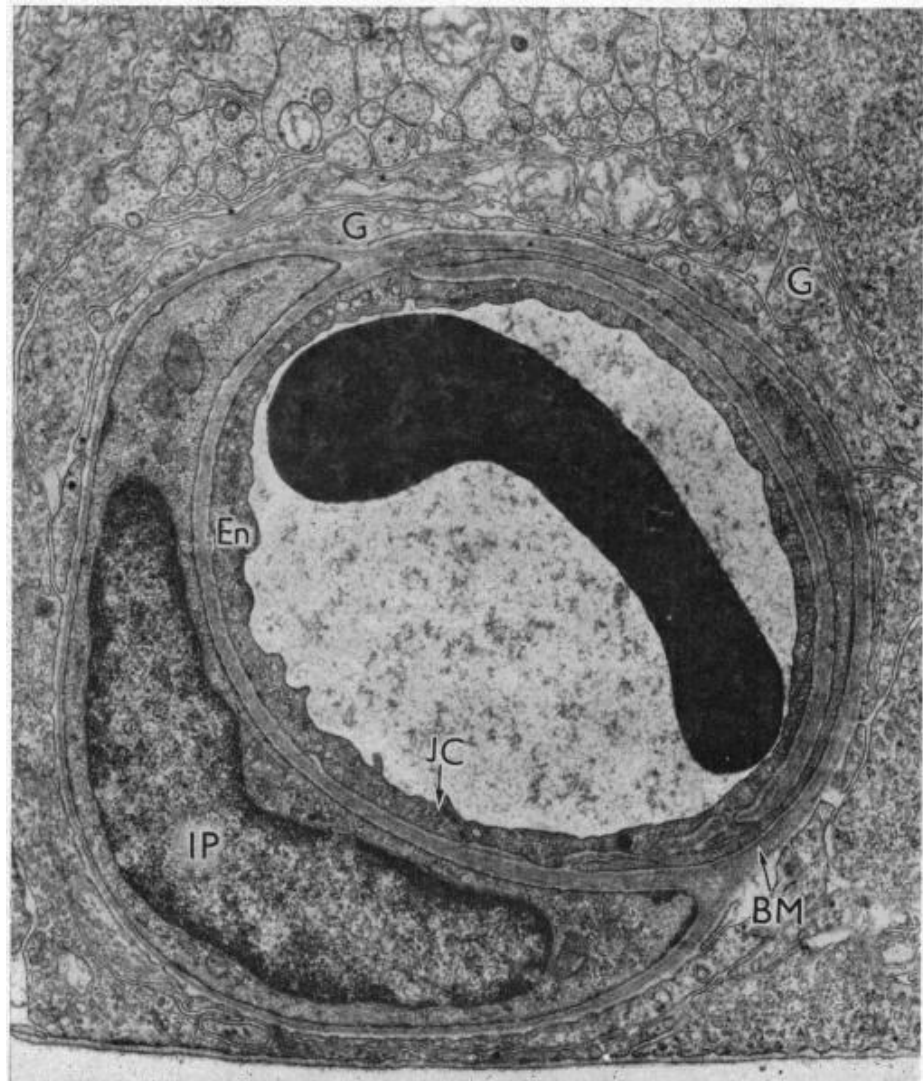


Figure 3. Electron micrograph on the retinal capillary.

Electron micrograph showing the cross-section of a rat retinal capillary consisting of the basement membrane (*B*), the endothelial cells (*En*), intramural pericyte (*IP*), the glial cells (*G*), and the cell junction (*CJ*) (Cunha-Vaz, 1965).

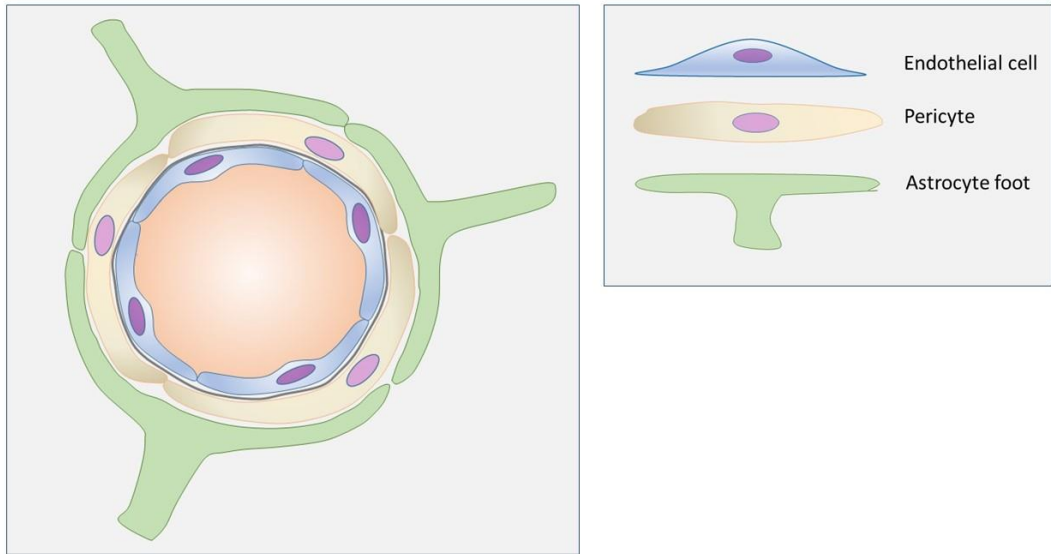


Figure 4. Schematic structure of microvascular endothelial cells.

Just as in the brain, retinal EC are partially covered by pericytes and they share a basement membrane consisting primarily of fibronectin, laminin 1, and collagen type IV. The EC and pericytes are also in contact with another BRB component, the end feet of astrocytes. Functional interactions between ECs, astrocytes, pericytes, other glial cells, and neurons are key to regulating neuronal homeostasis. The EC function in a cylindrical geometry with high curvature and experience shear stress resulting from blood flow. Adapted from (Wong, 2013).

Differences between BBB and BRB

In contrast to BBB, BRB is composed of outer barrier, formed by the retinal pigment epithelial (RPE), and inner barrier formed by microvascular endothelial cells (EC), which line inner side of the microvasculature in the retina. I will focus on comparing BBB and inner BRB.

BBB and BRB maintain a similar function, which is a gate keeping role between the blood stream and delicate neuronal tissue in the brain, and in the retina, respectively. They are both formed out of endothelial cells placed at the interface of blood flow and in both BBB and BRB, junctional structures play the main role in maintaining barrier function.

There is not much known about the differences in the structure between BRB and BBB, however there are reports pointing important divergences between the endothelial wall in the retina and in the brain. Stewart *et al.*

reported, that retinal endothelial cells have a higher density of interendothelial junctions and vesicles in comparison to the brain EC, suggesting that the inner BRB exhibits higher paracellular transport than BBB. Interestingly, pericytes which contribute to the second “line of defence” in the BBB and BRB, are approximately four times as numerous in the retina as in the brain. We can hypothesise, that higher numbers of pericytes act to compensate higher density of junction in the retinal EC (Stewart, 1994).

BBB and BRB exhibit differences in permeability for various drugs. For example, high-lipophilic compounds like verapamil and quinidine, showed higher permeability across BRB, compared to the BBB (Toda, 2011).

One of the most apparent differences between BBB and BRB, is the time point of its formation and acquisition. BBB is forming during the embryonic development, whereas BRB within 3 weeks after birth. Embryonic tracer studies showed that BBB becomes functional at embryonic day E15.5. Prior to that stage, at E13, E14 E15 BBB is fully permeable, and injected tracers (HRP and NHS-biotin) leaks out at the telencephalon and mesencephalon of a murine embryo (Ben-Zvi, 2014, Risau, 1986). Surprisingly there is no published data showing the time point for BRB acquisition.

Endothelial cells

A primary component of the BBB and BRB are specialised endothelial cells. The endothelium not only provides a barrier function between the circulation and the underlying tissue, but also influences vascular haemodynamics and regulates the accessibility to nutrient substances. This endothelial barrier is regulated through the presence of membrane-bound receptors for numerous molecules including proteins (e.g. growth factors, coagulant, and anticoagulant proteins), lipid transporting particles (e.g. low-density lipoprotein [LDL]), metabolites (e.g. nitrous oxide and serotonin), and hormones (e.g. endothelin-1), as well as through specific junctional proteins and receptors that govern cell-cell and cell-matrix interactions (Cines, 1998). Because of their important gate-keeping role, endothelial cells are a key target of investigation of the molecular mechanism involved in BRB and BBB formation and function.

Vascular permeability

Vascular permeability is the flow of ions, particles, solutes, molecules of varying size, and even whole cells (e.g. lymphocytes) across the vessel wall. Under normal physiological conditions vascular permeability is highly regulated. A change in the permeability of the vasculature may occur in response to permeability agents like vascular endothelial growth factor A (VEGF-A), histamine, and thrombin. Other factors that can influence the permeability of the vasculature are blood flow, shear stress, pressure differences, and ion concentration gradients (Weis, 2008).

Normal blood-tissue exchange can occur within individual endothelial cells - transcellular permeability, or between closely apposed endothelial cells - paracellular permeability (Figure 5).

Transcellular permeability can take place via caveolae, invaginations in the luminal cell membrane that can “bud off” and move through the cytoplasm, thus acting as transcytotic vesicles. Another shuttling route is via vesiculo-vacuolar organelles (VVOs) or through transendothelial channels (TE). Further transcellular blood-tissue exchange is through endothelial fenestrae, pores that span the entire cell, thus allowing rapid exchange.

Paracellular permeability occurs at the cell-cell junctions between adjacent endothelial cells through modulation of tight junctions (occludins, claudins, junctional adhesion molecules) and adherens junctions (cadherins) (Yuan, 2010).

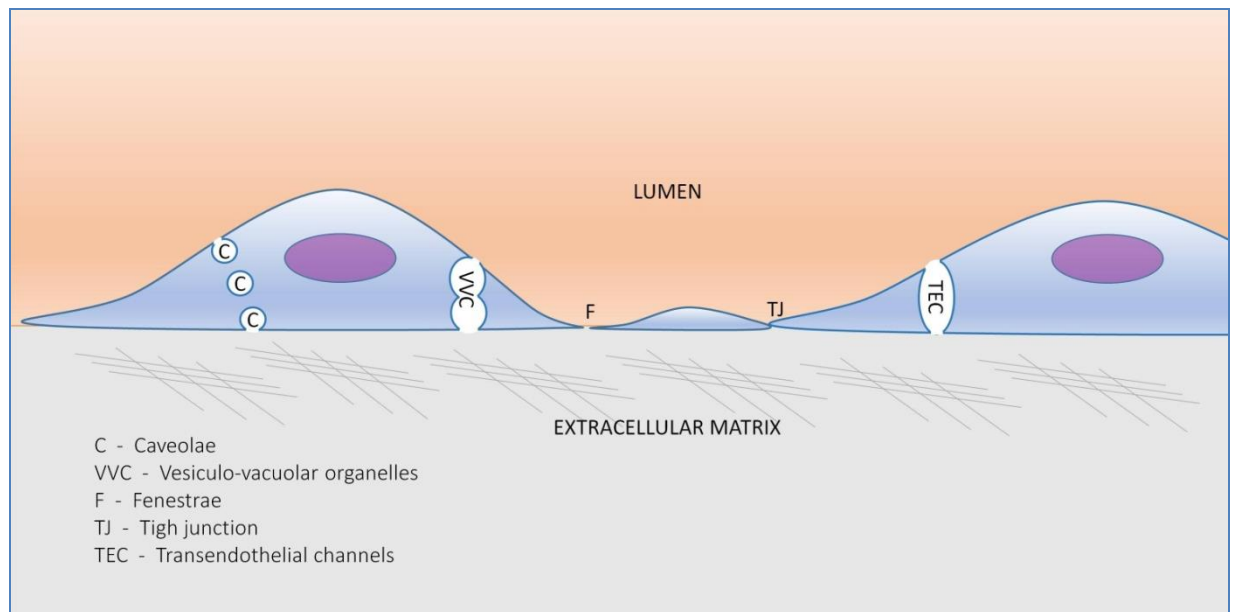


Figure 5. Schematic of structures mediating paracellular and transcellular permeability (JU, 2013).

Diseases that are characterised by BRB dysfunction

Many physiological regulators and factors work together to maintain proper vascular homeostasis.

In the eye, where endothelial cells maintain a gate keeping role, central mechanism of abnormal BRB function is characterised by excessive blood vessel growth and changes in the permeability of retinal endothelial cells. This is caused by elevated levels of growth factors, cytokines, inflammation, hyperglycemia and loss of pericytes (Klaassen, 2013). Deregulation of these factors is likely to contribute to disruption of barrier function and permits for the extravasation of serum components into the surrounding tissue (Cunha-Vaz, 2011, Rigor, 2012)

Perturbation of vascular permeability is resulting in endothelial dysfunction, contributes to age related macular degeneration, diabetic retinopathy, macular oedema, hypertensive retinopathy, branch vein occlusion, uveitis and other chronic retinal diseases, this results in vasogenic edema and neural tissue damage, causing loss of vision and if unmanaged, may lead to blindness (Weis, 2008, Penn, 2008, Stewart, 2012, Klaassen, 2013).

Macular oedema, a nonspecific sign of ocular disease is relevant for its frequency in diabetic retinopathy, it occurs as a consequence of fluid accumulation in the retina layers especially around the fovea, and in most cases is associated with alteration of the BRB (Cunha-Vaz, 2011).

Retinopathy of prematurity (ROP), diabetic retinopathy (DR) and age-related macular degeneration (AMD) are conditions that affect different age groups of patients. ROP, DR, and AMD have one feature in common, which is pathological proliferation of new blood vessels (neovascularisation). In DR and ROP, new vessels growth originates in the retina. Permeable vessels leak into the vitreous and subsequently cause fibrosis, retinal detachment and visual loss. In AMD, neovascularisation originates in the choroid and invades the overlying retina, and may lead to the bleeding and exudation, which in consequence leads to scarring and permanent loss of central vision. These neovascularisations in ROP, DR and AMD are driven by angiogenic cascade, and VEGF-A is a main mediator of these changes (Anderson, 2010).

The initial phase of many pathological conditions in the eye starts with the changes in the permeability of BRB. This is the reason why it is so crucial to understand the mechanisms behind fluctuations in endothelial barrier functions. VEGF-A is a main factor that drives changes in vascular permeability, and that is the reason why anti angiogenic and anti VEGF-A therapies became effective treatments for those conditions. However, VEGF-A is a major player in vascular homeostasis, this is why targeting it directly causes side effects and complications. Better understanding of the mechanism, lining behind the VEGF-A driven increase in permeability and neovascularisation, could lead to better and more efficient treatment. However, it is still not clear how VEGF-A induces vascular permeability.

There are reports showing that this might occur via phosphorylation of TJ and AJ molecules. It was first demonstrated by Antonetti, that VEGF-A increases occludin and ZO-1 tyrosine phosphorylation which are likely to contribute to the regulation of endothelial cell permeability (Antonetti, 1999). Murakami *et al.* published a paper where they are showing, that VEGF-A induces occludin phosphorylation on Ser490, and subsequent ubiquitination changes, the

distribution of TJ proteins in retinal endothelial cells from cell border to intracellular puncta, promoting endothelial permeability (Murakami, 2012).

The selective and rigorous function gate keeping function of BRB is a big challenge for drug administration, as any possible medication cannot pass the endothelial barrier. Alternative administration via the anterior pathway, such as eye drops or intraocular injections have significant disadvantages like drug effectiveness and side effects that might accompany intraocular injections. An emerging administration route is through the sclera, which is more permeable than the cornea and closer to the retina (Tervonen, 2014). Both anterior and sclera drug administration are charged with some disadvantages. Most of the time, the preferred administration would be systemic, but this requires a better understanding of the BRB function.

Up-regulation in VEGF-A expression, has pathological consequences not only in the eye, but can also lead to carcinogenesis. VEGF-A drives tumour angiogenesis and tumour progression, where VEGF-A also stimulates an increase in microvascular permeability and tumour oedema (Crawford, 2009). Thus, better understanding the mechanism of the VEGF-mediated angiogenesis and changes in vascular permeability are important targets also for anti-cancer therapies.

In order to target pathologic angiogenesis, and excessive vascular permeability in cancers and eye diseases, many anti-VEGF-A compounds have been developed. This rapidly expanding group of therapeutics acts by blocking VEGF-A receptors.

Currently, more than 1500 clinical trials of anti-VEGF receptors are in process. Several compounds have received US Food and Drug Administration Approval. One of those is bevacizumab, which has been approved for the intravenous treatment of advanced carcinomas. However, bevacizumab has been also used extensively in ophthalmology for exudative AMD, diabetic retinopathy, retinal vein occlusions, retinopathy of prematurity, and other chorioretinal vascular disorders. Pegaptanib and ranibizumab have been developed specifically for intraocular use, whereas aflibercept (VEGF Trap-Eye) is moving through clinical trials for both intraocular and systemic use (Stewart, 2012).

Early studies in rodent model and preclinical studies in non-human primates and rabbits showed that anti- VEGF therapy exhibits a safety profile and that side effects might be minimal. However, within the time, as the number of patients treated with these agents increased some toxicity of this therapy was reported. A small subset of patients receiving anti-VEGF therapy, as well as pregnant patients with elevated circulating levels of soluble FLT1 (an endogenous VEGFA decoy/antagonist), develop thrombotic microangiopathy (TMA) — a disease characterised by dramatic glomerular endothelial injury (Quaggin, 2012). This shows that specific analysis, of the VEGF-A pathway and its role, in both angiogenesis and increased permeability is required in order to improve current anti-VEGF therapies.

Junction structure - formation and function

Crucial for the maintenance of the integrity of endothelial cells and establishing BBB/BRB are junctional structures consisting of a complex of adhesive proteins, forming a zipper-like organization on the lateral surface of the adjacent cells (Rigor, 2012). These organized structures between endothelial cells contribute to the establishment of cell polarity, differentiation and are important for maintenance of tissue integrity (Gavard, 2008).

The adhesive structures are also stabilized from inside the cells, where they are directly or indirectly linked to the actin cytoskeleton (Hartsock, 2008). EC are connected by adherens junctions (AJ), tight junctions (TJ) and gap junctions (GJ) (Figure 6). GJ are often observed close to the luminal side of the endothelium, and play crucial role in cell–cell communication (Wallez, 2008). They are formed by hexamers of connexins, which connect the cytoplasm of two cells and allows various molecules, ions and electrical impulses to directly pass through. At TJ adhesion is established by claudins, occludin, junctional adhesion molecules (JAM), and endothelial cell selective adhesion molecule (ESAM) (Dejana, 2004). TJ take part in sealing the interendothelial cleft and formation of blood vessels, AJ are important for initiating and maintaining endothelial cell-cell contact. TJ and AJ play a major role in maintaining endothelial cell integrity lead to high endothelial electrical resistance and low paracellular permeability.

The electrical resistance in the BBB/BRB is in the range of 1500-2000 $\Omega\cdot\text{cm}^2$ at the pial vessels in comparison to 3-33 $\Omega\cdot\text{cm}^2$ in other tissues (Stamatovic, 2008, Kerns, 2015).

One of the first TJ transmembrane proteins described was occludin (Shen, 2011a). Occludins contain four transmembrane domains and three cytoplasmic domains: one intracellular short loop, a small N-terminal domain and a long carboxyl (C-) terminus. It is thought that the c-terminal domain can directly associate with ZO-1, ZO-2 and ZO-3, which bind to F-actin (Stamatovic, 2008). Several studies reported that the N-terminal region of occludin is critical for occludin function. Huber et al analysed neutrophil migration across monolayers formed by stably transfected epithelial cells expressing wild-type and mutant occludin. The expression of mutants with a modified N-terminal cytoplasmic domain up-regulated neutrophil migration, whereas deletion of the C-terminal cytoplasmic domain did not have an effect (Huber, 2000).

Claudins are major components of tight junctions in brain and retinal endothelial cells (Dejana, 2004). There are 27 different claudins expressed in different tissues and they all share the same structural pattern (Mineta, 2011). Claudins consist of four transmembrane regions, two extracellular loops and two cytoplasmic termini (Furuse, 2010). The first extracellular loop influences paracellular charge selectivity, while the second extracellular loop is the receptor for a bacterial toxin in some claudins for example claudin-3 and -4, but not to claudin-1 or -2. (Fujita, 2000). The C-terminus possesses the binding site for the cytoplasmic proteins ZO-1, ZO-2, ZO-3. Claudin function in the TJ complex is to limit paracellular ion movement selectively and this produces the high electrical resistance of the barrier. Brain endothelial cells possess claudin-5 and claudin-12 and possibly other claudins. Claudins present in brain endothelial cells may form pores of variable size ($\sim 10\text{\AA}$) which may be involved in transjunctional movement of water (Stamatovic, 2008) Deficiency of Claudin-5 does not inhibit tight junction formation and does not alter morphology of blood vessels. However, tracer experiments and magnetic resonance imaging revealed that in the Claudin-5 deficient mice, the BBB permeability for small molecules ($<800\text{ D}$), but not larger molecules, was selectively affected (Nitta, 2003).

JAMs (JAM-A, -B, -C) are members of the immunoglobulin superfamily. These molecules structurally are composed of a single transmembrane domain, an extracellular domain, an extracellular N-terminus, and a short cytoplasmic C-terminus. The short C-terminus cytoplasmic tail (40 amino acids) contains a PDZ binding domain which facilitates interactions with TJ associated scaffold proteins such as ZO-1, AF-6, ASIP/Par3, and cingulin. The cytoplasmic tail also contains consensus phosphorylation sites that may serve as substrates for PKC and PKA (Stamatovic, 2008).

At adherens junctions, adhesion is mostly mediated by vascular endothelial cadherin (VE-cadherin) (Dejana, 2004). VE-cadherin is a member of a large family of cadherins, and another cadherin present in endothelial cells is N-cadherin. Unlike VE-cadherin, N-cadherin does not localise at AJ and is diffusely distributed on the cell membrane which might suggest that the two proteins play different functions in EC. One of the hypotheses is that N-cadherin might promote cell adhesion and communication with pericytes, smooth muscle cells, and astrocytes that also express N-cadherin. This conjecture confirms localisation of N-cadherin at the basal side of EC in contact with pericytes and astrocytes in the brain (Bazzoni, 2004, Derycke, 2004). The AJ cytoplasmic plaque includes also proteins of the catenin family: α , β , γ , p120. VE-cadherin is an important determinant of microvascular integrity both *in vitro* and *in vivo* and together with catenin forms a complex that function as an early recognition mechanism between endothelial cells (Lampugnani, 2007, Stamatovic, 2008). VE-cadherin, through its carboxyterminal region binds β -catenin and γ -catenin (plakoglobin), both of these proteins associate with α -catenin which anchors this complex to actin, stabilising it from inside of the cell. α -catenin has been suggested to also bind α -actinin and vinculin for further stabilisation of the complex (Bazzoni, 2004).

Outside junction structures, EC express other cell-specific homophilic adhesion proteins, from which best studied is platelet endothelial cell adhesion molecule (PECAM or CD31). PECAM can bind β -catenin and limit its transcriptional activity. Therefore, although PECAM is located outside of AJ it might contribute to endothelial cell-cell adhesion (Figure 6) (Dejana, 2004).

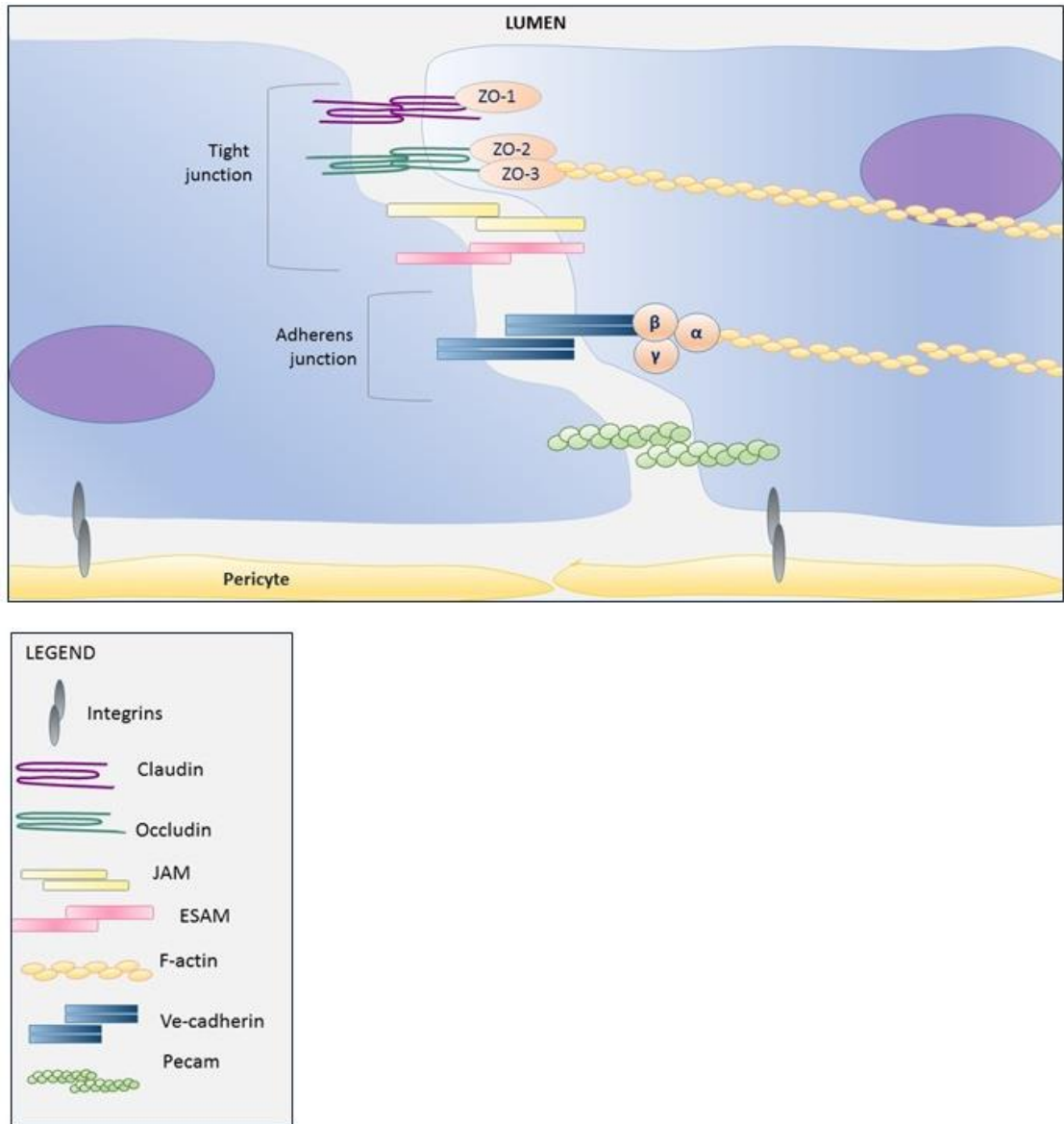


Figure 6. Endothelial cell junctions.

EC junctions are formed by tight junction and adherence junction. At TJ adhesion is mediated by claudins, occludins, junctional adhesion molecules (JAM), endothelial cell selective adhesion molecule (ESAM), and main adhesive molecule at AJ is vascular endothelial cadherin (VE-cadherin). TJ are connected to the cytoskeleton via adaptor proteins such as zona occludens 1 (ZO-1), ZO-2 and ZO-3, and AJ are connected via Catenin $-\alpha$, $-\beta$, and $-\gamma$. Adapted from (Dejana, 2004).

Table 1. Proteins involved in EC junction complex.

Adapted from (Stamatovic, 2008, Hartsock, 2008, Wallez, 2008).

Tight Junction
Transmembrane molecules
Occludin - formation and regulation of TJ paracellular barrier permeability, interacts with ZO-1, ZO-2, ZO-3, F-actin
Claudins-3,-5,-12 - tight junction-specific obliteration of the intercellular space; directly interacts with ZO-1, ZO-2 and ZO-3.
JAM-A -tight junction formation, neutrophil and monocytes transmigration; interaction with Par3
JAM-B - lymphocytes transmigration; interaction with JAM-C
JAM-C - cell-cell adhesion, leukocytes transmigration; interaction with JAM-B
ESAM -endothelial cell-selective adhesion molecule- participates in TJ assembly
Intracellular molecules
ZO-1 - stabilisation of junctions, signal transduction; interact with occludin, claudins, cingulin, ZO-3
ZO-2 - stabilisation of TJ and AJ, interacts with occludin
ZO-3 - interacts with occludin, claudins and ZO-1
Par-3, Par-6 - TJ assembly
Afadin/AF-6 - assembly of TJ and AJ; interaction JAMs, cadherins catenins, F-actin
Cingulin - formation and regulation of the TJ permeability, anchoring the TJ proteins to actin based cytoskeletons; interaction with ZO-1 and JAMs
7H6 - F-actin cross-linking protein, anchor actin to other TJ and AJ proteins; interact with ZO-1, β -catenin
Rab3b, Rab13 - participation in polarised transport, assembly and/or activity

of TJ
<p>PKCζ, PKCγ - cell polarisation processes, biogenesis of TJ; interaction with Par3, Par6, Rac, Cdc42, actin cytoskeleton</p> <p>G protein - TJ biogenesis, stabilisation of TJ, regulation of permeability</p>
<p>Adherence Junction</p> <p>VE-cadherin - control the cohesion and organization of the intercellular junctions</p> <p>Catenin α, β, γ (plakoglobin) - with VE-cadherin produces a complex which is linked to the actin filament network, and it is important for VE-cell-adhesion properties</p>
<p>Outside Adherence Junction</p> <p>N-cadherin - promotes endothelial cell adhesion and communication with mesenchymal cells expressing N-cadherin, such as pericytes, smooth muscle cells, and astrocytes</p> <p>PECAM - promotes adhesion</p> <p>SHP-2 - play a role in the Ras-mitogen-activated protein kinase (MAPK) activation cascade</p> <p>S-endo1 - induces homophilic cell adhesion</p>

VEGF-A controls EC growth and permeability

Vascular endothelial growth factor A (VEGF-A) was first identified as a potent permeability factor in the early 1980's and was originally named 'vascular permeability factor' (VPF) (Senger, 1983). Now known as VEGF-A, this growth factor promotes rapid endothelial cell proliferation, vascular permeability and the associated tissue oedema. However, the molecular mechanism that drives such a diverse role of VEGF-A in the vasculature is still under debate (Gavard, 2006).

VEGF-A is one of the key players in angiogenesis as it induces various distinct behavioural responses of endothelial cells including proliferation, migration, specialisation and survival (Ruhrberg, 2003). VEGF-A guides endothelial cells situated at the tips of retina vasculature, which sprout and extend long filopodia. An extracellular gradient of VEGF-A guides filopodia, leading to directed migration of the tip cells, and proliferation of stalk cells (Gerhardt, 2003).

The defective vasculature and embryonic lethality in mice seen at day 11-12 underlines the fact that the loss of even a single allele of VEGF-A has a significant role in hetero-embryonic development (Carmeliet, 1996, Ferrara, 1996).

VEGF-A belongs to a gene family that also includes VEGF-B, C, D, E, and PlGF. The VEGF family members are secreted, dimeric glycoproteins of approximately 40 kDa. VEGF-A actually refers to a collection of protein isoforms, ranging in size from 121 to 206 amino acid residues and differing in their ability to bind heparin and extracellular matrix.

The production of VEGF-A is stimulated by hypoxia and inflammatory cytokines. VEGF-A is produced in the retina by retinal pigment epithelial cells, ganglion cells, Muller cells, amacrine cells and smooth muscle cells and plays an important role in both choroidal vasculature formation and retinal vascular growth (Stewart, 2012, Famiglietti, 2003) neuronal development and neuroprotection (Foxton, 2013).

VEGF-A derived from RPE is important for the physiological regulation of choroidal vasculature and its overexpression has been implicated as an important factor in the pathogenesis of choroidal neovascularisation in age-related macular degeneration. It has also been reported that inactivation of VEGF-A expression in the RPE (in *VEGF^{rpe-/-}* mice) causes absence of choriocapillaris, occurrence of microphthalmia, and the loss of visual function. Severe abnormalities in choriocapillaris were observed even when VEGF-A levels were reduced (in *VEGF^{rpe+/-}* mice) (Marneros, 2005).

During vascular development, the primary role in angiogenesis may involve VEGF-A delivered from astrocytes and Muller cells. Astrocytes spreading across the retinal surface detect hypoxia in the inner layers of retina and in response to

hypoxia, secrete VEGF-A, which in turn causes vessel growth. Vessel function and the supply of oxygen cause a downregulation of VEGF expression. Müller cells might function as detectors of hypoxia in the middle layers of retina, and in response secrete VEGF - which causes the growth of the deep layer of retinal vessels (Stone, 1995). Astrocytes main role vascular growth confirms a very interesting observation, that in animals with only partially vascularised retinas like horses and rabbits, astrocytes are absent in the avascular region in the retina (Scott, 2010).

VEGF receptors

All VEGF isoforms bind to three main receptor tyrosine kinases (RTKs) - vascular endothelial growth receptors (VEGFR) that mediate their diverse functions: VEGFR-1, VEGFR-2 and VEGFR-3 and distinct coreceptors such as neuropilins or heparan sulfate glycosaminoglycans. VEGF-A, -B, and PlGF bind to VEGFR-1; VEGFR-2 mediates signalling from VEGF-A, -C, and -D, and VEGFR-3 is specific for VEGF-C and -D (Olsson, 2006, Ferrara, 2003, Gavard, 2006, Crawford, 2009).

VEGFR-1 (Flt-1) and VEGFR-2 (Flk-1) are the two prominent and best described VEGF receptors. VEGFR-2 plays a pivotal role in endothelial cell development and generation of mice deficient in this receptor results in death of homozygous embryos in utero between 8.5 and 9.5, as a result of a defect in the development of haematopoietic and endothelial cells (Shalaby, 1997, Shalaby, 1995). Interestingly in VEGFR-1 deficient mice endothelial cell formation was normal, however, these animals had a disorganised vasculature and died at embryonic days 8.5–9 (Fong, 1999, Fong, 1995).

VEGFR-1 and VEGFR-2 are primarily involved in angiogenesis. VEGFR-1 and VEGFR-2 are structurally similar. Overall, there is 43.2% sequence homology between VEGFR-1 and VEGFR-2. They are composed of an extracellular ligand-binding domain with seven immunoglobulin (Ig)-like motifs (ECD), a single transmembrane domain (TMD) and a juxtamembrane domain (JMD), a kinase domain split by a kinase insert, and a carboxyl terminus (Rahimi, 2006). The extracellular domain is responsible for binding the ligand,

the transmembrane domain anchors the receptor to the plasma membrane, and the juxtamembrane domain has been shown to regulate kinase activity by properly positioning kinase monomers.

Similar to other receptor tyrosine kinases, signalling by VEGFRs is activated upon ligand-mediated dimerisation. VEGFRs transduce signal upon binding of a covalently linked ligand dimer to the extracellular receptor domain (Figure 7). This interaction promotes receptor homo- and heterodimerisation. Kinase dimerisation can be mediated in multiple ways. As long as the kinase domains are properly oriented relative to each other, dimeric receptor constructs will be enzymatically active. Receptor dimerisation is followed by phosphorylation of specific tyrosine residues located in the intracellular JMD, the kinase insert domain, and the carboxyterminal tail of the receptor. Subsequently, a variety of signalling molecules are recruited to VEGFR dimers giving rise to the assembly of large molecular complexes, that activate distinct cellular pathways (Rahimi, 2006, Stutfeld, 2009).

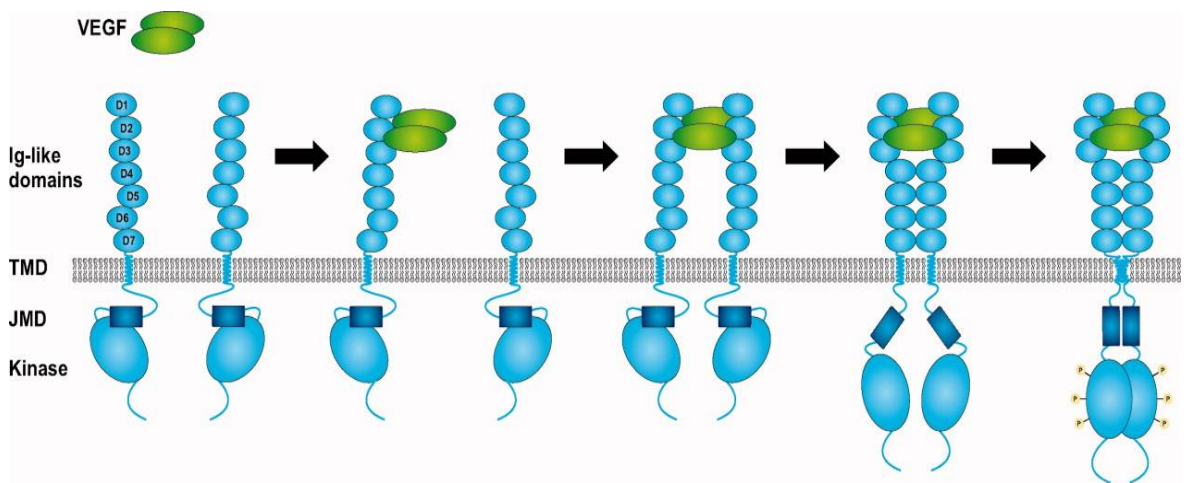


Figure 7. Schematic illustrating VEGFR activation.

Ligand (VEGF) mediates extracellular domain dimerisation. This interaction promotes receptor homo- and heterodimerisation followed by phosphorylation of specific tyrosine residues located in the kinase insert domain. Subsequently, a variety of signalling molecules are recruited to VEGFR dimers. Figure adapted from (Stutfeld, 2009).

VEGF-A mediates a plethora of biological processes in endothelial cells such as cell proliferation, migration, survival, cell-cell communication, and

vessel permeability via its receptors. VEGFR1 is required for the recruitment of haematopoietic precursors and migration of monocytes and macrophages, whereas VEGFR2 and VEGFR3 are essential for the functions of vascular endothelial and lymphendothelial cells, respectively (Olsson, 2006, Rahimi, 2006).

Cytoskeleton compartments in the endothelial cells

Determination of proper cellular shape, organisation, and segregation of components as they grow and divide, are critical for proper cell function and proliferation. In eukaryotic cells those roles are dependent on an astonishing system of filaments called the cytoskeleton. Actin filaments, microtubules and intermediate filaments are the three main components that build the cytoskeleton (Alberts, 2007)

Actin filaments form a very dynamic structure, which determine the shape of the cell surface and are necessary for cell locomotion. The basic element of the actin cytoskeleton is globular actin (G-actin). Several G-actin elements can be polymerised to actin filaments (F-actin). F-actin represents the structural basis of the actin cytoskeleton (Wabnitz, 2015).

A second major element of the cytoskeletal structure of an endothelial cell is the microtubule system. Microtubules are formed by polymers of α -, β - and γ -tubulin.

γ -tubulin is specifically localised to the centrosome, where it plays a critical role in initiating microtubule assembly. α - and β -tubulin forms dimmers, which polymerise to form microtubules. Microtubules consist of 13 linear protofilaments assembled around a hollow core. This lattice network spans the cells in a polarised fashion from the nucleus to the periphery (Cooper, 2000, Stamatovic, 2008). Microtubules determine the position of membrane enclosed organelles and direct intracellular transport, but also participate in organisation of actin filaments, focal adhesion, isometric cellular contraction and transendothelial leukocyte migration (Stamatovic, 2008).

Intermediate filaments are the third main component of the cytoskeleton, which mainly play a structural role by providing mechanical strength to cells

and tissues. In contrast to actin filaments and microtubules, which are constructed with specific proteins, actin and tubulin respectively, intermediate filaments are composed of a variety of proteins that are expressed in different types of cells. The subunits composing intermediate filaments constitute a superfamily of highly α -helical proteins that are divided into six major classes or types on the basis of similarities in sequence. In endothelial cells, intermediate filaments are mostly composed of vimentin. Vimentin filaments help support cellular membranes and may help keep the nucleus and other organelles in a defined place within the cell (Cooper, 2000, Lodish, 2000).

The cytoskeleton plays a crucial role in determining cell shape, and establishing interendothelial junctional integrity (Hoelzle, 2012). The actin microfilament system is linked to multiple membrane adhesion proteins including cadherins, occludin, glycocalyx components, functional intercellular proteins like zona occludens (ZO), catenins and focal adhesion complexes. This makes the organisation of actin filaments intimately linked to the assembly and function of junction structures in endothelial cells. Through disruption of cytoskeleton and actin stress fibre formation, driven by activated myosin light chain, can be generated force that might destabilise the position of junctional molecules, connected to the actin cytoskeleton, and cause their internalisation and barrier disruption (Stamatovic, 2008).

The link between the Rho GTP-ase pathway and endothelial barrier function

Crucial role in signalling transduction, that controls cytoskeletal reorganisation, cell shape, polarity and adhesion play Rho GTP-ases. They belong to the Ras superfamily of small (20-30 kDa) GTPases, which share a conserved structure and biochemical properties, acting as binary molecular switches turned on by binding GTP, and off by hydrolysing GTP to GDT. Despite structural and biochemical similarities, these proteins play multiple and diverse roles: proliferation, differentiation, morphology, polarity, adhesion, migration, survival and apoptosis. The Ras protein members are divided into five major

branches: Ras, Rho, Rab, Ran and Arf (Figure 8) (Wennerberg, 2005, Trabalzini, 2014).

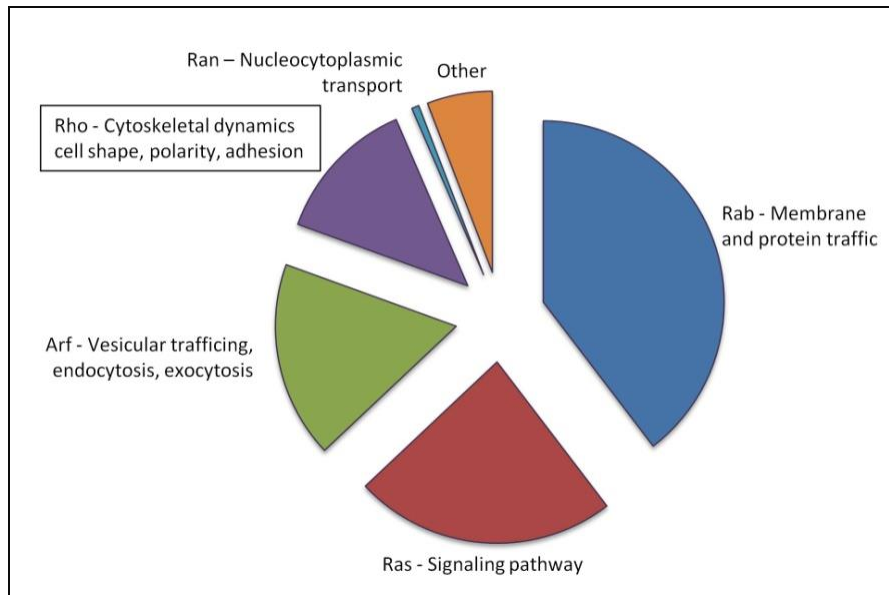


Figure 8. Schematic representation of the Ras proteins.

Ras, Rho, Rab, Ran and Arf and their main functions. Based on (Trabalzini, 2014, Wennerberg, 2005).

The most recognised and described members of Rho GTP-ases family are Rac1, RhoA, and CDC42.

Rho GTP-ases can be activated by VEGF-A, and regulate activity of p21-activated kinase (PAK) and serine/threonine protein kinase (ROCK). Both ROCK and PAK are very important in regulation of myosin regulatory light chain (MLC), Myosin light-chain phosphatase (MLCP) and myosin light chain kinase (MLCK) activity, which are highly important in modulation cytoskeletal remodelling (Figure 9).

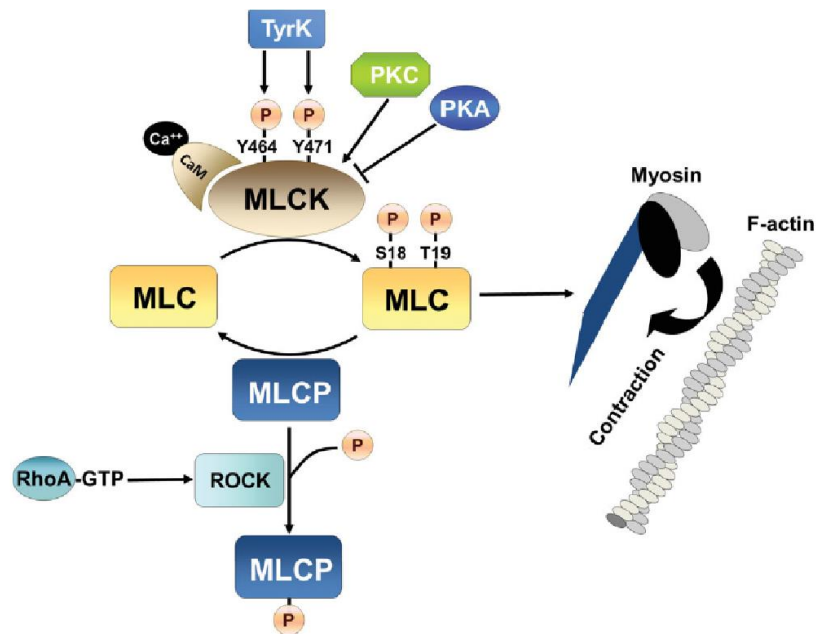


Figure 9. The control of actin-myosin contraction in endothelium.

Increased myosin light chain (MLC) phosphorylation at Ser-18 and Tyr-19, in response to MLCK activation or myosin light chain phosphatase (MLCP) inhibition, increases MLC ATPase-driven force generation relative to actin. MLCK activity is increased by Ca^{2+} -calmodulin binding, and/or by phosphorylation by protein kinase C (PKC) or tyrosine kinase phosphorylation at Tyr-464 and Tyr-471. MLCK activity is decreased in response to protein kinase A (PKA) activity. Inhibition of MLCP is achieved by ROCK activation downstream of RhoA activation, resulting in phosphorylation-dependent inhibition of MLCP. Adopted from (Rigor, 2012).

Phosphorylation of the 20 kD MLC can be categorised based on effects on myosin function for inhibitory and activating. Phosphorylation of Ser-19, Thr-18 stimulates myosin activity, whereas Ser-1, Ser-2 and Thr-9 its inhibition. Ser-19 can be phosphorylated by MLCK, and PAK, Rho kinase. These kinases are regulated by distinct upstream signals such as $[\text{Ca}^{2+}]_4$ /calmodulin and Rho family GTPases. Many of these pathways interact and this complexity suggests that cells specially and temporally compartmentalise their signals (Chew, 2002, Rigor, 2012).

The activity of MLC is also regulated by myosin light chain phosphatase (MLCP) activity, which dephosphorylates MLC and reduces its contractile

activity. MLCP is a trimeric holoenzyme consisting of catalytic subunit of protein phosphatase 1 (PP1), regulatory complex MYPT1 and a 20-kDa subunit (M20) with unknown function (Hurley, 2007, Terrak, 2004). MYPT1 plays a key part in determining the physical and functional integrity holoenzyme. At the N terminus of MYPT is located a PP1, this N-terminal domain together with catalytic subunit forms the active site of the MLCP. The C-terminal region of MYPT1 controls the substrate specificity and directly binds to substrates such as myosin (Khromov, 2009).

MLC-dependent stimulation of myosin II activity, and thus cytoskeleton reorganisation in the EC, appears to be an important concept in the study of barrier function.

Hypothesis and aims of the PhD project

The Blood-retinal barrier (BRB) and blood-brain barrier (BBB) protect, respectively, retina and brain from substances circulating in the blood that may affect the homeostatic regulation of the delicate and intricate neural microenvironment.

My project will focus on BRB formation during mouse postnatal development, with a particular focus on the inner BRB, a highly specialised endothelial barrier. The murine developmental model gives us an excellent opportunity for barrier function study, because retinal vascular development occurs postnatally and over a brief 2-3 week period. In Chapter 3, by using tracer study, I would like to provide analysis of the BRB function among early stages of murine development. These experiments will help us define the time point for BRB acquisition.

In Chapter 4, I would like to define the role of VEGF-A and VEGF- receptors during BRB formation. Postnatal development, in contrast to embryonic development, allows for the assessment of barrier function using tracers, and also affords the opportunity to explore mechanisms through pharmacological manipulations (Weis, 2008). Using VEGFR2 blocking antibody injection and VEGF-A injection study, I would like to attempt to understand the importance of VEGF-A activity during BRB formation.

In Chapter 5, I would like to present the results from the phosphoproteomic study, where I will present the differences in the protein phosphorylation state between P5 - early stage of retina development, when BRB does not maintain or prepare BRB function, and P15 when BRB maintains its gate keeping role. This comparison would help us define possible mechanisms involved in poor barrier function at early stages of murine retina development.

In Chapter 6, I would like to explore the role of the cytoskeletal remodelling during BRB development. Using western blotting technique and immunofluorescent staining, I will confirm previously identified differences in phosphorylation of various molecules implicated in cytoskeleton remodelling. Using small PIK peptide, which is MLCK inhibitor, I will present the effect on BRB function after blocking MLCK driven MLC phosphorylation.

In the last Chapter 7 I will present suggested methods for BRB function study in the in-vitro model.

This work will provide an analysis of BRB function during retina development, and suggest the mechanism that might be implicated in poor BRB function, at early stages of retina vasculature formation. At the root of many pathological conditions in the eye, lies a change in vascular permeability. Better understanding of the changes implicated in the increased BRB permeability will likely provide information that is useful in understanding disorders characterised by BRB and BBB dysfunction.

Materials and Methods

Chapter 2.

Materials and Methods

Reagents

All chemicals were purchased from Sigma-Aldrich (Dorset, UK), unless otherwise indicated.

In-vivo experiments

Experiments were performed on C57BL/6 mice (Charles River) and Lewis rats (Harlan Laboratories). Animals were kept on a 12-hour light–dark cycle. All experiments were conducted in accordance with the ARVO Statement for the Use of Animals in Ophthalmic and Vision Research, and with Home Office standards and were reviewed by an institutional animal care committee.

Retina dissection

C57BL/6 mice at the different stages of development, were euthanized in CO₂ chamber or anesthetised with a mixture of Ketamine/Xylazine, depending on the type of experiment. Eyes were carefully enucleated, and placed in microcentrifuge tubes filled with 4% paraformaldehyde (Electron Microscopy Sciences) in phosphate buffer solution (PBS). After 1 hour of fixation, eye was transferred into a dish filled with PBS. Retina dissection was performed under binocular dissecting microscope (Figure 10). The tissue around sclera and optic nerve was removed. Then a cut was made at the boundary between the cornea and the sclera. The pupil, lens, iris and vitreous (with hyaloid vessels in case of animals below P10) were removed. Then the choroid/RPE was peeled of and 4

cuts were made on the retina tissue. Finally, the retina was flat mounted on the microscopic slide.

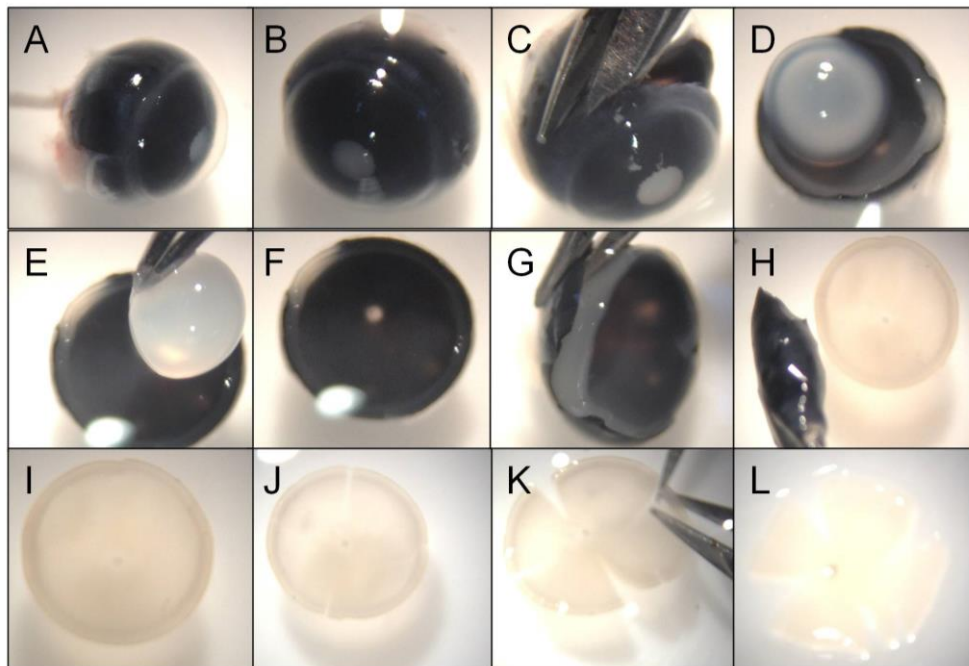


Figure 10. The procedure of retina flat mounting.

After enucleating the eye, the tissue around sclera and optic nerve was removed. Then a cut was made at the boundary between the cornea and the sclera. The pupil, lens, iris and vitreous with hyaloid vessels were removed. Then 4 cuts were made and choroid pulled off. Finally, the retina was flat mounted on the microscopic slide.

Immunofluorescence staining of the whole mount retina tissue and cryostat section

C57BL/6 mice at the different stages of development, were euthanised in CO₂ chamber or anaesthetised with a mixture of Ketamine/Xylazine. Eyes were carefully enucleated, and placed in microcentrifuge tubes filled with 1ml of 4% paraformaldehyde (Electron Microscopy Sciences) in PBS. After 1 hour fixation at room temperature, retina tissue was dissected as described above.

For PFA-fixed retina, fixation was followed by 3 washes in PBS and a 1 hour permeabilisation step in 1% Triton X-100 in PBS. That retina was blocked for 1 hour in blocking solution (5% goat or donkey serum, 0.1% Triton X-100 in PBS). Primary antibody incubation was performed in diluted blocking solution (2%

goat or donkey serum, 0.05% Triton X-100 in PBS) for 16-18 hours at 4^oC. The list of primary antibodies is presented in Table 2.

After primary antibody incubation tissues were washed 3 times for 30 minutes in diluted blocking solution. Secondary antibody incubation was performed for 1 hour at room temperature in diluted blocking solution. The list of secondary antibodies is presented in Table 3. The retina was washed 3 times for 30 minutes in PBS.

After last wash retina was placed on the microscopic slide and mounted with the Vectashield mounting medium (Vector Laboratories), covered with the coverslip and sealed with varnish.

For immunolabelling of ocular cryosections, eyeballs were fixed for 16-18 hours in 4% PFA at 4^oC, and embedded in OCT. Cryosections of 8-10 µm were cut, and stored at -80^oC until use. Immediately before use cryosections were air-dried for 5 minutes at room temperature. After 3 washes in PBS, cryosection samples were permeabilised for 15 minutes in 0.5% Triton X-100 in PBS. The retina was blocked for 1 hour in blocking solution (5% goat or donkey serum, 0.1% Triton X-100 in PBS). Primary antibody incubation was performed in diluted blocking solution (2% goat or donkey serum, 0.05% Triton X-100 in PBS) for 1-2 hours at room temperature.

After primary antibody incubation tissues were washed 3 times for 15 minutes in diluted blocking solution. Secondary antibody incubation was performed for 1 hour at room temperature in diluted blocking solution. Then retina was washed 3 times for 15 minutes in PBS.

After last wash microscopic slide was covered with Vectashield mounting medium (Vector Laboratories), cover-slipped and sealed with varnish.

Table 2. Primary antibodies and conditions used in immunofluorescent retina staining.

Antibody	Dilution	Company and catalogue number
Isolectin B4	1 : 200	Vector Laboratories - FL-1201
Isolectin B4	1 : 200	Sigma - L3759
Rb anti-Collagen IV	1 : 200	Abcam - ab19808
Rb anti-Collagen IV	1 : 200	Abcam - ab6586
Ms anti-PECAM-1	1 : 200	BD Pharmingen™ - 550300
Rt anti-PECAM-1	1 : 200	BD Pharmingen™ - 553370
Rb anti-von Willebrand Factor	1 : 500	Abcam - ab6994
Rb anti-IBA-1	1 : 200	Abcam - ab5076
Rb anti-Claudin 5	1 : 200	Abcam - ab53765
Rb anti-Occludin	1 : 200	Abcam - ab31721
Rb anti-ZO-1	1 : 200	Invitrogen - 61-7300
Rb anti-VE-cadherin	1 : 200	Abcam - ab33168
Rb anti-VEGF-A	1 : 200	Abcam - ab46154
Rb anti-VEGF-A	1 : 200	Abcam - ab51745
Gt anti-VEGFR1	1 : 100	Santa Cruz - sc-31173
Rb anti-VEGFR2	1 : 100	Rerearch&Development MAB4431
Rt anti-DC101	1 : 100	Kindly donated by Prof. Patrick Turowski
Rb anti-MLCK	1 : 200	Abcam - ab76092
Rb anti-MLCK-P	1 : 200	Invitrogen - 441085G
Rb anti-PAK	1 : 200	Abcam - ab40852
Rb anti-PAK-P	1 : 200	Abcam - ab40795
Rb anti-MLC-P	1 : 200	Abcam - ab2480
Ms anti β -actin	1 : 200	Sigma - A2228
Rb anti β -actin	1 : 200	Sigma - A2066
Phalloidin Alexa Flour 594	1 : 200	Life Technologies - A12381

Table 3. Secondary antibodies used in immunofluorescence staining of retina.

2° Ab	Conjugation	Dilution	Company and Cat#
Gt anti-ms IgG (H+L)	AlexaFluor 488	1 : 500	Invitrogen (A11029)
Dk anti-rt IgG (H+L)	AlexaFluor 488	1 : 500	Invitrogen (A21208)
Gt anti-rt IgG (H+L)	AlexaFluor 594	1 : 500	Invitrogen (A11007)
Gt anti-rb IgG (H+L)	AlexaFluor 488	1 : 500	Invitrogen (A11008)
Gt anti-rb IgG (H+L)	AlexaFluor 594	1 : 500	Invitrogen (A11012)
Dk anti-rb IgG (H+L)	AlexaFluor 488	1 : 500	Invitrogen (R37118)
Dk anti-rb IgG (H+L)	AlexaFluor 594	1 : 500	Invitrogen (R37119)
Dk anti-gt IgG (H+L)	AlexaFluor 594	1 : 500	Invitrogen (A11058)

Ms – mouse; Rt - rat; Rb – rabbit; Gt – goat; Dk – donkey; Ht – hamster

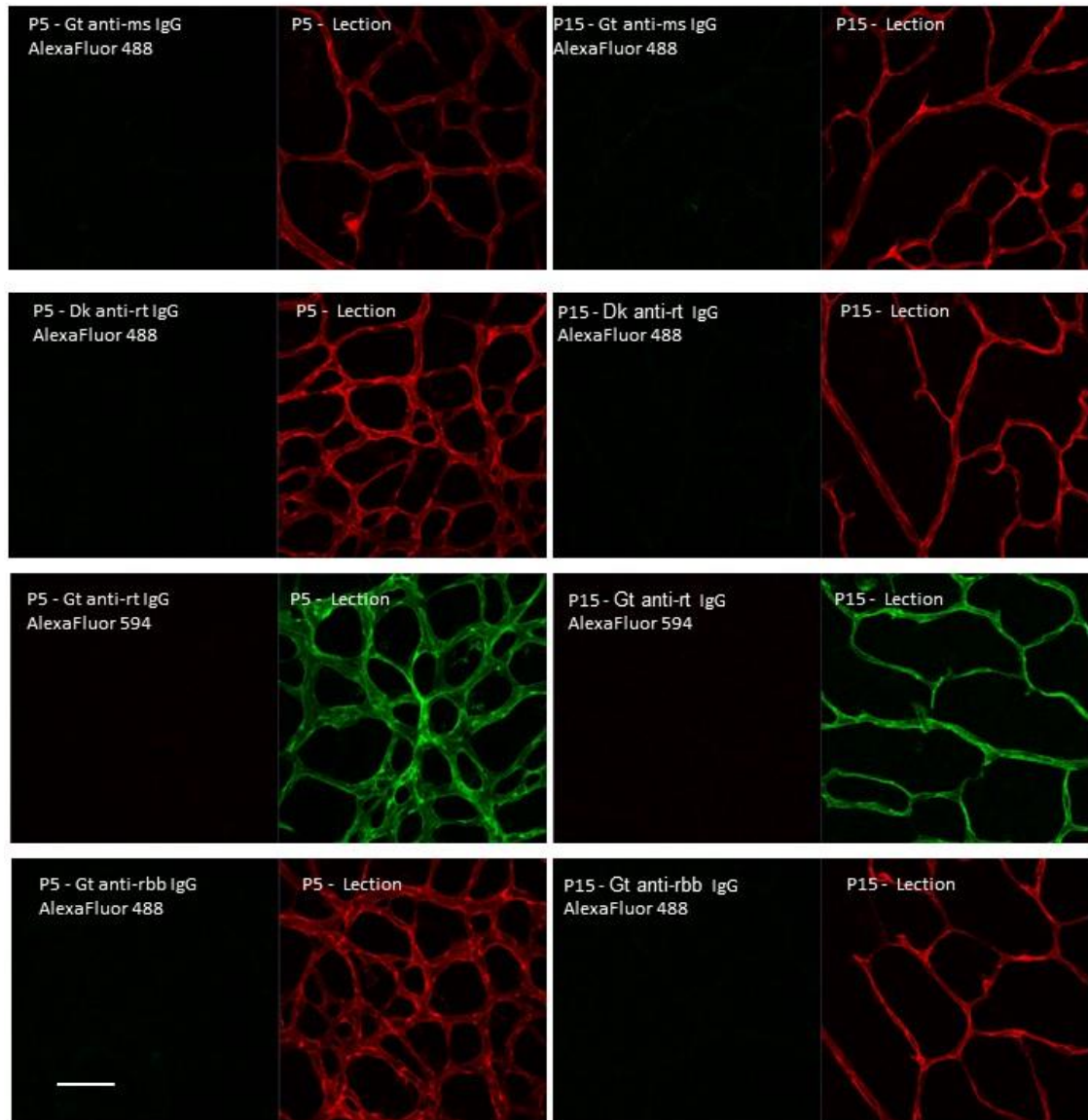


Figure 11. 2° Antibody control staining (part1).

The retinas were immunostained with 2° Antibody and Lectin. The scale bar indicates 50 μ m for all pictures.

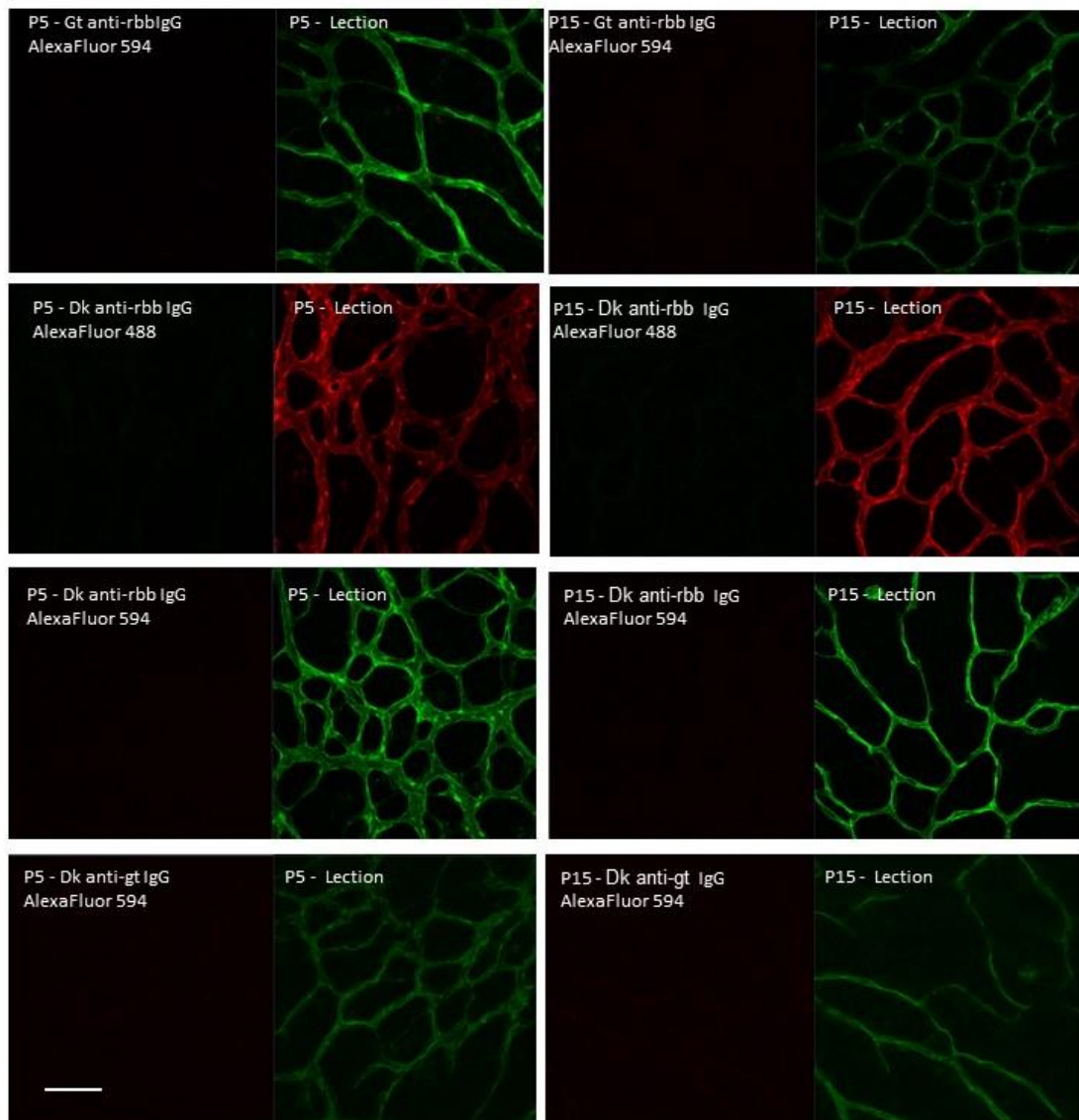


Figure 12. 2° Antibody control staining (part2).

Leakage assay in the retina with NHS- Biotin

At the age of postnatal day (P) 5, 10, and 15 mice were anesthetized with a mixture of ketamine (75 mg/kg body weight, Fort Dodge Animal Health, USA) and xylazine (25 mg/kg body weight, IVX Animal Health USA). After the animals reached deep anaesthesia the chest was opened and a cut was made on the left side of the ribs. Then within 1 minute NHS-Biotin (Pierce EZ-Link Sulfo-NHS-Biotin, Thermo Scientific, 21217) was injected into the left ventricle (0.05 mg per 1g animal). After a delay of 30sec to allow NHS-Biotin to enter the circulation, animal was euthanized by overdose anaesthesia, and eyes were

removed and placed into 1ml of 4% PFA for 1h at room temperature. The retinas were dissected, blocked and permeabilised in 5% FBS (blocking serum) 1% Triton X-100 in PBS for 1h. Tissue was incubated overnight with Streptavidin (1:500 Alexa Fluor conjugate 594 - Invitrogen S32356) in blocking solution, followed by three 30 minute washes in PBS. Finally, the retinas were flat mounted with Vectashield (Vector Laboratory). Microscopic analysis was done with LSM710 laser scanning confocal microscope (Zeiss Imager Z.2) and Zen2009 software (Zeiss).

Dextran – blood concentration measurement

P5, P10 and P15 C57BL/6 mice were injected intraperitoneally with 3 kD dextran or 70 kD dextran according to their body weight (0.1mg per 1g body weight). After 2 hours (for the animals injected with 3 kD dextran) or after 4 hours (for animals injected with 70kD dextran), mice were anaesthetised with a mixture of ketamine and xylazine. When animals were under deep anaesthesia, chest was opened and 50 µl of blood sample was withdrawn from the right ventricle (before inserting needle into the heart, needle and syringe was washed in 0.5M EDTA) and 100µl EDTA (0,5M) was added to the blood sample. Samples were spin at 9000rpm and 100µl of the solution from each sample was located in the black plate. Fluorescent intensity was measured with Plate Reader and compared between the groups of P5, P10, and P15.

Leakage assay in the retina with 3kD fixable dextran

P5, P10, P15 mice were injected intraperitoneally with 3 kD fixable dextran (Dextran, Fluorescein, 3000MW, Anionic, Lysine Fixable, Life Technologies D-3306) animals were left for 1 or 2 hours, to allow for dextran get into the blood circulation. Then animals were anaesthetized with a mixture of ketamine and xylazine and cardiac perfusion was done. After that, eyes were removed and fixed in 1ml of 4% PFA for 1h. The retina was dissected and flatmounted with Vectashield (Vector Laboratory) for microscopic analysis. Pictures were taken with LSM710 laser scanning confocal microscope (Zeiss

Imager Z.2), under the same settings, and Zen2009 software (Zeiss). Retina was observed with the objective Zeiss Apochromat 10x/0.45W.

For analysis, 9 pictures were taken and stitched together in order to reconstruct one quarter of the retina. At least 3 pictures, each representing one quarter of the retina were taken for each animal. Images were analysed with ImageJ software. The intensity of the fluorescence of the retina was measured, by circling the retina tissue and measuring the intensity of fluorescence of the tissue. The average fluorescence intensity of the retina from 1 animal, was assigned as 1 representative sample.

Statistical analysis was performed using GraphPad Prism Software. For normal distribution a D'Agostino-Pearson normality test was run. Differences between multiple groups were compared using one-way ANOVA followed by the post hoc t-test. The criterion for statistical significance was p-value < 0.05 (*), 0.01(**) or 0.001 (***) specified in figure legends.

Leakage assay in the retina with 70kD fixable dextran

P5, P10, P15 mice were injected intraperitoneally with 70 kD fixable dextran (Dextran, Fluorescein, 70 000MW, Anionic, Lysine Fixable, Life Technologies D-1822) animals were left for 4 hours, to allow for dextran get into the blood circulation. Then animals were euthanized using CO2 chamber. After that, eyes were removed and fixed in 1ml of 4% PFA for 1h at room temperature. The retina was dissected and flatmounted with Vectashield (Vector Laboratory) for microscopic analysis. Pictures were taken with LSM710 laser scanning confocal microscope (Zeiss Imager Z.2) and Zen2009 software (Zeiss) was used under same settings. Retina was observed with the objective Zeiss Apochromat 10x/0.45W. 9 tile pictures for each retina were taken and stitched together.

VEGF-A triggered leakage assay in the retina

The pupils of the P15 mice were dilated with 2.5% tropicamide (Bausch & Lomb) and atropine (Bausch & Lomb). After pupils were fully dilated animals

were anaesthetised with a mixture of ketamine and xylazine. Followed by deep anaesthesia mice were intravitreally injected with 1µl VEGF-A or PBS (Recombinant Rat VEGF 164, CF Research and Development 564-RV-010/CF – 100µg/ml stock concentration). After 24 hours, 3kD dextran or 70 kD dextran, with the volume adjusted according to the body weight, was injected intraperitoneal. After 2 (for 3 kD dextran injected animals) or 4 hours (for 70 kD dextran injected animals) from dextran injection, animals were terminally anaesthetised. Eyes were enucleated, treated and examined in the same way as for the developmental leakage assay procedure. For 3kD dextran injected animals the same statistical analysis was used as for developmental leakage assay.

VEGFR1 and VEGFR2 in-vivo staining

C57BL/6 animals at the age P20 were anaesthetized with a mixture of Ketamine and Xylazine. After animals reached deep anaesthesia the chest was opened and a cut was made on the left side of the ribs. Then rat anti-mouse VEGFR2 (MAB 4431-R&D systems) or goat polyclonal anti-VEGFR1 (Cruz Biotechnology, Inc. sc-31173) 7 mg/kg was slowly injected into the left ventricles. After 5 min delay to allow for the antibody getting into the circulation, animals were perfused with PBS. Eyes were removed and fixed for 1 hour in 4% PFA, then the retina was dissected and blocked for 1 hour in 10% FBS 1% Triton in PBS. The tissue was incubated overnight with secondary antibodies, washed and analysed with the microscope (LSM710 laser scanning confocal microscope (Zeiss); Zen2009 software (Zeiss)). Cardiac injected antibodies represent the luminal localisation of VEGFR1 and VEGFR2. For the abluminal localisation of VEGFR1 and VEGFR2 staining without permeabilisation step was done.

VEGFR2 blocking antibody injection

C57BL/6 animals at the age P5, were injected intraperitoneally with the mouse VEGFR2 blocking antibody (MAB 4431-R&D systems; 10mg antibody/kg

of the animal). 24 hours after blocking antibody injection, 3kD dextran leakage assay was performed. The procedure, examination and statistical analysis was the same as for the developmental leakage assay.

Leakage assay after PIK injection

PIK peptide (DLys-DArg-DArg-DTyr-DLys-DTyr-DLys-DLys-DArg-NH₂) used in this assay was kindly donated by Prof Randall Mrsny from University of Bath. PIK control peptide was commercially synthesised by GenScript (DLys-DArg-DArg- DAla-DAla-DAla- DLys-DLys-DArg-NH₂).

C57BL6 animals at the age P6, were injected intraperitoneal with the PIK peptide (20mg/kg), for the control PBS or with PIK control peptide (20mg/kg) was used. An hour after PIK/PIK control/PBS injection 3 kD dextran leakage assay was performed, the same way as for the developmental leakage procedure. The procedure, examination and statistical analysis was the same as for the developmental leakage assay.

Protein techniques

Protein extraction from the retina for western blot

C57BL/6 mice at the different stages of development, were euthanised in a CO₂ chamber. After performing Schedule 1, eyes were enucleating and placed in PBS on ice. Straight after eye enucleation, retina dissection on ice was performed. After dissection, retina was washed in PBS at 4°C. Tissues were re-suspended in about 200 µl of radioimmunoprecipitation assay buffer (RIPA buffer; Sigma) with protease and phosphatase inhibitors (Halt Protease and Phosphatase Inhibitor Cocktail (100X) -Thermo Scientific), and left on ice for 10 minutes, after that, spun at 14,000 rpm for 10 minutes at 4°C. Supernatant from each sample was collected, and mixed 1:5 with a reducing lane marker sample buffer (Thermo Scientific) and heated at 98°C for 5 minutes.

Protein concentration determination

Protein concentrations were determined using a BCA kit (Thermo Scientific). BSA (Bovine serum albumin) standards diluted in water and sample diluents were incubated with BCA reagent for 30 minutes at 37°C. The absorption wavelength of a microplate reader was set to 562 nm and the absorbance was measured in a spectrophotometer of all Standards and samples (OD562). Standard curve was created based on the absorbance of BSA standards and was used to assign protein concentrations of samples.

SDS-PAGE (sodium dodecyl sulfate polyacrylamide gel electrophoresis)

Gels were poured at a thickness of 1.5 mm using the Bio-Rad Mini gel assembly kit and acrylamide solutions from Bio-Rad. The separating gel and stacking gel were prepared as in Table 4-5.

Table 4. Separating gel

Gel	DDI (Distilled De-Ionised) water	29:1 Acrylamide : Bisacrylamide	1.5 M Tris-HCl (pH 8.8)	10% SDS (sodium dodecyl sulphate)
7.5%	4.9 ml	2.5 ml	2.5 ml	0.1 ml
10%	4.1 ml	3.3 ml	2.5 ml	0.1 ml
12%	3.4 ml	4.0 ml	2.5 ml	0.1 ml

Just before the gel was poured, 50 µl of freshly made 10% APS (ammonium persulfate) and 5 µl of TEMED (N, N, N', N'-tetramethylethylenediamine) were added.

Table 5. Stacking gel

Gel	DDI water	29:1 Acrylamide : Bisacrylamide	0.5 M Tris-HCl (pH 6.8)	10% SDS
-----	-----------	---------------------------------	-------------------------	---------

Stacking gel	4.1 ml	3.3 ml	2.5 ml	0.1 ml
--------------	--------	--------	--------	--------

Just before the gel was poured, 50 µl of freshly made 10% APS and 10 µl of TEMED were added.

Samples were boiled at 95°C for 5 minutes prior to loading on the gel. Gels were run in Tris-glycine buffer (25 mM Tris, 250 mM glycine pH 8.3, 0.1% SDS) at 70-120 V.

Western-blot

Following electrophoretic separation, proteins were blotted onto Hybond-P PVDF (Amersham Biosciences) membranes using a semi-dry blotter (Bio-Rad). Membranes and pieces of Whatman paper were pre-soaked in transfer buffer (150 ml methanol, 100 ml tris-glycine buffer, in a total volume of 1000 ml) for 30 minutes. After a brief incubation of the gel in transfer buffer, gel and membrane were sandwiched between six pieces of Whatman paper, with the membrane facing the anode of the electroblotting apparatus. Transfer was carried out at 120 mA per gel for 1 hour (1.5mm thick gels). Blots were incubated with blocking buffer (5% non-fat dry milk in TBST -0.1% tween 20 in 0.1 M Tris buffer) for 2 hours at room temperature or overnight at 4°C. The primary antibody was diluted in blocking buffer and applied for 2 hours at room temperature or overnight at 4°C. After 3 ten-minute washes in TBST, horseradish peroxidase (HRP)-conjugated secondary antibodies were diluted in a similar fashion and applied for 1 hour at room temperature. Blots were washed 3 times in TBST. The product of the horseradish peroxidase reaction was detected by chemiluminescence (Amersham Biosciences). The primary and secondary antibodies used in experiments are listed in Table 6-7.

Table 6. Primary antibodies and conditions used in Western blotting.

Antibody	Dilution	Company and catalogue number
Rb anti-MLCK	1 : 5000	Abcam - ab76092
Rb anti-MLCK-P	1 : 1000	Invitrogen - 441085G
Rb anti-PAK	1 : 500	Abcam - ab40852
Rb anti-PAK-P	1 : 10 000	Abcam - ab40795
Rb anti-MLC-P	1 : 1000	Abcam - ab2480
Rb anti-MLC-P	1 : 1000	Cell Signalling - 3674
Rb anti-MLC-P	1 : 1000	Cell Signalling - 3671
Ms anti β -actin	1 : 1000	Sigma - A2228
Rb anti β -actin	1 : 1000	Sigma - A2066
Ms anti- P-glycoprotein 1	1 : 100	Enzo - C219
Ms anti- P-glycoprotein 1	1 : 100	Enzo - C219

Table 7. Secondary antibodies used in Western blotting.

Antibody	Dilution	Company and catalogue
Sheep anti-ms IgG (HRP)	1:1000	GE Healthcare, NA-931-1ML
Donkey anti-rb IgG (HRP)	1:1000	GE Healthcare, NA-934-1ML

Ms – mouse; Rt - rat; Rb – rabbit; Gt – goat

Phosphoproteomic

Phosphoproteomic analysis of the protein extracts was performed by the Roche Innovation Center Basel. Experimental procedure was kindly provided by PhD Manuel Tzouros.

Abbreviations

ACN, acetonitrile; AmBic, ammonium bicarbonate; FA, formic acid; IP, immunoprecipitation; PSM, peptide to spectrum match; RT, room temperature; TFA, trifluoroacetic acid; TMT, Tandem Mass Tags.

Materials

TMT10plex isobaric label reagents were from Thermo Fisher Scientific (Rockford, IL, USA). Titansphere TiO₂ beads were from GL Sciences Inc. (10 μm, Japan). Anti phosphotyrosine antibody PTMScan P-Tyr-1000 kit was from Cell Signaling Technology (Danvers, MA). All chemicals were from Sigma-Aldrich (Steinheim, Germany) unless otherwise stated.

Mice

Retina homogenization and protein digestion

Pooled retina were homogenized in cold lysis buffer (1% SDS, 8 M urea, 50 mM AmBic pH 8.8, protease (cOmplete), and phosphatase (PhosSTOP, both Roche Diagnostics) inhibitors) at a tissue concentration of 50 mg/ml using a tip sonifier (QSonica, Newtown, CT), applying 3 × 10 s bursts (55% amplitude) and cooling the samples between bursts for 1 min on ice. Insoluble material was removed by centrifugation at 14'000 × *g* for 10 min at 15 °C and protein concentrations were determined using the bicinchoninic assay (BCA, Pierce). Proteins were precipitated using methanol/chloroform. Briefly, four, one, and three volumes of methanol, chloroform, and water, respectively, were added to the lysates followed by vortexing after each solvent addition, and final centrifugation at 14'000 × *g* for 5 min at RT. After removal of the supernatant, pellets were washed twice with methanol and air dried. Proteins were re-dissolved in digestion buffer (8 M urea, 50 mM AmBic pH 8.8, protease, and phosphatase inhibitors), reduced with 10 mM DTT for 30 min at 56°C, alkylated with 20 mM iodoacetamide for 30 min at RT (dark), and pre-digested with 1:100 w/w lysyl endopeptidase (Lys-C, Wako Pure Chemical Industries Ltd., Japan) for 4 h at 37 °C. After dilution of urea to 2 M with 50 mM AmBic solution, digestion was continued by the addition of 1:100 w/w trypsin (Promega, Madison, WI) and incubation overnight at 37 °C. Samples were acidified with FA to a final 5% v/v content, vortexed, and centrifuged at 7'000 × *g* for 10 min at 4 °C to remove insoluble material. Peptides were desalted by solid-phase extraction (SPE) (100 mg C18 Sep-Pak, Waters, Milford, MA) and freeze-dried overnight.

Peptide Tandem Mass Tag labelling and phosphopeptide enrichment

TMT labelling was performed similar to the method reported by Paulo and Gygi (Paulo, 2015). Lyophilized peptides (2 mg per condition) were reconstituted in 100 mM HEPES pH 8.5 buffer (3 mg/ml final concentration) and labelled with TMT10plex reagents (5 mg, dissolved in 0.3 ml of anhydrous ACN) for 1 h at RT. The reaction mixtures were quenched with hydroxylamine (0.3% v/v end concentration) for 15 min at RT followed by acidification with FA (5% v/v end concentration). Using an aliquot, labelling efficiency was individually verified to be >99.5% (based on spectral counts of TMT- vs. un-labelled PSMs). Samples were combined, freeze-dried overnight, and desalted by SPE (500 mg C18 Sep-Pak, Waters). A 0.5 mg fraction was removed, dried *in vacuo*, and stored at -20 °C for subsequent proteome-level analysis.

Phosphopeptide enrichment was performed similar to the procedure described by Kettenbach and Gerber (Kettenbach, 2011). Peptides eluted from the SPE (in 50% v/v ACN) were acidified with lactic acid (2 M end concentration and 50% v/v ACN) (2 mg/ml end peptide concentration), mixed with pre-washed TiO₂ beads (1:4 peptide/bead ratio) (GL Sciences Inc, Japan) and rotated head-over-head for 1 h at RT. After spin down and transfer of the supernatant to a new tube (saved for pTyr IP), beads were washed 2 × with 2 M lactic acid/50% ACN, 3 × with 0.1% TFA/50% ACN, eluted with 5% NH₄OH pH 11 and directly acidified with a 10% FA solution. TiO₂-flowthrough was desalted by SPE (500 mg C18 Sep-Pak), freeze-dried overnight and used for phosphotyrosine IP (PTMScan p-Tyr-1000 kit, Cell Signalling Technologies) following the manufacturer's protocol. Phosphopeptide samples were finally desalted by stop and go extraction (StAGE) (Rappsilber, 2003) and stored at -20 °C.

Offline high pH RP fractionation

Samples for proteome- and phosphoproteome-level (TiO₂) analysis were fractionated by high pH (HpH) reversed-phase (RP) chromatography using an Agilent 1100 series HPLC system (Agilent Technologies, Waldbronn, Germany) equipped with a binary pump, degasser, multiple wavelength detector, refrigerated autosampler and fraction collector. Peptides (200 µg for the proteome, and total TiO₂-enriched fraction for the phosphoproteome) were

separated on a Zorbax Extend-C18 column (4.6 mm × 250 mm, 5 μm particle size) using the following gradient at 0.8 ml/min: 100% A for 5 min, 0-20% B in 5 min, 20-45% B in 50 min, 45-100% B in 1 min, 100% B for 4 min, 100-0% B in 1 min, and 100% A for 9 min (buffer A: 10 mM AmBic pH 8.0/5% ACN; buffer B: 10 mM AmBic pH 8.0/90% ACN) (Erickson, 2015). A total of 96 fractions were collected from min 10 to 70, consolidated by columns into 12 samples (end volume ca. 4 ml), acidified with 5% v/v FA (end concentration), and freeze-dried overnight. Samples were stored at -20 °C until LC-MS analysis.

LC-MS/MS

LC-MS/MS was performed using an EASY-nLC 1000 ultrahigh pressure liquid chromatography (UHPLC) connected to an Orbitrap Fusion Tribrid and equipped with an EASY-spray source (Thermo Fisher Scientific). Samples were re-suspended in 5% FA/2% ACN, and concentrated on an Acclaim PepMap C18 trapping column at a controlled maximum backpressure of 500 bar. One tenth of, and the whole HpH RP fractions were injected for the proteome, and the phosphoproteome (TiO₂ and pTyr) analyses, respectively. Peptides were separated on an Acclaim PepMap C18 EASY-spray column heated at 45 °C and using the following gradient at 300 nl/min: 5-15% B in 60 min, 15-35% B in 60 min, 35-80% B in 2 min, 80% B for 18 min, corresponding to a total acquisition time of 140 min (buffer A: 0.1% FA; buffer B: 0.1% FA/ACN). For the pTyr sample, the first two ACN steps were increased 30 min each, and the total acquisition time was 200 min. The spray voltage used was 1.9-2.2 kV.

MS acquisition parameters were selected as described by Erickson and Gygi with some minor modifications (Erickson 2015). The instrument was operating in the data-dependent mode, collecting Orbitrap full MS1 scans over a mass range from *m/z* 390 to 1400, using wide quadrupole isolation, a resolution of 120k (at *m/z* 200), an automatic gain control (AGC) target value of 2E5 (5E5 for the pTyr), and a maximum injection time (IT) of 100 ms. Data were on-the-fly recalibrated using ambient air hexacyclodimethylsiloxane at *m/z* 445.12002. The ten most intense precursor ions, with charge states between 2 and 6, a minimum intensity of 5E3, were mono-isotopically selected for collision induced dissociation (CID), using a quadrupole isolation of *m/z* 0.5, AGC target

of 4E3, maximum IT of 35 ms (150 ms, and 200 ms for TiO₂, and pTyr, respectively), collision energy of 35%, and ion trap readout with rapid scan rate. Only a single charge state per precursor was selected for MS2. Interrogated precursor ions were dynamically excluded for 75 s using a ± 10 ppm mass tolerance. TMT reporter ions were generated using synchronous precursor selection (SPS), a quadrupole isolation of m/z 2, high-energy collision dissociation (HCD) at a normalized collision energy of 55%, and readout in the Orbitrap with a resolution of 60k, scan range of m/z 100 to 1000, an AGC target of 5E4, and a maximum IT of 150 ms (250 ms, and 350 ms for TiO₂, and pTyr, respectively). The mass range for selecting the SPS (MS3) precursors was from m/z 400 to 2000, excluding the MS2 precursor with a tolerance of m/z 40 (low) and 5 (high), and any TMT neutral loss from it. The number of SPS precursors was set to 10 for all except for the TiO₂ enriched samples where it was lowered to 5.

Data processing

Raw data were processed using Proteome Discoverer 2.1 (Thermo Fisher Scientific) and Mascot Server 2.5.1 (Matrix Science, London). A processing workflow was designed to search MS2 data against the UniProt/SwissProt mouse protein database (08.2015 release, 16'724 entries) using trypsin/P as an enzyme, a maximum of two missed cleavage sites, 10 ppm, and 0.5 Da as the precursor, and fragment ion tolerances, respectively. Carbamidomethylated cysteines (+57.02146 Da), TMT10 labelled lysines and peptide N-termini (+229.162932 Da) were set as static, while oxidized methionines (+15.99492 Da), phosphorylated serines, threonines, and tyrosines (+79.966331 Da) (only for the TiO₂ and pTyr data) were set as dynamic modifications. PSMs false discovery rates (FDRs) were controlled for candidates with a max. delta Cn of 0.05 using Percolator and setting a q-Value threshold of 0.01. Site localization probabilities were estimated using ptmRS 2.0 (only for TiO₂/pTyr) with 0.5 Da as fragment ion mass tolerance, neutral loss peaks enabled, 8 as maximum peak depth, 500 and 10 as maximum position isoforms, and PTMs per peptide, respectively. Reporter ion quantitation was performed with the HCD MS3 data using a 3 mmu peak integration and most confident centroid tolerances.

Reporter ion intensities were adjusted to correct for the isotopic impurities of the different TMT reagents (manufacturer specifications). Reporter ions signal to noise (S/N) ratio were used to express abundances as described by Gygi and colleagues (McAlister, 2014, Erickson 2015). A minimal average S/N of 40 for phosphopeptides, 10 for proteins, and not more than 50% co-isolation thresholds were set to keep only quantitative information with sufficient quality.

A consensus workflow was defined to group PSMs into peptide and proteins. For the phosphopeptide analysis, only ranked 1 PSMs with 25 as site localization probability threshold were considered. Peptide FDRs were controlled by setting a q-Value threshold of 0.01 and allowing the software to automatically select PSM q-Value or ion score for the grouping. High confidence peptides with a minimal length of 6 residues were further grouped into proteins and protein FDR was set to fulfil a q-Value threshold of 0.01. For protein grouping, strict parsimony principle was applied. Peptide and protein quantitation was performed by summing S/N for each channel and normalizing each value with the highest TMT channel total. For protein quantitation, unique and razor peptides were considered. Finally, individual peptide and protein S/N were scaled to an average of 100.

Tissue culture

MVEC isolation

Microvascular endothelial cells were isolated from rat cortical grey matter according to the protocol adapted from Abbot 1992 (Abbott, 1992).

6-8 weeks old Lewis rats were euthanized by CO₂ asphyxiation, brains were removed and placed in working buffer (calcium- and magnesium-free Hanks' balanced saline solution (Ca,Mg-free HBSS Invitrogen), buffered with 10 mM HEPES-buffer, containing 100 i.u./ml penicillin and 100 µg/ml streptomycin (Sigma), with 0.5% bovine serum albumin (BSA, First Link PF 253-50)). Brain dissection was performed under a laminar flow hood, on the dish with sterile lint moisture with working buffer. Cerebellum and brain stem

were removed. Meninges and choroid plexus were peeled off. White matter from the hind- and mid-brain was removed. The remaining grey matter was transferred to fresh working buffer and chopped with scalpel. The suspension was spun at 600g at 4°C for 5 min.

Tissue was digested in 15 ml digestion medium (10 mg/ml Collagenase/dispase from Roche or Worthington in Ca,Mg-free HBSS containing 10 mM HEPES, 100 i.u./ml penicillin and 100 µg/ml streptomycin, 20 units/ml DNase I (deoxyribonuclear- 5'oligonucleotideo-hydrolase), 0,147 µg/ml TLCK (tosyl-lysine-chloromethyl- ketone)) for 1 hour at 37°C water bath with gentle agitation every 15 min.

The suspension was triturated with narrowed in flame Pasteur pipette until creamy texture achieved. The suspension was centrifuged for 5 min at 600g.

After removing supernatant, vessels were re-suspended in 22% BSA and spun for 20min at 1000g. The top layers of the BSA gradient were removed and the pellet was re-suspended in washing buffer and spun for 5 min at 600g. After removing supernatant, pellet was re-suspended in 5 ml digestion medium, for second 3hour digestion at 37°C.

Percoll gradient was prepared before the end of 2nd digestion. Plastic ultracentrifuge tubes were sterilised in 70% ethanol and washed in washing buffer, to prevent cell adhesion. Washing buffer was removed from the tubes and 7ml 50% Percoll gradient solution (Percoll gradient stock solution: 50ml Percoll plus 5ml 10X HBSS with Calcium and Magnesium, plus 45ml HBSS with Calcium and Magnesium) was added to the tubes. Percoll balance was prepared by spinning at 4°C at 25 000g for 1 hour.

Digestion solution was spun for 5 min at 600g, and after that percoll gradient was done.

The suspension from 2nd digestion was gently layered on the top of the Percoll gradient and spun for 20 min at 1000g.

Capillaries are found between two clear bands on gradient, and should be visible as flocculated red particles. Capillaries were transferred with Pasteur pipette and placed in 20 ml washing buffer and spun for 5 min at 700g.

Finally capillaries were re-suspended in growth medium with 5 µg/ml puromycin (EGM2-MV Lonza) and seeded at a high density (vessels from 6 rat brains per 40 cm²) on transwells (12-mm Costar Transwells (3460)) or dishes coated with collagen IV/fibronectin.

4 days after isolation cells were washed in PBS and growth medium without puromycin was added.

On the day 8 TEER was measured, and growth medium was changed. This procedure was repeated on day 13, and wells with TEER above 200 Ωcm², were used for the experiments.

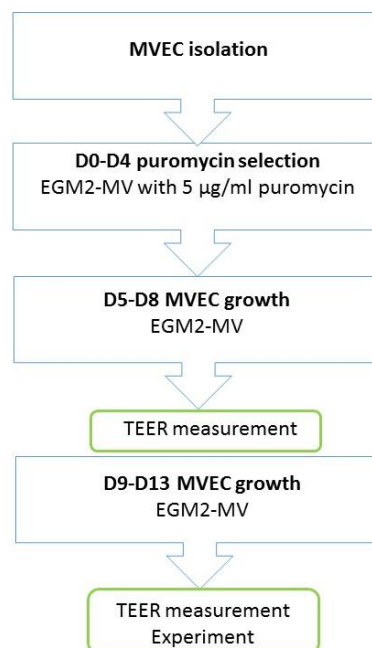


Figure 13. Schematic representations of the MVEC post isolation treatment.

Immunostaining of cells cultured on dishes and filters

Cells on dishes or transwells were fixed either in -20°C methanol for 5 minutes or in 4% paraformaldehyde (PFA) at room temperature for 10 minutes. For PFA fixed cells, fixation was followed by 3 washes in PBS and a 10 minutes permeabilisation step in PBST (0.1% Triton X-100, PBS). Cells were blocked for 15 minutes in blocking solution (5% goat or donkey serum in PBS). After the blocking step cells were incubated for 1 hour with the primary antibody. List of primary antibodies is presented in Table 8. Then 3 washes in PBS were carried

out followed by 1 hour incubated with Secondary antibodies. List of Secondary antibodies is presented in Table 9. Then three 5 minutes washes in blocking solution was performed. Finally, cells were mounted with Vecta Shield (Vector Laboratory).

Cells plated on a dish were mounted and covered with a coverslip directly on a dish. For the staining maintained on a transwell, the filter was catted out of the transwell and placed on the microscopic slide, than mounted and covered with a coverslip.

Table 8. Primary antibodies and conditions used in immunofluorescent PRBEC staining.

Antibody	Dilution	Company and catalogue number
Rb anti-von Willebrand Factor	1 : 100	Abcam - ab6994
Rb anti-Claudin 5	1 : 100	Abcam - ab53765
Rb anti-Occludin	1 : 100	Abcam - ab31721
Rb anti-VE-cadherin	1 : 100	Abcam - ab33168

Table 9. Secondary antibodies used in immunofluorescence staining of PRBEC.

2° Ab	Conjugation	Dilution	Company and Cat#
Gt anti-rb IgG (H+L)	AlexaFluor 488	1 : 500	Invitrogen (A11008)
Gt anti-rb IgG (H+L)	AlexaFluor 546	1 : 500	Invitrogen (A11010)
Dk anti-rb IgG (H+L)	AlexaFluor 488	1 : 500	Invitrogen (R37118)
Dk anti-rb IgG (H+L)	AlexaFluor 594	1 : 500	Invitrogen (R37119)

Ms – mouse; Rt - rat; Rb – rabbit; Gt – goat; Dk – donkey; Ht – hamster

TEER measurement

Primary endothelial cells were plated on Transwell filters (12-mm Costar Transwells (3460)) with growth media (EGM2-MV Lonza). TEER

measurements were recorded using EVOM2 Epithelial Voltohmmeter for TEER device (World Precision Instruments). STX2 “chopstick” electrodes pair (4mm wide and 1mm thick) were washed with ethanol and PBS and placed on the well: one electrode was inside the Transwell and the other one outside of the Transwell. When the electrode was placed the measurement was taken. The electrodes were washed with PBS between each measurement.

Flux measurement

MVEC were grown on Transwell filters (12-mm Costar Transwells (3460)) and starved for 12 hours in EBM2 media, 0.5% FCS. 4kDa FITC dextran was added at 1 mg/ml to the apical side of the cells and 50 μ l samples were removed from the basal chamber and replaced with fresh medium. Sample was taken every 20-30 min for 120 min before and 120 min after addition VEGF-A at the concentration 50ng/ml. Fluorescence of the samples was plotted against the time and permeability changes were determined from linear slope changes before and after addition of the compound.

Capillaries isolation

Microvessels were isolated from the eyes C57BL/6 mice at the age P5 and P15. Animals were euthanized with CO₂ chamber and eyes were taken and placed on ice in the microcentrifuge tube with a washing buffer (HBSS 1X - without Ca²⁺ or Mg²⁺, 10mM HEPES, 0.1% BSA Firs Link Solution).

Retina was carefully dissected on ice. After dissection retina was homogenised and passed through the 70 μ m filter. Next tissue that passed through the filter was centrifuged at 1000g for 7 min. Supernatant was re-suspended in 3ml (per 10 eyes) collagenase/dispase buffer (2mg/ml Collagenase/dispase Roche, TLCK 0.147 μ g/ml, DNA-ase 20 U/ml) and incubated at 37C for 30min.

After digestion step, tissue was centrifuged for 5 min at 1000g at 4°C. Pellet was re-suspended in washing buffer and centrifuged again for 5min at 600g at 4°C. Retina capillaries were ready for further experiments: sample preparation for western blotting, VEGF-A treatment and immunostaining.

VEGF-A treatment on the retina capillaries

Retina capillaries received from P5 and P15 retinas (4 retinas were used for 1 sample preparation) were re-suspended in 420µl working buffer (prepared as for capillary isolation). VEGF-A was added (25ng/ml, 50ng/ml, 100ng/ml) and left for incubation for 10 or 30 min at room temperature. After incubation, capillaries were centrifuged and pellet washed with working buffer. After another spin, capillaries were ready for protein extraction.

Protein extraction from the retina capillaries

Retina capillaries received from P5 and P15 retinas (4 retinas were used for 1 western blotting sample preparation) were re-suspended in 100 µl of radioimmunoprecipitation assay buffer (RIPA buffer; Sigma) with protease and phosphatase inhibitors (Halt Protease and Phosphatase Inhibitor Cocktail (100X) -Thermo Scientific), and left on ice for 10 minutes, after that time cleared at 14,000 rpm for 10 minutes at 4°C. Supernatant from each sample was collected, mixed 1:5 with a reducing lane marker sample buffer (Thermo Scientific) and heated at 98°C for 5 minutes.

Retina capillaries immunostaining

Retina capillaries received from P5 and P15 retinas were fixed in 4%PFA for 10 min, and centrifuged for 5min at 600g at 4°C. Then blocking solution – 5% BSA with 0,2% Triton X-100, was added and after 1h of incubation, capillaries were centrifuged. To the pellet, primary antibody re-suspended in blocking buffer, was added. Incubation with primary antibody was done for 1 hour at room temperature or overnight at 4°C. List of primary antibodies is presented in Table 10.

After incubation with primary antibody, capillaries were washed for 10 min in blocking solution with centrifugation step after each wash. Then secondary antibody (Table 11) in the blocking solution was added and left for an hour incubation. After that capillaries were washed 3 times for 10min in blocking buffer. After final centrifuge, capillaries were re-suspended in 100µl of

PBS, transferred on the microscopic slide and left to dry. When slide was completely dry, capillaries were mounted (VectaShield) and covered with coverslip.

Table 10. Primary antibodies and conditions used in immunofluorescent capillary staining.

Antibody	Dilution	Company and catalogue number
Rb anti-Claudin 5	1 : 100	Abcam - ab53765
Rb anti-VE-cadherin	1 : 100	Abcam - ab33168
Phalloidin Alexa Flour 594	1 : 100	Life Technologies - A12381

Table 11. Secondary antibodies used in immunofluorescence staining of capillaries.

2° Ab	Conjugation	Dilution	Company and Cat#
Gt anti-rb IgG (H+L)	AlexaFluor 488	1 : 500	Invitrogen (A11008)
Gt anti-rb IgG (H+L)	AlexaFluor 546	1 : 500	Invitrogen (A11010)
Dk anti-rb IgG (H+L)	AlexaFluor 488	1 : 500	Invitrogen (R37118)
Dk anti-rb IgG (H+L)	AlexaFluor 594	1 : 500	Invitrogen (R37119)

Ms – mouse; Rt - rat; Rb – rabbit; Gt – goat; Dk – donkey; Ht – hamster

Morphology

Light microscopy

Images were captured using the following instruments and software packages:

- 1) LSM710 laser scanning confocal microscope (Zeiss); Zen2009 software (Zeiss).
- 2) Olympus Fluorescence microscope (Olympus); Image Pro-Plus 6.1 software (Olympus).

Results

Chapter 3.

Onset of Blood Retinal Barrier function

During murine development blood vessels that supply the retina undergo extensive reorganisation through sprouting angiogenesis, vascular remodelling, vessel regression, and, vessel differentiation (Fruttiger, 2007). In the periphery, developing vasculature is relatively dense and over time, as more vessels grow, undergoes intense remodelling, to finally reach the characteristic hierarchical tree architecture (Figure 14). This vascular architecture is formed by endothelial cells with particularly tight and restrictive physiological barrier function that controls the flow of ions, proteins, and water flux in and out of the retina (Cunha-Vaz, 2011). However, there is virtually no published data mapping the development of the retinal vasculature to the onset of the BRB.

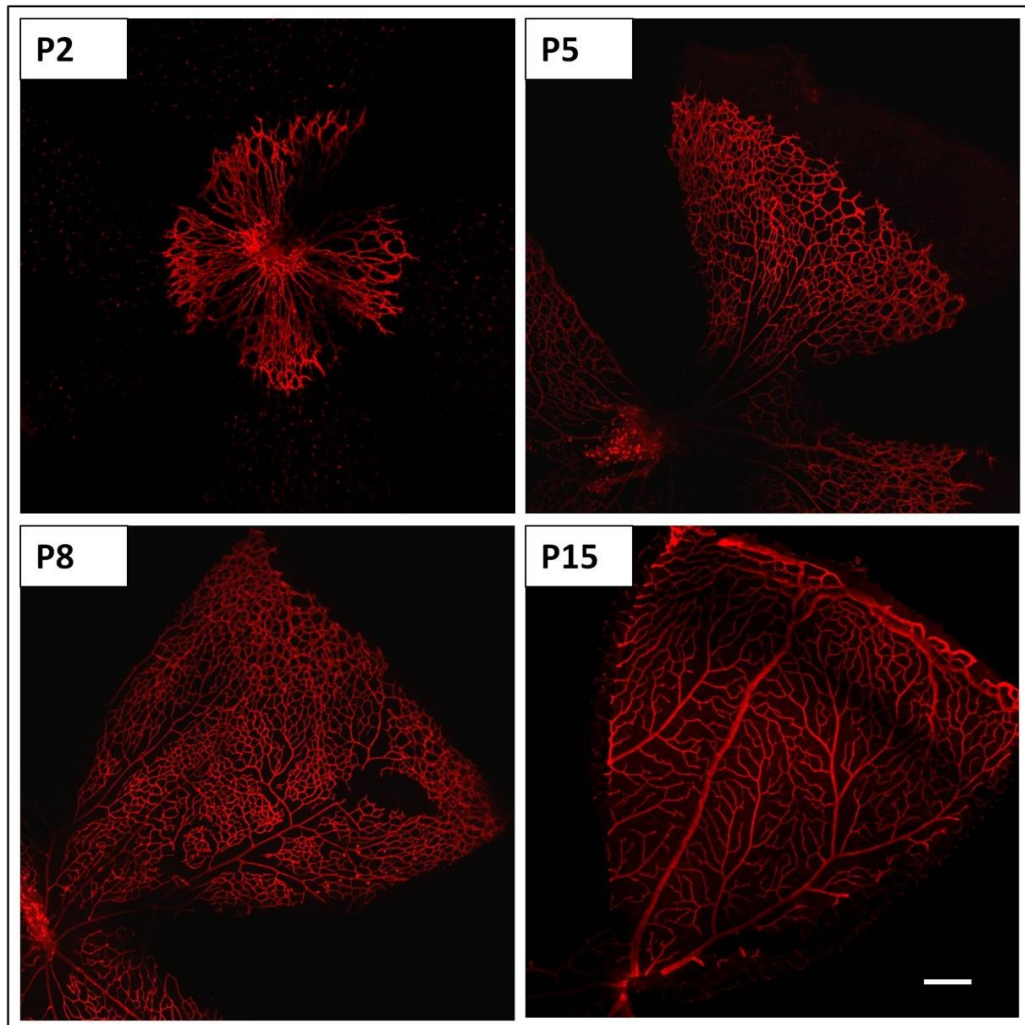


Figure 14. Morphological assessment of vascular development in the retina.

P2, P5, P8, P15 retina vasculature staining with Collagen IV antibody – visualisation of vascular growth among early stages of murine development. The scale bar indicates 200 μ m for all images.

Demonstration of poor BRB function at early stages of murine development

During retina dissection at early stages of postnatal development, blood patches at the periphery of growing vessels can be easily observed under the dissecting microscope (Figure 15). These blood patches, at the head of the developing vascular tree suggest that endothelial cells lining the lumen of the growing vessels, allow for the exudation of the substances moving within the blood stream into the surrounding tissue. This may suggest that at the time

when blood vessels grow, they do not fulfil their gate keeping role. Thus, mapping the spatial and temporal changes in retinal barrier function may provide insight into BRB acquisition and potential mechanisms involved.

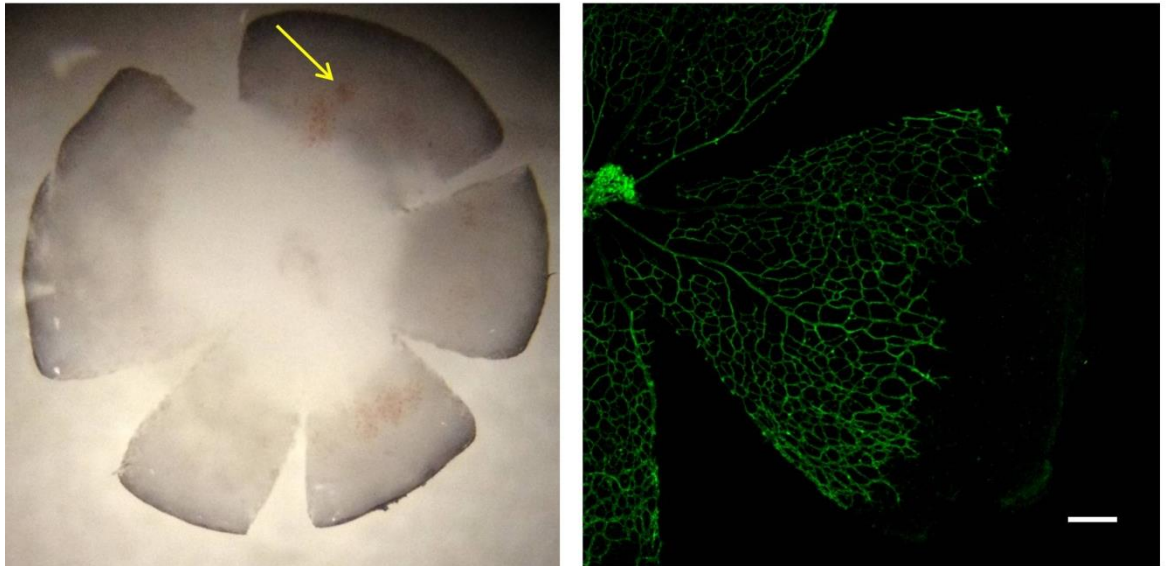


Figure 15. Blood cell leakage at the periphery of growing vasculature.

Left pictures shows blood patches at the periphery of growing vasculature – pictures taken under dissecting microscope. Right picture shows representative lectin staining of the vasculature in the retina at P6. The scale bar indicates 200 μ m.

There are a number of different techniques that allow for BRB examination, for example fluorescein angiography (FA), optical coherence tomography (OCT), ocular fluorophotometry (OF). FA, OCT, OF are widely used both in clinics and for in-vivo experiments for measuring blood–retinal barrier function, blood-aqueous barrier function and even aqueous flow. However the murine developmental model has limitations that do not allow for adapting these techniques for mapping BRB function. One of the obstacles is that up until around day 10-13 of postnatal development, the pups have closed eyelids and all the above methods require pupil dilation and imaging of the back of the eye. This is why mapping BRB function in the murine model requires a novel approach and development of new techniques.

To examine the onset of barrier function during post-natal vascular development, an in-vivo tracer assay was developed. The initial tracers used were different sizes of a hydrophilic polysaccharide – dextran. Good water solubility, availability of different sizes and low toxicity makes dextran an effective and valuable tool for in-vivo experiments. Additionally, a fluorescent conjugate allows for the visualisation of injected dextran. Dextran, injected intraperitoneally into mice at different stages of development reaches the circulation, including the retinal vasculature and can be visualised with fluorescent microscopy.

An initial set of dextran leakage assays were performed with 4 kDa FITC dextran - fluorescent conjugated dextran. Animals were injected with dextran at the dose 0.1mg per 1g body weight and left for 2 to 3 hours to let dextran enter into the circulation. Before performing termination of the in-life part of the experiment and eye nucleation, animals were perfused with PBS, followed by fixative perfusion, to help ensure that all fluorescent signals will be from extravasated dextran. Then eyes were removed and the retina flat mounted.

Initial experiments with 4 kDa FITC dextran did not give expected results and did not allow for leakage visualisation in the retina at P5. There was no significant difference between retina from the animals injected with dextran and retina from the animals injected with PBS (Figure 16).

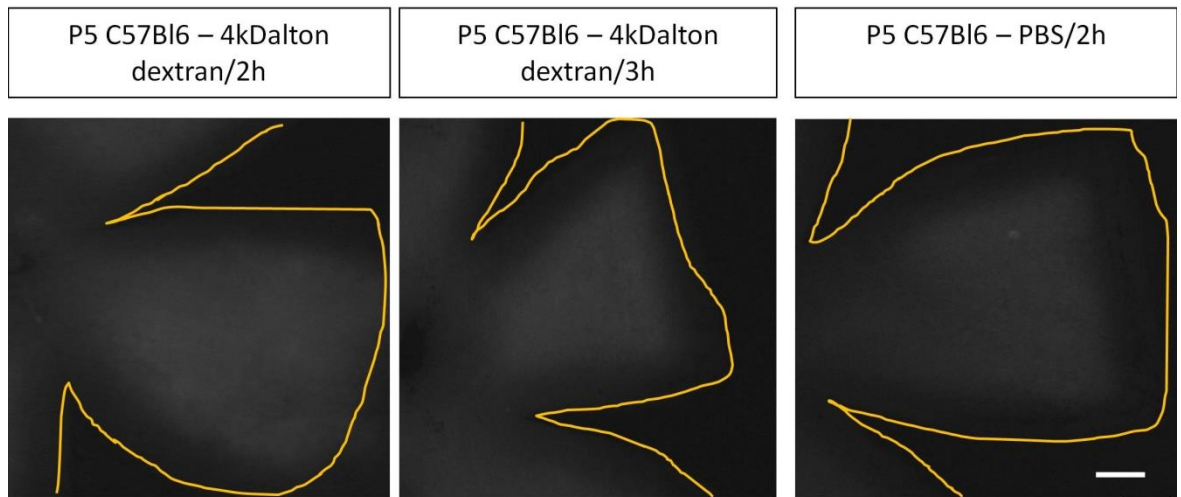


Figure 16. P5 flat mounted retina after 4kD dextran injection.

P5 flat mounted retina after 4kD fluorescein conjugated dextran and PBS injection, followed by perfusion with PBS and fixative. The scale bar indicates 400 μ m for all pictures.

A similar experiment with 4 kDa FITC dextran was performed, but this time without perfusion in order to track the dye in the eye vasculature. Surprisingly dextran was detected in P15 retina but not at P5, even though both groups were not perfused (Figure 17). These experiments lead us to believe, that 4 kDa FITC dextran might not be a sufficient tool for this study, since after extravasation from vessels at P5, it cannot be detected.

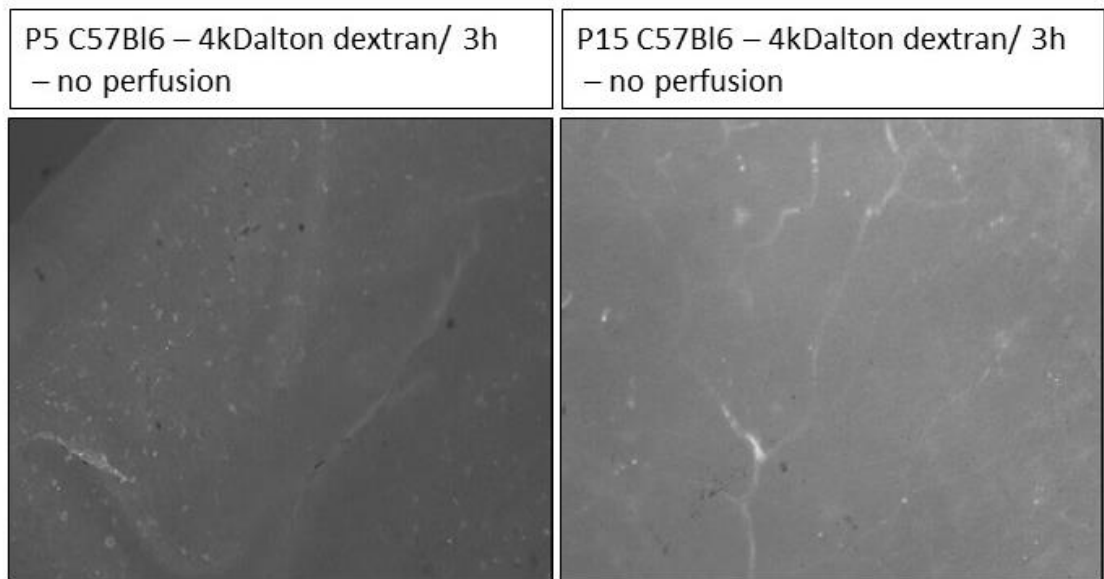


Figure 17. P5 and P15 flat mounted retina after 4kD dextran injection.

P5 and P15 flat mounted retina after 4kD fluorescein conjugated dextran intraperitoneal injection, without perfusion.

One potential reason for problems detecting signal from FITC dextran might be that after dextran leaks out of the vessels, it can be easily washed away, during the retina dissecting procedure.

To test this hypothesis, the permeability of the developmental retinal vasculature was assessed using a 3kD FITC fixable dextran conjugated to fluorescein. Fixable dextran is used when an experiment requires subsequent treatment with formaldehyde or glutaldehyde. Fixable versions of dextrans have covalently bound lysine residues that permit dextran tracers to be conjugated to surrounding biomolecules by aldehyde-mediated fixation for subsequent detection by fluorescent imaging and ultrastructural techniques.

A similar experiment to the initial tracer study was performed with 3kD FITC fixable dextran injected intraperitoneally into P5 and P15 C57Bl/6 mice. Two hours after injection, the animals were perfused. For the control, a group of animals was not perfused, in order to see if it will be possible to detect signal from fixable dextran without clearing it from the circulation (Figure 18).

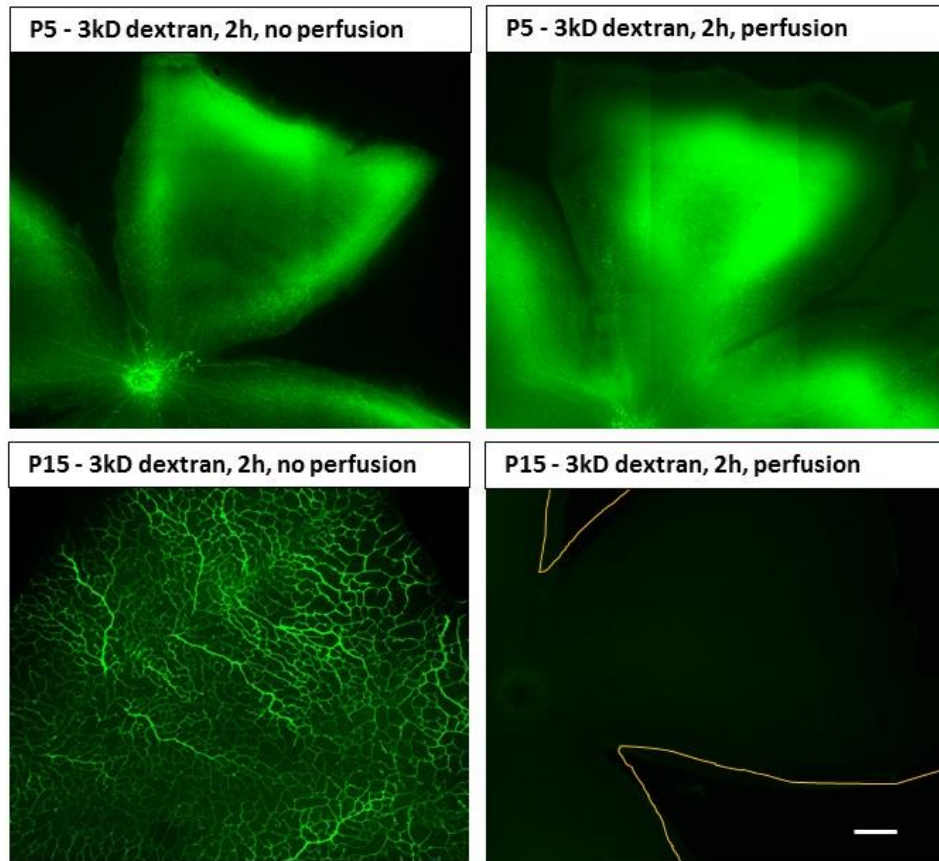


Figure 18. P5 and P15 retina after 3kD dextran injection.

P5 and P15 flat mounted retina 2h after 3kD fluorescein conjugated, fixable dextran injection. Pictures on the left shows retina without perfusion, pictures on the right with PBS perfusion. The scale bar indicates 200 μ m to all pictures.

A leakage assay performed with fixable dextran suggests that at P5 endothelial cells do not fulfil their gate keeping role and allow for the dextran to extravasate from the vessels. At P5 and P15 pictures were taken using the same fluorescent imaging settings. There is no fluorescent signal at P15 after perfusion, which indicates that all of the dextran was removed after flushing the circulation. In comparison in non-perfusion P15 retina dextran is localised in the vasculature. This experiment suggests a significant difference in barrier function between P5 and P15 retina with early stages of development of endothelial cells associated with poorer barrier function.

Further investigation was carried out in order to discover at what stage of development we can observe the onset of barrier function. But firstly, I

checked for the optimal time point which allows 3kD dextran to reach the circulation.

P5 animals were injected with 3kDa dextran, the pups were perfused 1 hour and 2 hours after injection. The retina analysis protocol was carried out in the same way as the previous experiment.

1 hour after the injection of dextran, a diffuse fluorescence signal could be detected in the retina. The dye was extravascular, demonstrating that there was no significant barrier to this tracer. 2 hours after the injection, the fluorescence signal was stronger and equally diffused (Figure 19). The 2 hour time point was chosen for future experiments.

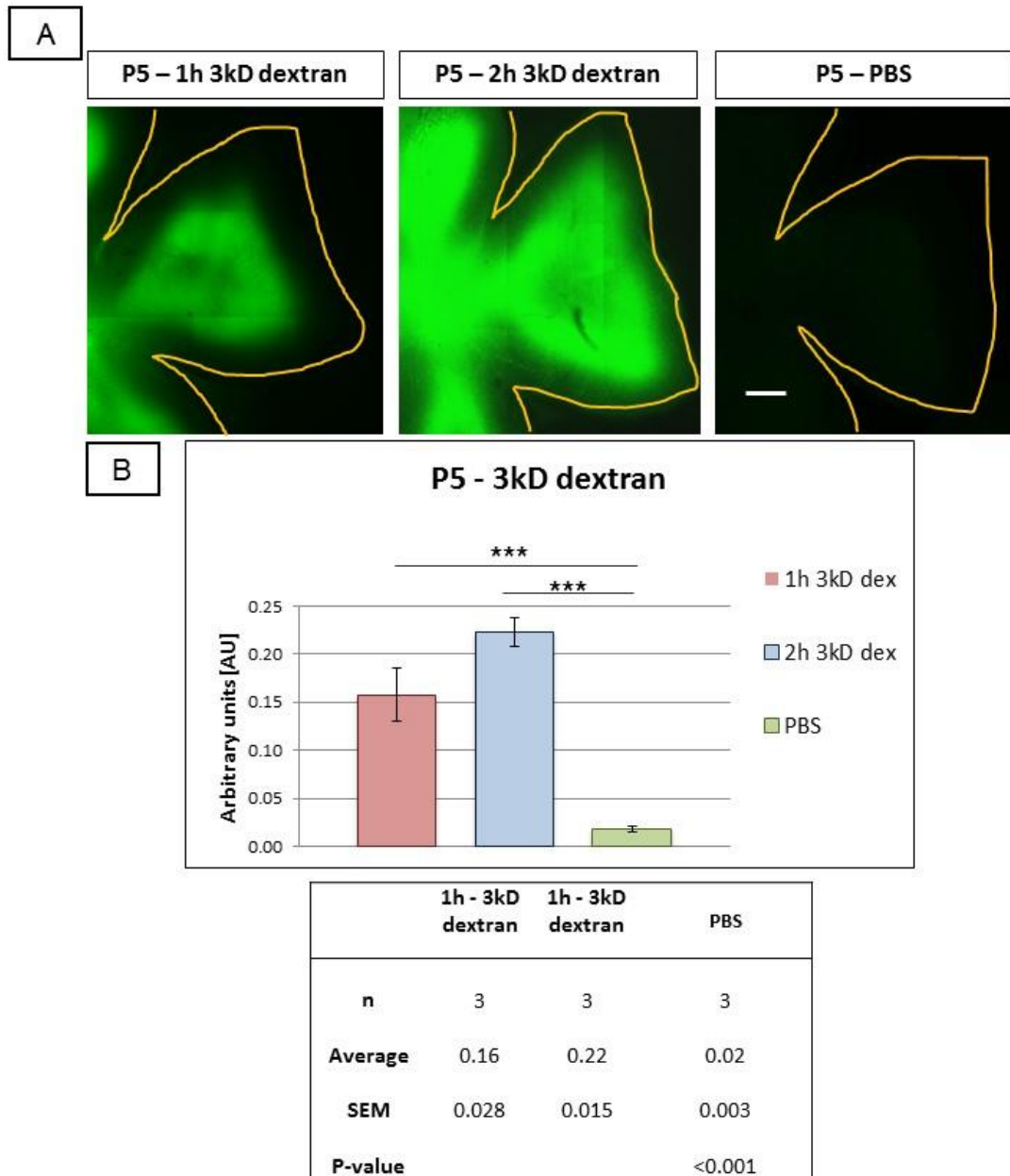


Figure 19. Measurement of the optimal time point for 3kD dextran leakage assay on P5 retina.

A-P5 flat mounted retina after 1 and 2 hours following 3kD dextran injection; PBS injection served as the negative control. The scale bar indicates 200 μ m for all pictures.

B-Measurement of the fluorescence intensity of the retina (N=3), error bars indicates SEM value

BRB formation based on 3kDa dextran leakage assay

The next step was measuring the dextran concentration in the plasma at the different stages of development. . Blood was drawn from pups at different time points to confirm that major changes in barrier function could not be attributed to the access of intraperitoneal tracer to the circulation. The fluorescent signal of plasma represents dextran concentration after 2 hours from injecting the tracer into P5, P10 and P15 mice (Figure 20).

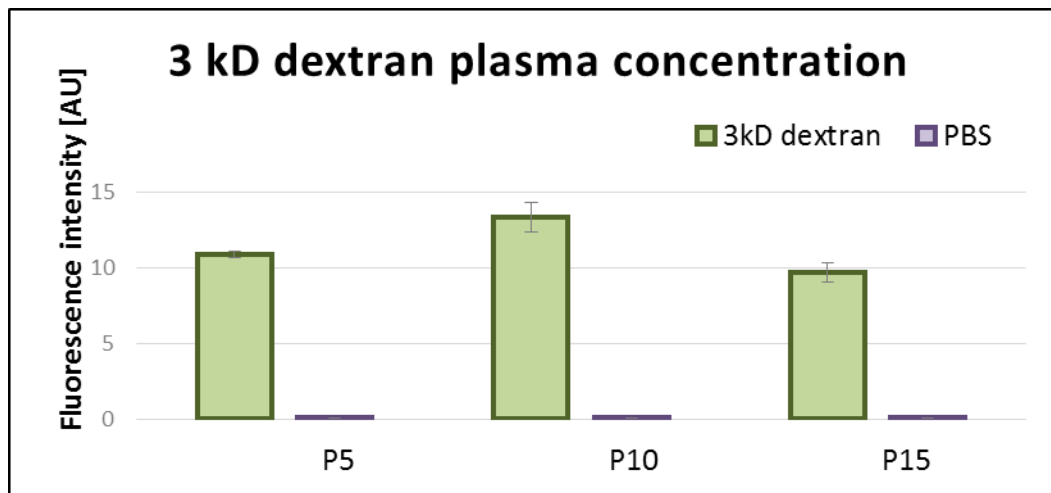


Figure 20. 3kD dextran plasma concentration at the P5, P10, and P15.

3 kD dextran plasma concentration was measured based on fluorescent intensity of the blood samples taken 2h after IP injection of 3kD dextran.

This experiment shows that 2 hours after injection, dextran reaches the circulation to a similar degree at P5, P10 and P15.

Based on these experiments barrier function at P5, P6, P8, P10 and P15 was measured (Figure 21).

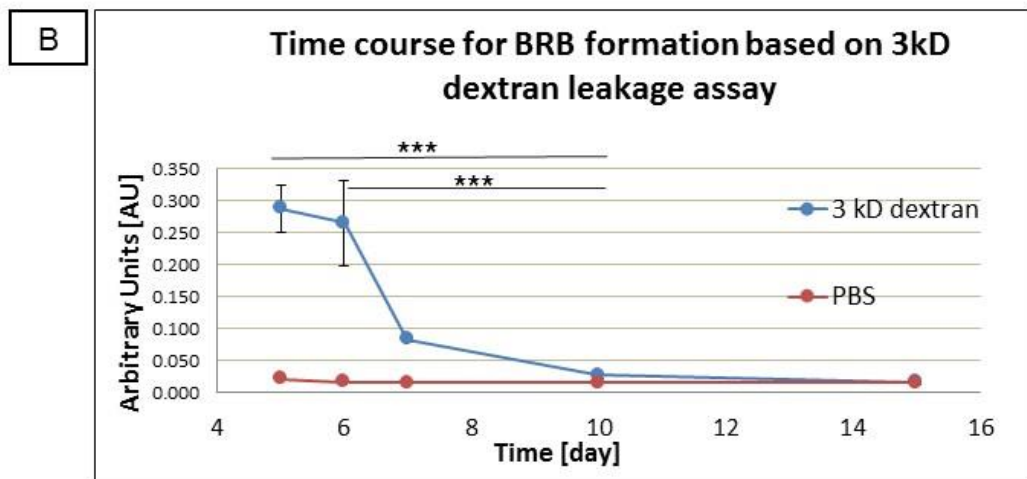
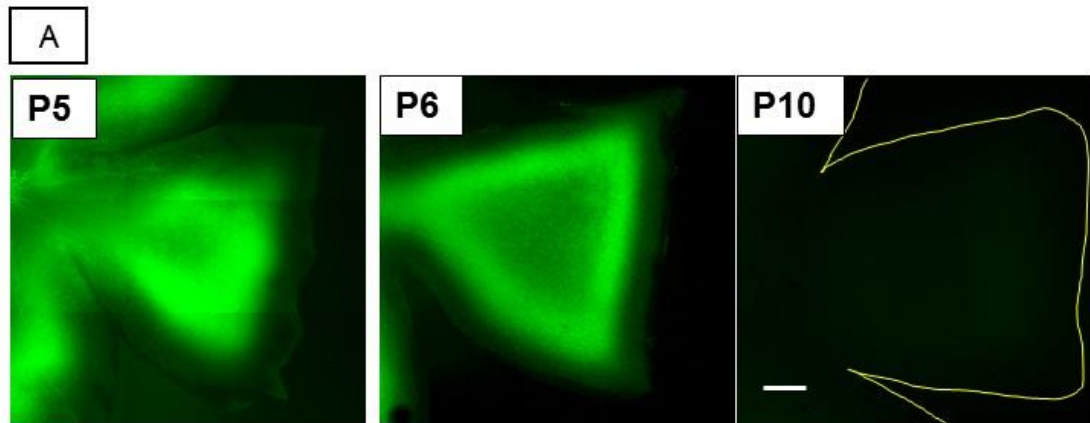


Figure 21. BRB formation based on the 3kD dextran permeability assay.

A- Flat mounted retina after 3kD fixable, fluorescent conjugated dextran and a PBS control injection at P5, P6, and P10. The scale bar indicates 200 μ m for all images.

B- Fluorescence intensity of the flat mounted retina, 2 hours following injection and perfusion, was measured with ImageJ Software. The graph shows the average intensity of fluorescence at different stages of development, plotted against the post-natal day of development, error bars indicates SEM. Number of animals used for the experiment: 3kD dextran - P5=17; P6=8; P7=2; P10=5; P15=10; PBS control - P5=7; P6=5; P7=1; P10=2; P15=6

Based on 3kD dextran tracer experiments, the leakage of fluorescence declined between P5 and P8, and by P10, there was no observed leakage of the tracer, suggesting the formation of the endothelial barrier at this point in retinal vascular development.

Assessing barrier formation we are mainly focusing on superficial plexus layer as this is the only vascular layer present prior to the P10.

We also looked at the permeability of the skin tissue, after 3kD dextran leakage assay (Figure 22). Interestingly at P10, when 3kD dextran after flashing out from the circulation is no longer detected in the retina, the skin tissue exhibit permeable properties.

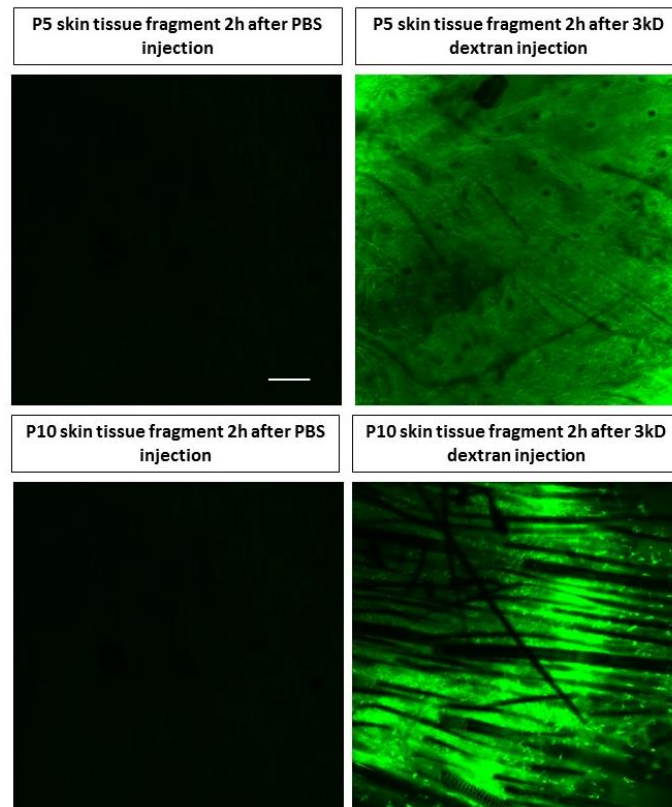


Figure 22. P5 and P10 skin tissue fragment 2h after 3kD dextran injection.

Skin tissue fragment was taken after performing 3kD dextran leakage assay. 3kD dextran leaks out from the skin vasculature both at P5 and P10. The scale bar indicates 100 μ m for all pictures.

BRB formation based on 70kD dextran leakage assay

Endothelial cells in the early developing retina vasculature permit leakage of the small sized dextran, but the question remains if the endothelial wall will be permeable for higher sizes of molecules. We next explored if there were differences in endothelial cell permeability as a function of size. To investigate vessel permeability for higher molecular weight and sized molecules 70 kDa FITC dextran was used for further experiments.

Pilot experiments suggested that the larger tracer required longer time to reach a significant concentration level in the circulation; therefore, the pups were perfused and eyes were taken 4 hours after intra-peritoneal injection, when 70kD dextran reached a similar concentration in the circulation as 3kD dextran after 2 hours (Figure 23).

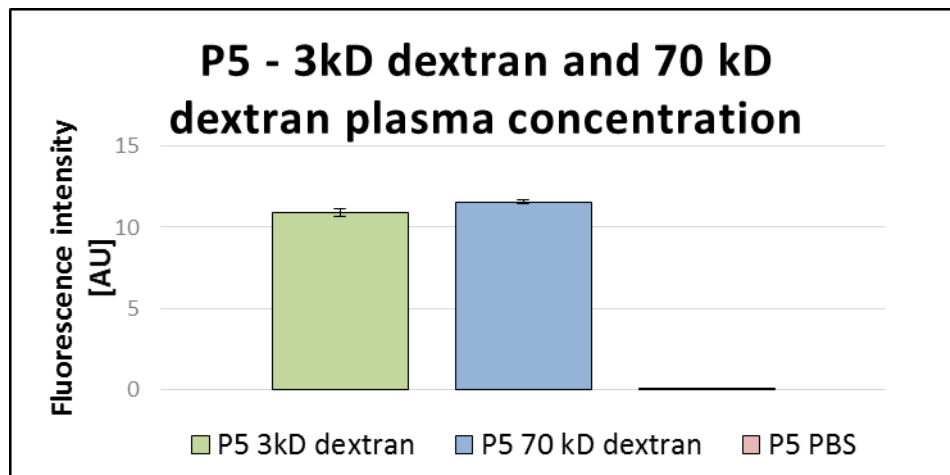


Figure 23. 3kD dextran and 70kD dextran plasma concentration at P5.

3 kD dextran and 70 kD dextran plasma concentration was measured based on fluorescence intensity of the blood samples taken 2 hours and 4 hours, respectively, after IP injection of the appropriate dextran; PBS injection was used as a control.

Similar to 3kD dextran, the retinal vasculature at P5 permits leakage of 70 kD dextran, which accumulates at the retinal periphery, where the endothelium is most immature. In contrast to 3kD dextran, perfusion with PBS did not completely remove the intravascular 70kD dextran and for further experiments with this tool no perfusion was done, as more clear data in terms of dextran localisation was achieved with this approach.

70kDa dextran extravasation occurred with a different pattern than the smaller tracer. In contrast to 3kD dextran, 70kDa dextran exhibits a non-vascular signal in the periphery of the developing vasculature. This suggests that during development the vascular front might be more permeable than more mature vessels closer to the optic nerve and BRB acquisition occurs in a spatial manner (Figure 24-25).

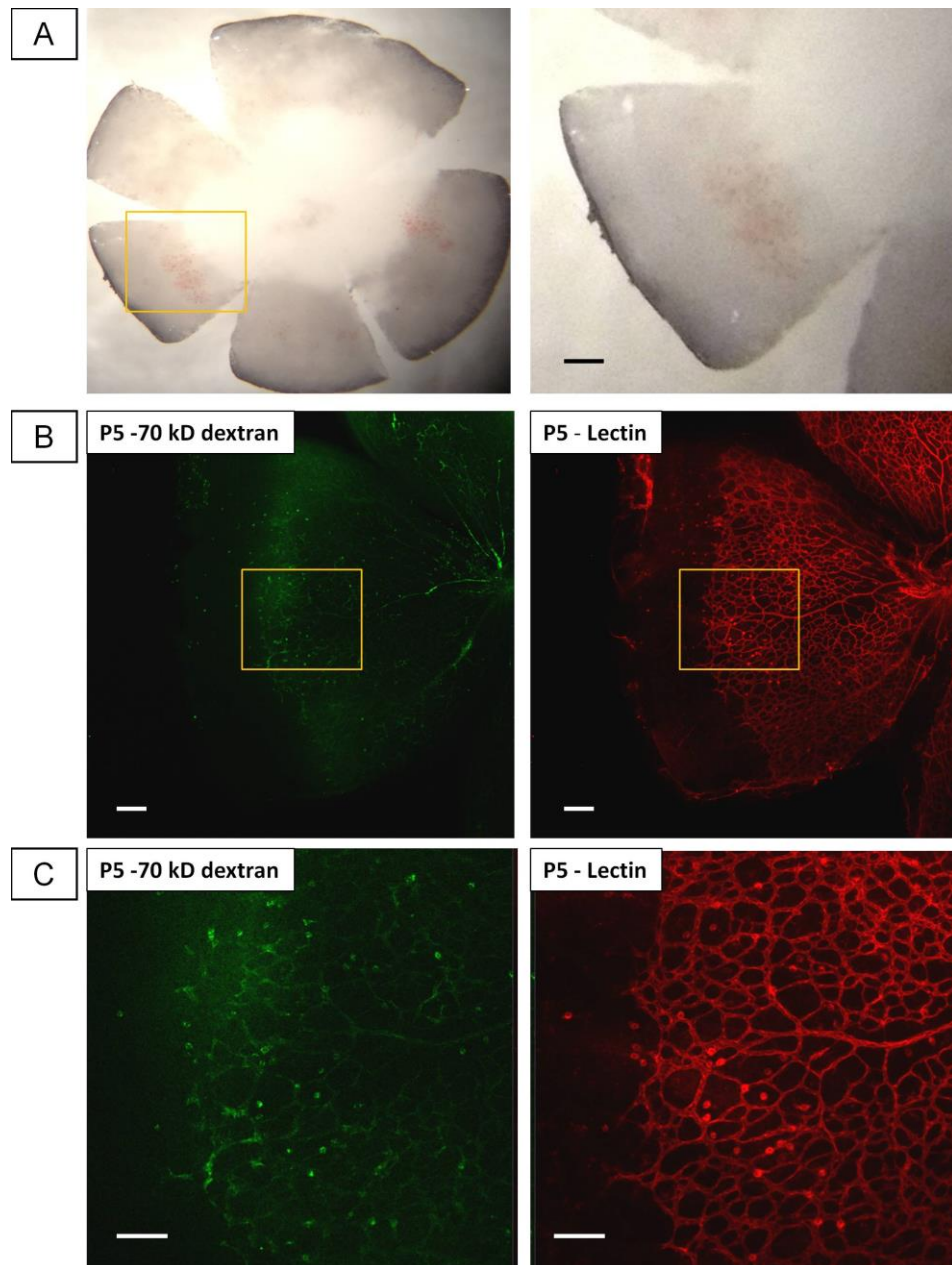


Figure 24. P5- flat mounted retina 4 hours after 70 kD dextran IP injection.

A dissected P5 retina with visible patches of blood in the periphery. B- Leaf of the retina after 70kDa dextran injection (3x3 pictures stitched together) and Lectin staining for co-localisation. C- High magnification view for the marked area. The scale bar indicates 200µm.

70kD dextran / Lectin

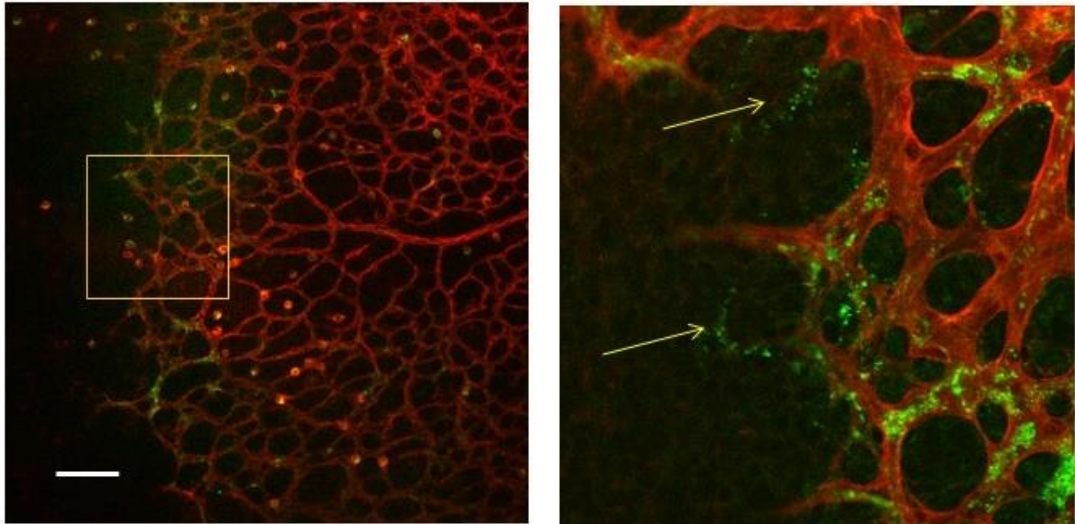


Figure 25. Leakage of the 70kD dextran at P5 retina.

Periphery of P5 retina 4 hours after 70 kD dextran IP injection, on the right is a high magnification view for the marked area. The scale bar indicates 200 μ m.

70kDa dextran plasma concentration, 4 hours after intraperitoneal injection was measured (Figure 26). Similar 70kDa dextran concentration at P5, P10 and P15 demonstrated that the difference in accessibility of the tracer in the circulation was similar in this assay.

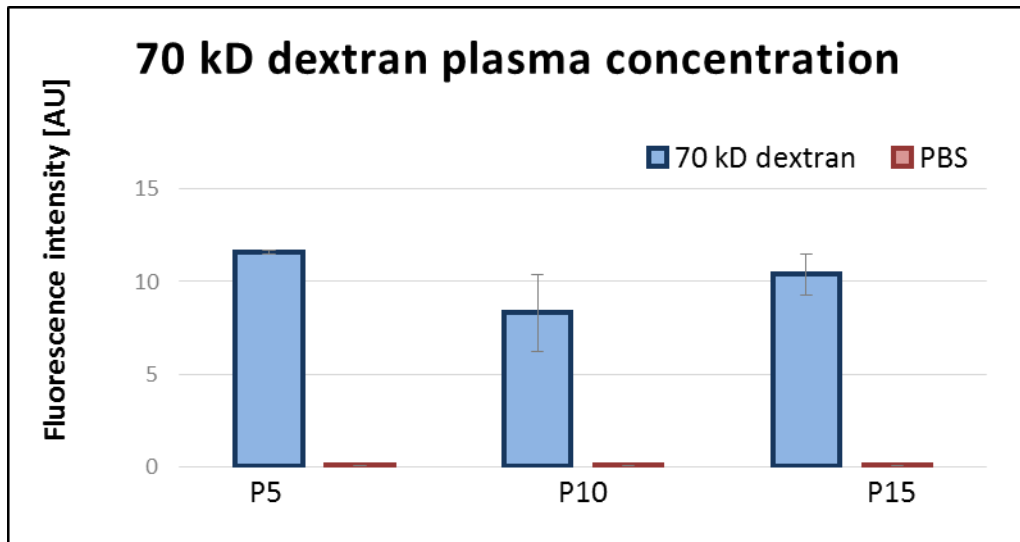


Figure 26. 70kD dextran plasma concentration at P5, P10 and P15 post-natal stage of development.

70 kD dextran plasma concentration was measured based on fluorescent intensity of plasma derived from the blood samples taken 4 hours after IP injection of the dextran; PBS injection was used as a control.

To determine the time point for BRB formation based on the 70kD dextran leakage assay, a similar time course experiment to the 3kD dextran leakage assay was performed. 70 kD fixable fluorescein conjugated dextran was injected at different stages of post-natal development. 4 hours after IP injection eyes were taken and the retina was processed as described in the Methods. An extracellular fluorescence signal was detected up to P8, but not at P10 or thereafter. At P9, there was variability in the number of retinas that exhibited leakage (Figure 27). This data appeared to mirror the data using 3kD dextran, suggesting that an endothelial barrier develops at P10 and is equally effective for large and small substances.

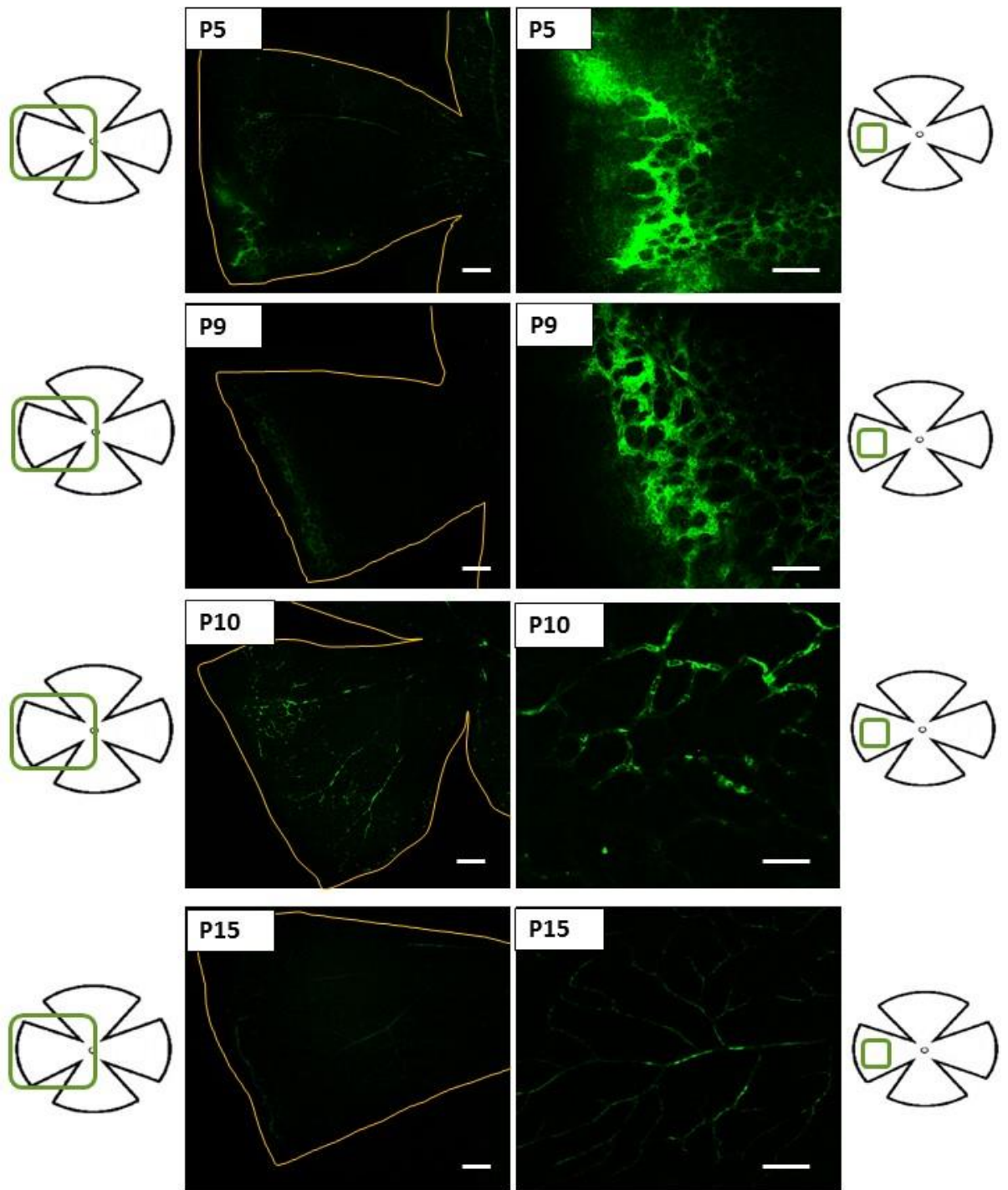


Figure 27. Time point for BRB formation based on the 70kD dextran tracer.

P5, P9, P10 and P15 flat mounted retina 4h after 70kD dextran intraperitoneal injection. The scale bar indicates 200 μ m, for all pictures.

BRB formation based on an NHS-biotin tracer assay

Size selectivity of the barrier was further investigated using sulfo-NHS-Biotin (sulfosuccinimidobiotin) which enables crosslinking of the tracer to primary amine containing molecules. These very small sized molecules – 244Da - react very effectively to form stable amide bonds (Figure 28).

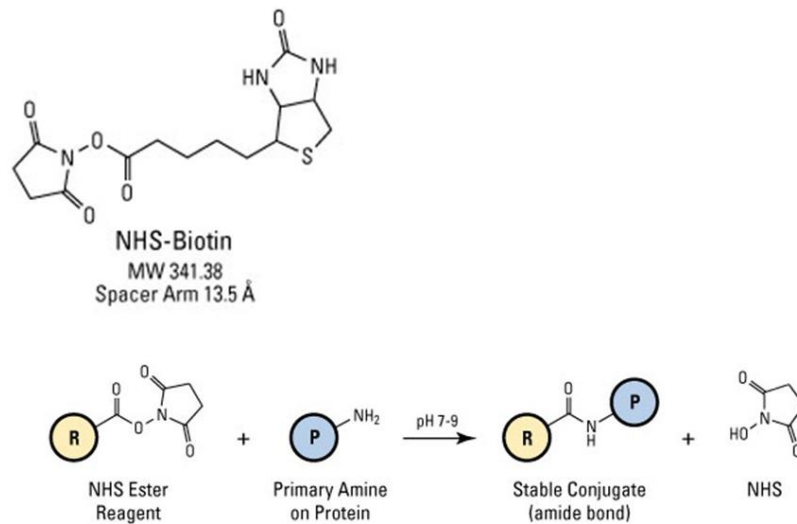


Figure 28. The reactivity of NHS-biotin.

NHS-Biotin – reacts with primary amines (-NH₂), such as the side-chain of lysines (K) or the amino-termini of polypeptides (*Thermo Scientific Pierce Protein Biology*)

Because of its high reactivity NHS-biotin was perfused via the heart of anaesthetised animals, and after 3 minutes, eyes were taken, retinas dissected and labelled with streptavidin (Figure 29). NHS-biotin remained localised and following the assay confirmed that the peripheral, more immature vasculature, lacked proper barrier function. Overall, NHS-biotin gave results consistent with the dextran leakage assays, with permeable retinal vasculature at early stages of development and only intravascular tracer present by P10.

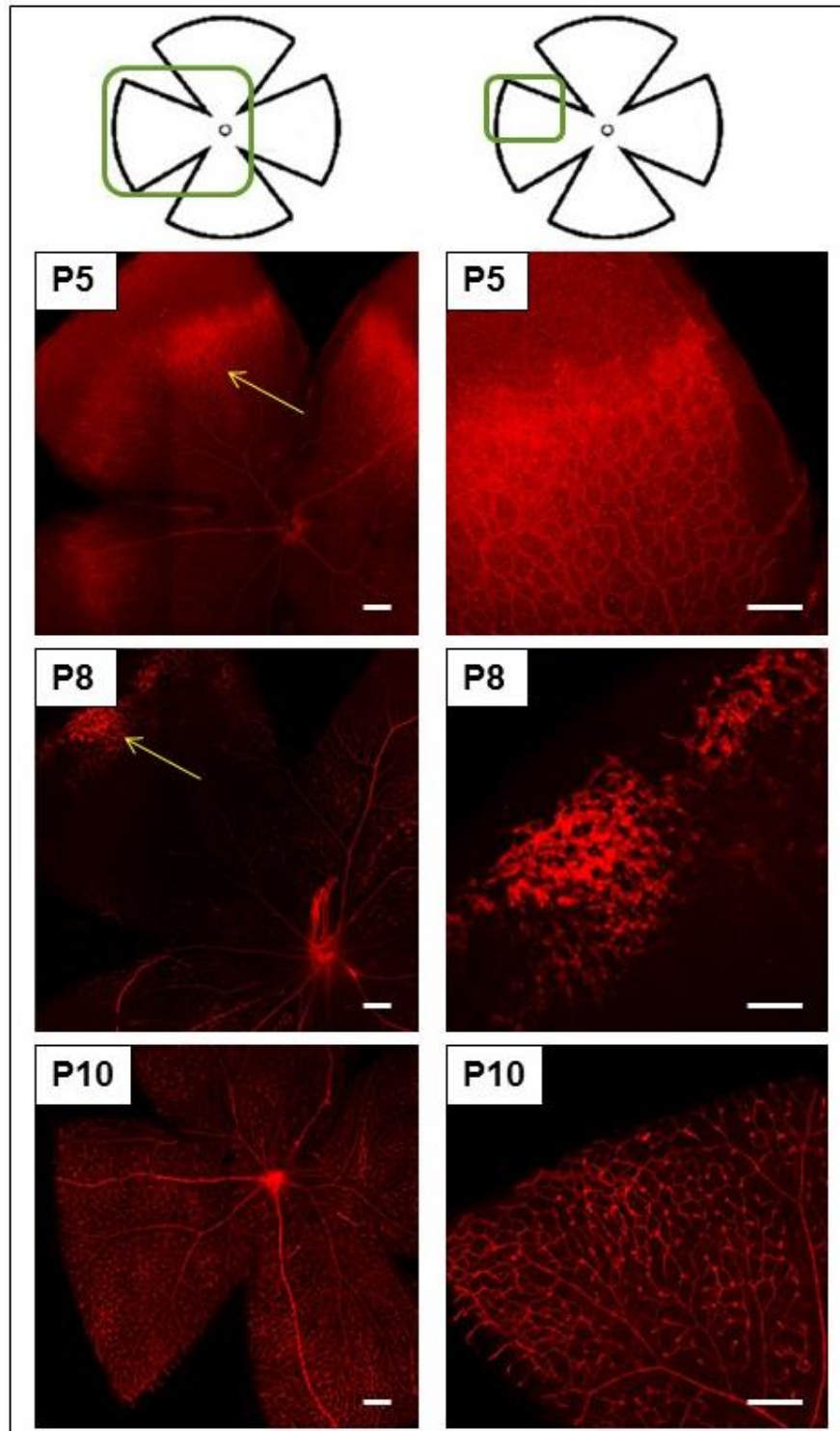


Figure 29. The permeability study of retina vasculature using NHS-biotin.

NHS-biotin was cardiac infused at P5, P8 and P10, and after retina dissection, visualised using Streptavidin (Alexa Fluor conjugate 594). Arrows point periphery of the retina. The scale bar indicates 200 μ m, for all pictures.

Junction protein localisation in the retina

Having identified P10 as the time of BRB acquisition, I next began to explore potential molecular changes that might accompany, and potentially play a role in BRB formation. TJ and AJ significantly contribute to cell-cell adhesion and sealing of the intercellular space. For this reason as a next step immunohistochemical screening in terms of presence and localisation in the endothelial cell wall of TJ and AJ components was carried out.

Claudin-5 is a major cell adhesion molecule of tight junctions in endothelial cells, highly expressed in the brain and retinal vasculature, and it has been suggested that Claudin-5 may play an important role in BBB/BRB formation.

Cld-5 immunohistochemical localisation was probed at P5, pre-BRB formation in the retina. Cld-5 in the mature retina is localised primarily to the plasma membrane, which is not surprising considering the role that it plays in tight junction formation. Interestingly Cld-5 immunostaining at P5 shows that the protein is primarily localised to the plasma membrane in the central retina, but in the peripheral, immature vessels Cld-5 staining appeared more diffuse (Figure 30).

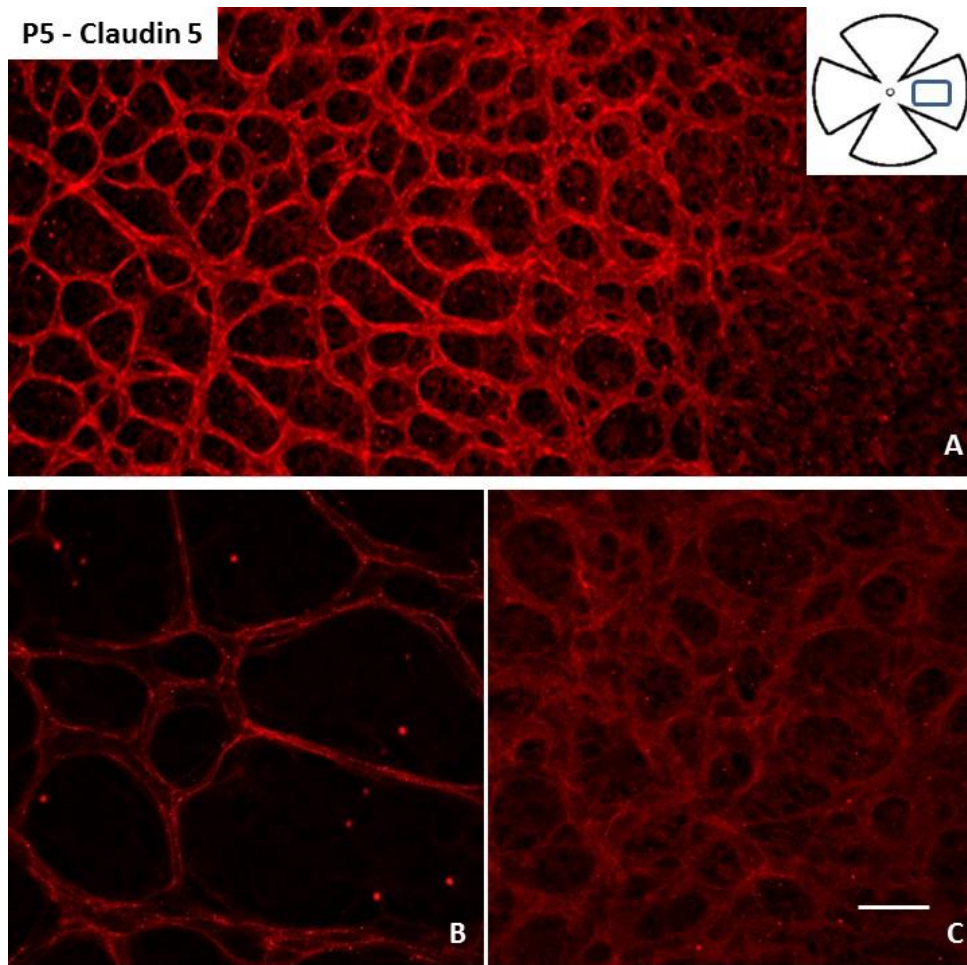


Figure 30. Claudin-5 localisation in the retina at P5.

A - Portion of the retina

B - Central vessels C - periphery vessels. The scale bar indicates 50 μ m, for all pictures.

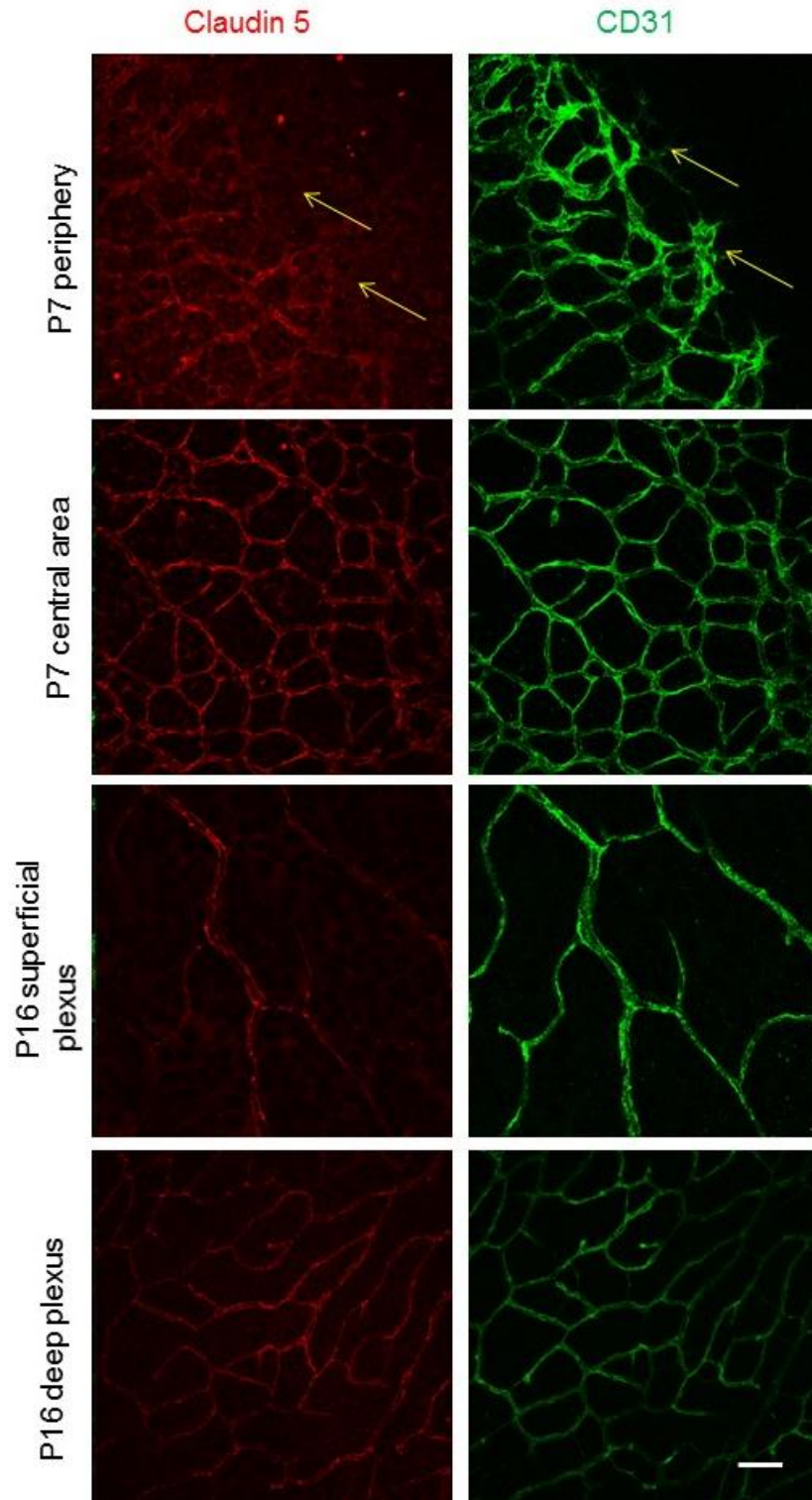


Figure 31. The localisation of Claudin-5 in the retina at P7 and P16.

Claudin-5 staining at P7 retina (central part and periphery) and P16 (superficial and deep plexus layer) with CD31 vascular co-localisation. The scale bar indicates 50 μ m, for all pictures.

Different organisation of Cld-5 between more mature and peripheral regions, led us to examine P7 and P16, when the BRB is intact. The retina vasculature gets fully developed within 3 weeks of birth, and P10 is the time point when the superficial layer is usually fully developed but the deep plexus and intermediate plexus are still growing. This is why an important issue to address is not only localising Cld-5 at the different stages of development, but also at in different areas and plexi.

Cld-5 expression at the periphery of P7 retina vasculature is not only more diffuse compared to the more mature central area and deep plexus layer, but also appeared to be less abundant in the periphery (Figure 31). This data might be explained by the fact that VEGF-A can increase permeability by altering the expression of tight junction proteins. It has been shown that TJ proteins are reduced in retinal and brain endothelial cells exposed to VEGF-A (Nag, 2011).

Another important component of TJ is the cytoplasmic plaque protein zonula occludens 1, or ZO-1, which is believed to be crucial in TJ formation. For example, silencing the gene encoding ZO-1 cause delays in formation of TJ (Chlenski, 2000, McNeil, 2006, Katsuno, 2008). Interestingly, unlike Cldn-5, immunostaining of ZO-1 at P5 did not reveal significant differences in terms of distribution of ZO-1 between central (more mature) and the peripheral area of the retina, and ZO-1 appeared primarily localised to the plasma membrane (Figure 32). This is surprising, as ZO-1 is a potential TJ protein downregulated by VEGF-A. One of the possibilities is that ZO-1 is regulated by phosphorylation, and it would be interesting to see the immunostaining of ZO-1 in phosphorylated form, and analyse if there would be a different distribution between the peripheral and the more mature vasculature.

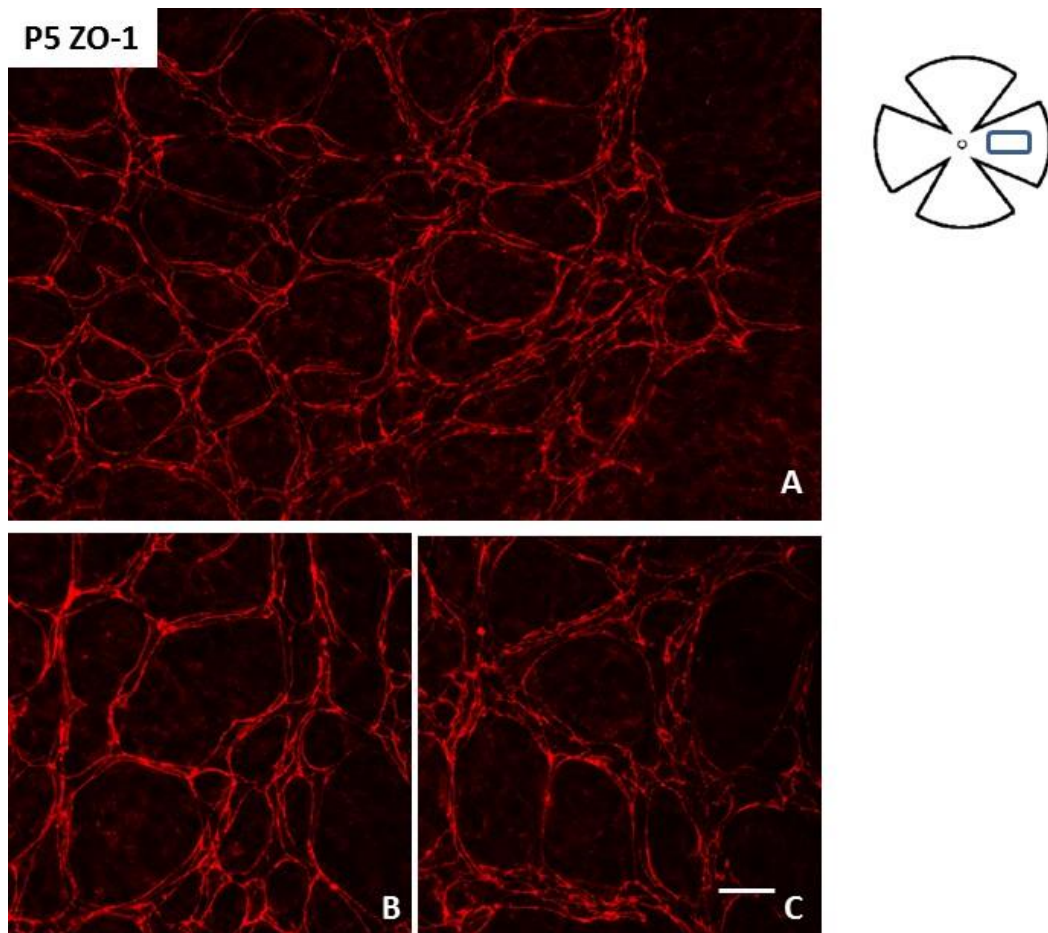


Figure 32. ZO-1 localisation in the P5 retina.

A - Portion of the retina

B - Central vessels C - periphery vessels.

The scale bar indicates 50µm, for all pictures.

Besides the tight junction, another adhesive structure crucial for proper barrier function are the adherens junctions (AJs), of which the main adhesive protein in endothelium is vascular endothelial cadherin (VE-cadherin) (Dejana, 2004).

In the developing retina the difference in VE-cadherin localisation in the retinal vessels at different stages of development was less apparent (Figure 33). Similar to ZO-1, VE-cadherin staining did not indicate any differences between the more mature and peripheral vasculature. VEGF-A driven modification of VE-cadherin could involve phosphorylation, this is why it would be interesting to localise phospho VE-cadherin in developing retina. Another possibility is that

VE-cadherin and ZO-1 may play a more general role in cell-cell adhesion, and that Cld-5 may be added to fortify junctions as part of formation of the BRB.

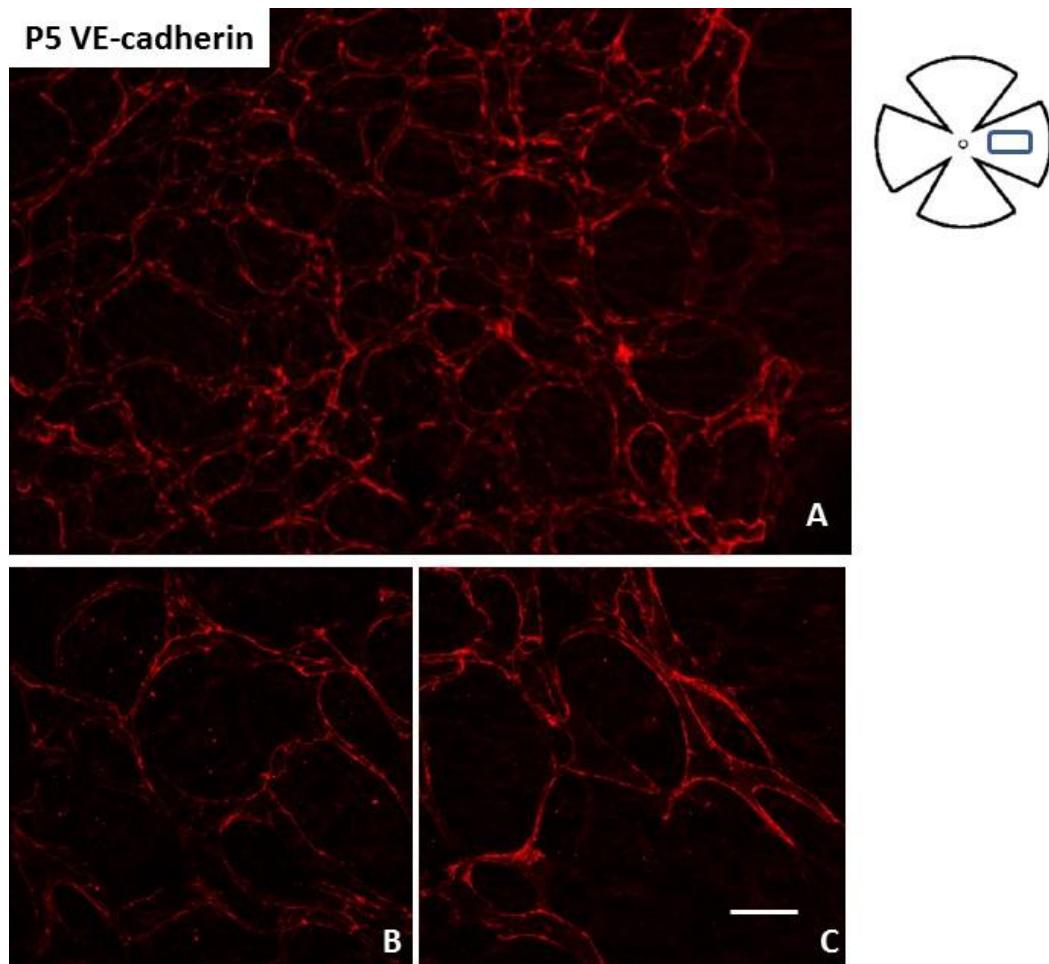


Figure 33. VE-Cadherin localisation in the P5 retina.

A - Portion of the retina

B - Central vessels C - periphery vessels.

The scale bar indicates 50 μ m, for all pictures.

Macrophage activation during BRB development

Endothelial cell interaction with immune cells is important in the modulation of vascular function (He, 2012). Inflammatory processes in the vasculature are highly regulated and form very complex multistep pathways (Takahashi, 1996, Woollard, 2010, Mestas, 2008).

Interaction between monocytes/macrophage and endothelial cells, appears to be a first step in many permeability-related conditions in the vasculature, including in the retina. For example, in models of diabetic retinopathy and neovascular age-related macular degeneration, reduction of leukostasis and of macrophage numbers in the retina leads to a reduction in vascular permeability (Nagai, 2015, Jousen, 2004). Thus, we decided to look at the myeloid cells during retina vascular development and determine if there may be an obvious qualitative change during the transition from leaky to BRB vessels.

Whole mount retinas at P5 and P15 were stained with IBA-1 - ionized calcium binding adaptor molecule 1, which is a calcium binding protein, a good marker for the resident microglia and macrophage.

IBA-1 positive cells were present in the P5 whole mount retina, both in close proximity to the vasculature and in the extravascular spaces (Figure 34). There was no obvious change in IBA-1-positive cell numbers found in the developing versus more mature vasculature

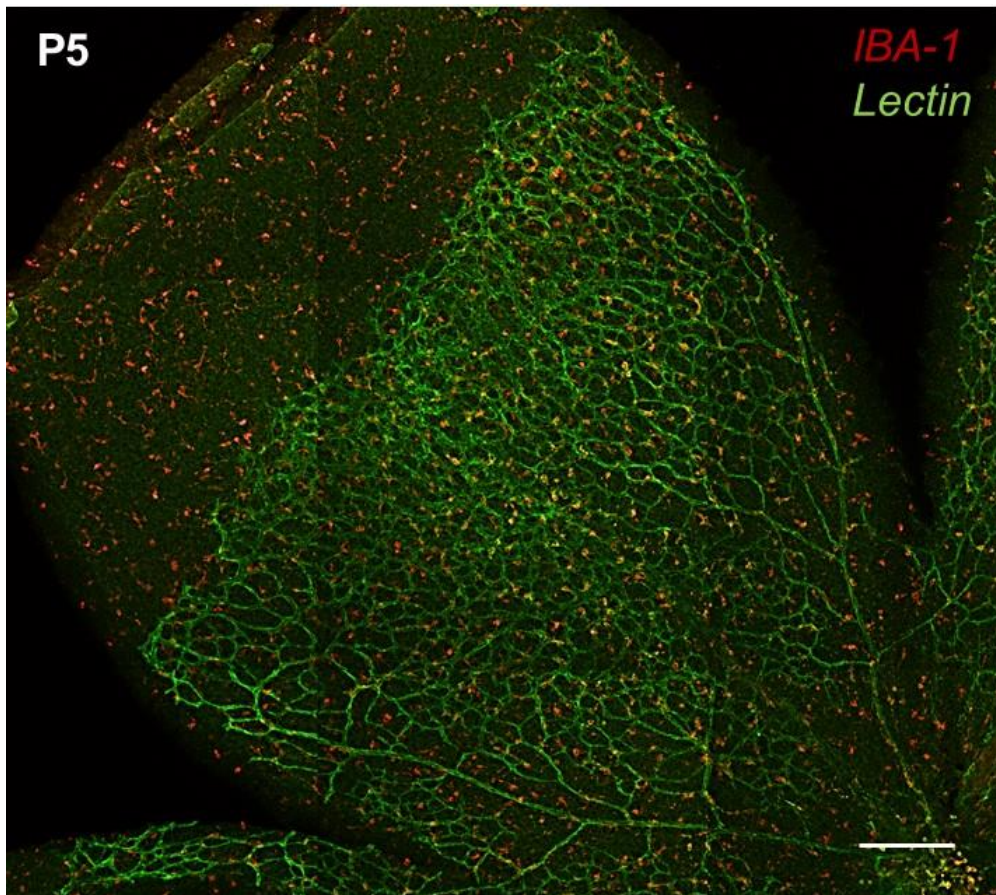


Figure 34. P5 whole mount retina stained with IBA-1 and Lectin.

The scale bar indicates 200 μm .

However, high magnification view of IBA-1 positive cells (Figure 35) showed differences in the morphology between P5 and P15. The morphology of IBA-1 stained cells looked different at the periphery compared to the more mature central area of P5 retina, and distinct morphology was also found between the superficial and deep plexus in the P15 retina. For example, the cells in the immature area of the retina were more flattened in appearance whilst the central retinal cells were more spindle shaped. The significance of the differential morphology of the IBA-1 positive cells during BRB formation is as yet unclear.

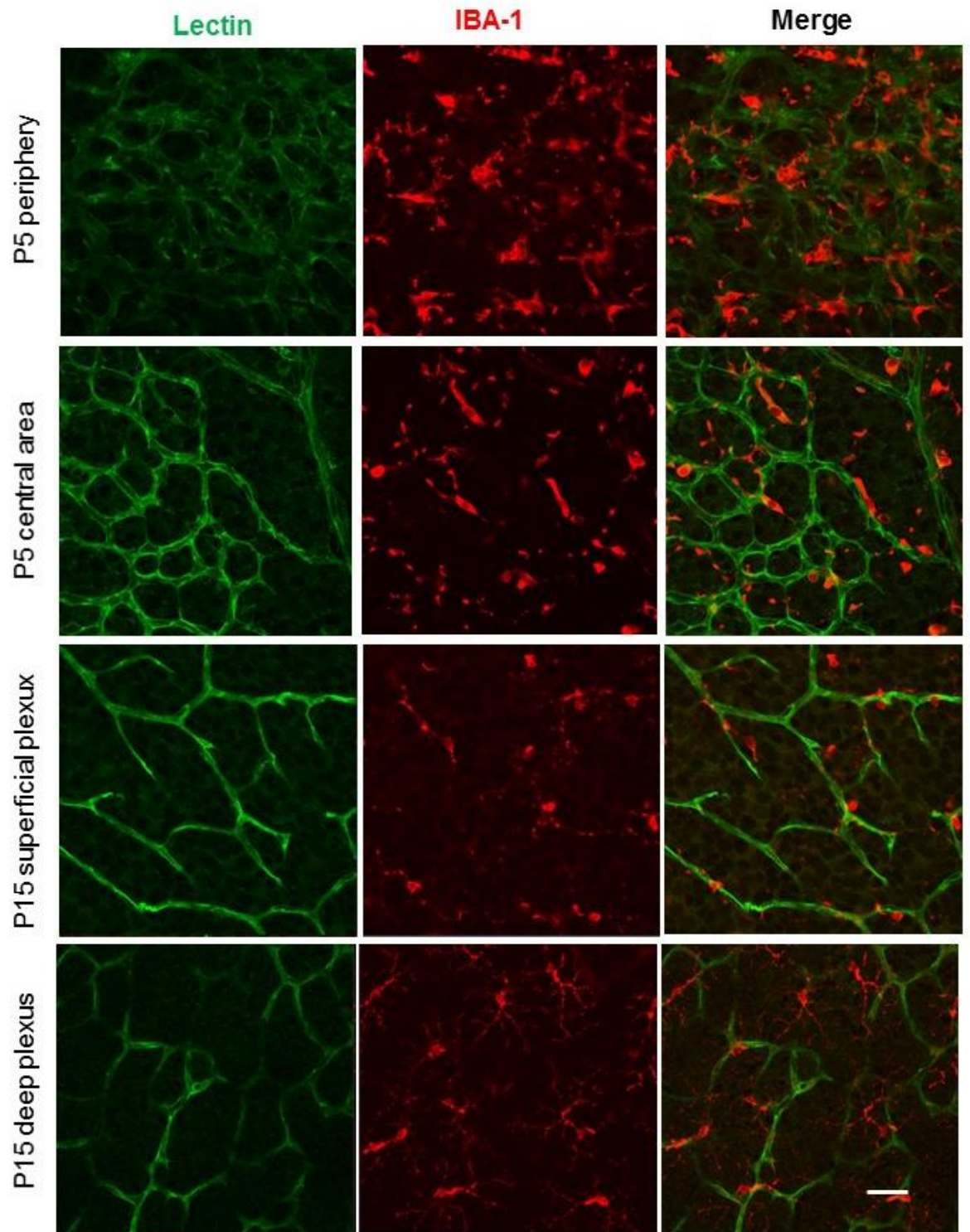


Figure 35. IBA-1 localisation in the retina at P5 and P15.

IBA-1 localisation at P5 (central part of the retina periphery) and P15 (superficial plexus and deep plexus) and Lectin co-localisation. The scale bar indicates 50µm, for all pictures.

Onset of Blood Retinal Barrier function – conclusions and discussion

There are many assays that can be used both in the clinic and in animal studies for investigating permeability of the vasculature in the retina, for example FA, and OCT. Unfortunately none of these techniques can be applied for studies in the rodent retinal vascular development model.

The in-vivo leakage assay I have developed – visualisation of tracers on flat mounted retina - appears to be a valuable tool for the study of BRB formation and function during different stages of retina development. The protocol is relatively fast and easy. Different size tracers can be used to study barrier function.

At P5, vasculature reaches the middle part of the retina, the superficial plexus that spreads from the optic nerve, is half way from the optic nerve to the ciliary body, and at this stage the leakage was the strongest.

P10 appears to be a time associated with a very significant change in barrier function, and it is a time when the superficial vascular plexus is nearly complete, in terms of growth and remodelling. After P10, retina vasculature still undergoes a growth and remodelling process, when vessels begin to penetrate into the deeper retinal layers to form the deeper plexus, and intermediate plexus (Figure 36); however, the tracer studies suggest no leakage occurs after that stage of development.

This interesting finding suggests that early vascular growth in the retina is accompanied by poor barrier function, but the proliferation, migration and remodelling that accompanies the formation of the deeper vascular beds, occurs whilst maintaining the BRB. Just how the BRB is maintained during this period is completely unknown.

In order to determine the changes in the retina vasculature that might be involved in fluctuations in the BRB permeability functions, I decided to focus on comparisons P5 and P15 retina vasculature. P5 is the stage when BRB functions are the poorest in opposition to P15, when leakage was not detected.

Interestingly, in a very well described murine model of retinopathy of prematurity (ROP) the time point, chosen for studying the changes in vasculature upon high oxygen exposure is P7. This is in order to balance in

retinal development between hyaloid regression and incomplete retina vascularisation (Smith, 1994).

During superficial plexus development, endothelial cells follow an astrocyte template based on VEGF-A cues. VEGF-A is also a very potent permeability factor. In the next chapter, I perform experiments which aim to provide a better understanding of BRB acquisition, with relation to VEGF-A expression and distribution in the retina at various stages of post-natal development.

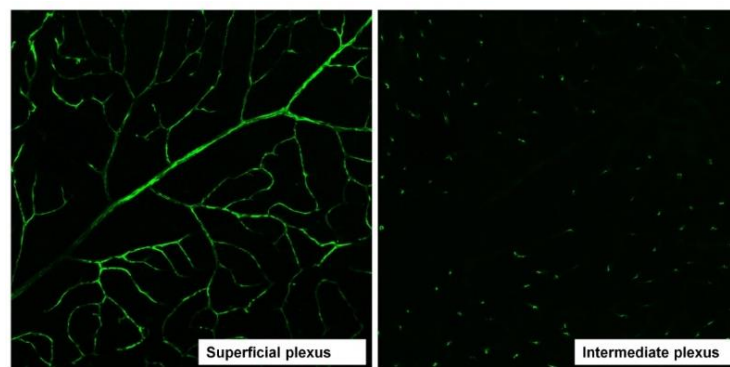


Figure 36 Superficial and intermediate plexus at P10.

Visualisation of retina vasculature at P10 using 70 kD dextran. P10 stage of post-natal development is the time point for BRB onset based on numerous tracer studies.

Chapter 4.

The role of VEGF-A during Blood Retina Barrier development

Does VEGF-A expression reduce barrier function prior to P10?

VEGF-A is a critical growth factor for blood vessels, implicated both in normal physiological growth and during pathology of blood vessels. Large numbers of studies, investigating the level of protein expression have shown that whenever angiogenesis occurs, VEGF-A is present, or its level is elevated. It has also been demonstrated that one driving force for the expression of VEGF-A and vascular growth is hypoxia (Woolard, 2004). This would make sense considering that during vascular growth, there is a high demand for oxygen and nutrition for growing neuronal cells.

VEGF-A is known to orchestrate assembly of the superficial vascular plexus in the developing retina. After establishing the time frame for BRB formation, we have begun to explore if VEGF-A is expressed at high levels adjacent to the immature vascular front, and if this could be, in part, responsible for vascular leakage in the premature retina.

VEGF-A localisation in the developing retina by in situ hybridisation

In previous work demonstrated that VEGF-A is most strongly expressed by pre-vascular retinal astrocytes, but also by retinal astrocytes within the developing vascular plexus, suggesting a role for retinal astrocyte-derived VEGF-A in angiogenesis and vessel network maturation (Scott, 2010) (Figure 37).

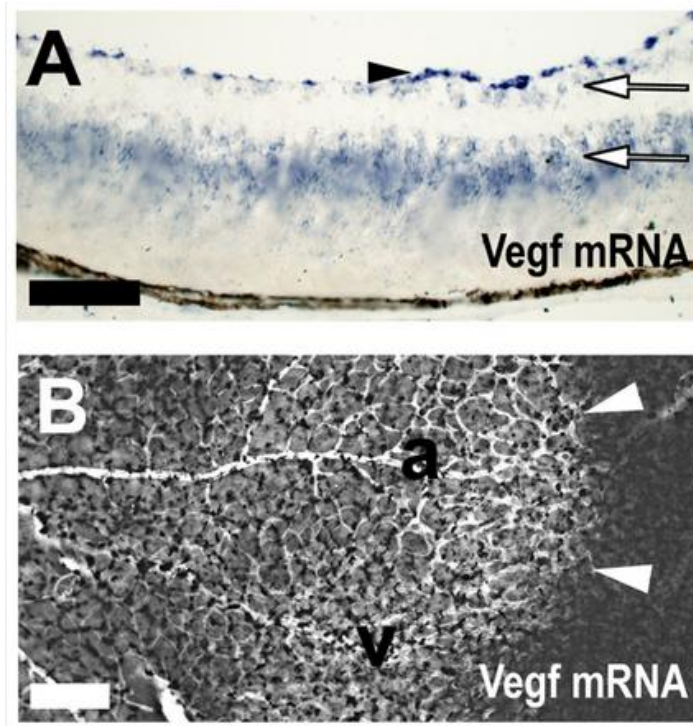


Figure 37. VEGF mRNA expression in the retina.

In situ hybridisation showed Vegf mRNA expression in a retinal cross-section (A) and a retinal whole mount (B) at P5. (A) Vegf mRNA was most strongly expressed in retinal astrocytes (arrowhead), and weakly in retinal ganglion cells and the inner nuclear layer (arrows). (B) Retinal astrocytes expressed VEGF strongest distal to the edge of the growing vascular plexus (white arrowheads), at intermediate levels around veins (v) and weakest along arteries (a). Adopted from (Scott, 2010).

Identification and localisation of VEGF-A in the retina at different stages of BRB development

The retina has the highest metabolic needs of any tissue in the body. At the early stages of retina development, the onset of neuronal activity increases metabolic activity in maturing retinal neurons and photoreceptors, can causes 'physiological hypoxia'. In response, astrocytes and Müller cells respond by secreting VEGF-A that drives vascular growth (Kur, 2012).

VEGF-A staining in the retina, at different stages of development, shows that VEGF-A is highly expressed at P5 (Figure 38). VEGF-A expression at the early stage of retina vascularisation is also significantly higher than it is at P15

(Figure 39-40). Co-localisation with lectin staining shows that the VEGF-A signal is mainly non-vascular. Interestingly P5 retina peripheral staining shows a strong VEGF-A expression at the edges of growing EC (Figure 38).

This data is consistent with previously described in-situ hybridisation of VEGF-A mRNA. Both of these sets of data imply the importance and driving force of VEGF-A during retina vascular development.

Furthermore, astrocytes that accompany the developing vessels may also play an important role in vascular development in the retina. Firstly, as they express VEGF-A, secondly as they form the platform that EC follow, moving from the optic nerve towards the periphery, and thirdly stabilising new vessels. The importance of neuroglia in the development and maintenance of a healthy retinal plexus is supported by the fact that the only species with retinal astrocytes have vascularised retinas (Kur, 2012). Interestingly the pattern of VEGF-A staining in the non-vascularised part of periphery of P5 retina seems to co-localised with GFAP staining, this would confirm the co-localisation of VEGF-A with astrocytes (Figure 41).

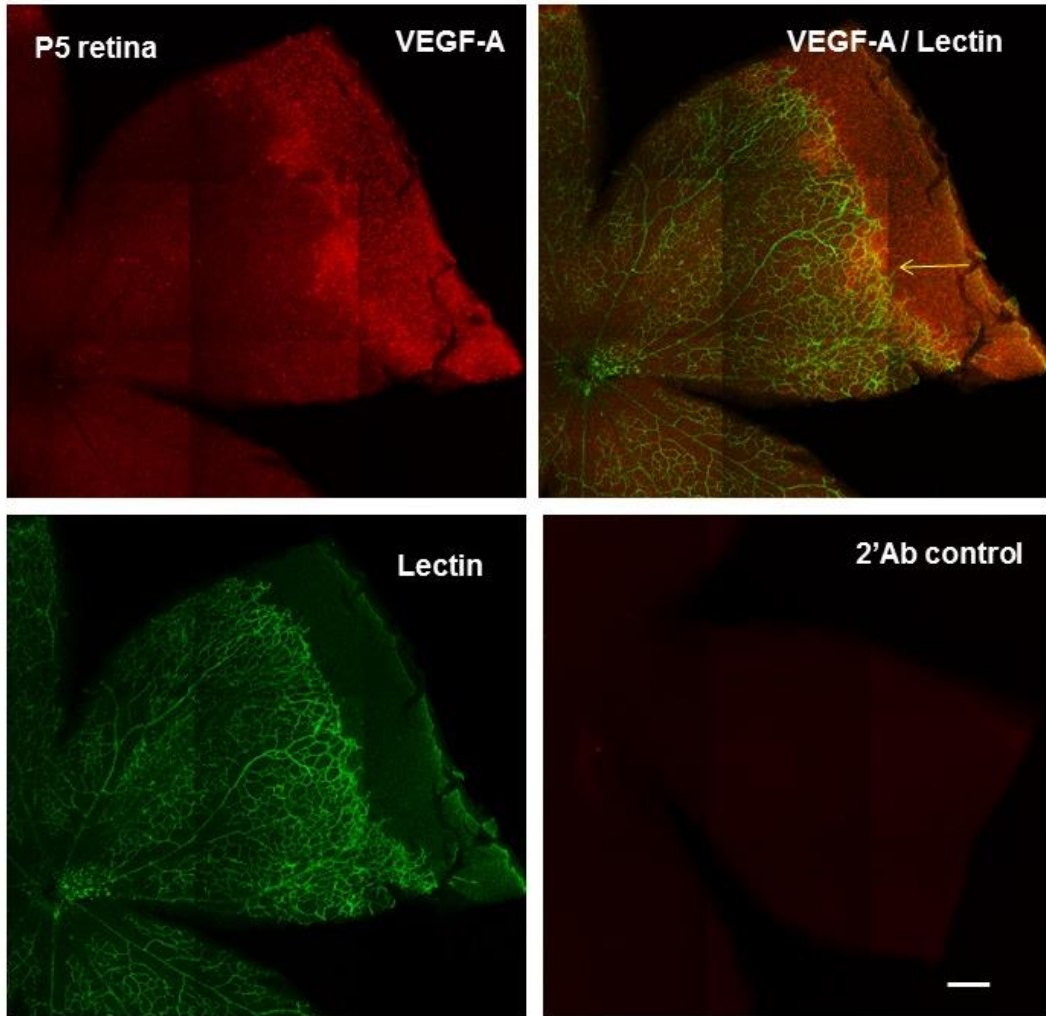


Figure 38. VEGF-A localisation in the P5 retina.

VEGF-A staining at P5 retina showing strong VEGF-A expression at the edges of growing EC. The scale bar indicates 200 μ m for both pictures.

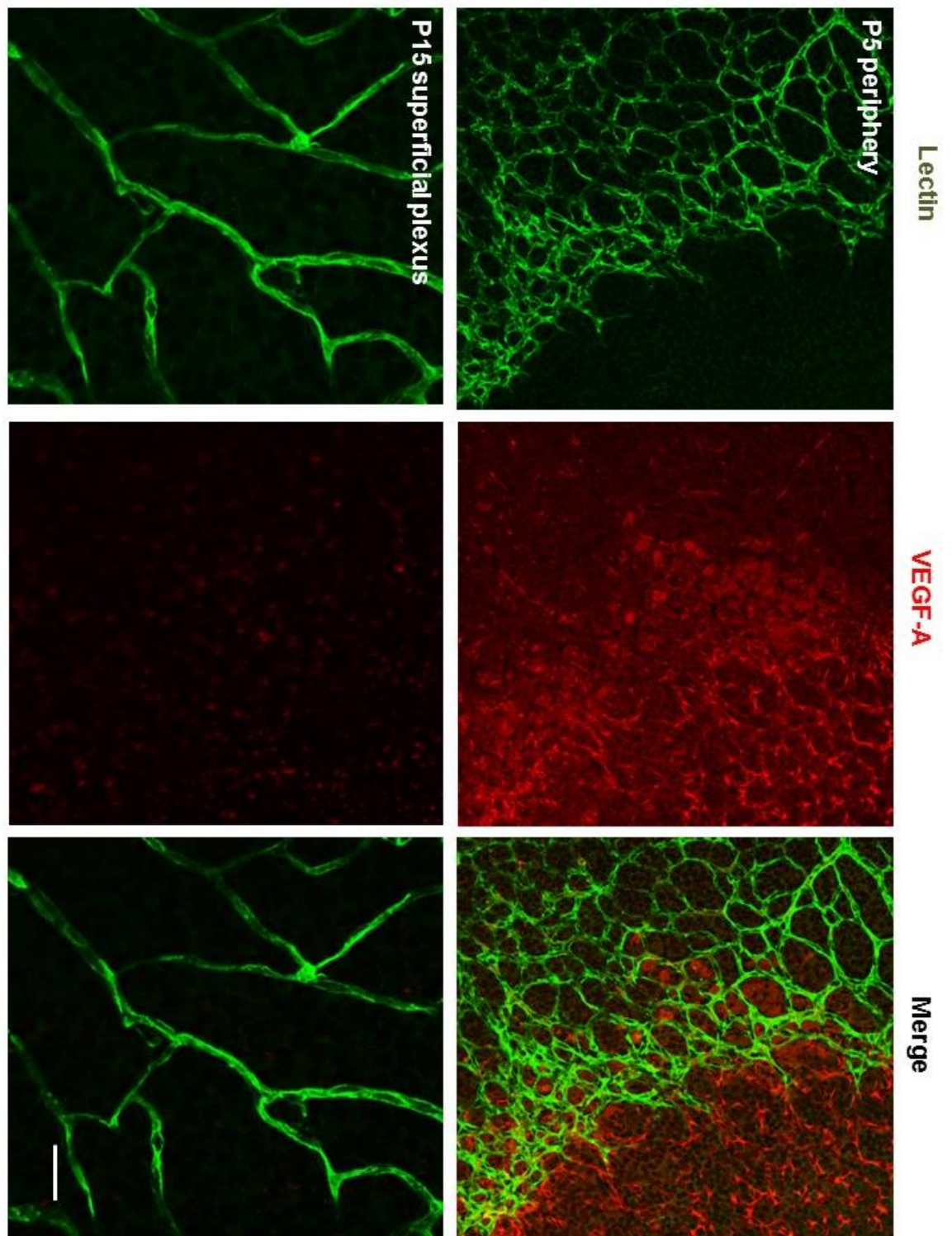


Figure 39. VEGF-A staining at P5 and P15.

High expression of VEGF-A at the periphery of growing vasculature at P5, compared to the superficial plexus layer at P15. The scale bar indicates 50 μm for all pictures.

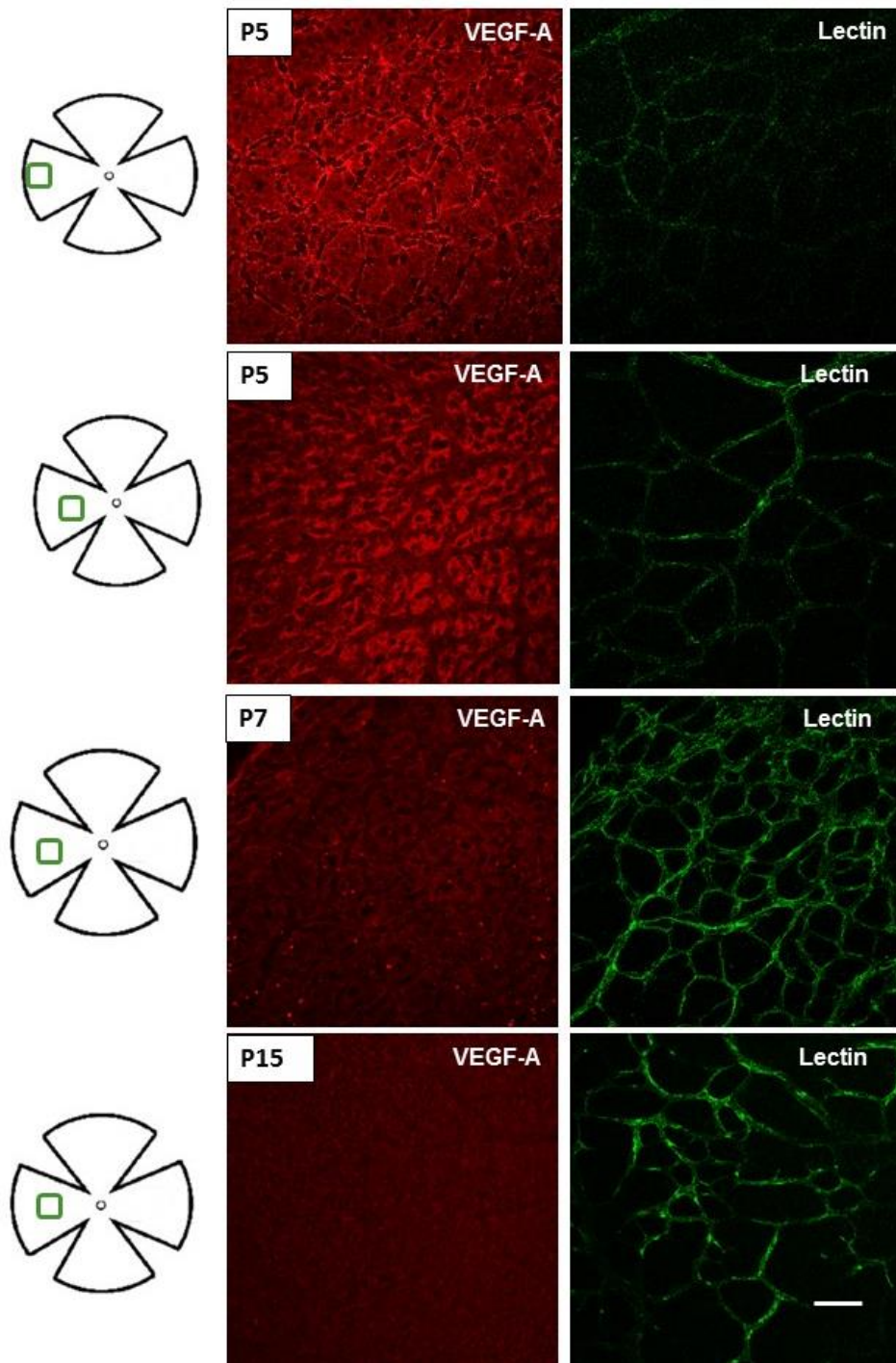


Figure 40. VEGF-A staining at different stages of retina development.

VEGF-A staining at P5, P7 and P15 retina, showing decrease of VEGF-A expression at P7 and P15.

The scale bar indicates 50 μ m, for all pictures.

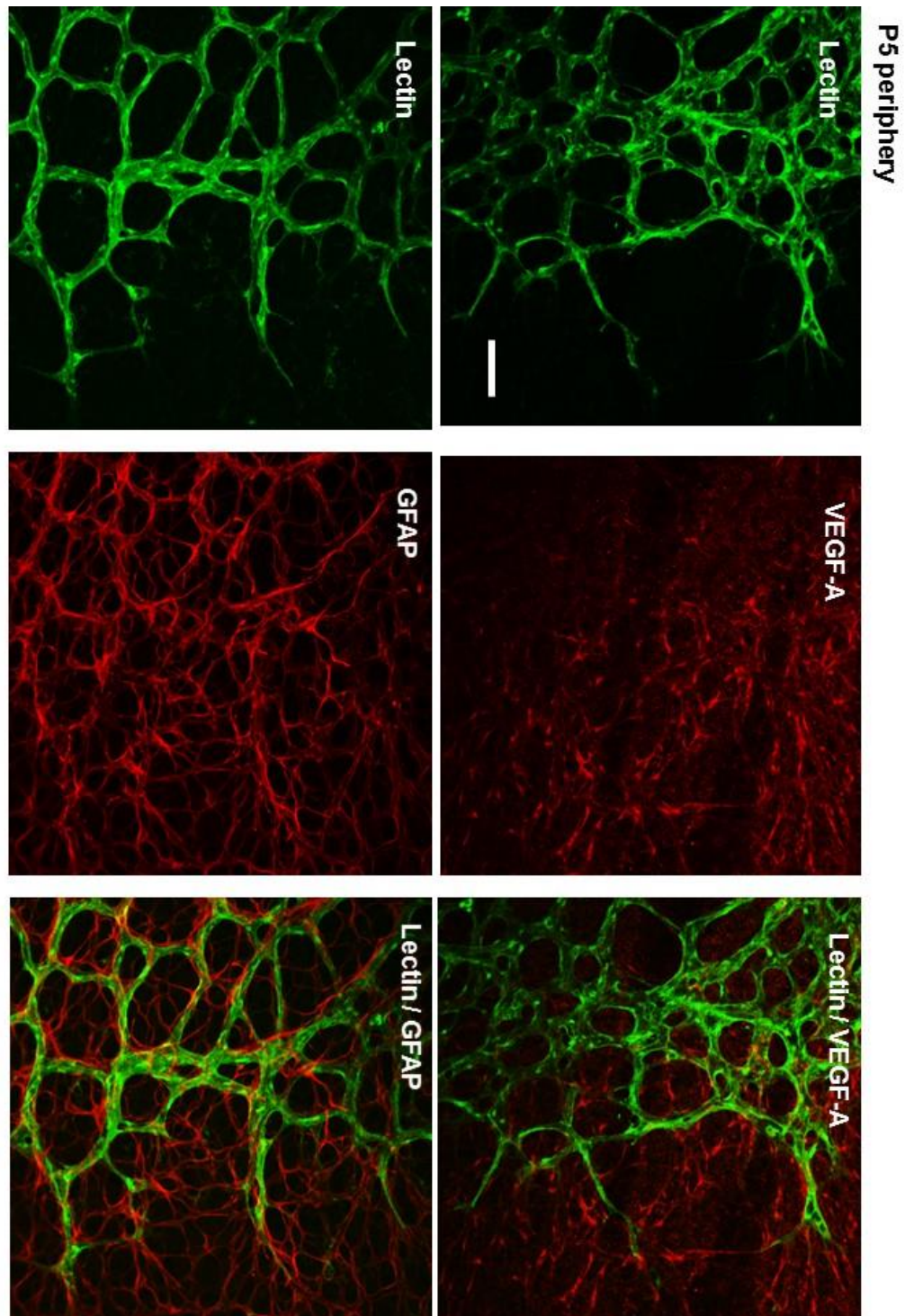


Figure 41. VEGF-A and GFAP staining in the periphery of P5 retina.

VEGF-A and GFAP localisation at P5 periphery of retina vasculature, showing similar pattern of expression suggesting that most of the VEGF-A in developing retina is expressed by astrocytes.

The scale bar indicates 50 μ m, for all pictures.

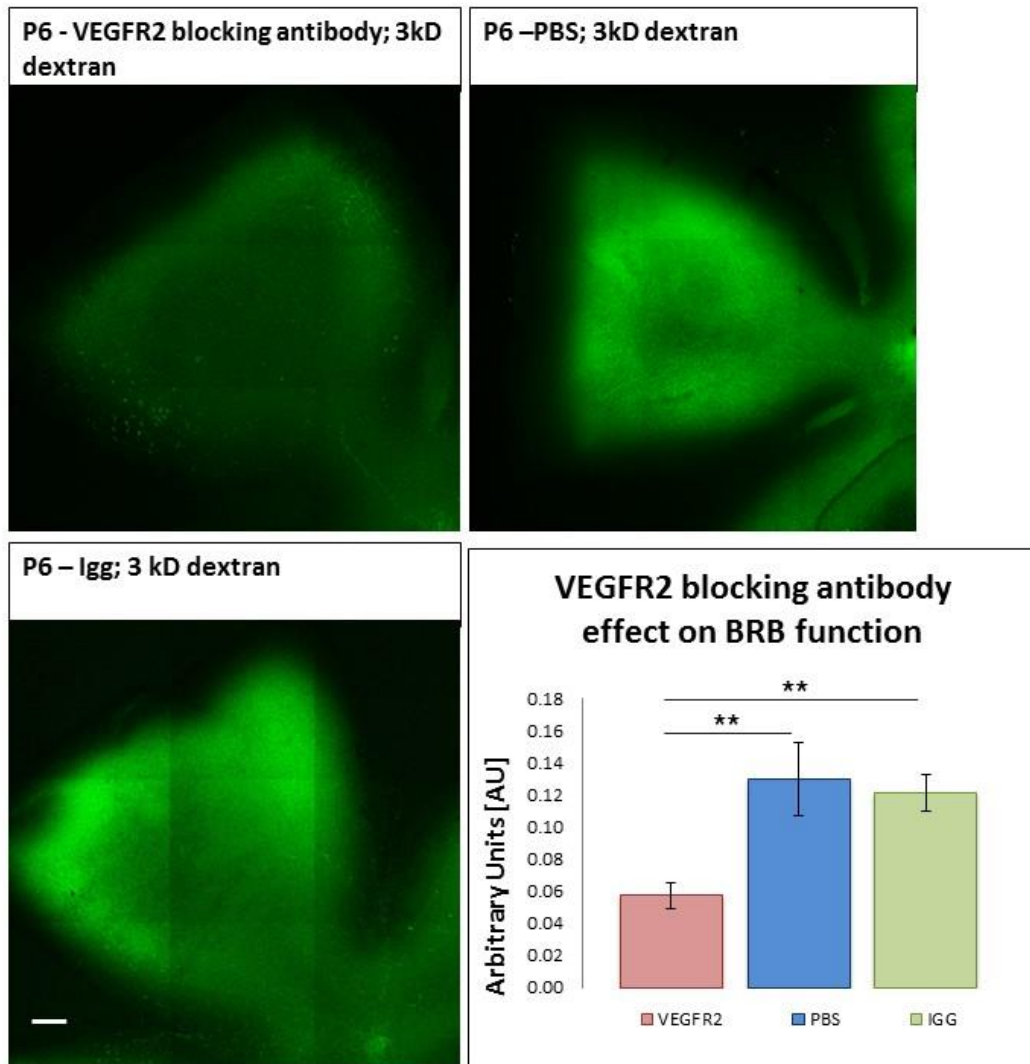
VEGFR2 blocking antibody injection

VEGF-A is a very potent vascular permeability factor, and therefore, VEGF-A expression at the vascular front could explain why there is a weak vascular barrier in the periphery. As a next step, I probed the role of VEGF-A signalling in the control of permeability during BRB formation.

There are two well-characterised receptors for VEGF-A expressed on endothelium: VEGF receptor 2 (VEGFR2, KDR, Flk-1) and VEGF receptor 1 (VEGFR1, Flt-1). VEGFR1 signalling is not required for retinal vascular development, whilst VEGFR2 is known to mediate endothelial cell mitogenesis and migration, and is known to be responsible for VEGF-A's acute effect on vascular permeability (Brekken, 2000). To test if VEGF-A signalling was responsible for the lack of barrier function during the formation of the superficial plexus, we injected rat VEGFR2 blocking antibody into P5 pups and the next day we visualised leakage using 3kD dextran.

In the animals that received rat anti VEGFR2 blocking antibody we could see a decrease in the vascular leakage compared to the animals that were injected with control IgG (Figure 42). The VEGFR2 blocking antibody decreased leakage by 50%.

This suggests that one of the mechanisms responsible for leakiness of the developmental vasculature is based on VEGF-A signalling. These data also suggest that vascular leakage accompanies vascular growth, and this concept intuitively makes sense given that endothelial cells must divide and migrate during vessel formation. However, the observation that the BRB is maintained during formation of the deeper plexi means that the growth of the vasculature is not always accompanied by vascular permeability.



	VEGFR2	PBS	IGG
Average	0.06	0.13	0.12
SEM	0.01	0.02	0.01
N	18	9	14

Figure 42. VEGFR2 blocking antibody effects on BRB function at P6.

Pictures show 3kD dextran leakage assay at P6 retina after VEGFR2 blocking antibody injection. Graph represents intensity of fluorescence of the retina; error bars indicates SEM value; N- Number of animals. The scale bar indicates 200 μ m for all pictures.

VEGF-A induced Blood Retina Barrier breakdown

Since blocking VEGF-A signalling enhanced endothelial barrier function, as a next step we wanted to explore the opposite- whether the P15 post-natal BRB was still responsive to VEGF-A induced permeability.

VEGF-A was injected intravitreal and on the following day a leakage tracer study was performed to see if the retina vasculature had been affected (Figure 43).

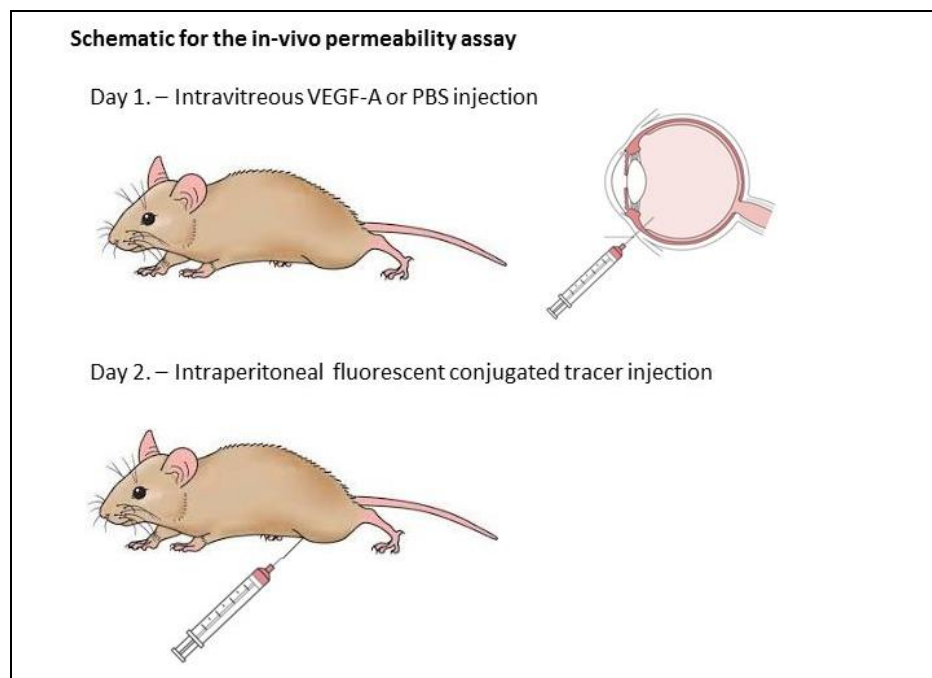
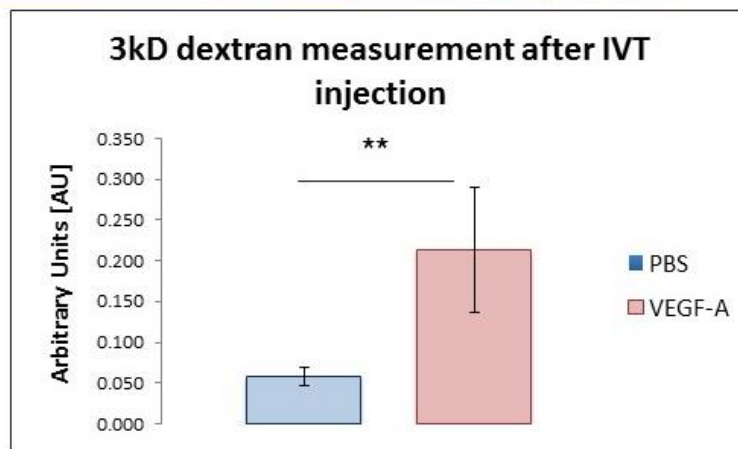
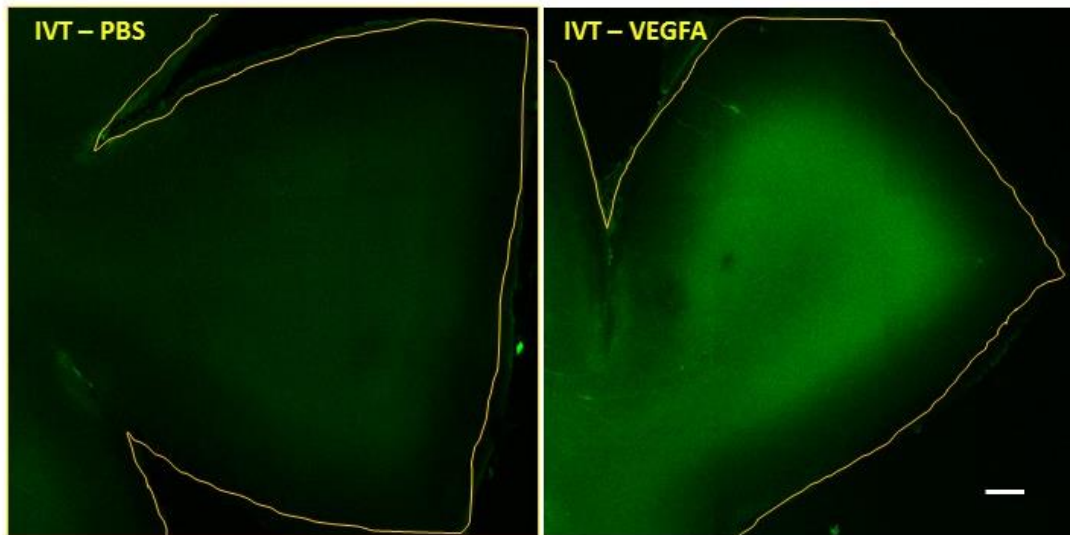


Figure 43. Schematic illustration of the in vivo VEGF-A permeability study.

In order to evaluate the effect of intravitreal injections of VEGF-A on the vasculature in the P15 retina, we firstly used 3kD fluorescein conjugated and fixable dextran tracer (Figure 44). As the figure shows after intravitreal injection of VEGF-A, we can observe a significant increase of the leakage compared to PBS injected animals.

Small size dextran tracer leaks out of the retina vasculature at P16 following exposure to VEGF-A. We also performed a similar experiment using 70kD dextran as a tracer to probe the size of molecules which may extravasate following VEGF-A exposure.



	PBS	VEGF-A
n	6	6
Average	0.059	0.214
SEM	0.021	0.098

Figure 44. Permeability study after VEGF-A intravitreal injection at P15 C57BL6.

IVT - VEGF-A injection (N=6); B) IVT PBS injection (N=6). C57Bl/6 animals intravitreally injected with VEGF-A or PBS at P15. BRB function was measured on the following day with 3kD dextran leakage assay. Graph indicates in intensity of fluorescence in the retina, error bars indicates SEM value. The scale bar indicates 200 μ m for both pictures.

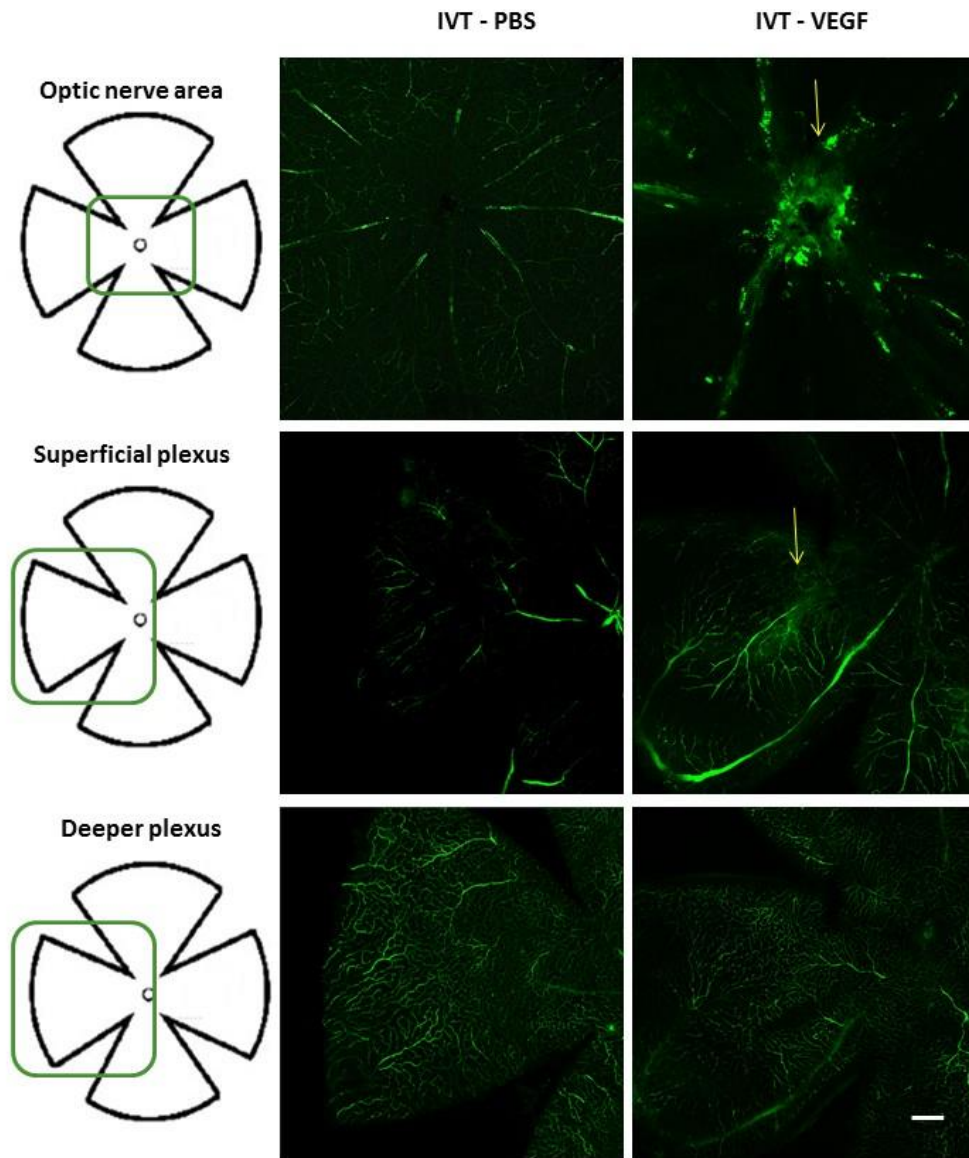


Figure 45. Permeability study after VEGF-A intravitreal injection at P15.

Permeability study after VEGF-A intravitreal injection at P15 C57Bl/6 with 70kD dextran used as the tracer. On the left represents pictures of animals injected with PBS, on the right represents pictures of animals injected with VEGF-A. The scale bar represents 200 μm for all pictures.

Using the 70 kD dextran, which remained localised following leakage from the vasculature, provided greater detail on the regions of the retinal vasculature that were most affected by VEGF-A exposure (Figure 45). The greatest areas of leakage were observed in the central superficial plexus, and the deeper plexus barrier was unaffected by VEGF-A. Possible reason for it is the higher concentration, and accessibility of VEGF-A in the superficial plexus layer.

This data gives us an interesting insight into the role that VEGF-A might play during vascular growth. By blocking VEGFR2 we can observe a decrease of the leakage at early stages of development, and by introducing VEGF-A at P15, we detect increases of the vascular permeability. Interestingly, a similar effect of VEGF-A on retina function has been previously reported in Tamim Qaum (2001), where in a 1-week diabetic rat model retinal VEGF-A mRNA levels was found to be significantly higher than age-matched non-diabetic controls. With this increased level of VEGF-A in the retina, coincided with BRB breakdown. To reverse early diabetic blood–retinal barrier breakdown VEGF TrapA₄₀, a soluble Flt/F_c chimera, was used. VEGF TrapA₄₀ reversed early diabetic blood–retinal barrier breakdown in a dose-dependent manner, moreover at a dose of 25 mg/kg, restored diabetic blood–retinal barrier breakdown to non-diabetic levels (Qaum, 2001).

Our experiments suggest that regulation of VEGF-A levels may be an important factor during the acquisition of the BRB, and warrants further investigation of the levels and localisation of VEGF-A especially around the P10 watershed period.

VEGFR1 and VEGFR2 localisation in the retina

Previous experiments underline the importance of the role of VEGF-A in barrier formation and function. The process of vascular growth in the retina depends on new cell growth, segregation of apical and basal membrane compartments, and subsequent junction formation. VEGF-A mediates a diversity of functions during vascular development in the retina, through the use of multiple receptors.

VEGF-A is a ligand for VEGFR1 and VEGFR2 and via those receptors triggers a number of molecular signalling events. VEGFR1 is required for the recruitment of haematopoietic precursors and migration of monocytes and macrophages, whereas VEGFR2 is essential for vascular endothelial cell growth (Olsson, 2006, Rahimi, 2006). Both receptors are involved in angiogenesis.

I decided to localise the main mediators of VEGF-A signalling: VEGFR1 and VEGFR2 in the retina, at different stages of development. VEGFR2

immunostaining in the retina (Figure 46) shows it has higher expression at P5 compared to P15 retina. Additionally VEGFR2 at P5 was localised both in the vasculature and in nonvascular tissue, specially at the periphery where the nonvascular signal was significantly stronger in comparison to the more central retina.

In contrast to VEGFR2, VEGFR1 was mostly found in the vasculature at P5 and at P15 (Figure 47).

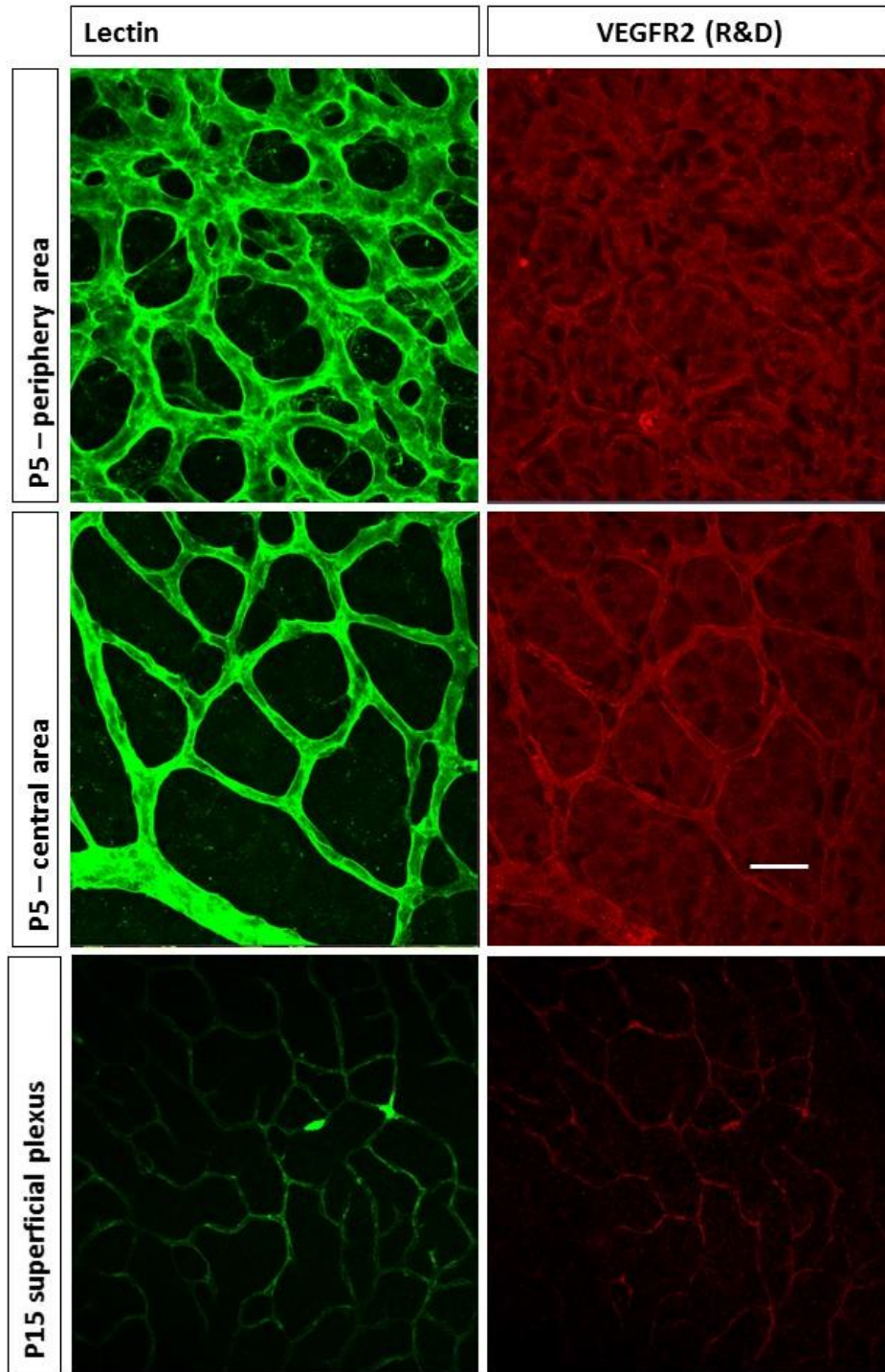


Figure 46. VEGFR2 immunostaining at P5 and P15 retina.

VEGFR2 immunostaining at P5 (periphery and central area) and P15 (superficial plexus). The scale bar indicates 50 μ m for all pictures.

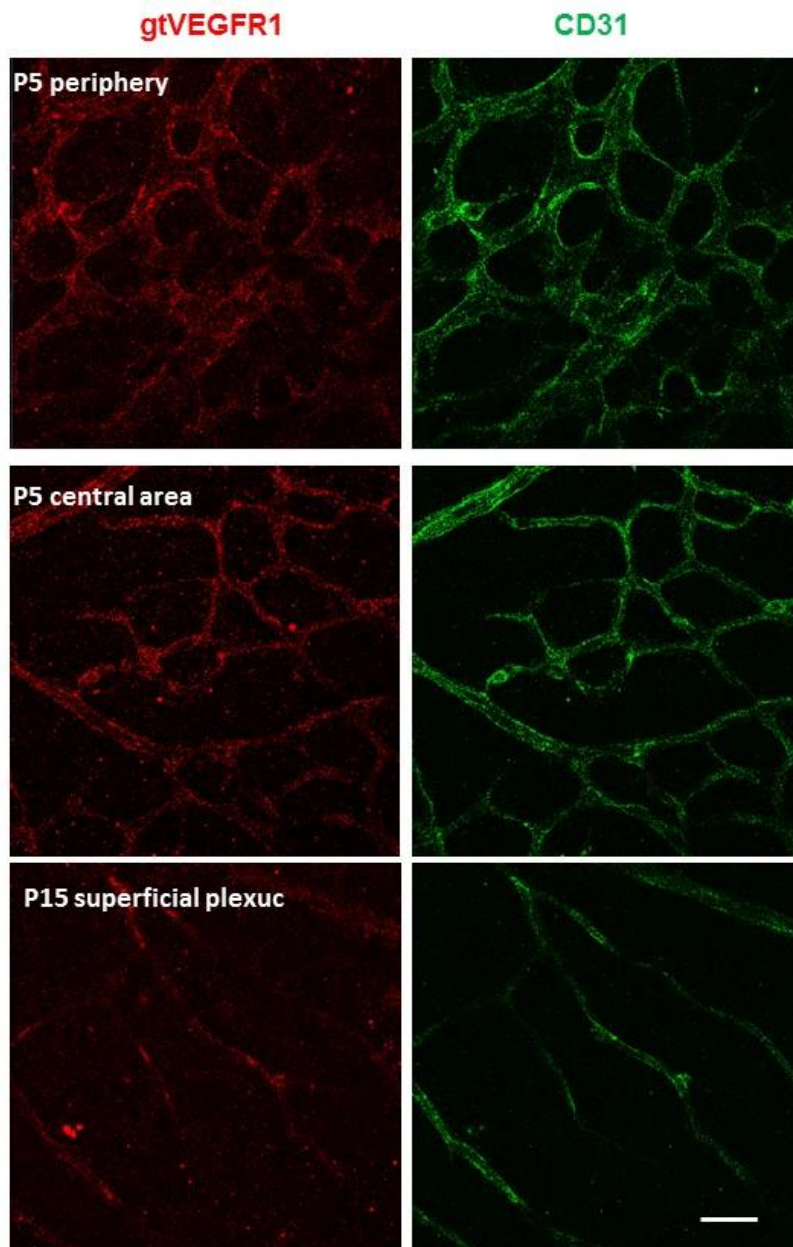


Figure 47. VEGFR1 immunostaining at P5 and P15 retina.

VEGFR1 immunostaining at P5 (periphery and central area) and P15 (superficial plexus). The scale bar indicates 50 μm for all pictures.

VEGFR1 and VEGFR2 polarity

Immunostaining of VEGFR1 and VEGFR2 demonstrated significant differences in localisation. VEGFR1 was mostly found in the vasculature and VEGFR2 was localised both, in the neuronal part of the tissue and the vasculature. It has been reported that the two receptors are differentially

segregated into luminal (VEGFR1) and abluminal (VEGR2) domains in endothelium of the BBB (Hudson, 2014). I next explored this possibility in the BRB.

To probe the luminal localisation of these two receptors in the retinal vasculature, VEGFR1 or VEGFR2 antibodies were perfused by cardiac injection into P20 pups. After a 5 minute delay to allow the antibodies to distribute, the pups were perfused to remove any unbound antibody. Investigation of luminal expression of VEGFR1 and VEGFR2 was carried out only for the superficial plexus layer, as control IgG experiments showed that antibodies might not get fully perfused out of that part of the retina. Afterwards, eyes were fixed, permeabilised, blocked and incubated with a secondary antibody. Cardiac infusion of primary antibody shows the luminal expression of VEGFR1/VEGFR2, as the antibody cannot cross the BRB.

To probe for abluminal localisation of VEGFR1 and VEGFR2 immunostaining was done without permeabilisation. The investigation of the abluminal localisation of the VEGF receptors, was carried out only on the superficial plexus, as without permeabilisation step the antibody does not have access to the deeper layers of the retina. Staining without permeabilisation step shows abluminal localisation of VEGFR1/VEGR2 in the retina, because antibodies cannot pass BRB in the un-permeabilised tissue.

This assay allows for distinguishing localisation of VEGFR1/VEGFR2, and shows if they are expressed on the luminal or abluminal side of the endothelial cell layer. Described method helped demonstrate the VEGF receptors polarised localisation *in vivo* (Hudson, 2014).

VEGFR1 was detected in the retina after antibody cardiac infusion, this suggest that it is expressed on the luminal side of the vasculature. VEGFR2 was not detected in the retina after antibody cardiac infusion, which indicates that it might be less expressed on the luminal side of the vessel (Figure 48). Interestingly DC101, VEGFR2 blocking antibody from GeneTex, was detected in the skin section after antibody cardiac infusion (Figure 49). This is a very interesting finding that shows the differences in permeability between the BRB and other tissues like skin.

VEGFR2 was detected by immunostaining of unpermeabilised retinas, whilst VEGFR1 was not detected after immunostaining without permeabilisation. This result suggests that VEGFR2 is mainly expressed on the abluminal side of the vessels, and VEGFR1 on the luminal side (Figure 50).

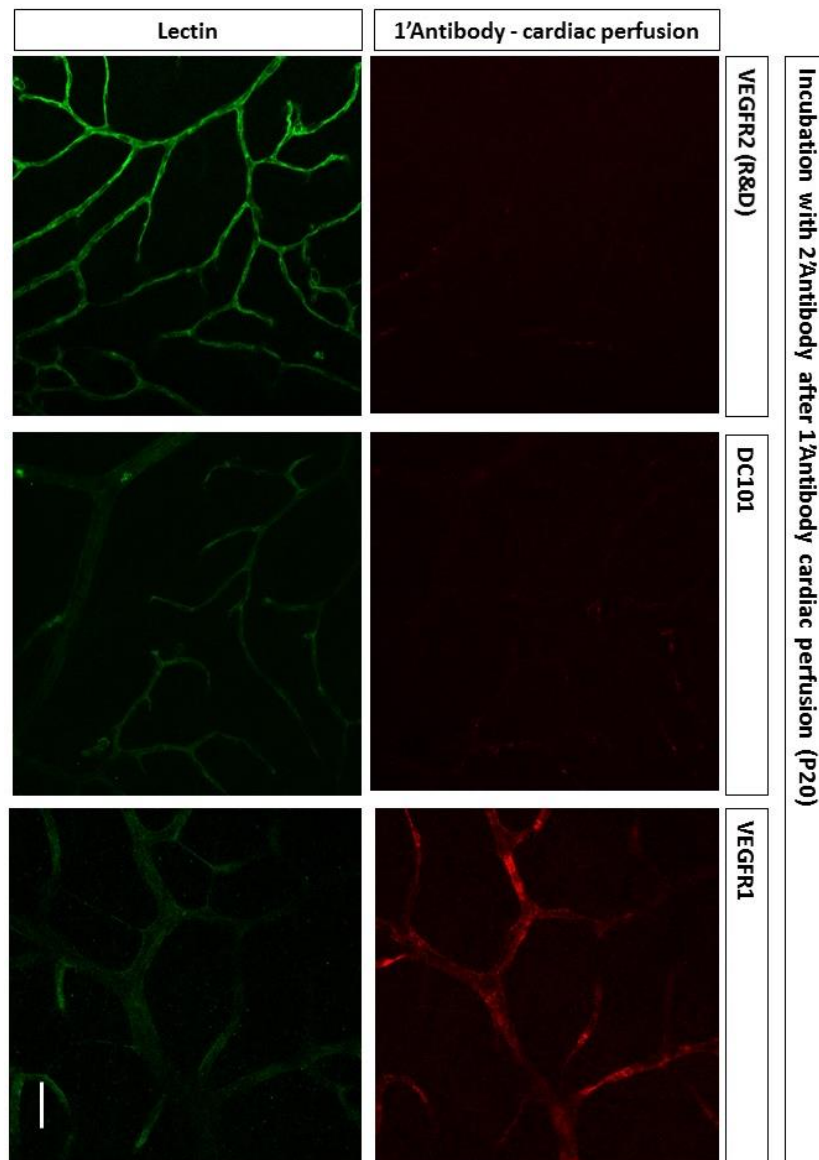


Figure 48. VEGFR1, VEGFR2 and DC101 cardiac infusion.

VEGFR1, VEGFR2, DC101 were cardiac injected into P20 C57Bl/6 animals, and left for 5 minutes to allow the antibody to reach the circulation. Next animals were perfused and eyes were taken, 4% PFA fixed, permeabilised and incubated with a Secondary Antibody.

The scale bar indicates 50 μ m for all pictures.

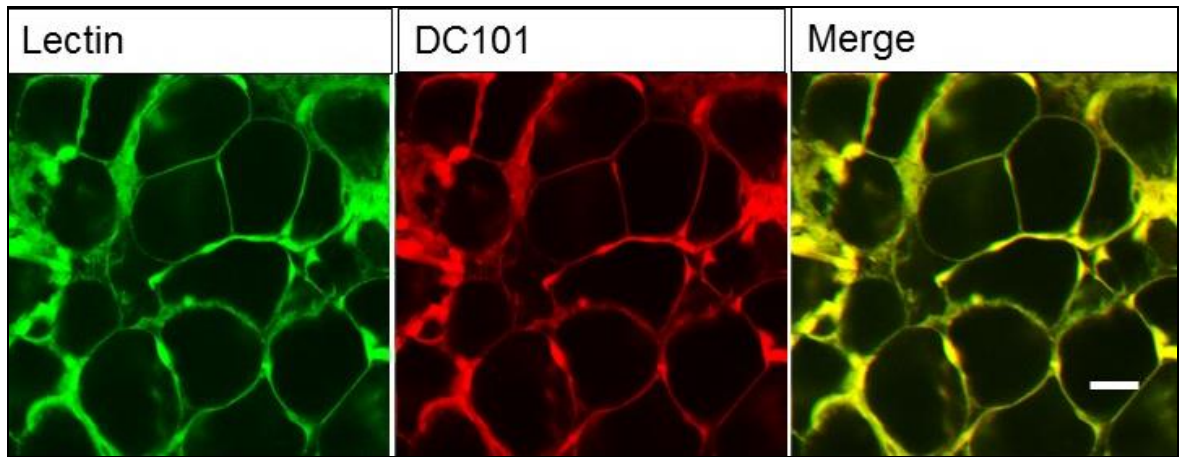


Figure 49. Fragment of the skin after DC101 cardiac infusion and perfusion.

DC101 was cardiac injected into P20 C57Bl/6 animals, and left for 5 minutes to allow the antibody to reach the circulation. Next animals were perfused and eyes were taken, fixed, permeabilised and incubated with Secondary antibody. The scale bar indicates 50 μm for all pictures.

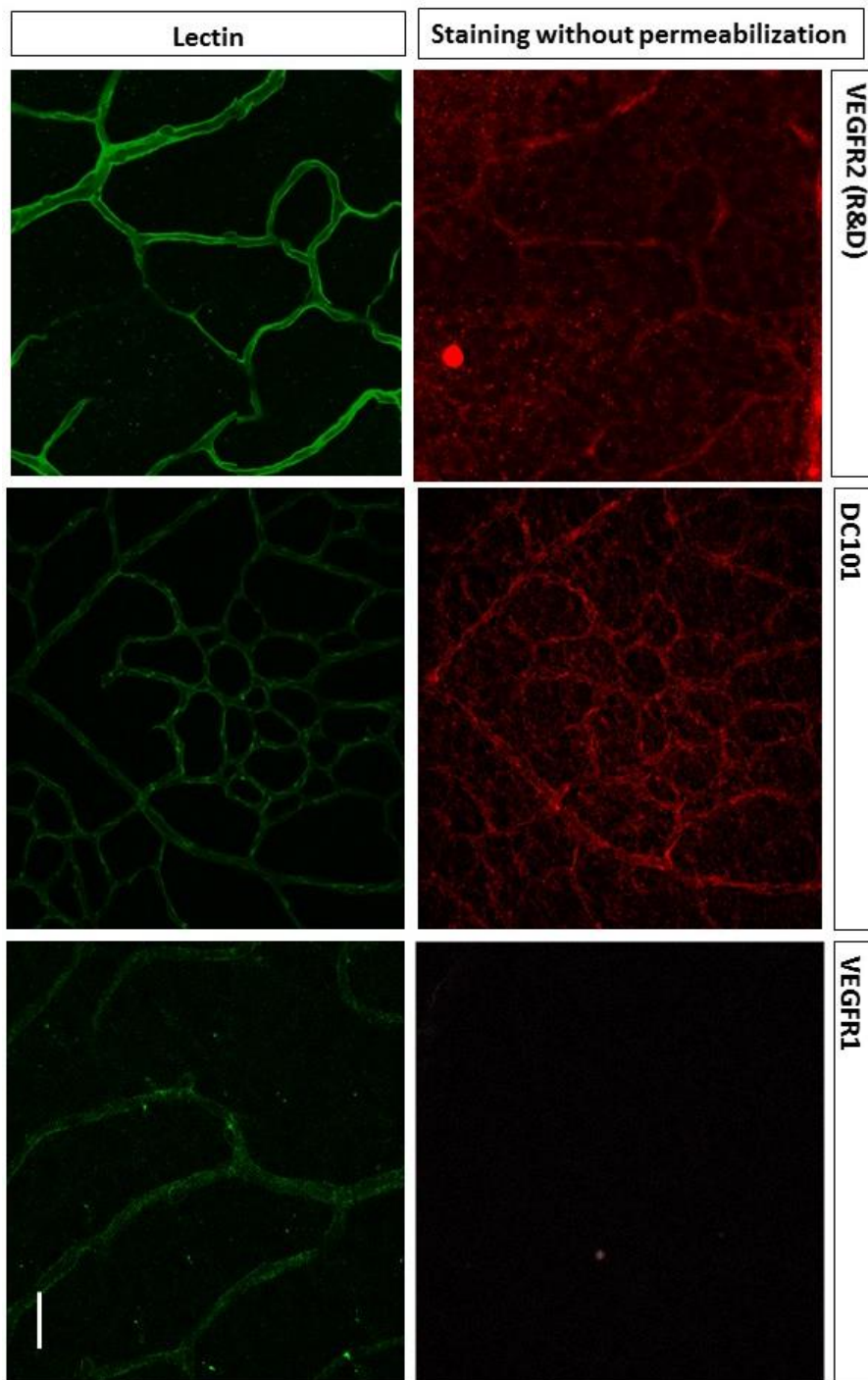


Figure 50. VEGFR1, VEGFR2 and DC101 staining without the permeabilisation step.

Eyes were processed as for routine immunofluorescent staining but the permeabilisation step was omitted.
The scale bar indicates 50 μm for all pictures.

The role of VEGF during Blood Retina Barrier development – discussion

VEGF-A is not only responsible for new vascular growth, but influences the permeability of EC. VEGF-A localisation in the retina matches the area where leakage has been detected with dextran and the biotin leakage assay, which enables crosslinking at sites of linkage and strongly highlighted the VEGF-A positive periphery. VEGF-A was implicated as an inhibitor of BRB formation, as shown in the experiments blocking VEGFR2 function where BRB function was improved in the animals injected with VEGFR2 blocking antibody.

Based on immunostaining of VEGFR-1 and -2 we can conclude that VEGFR-1 is mainly localised in the vasculature whereas VEGFR-2 exhibits vascular and nonvascular – neuronal localisation in the retina. I performed antibody tracer experiments, to explore if the BRB is associated with polarisation of the VEGFR's.

In-vivo or ex-vivo exposure of antibodies specific to the VEGF receptors and post- processing with or without permeabilisation suggested that, as with the BBB, VEGFR2 is mainly localised on the abluminal side of the EC, whereas VEGFR1 is expression is mainly luminal.

This interesting finding appears to confirm recently published data that VEGF-A induced permeability only, when presented to the abluminal side of the vasculature (Hudson, 2014). Hudson *et al.* found that VEGF-A did not promote permeability of microvessels in the brain or eye when intravenously injected into mice, but did increase permeability when administered directly into the eye or brain. Additionally they reported that in the primary cerebral MVECs isolated from rats, VEGF-A induced permeability only when administered to the basal side of the MVEC monolayer. These findings were supported with data that also shows polarised distribution of VEGF receptors.

Chapter 5.

Phosphoproteomic comparison of P5 and P15 retinas

The previous chapter suggests that VEGF-A expression promotes vascular permeability during postnatal development and hence prevents BRB formation. Yet, there is still little known of events downstream of VEGF-A signalling, and of mechanistic changes that accompany barrier formation. Knowing the timing of BRB formation allows us to probe for pathways implicated in barrier function, across the period of barrier acquisition using comparative methods such as subtractive proteomics, RNAseq or comparative phosphoproteomics.

Phosphoproteomic study of P5 and P15 retina protein extracts

We decided to explore the differences between P5 and P15 retina at a phosphoproteomic level, since we already had evidence that the VEGFR2 receptor tyrosine kinase may be involved in pre-barrier vascular permeability.

Phosphoproteomic analysis of the protein extracts was performed in collaboration with the Roche Innovation Center Basel.

Samples were analysed by Liquid chromatography and mass spectrometry (LC-MS) and data were processed using Proteome Discoverer Software. This software performs peptide grouping (assembling all identical phosphopeptide - same sequence and same mass) and keeps the one with highest identification score. This allows to remove redundancy in the data. Over 10000 different phosphopeptides were identified in the samples: 6331 single, 3610 double, 456 triple phosphorylations in peptide group. Most of the detected phosphorylations were Serine 88%, threonine 10.1%, tyrosine 1.6% and ambiguous phosphorylations 0.3% (Figure 51).

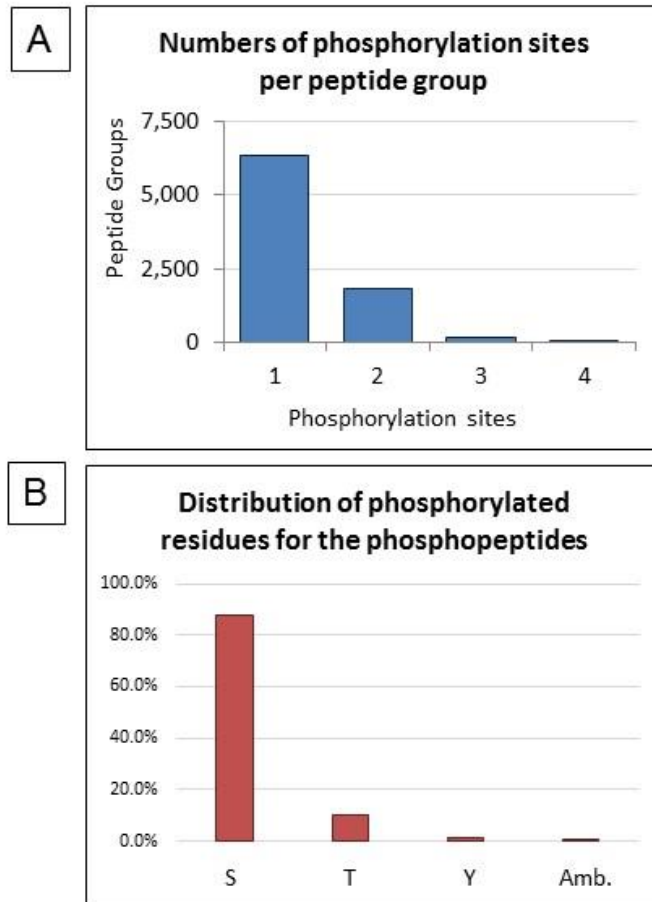


Figure 51. Phosphopeptides identified in the P5 and P15 samples.

A - Numbers of phosphorylation sites per peptide groups

B - Distribution of phosphorylated residues for the phosphopeptides. Ser, Thr, Tyr represent 88.0%, 10.1%, 1.6%, respectively.

Data provided by PhD Manuel Tzouros (Roche Innovation Center Basel).

Out of all identified phosphorylations we tried to determine the ones that were significantly different between P5 and P15 samples.

Using the Reactome Pathway Database we analysed the pathways associated with up-/down- phosphorylated proteins. Table 12 represents selected up-/down-regulated pathways and proteins that were modified between P5 and P15.

Table 12. Proteins that are differentially phosphorylated between P5 and P15.

Associated pathways were analysed with Reactome Pathway Database.

Junction interactions		Ratio P15/P5
Cadherin-10	S784	2.1759
Catenin alpha-1	S641	0.5740
	S641; S652	0.4347
Catenin alpha-2	T264	2.6693
	S640; S651	1.5277
	S901	1.5473
	S939	2.2140
Catenin alpha-3	S637	23.1834
Catenin beta-1	S191	0.5612
	S552	1.8678
	Y489	0.2499
Catenin delta-1	S47	0.3611
	S252	0.2516
	S268	0.4188
	S346	0.4320
	S346; S352	0.3809
	Zona occludens protein ZO-1	S353
Zona occludens protein ZO-1	S617	0.4952
	S125; S131	0.7085
	S275; S280	0.5124
	Zona occludens protein ZO-2	S684
Zona occludens protein ZO-2	S968	0.6734
	S1008	0.6360
	S1030; T1031	0.5663
	Zona occludens protein ZO-3	S195
Zona occludens protein ZO-3	S195	0.3293
VEGF-A Signalling		
Protein kinase Src	S17	0.4932
	S21	0.3795
	T73	0.4874

Focal adhesion kinase 1 (FAK)	Y608	0.7489
serine/threonine-protein kinase (Akt)	S122	0.4849
	S124	0.4021
	S124; S126	0.4858
	S126; S129	0.4131
Mitogen-activated protein kinase 1	T183; Y185	5.6231
Mitogen-activated protein kinase 3	T203; Y205	5.2628
Mitogen-activated protein kinase 6	S189	0.6659
Mitogen-activated protein kinase 8	Y185; Y223	3.6993
Protein kinase C alpha type	S319	10.1822
	S321	10.2009
Protein kinase C beta type	T642	2.7881
Protein kinase C epsilon type	S368	3.2744
	S388	5.4437
	S346; T349	6.5808
Signalling by Rho GTPases		
Rho GTPase-activating protein 1	S27	4.4188
	S44	2.4565
	S44; S47	6.1629
	S49; S51	2.6688
Rho GTPase-activating protein 5	S1194	1.8862
	S1201	1.5603
Rho GTPase-activating protein 7	S89	0.5207
	S505; S510	0.6569
Rho GTPase-activating protein 17	T736	0.5488
	T730; T736; S739	0.5827
Rho GTPase-activating protein 20	S46	3.8138
Rho GTPase-activating protein 21	S41	0.5441
Rho GTPase-activating protein 23	S12	1.4175
	S515	0.3481
	S594	1.6705
	S619	1.5363
Rho GTPase-activating protein 24	S414	3.7486

Rho GTPase-activating protein 26	S609	2.6012
Rho GTPase-activating protein 31	S1242	0.2628
Rho GTPase-activating protein 39	T165	1.3094
Rho GTPase-activating protein 42	Y759	2.5252
Rho guanine nucleotide exchange factor SYX	S938	0.6215
Rho guanine nucleotide exchange factor 2	S931	0.5520
	S955	0.5339
Rho guanine nucleotide exchange factor 6	S679	4.8226
Rho guanine nucleotide exchange factor 10	S34	0.7659
Rho guanine nucleotide exchange factor 12	T189	0.7385
	S309	0.7331
	S637	0.5549
Rho guanine nucleotide exchange factor 18	S927	0.5888
Rho guanine nucleotide exchange factor 7	S151	0.6436
	S155	0.4890
	S497	0.3840
	S673	1.6804
Rho guanine nucleotide exchange factor 40	S415	0.5938
	S959	0.3504
Smooth Muscle Contraction		
Myosin regulatory light chain	S19	0.4640
Protein phosphatase	S618	1.6290
	S870	0.5499
	T858	0.5763
Myosin light chain kinase	S355	1.9265
	S381	1.8065
	S802	1.4784
	S1795	2.9708
Regulation of beta-Catenin		
B-cell CLL/lymphoma 9 protein	S278	0.5655
	S688	0.4562
	S916	0.6228
	T115	0.2996

	S102; T115	1.4398
Transducin-like enhancer protein 3	S217	0.3127
	S240	0.4717
	S289	0.5887
	S203; S207	0.2228
	S240; S245	0.3940
	S263; S267	0.4105
	Signal Transduction	
Reticulon-4	S344	1.8022
	S768	1.4872
	S953	1.9245
	Y861	1.8013
	Serine/threonine-protein phosphatase 2B catalytic subunit alpha isoform	
	S469	3.3231
	S498	7.4922
Rhodopsin	S334	42.5197
	S338	33.2759
	S334; S339	15.2473
	S334; T340	41.1346
	T336; S338	24.6535
	S338; T340; S343	36.6474
	Prickle-like protein 1	
	S684	0.7550
Recoverin	S72	30.9000
Regulator of G-protein signaling 9-binding protein	S133	42.4244
	S140	25.7306
Transmembrane Transport of Small Molecules		
Protein unc-79 homolog	S1242	9.5560
Monocarboxylate transporter 1	S213	7.6226
	S230	5.5696
	S461	18.7000
	S210; S213	5.3143
	S461; T462	8.4596
	Sodium-driven chloride bicarbonate exchanger	
	S89	8.7250

	S276	15.6138
	S247	20.4620
	S276; S280	9.2472
High affinity choline transporter 1	S550	28.7705
	S573	16.8881
Solute carrier family 12 member 5	S963	12.3707
	S955	15.2748
	S963	12.3707
	S955; S963	3.5388
	S1044	5.7637
	S1044; S1047	7.2729
Phospholemman	S82	1.8598
	S83	1.8371
Sodium- and chloride-dependent GABA transporter 3	S21	4.3090



Pathways regulated by protein phosphorylation between P5 and P15

Adherens junction interaction

Phosphoproteomic analysis provided numerous examples of the regulation of known permeability and barrier-associated proteins which vary between P5 and P15 retina. One interesting set of proteins were associated with adherens junction interactions. There was a drastic change in phosphorylation of many proteins, involved in adherence and tight junction formation, at P15 retina compared to P5 (Table 12). This is particularly interesting as there are many reports indicating that phosphorylation of tight junction and adherens junction molecules is associated with increased permeability of endothelial cell monolayers. For example, Weiyong Shen and colleagues showed a dose dependent increase in paracellular permeability of retinal microvascular endothelial cells after TGF- β 1 treatment, and both decrease in expression of VE-cadherin and Claudin-5, and increase of tyrosine phosphorylation of VE-cadherin and Claudin-5 at zones of intercellular contact (Shen, 2011b).

Clayburgh and colleagues showed that upon disruption of the intestinal epithelial barrier, occludin was internalized into intracellular vesicles, but there was no changes in Claudin-1, Claudin-4 and Claudin-5 distribution (Clayburgh, 2005)

Interestingly no tyrosine phosphorylations for Claudin-5 and VE-cadherin were detected with the phosphoproteomic study, however many other significant junction molecules modifications were identified. One of the interesting changes recognised in the study, was an increase in S784 phosphorylation for Cadherin 10. It was previously reported that the pattern of expression of Cadherin-10 is consistent with a key role in forming and maintaining the barriers. Cadherin-10 is present in BBB endothelia, but absent from the endothelia of leaky brain vessels and non-brain vessels (Williams, 2005). This could suggest that Cadherin-10 might be involved in BRB function.

The association of Cadherins with cytoskeleton is mediated by β -catenin, a key protein in the cadherin-catenin cell adhesion complex. Our analysis also showed changes in β -catenin phosphorylation: a decrease of phosphorylation at S191 and Y489, and an increase of phosphorylation at S552 (Figure 52). The decrease in tyrosine phosphorylation at P15, is very interesting as there are reports showing that tyrosine phosphorylation is a major mechanism responsible for destruction of junctional apparatus via loss of cadherin - β -catenin complex (Tominaga, 2008, Rhee, 2002).

Cadherin - β -catenin complex is connected with actin cytoskeleton via α -catenin (Sarpal, 2012). Restoring expression of α -catenin in the prostate cancer cell line (PC3), which due to the chromosomal abnormalities, renders PC3 cells null for the expression of α -catenin, restores junctional complexes. These show that α -catenin has a critical role in supporting the cadherin cell-cell adhesion function and formation of junctional complexes. Inge *et al.* showed in their report that α -catenin protects β -catenin from Src phosphorylation by increasing the stability of its interaction with E-cadherin (Inge, 2008). These findings underline the importance of α -catenin in junction formation and function. For this reason we decided to analyse in detail the changes in α -catenins phosphorylation between P5 and P15 retina tissue.

Analysis of the phosphorylation of α -catenins showed a decrease in phosphorylation of α -catenin 1 (S641; S641/ S652) and an increase in phosphorylation of α -catenin 2 (T264, S640/S651, S901, S939) and a very significant increase in phosphorylation of α -catenin 3 on S637 (Figure 53). The remarkable increase of S637 phosphorylation of α -catenin 3 is particularly interesting, as it has been shown that phosphorylation of α -catenin contributes to intercellular adhesion in mammalian cells and *Drosophila* (Escobar, 2015).

Another important player in modulating cell-cell adhesion required for cadherin stability is δ -catenin, also called p120-catenin (p120) (Brown, 2009). In contrast to the β -catenin, which associates with α -catenin and is believed to participate in coupling the cadherin–catenin complex to the actin cytoskeleton, δ -catenin binding stabilises cadherins at the cell surface (Oas, 2013). Interestingly, phosphorylation of δ -catenin mediated by PKC α induces AJ disassembly and VE-cadherin internalisation (Vandenbroucke St Amant, 2012).

In the phosphoproteomic study, we found that most of the δ -catenin phosphorylations are decreasing at P15 compared to P5 (S47, S252, S268; S346; S346/S352) (Figure 54).

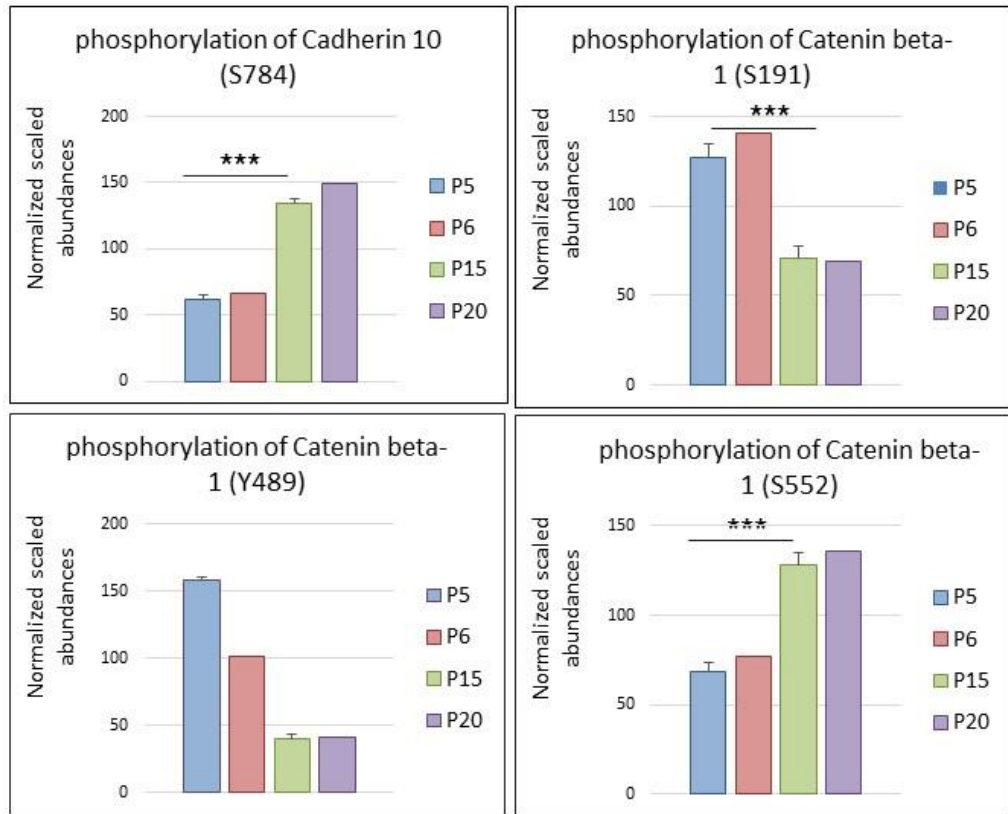


Figure 52. Changes in phosphorylation of AJ proteins between P5 and P20 retina.

For all the following phosphoproteomic analyses, the following will apply: Each sample of protein extract, was prepared from 16 retina tissues for P5 and P6, and 10 retina tissues for P15 and P20. The volume of protein extract used for the phosphoproteomic assay was determined by final protein concentration. The numbers of repetitions performed are as follow: P5 - N=4; P6 - N=1; P15 - N=4; P20 - N=1. A student t-test was run on P5 and P15 samples. The criterion for statistical significance was p-value < 0.05 (*), 0.01(**) or 0.001 (***)

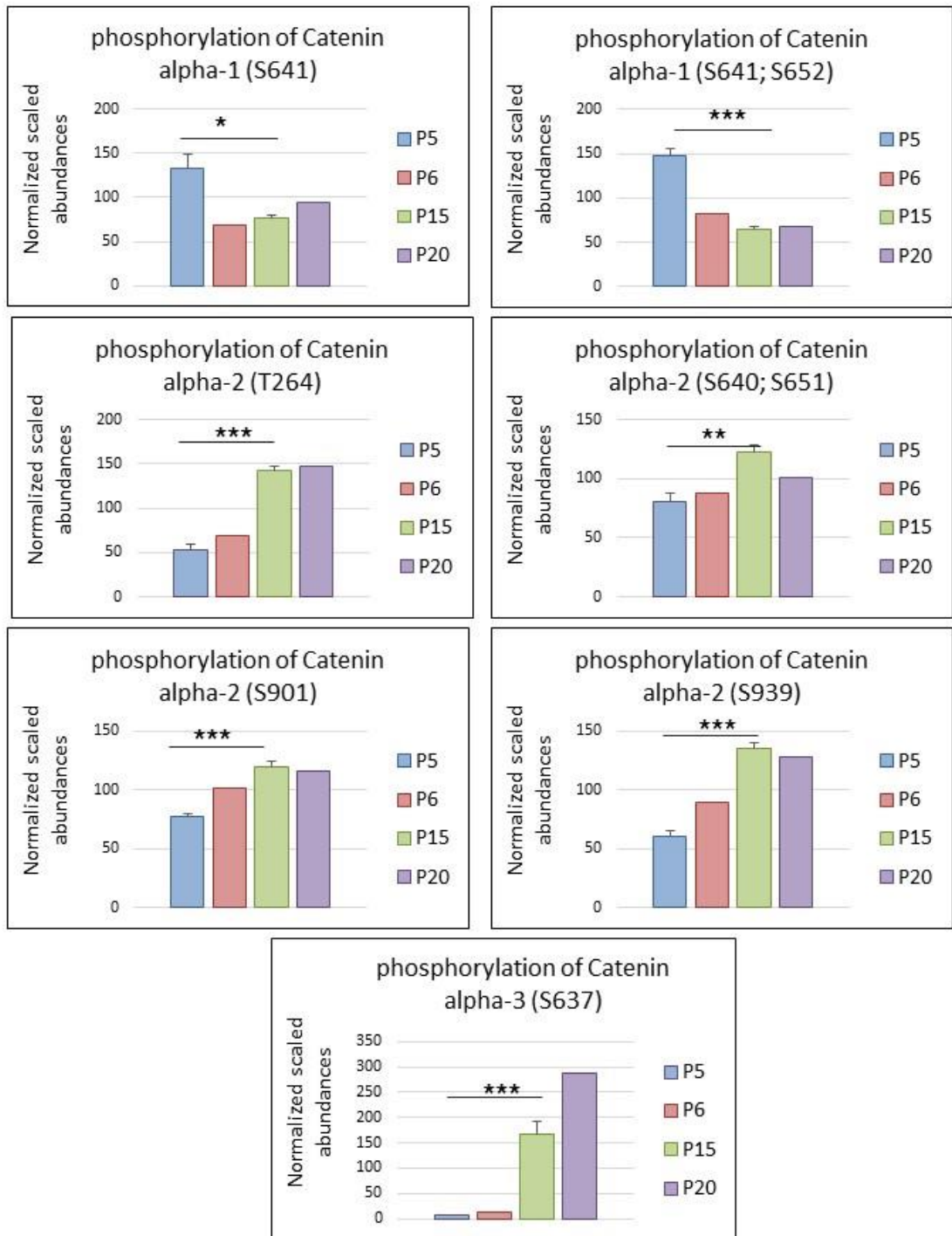


Figure 53. Changes in phosphorylation of α -catenin proteins between P5 and P20 retina.

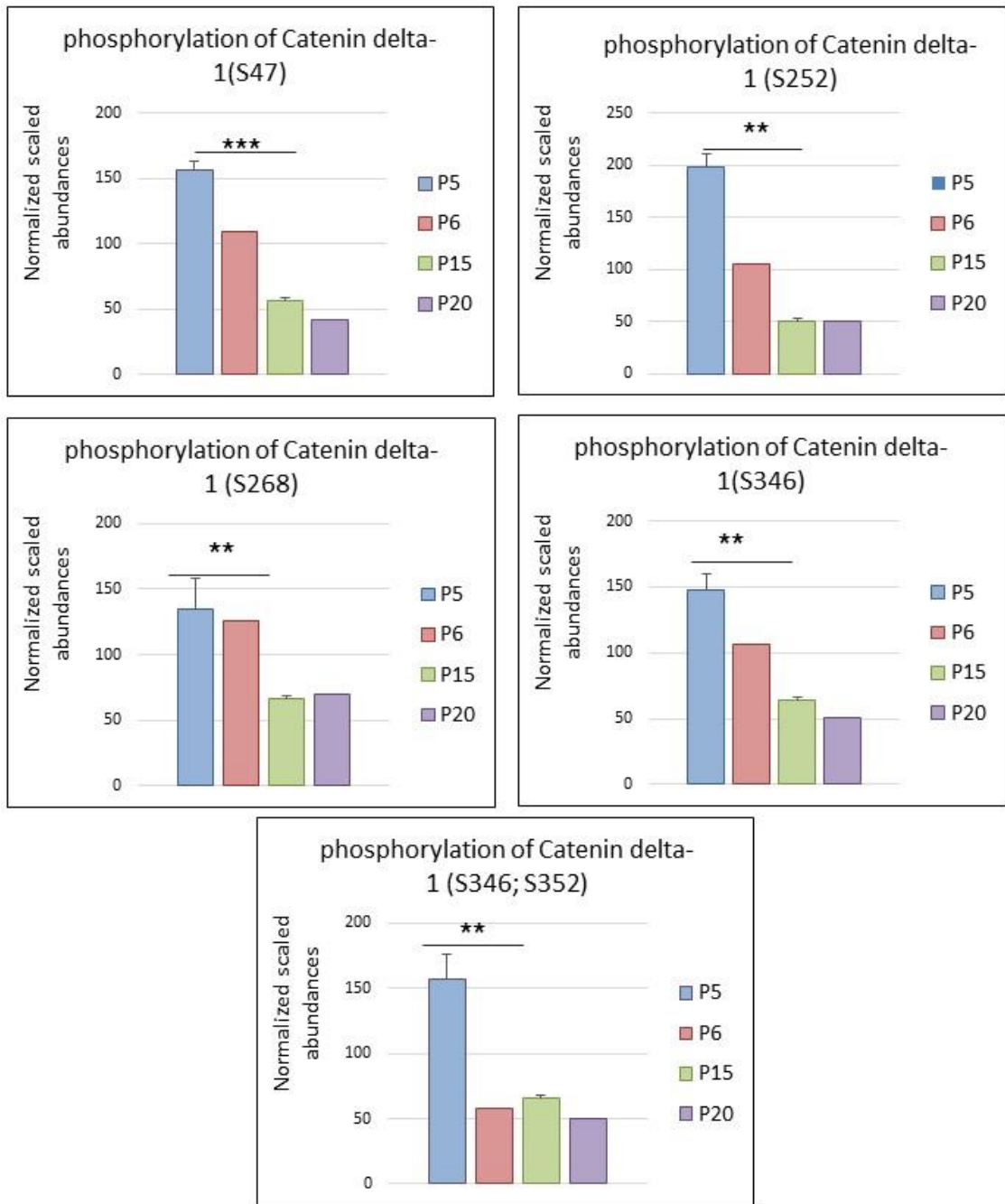


Figure 54. Changes in phosphorylation of δ -catenin between P5 and P20 retina.

Significant changes in phosphorylation were also found for proteins forming TJ – ZO-1, ZO-2 and ZO-3. Higher phosphorylation of ZO-1 (S353, S617, S125/S131, and S275/S280), ZO-2 (S684, S968, S1008, and S1030/T1031), and ZO-3 (S195) were found at P5, when BRB does not maintain barrier function, compared to P15 when BRB is fully formed (Figure 55-56). This is interesting,

as it has been reported that changes in ZO-1 phosphorylation and expression, are associated with the breakdown of the BRB in diabetic retinopathy (Antonetti 1999, Rincon-Choles, 2006).

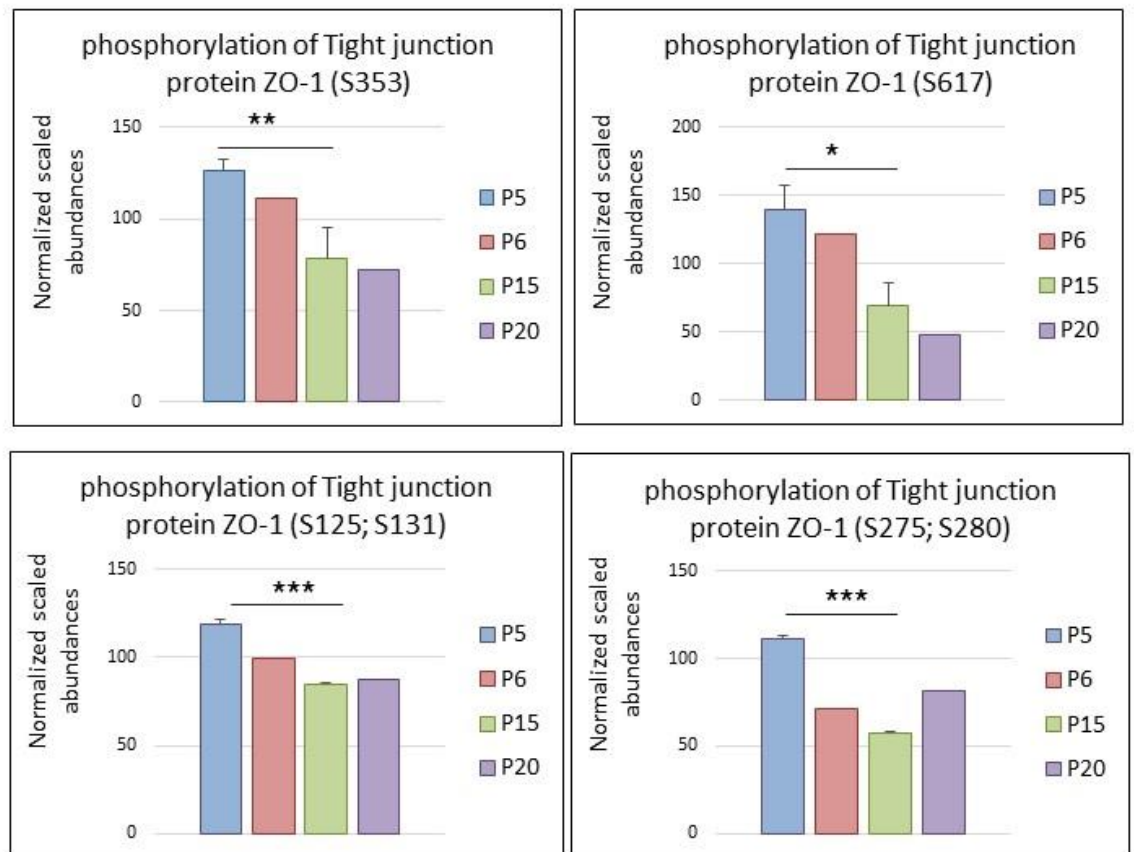


Figure 55. Changes in phosphorylation state of ZO-1 protein between P5 and P20 retina.

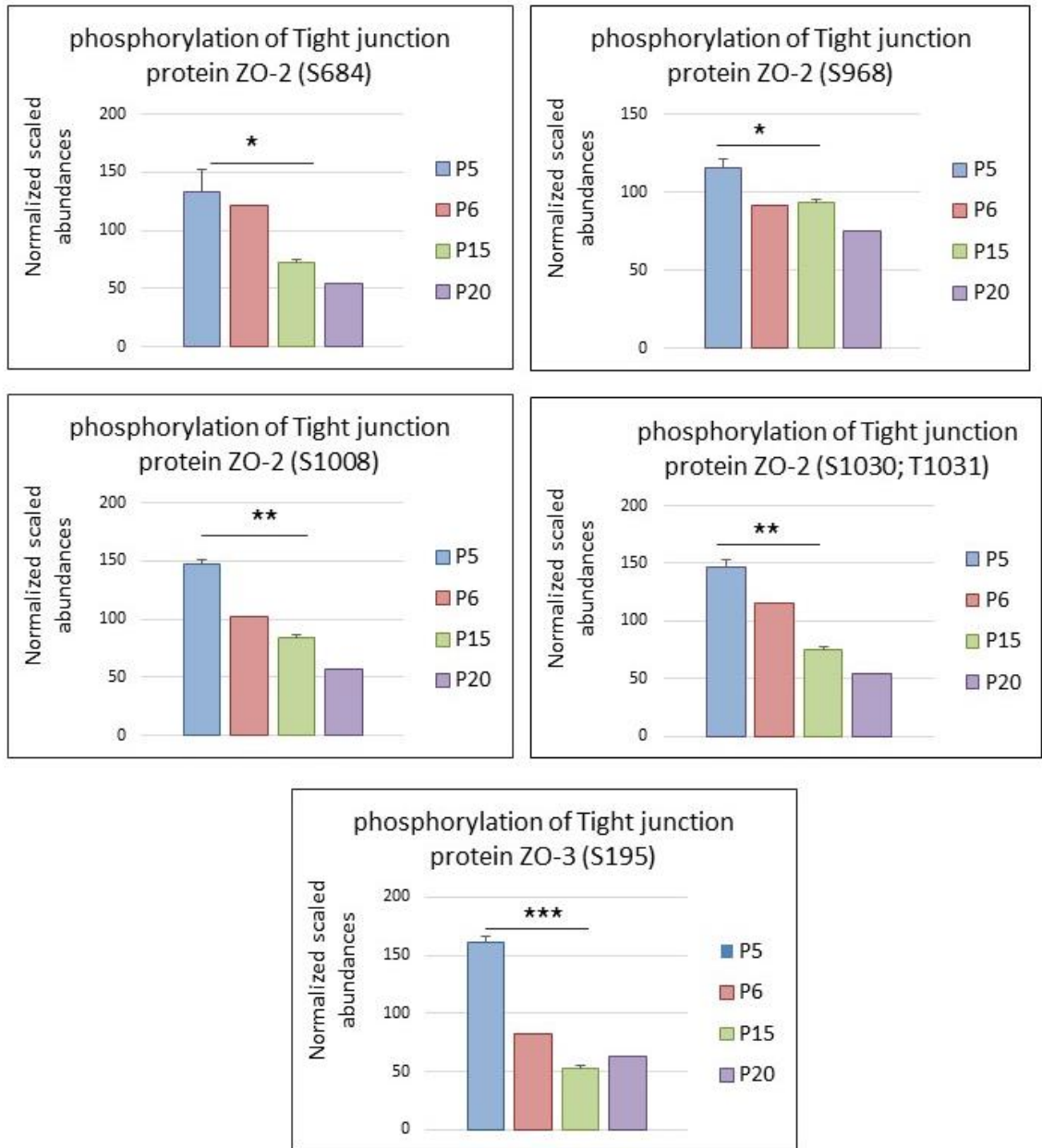


Figure 56. Changes in phosphorylation state of ZO-2 and ZO-3 protein between P5 and P20 retina.

This data strongly suggests that the transition from vascular permeability to BRB formation is accompanied by the dephosphorylation of a majority of AJ and TJ proteins.

VEGF-A signalling

VEGF-A signalling is also characterised by significant changes in protein phosphorylation. Given our data implicating VEGF-A as a negative regulator of

BRB acquisition during post-natal development, we examined some known downstream signalling proteins. A decrease in phosphorylation at P15 compared to P5 was found for tyrosine protein kinase Src (S17, S21, and T73) and Focal adhesion kinase (FAK) (Y608) (Figure 57).

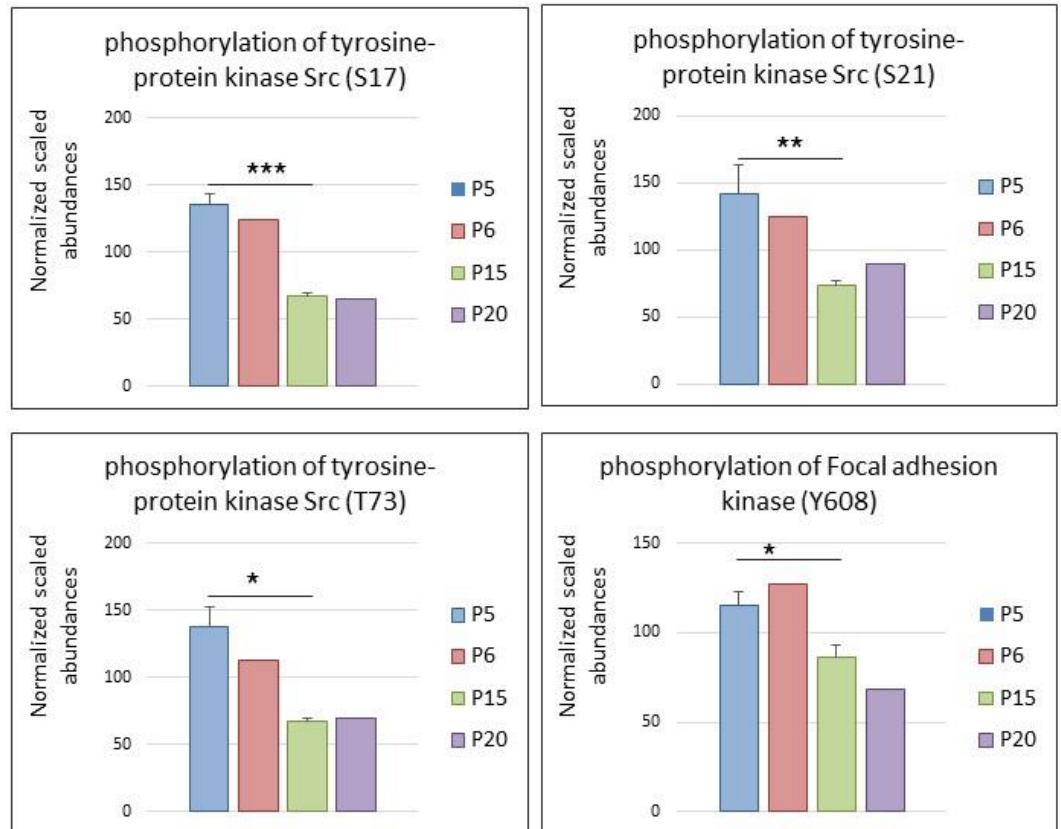


Figure 57. Changes in phosphorylation of tyrosine protein kinase Src and Focal adhesion kinase.

The Src family of protein kinases are implicated in a variety of vascular-related functions. VEGF-A driven angiogenesis has been shown to require Src kinase activity (Lamallice, 2006). It has also been demonstrated that VEGF-A via Src induces the site-specific tyrosine phosphorylation of FAK that is involved in angiogenesis (Eliceiri, 2002).

Akt-1 is a multifunctional serine-threonine protein kinase involved in a diverse range of cellular functions like cell metabolism, survival, migration, and gene expression. Genetic loss of Akt-1 in mice causes ischemia and defective VEGF-induced angiogenesis, reduced endothelial progenitor cell numbers (EPC)

as well as severe vascular disease (Ackah, 2005). Phosphoproteomic analysis indicated significantly stronger phosphorylation of Akt-1 (S122, S124, S124/S126 and S126/S129) at P5 (Figure 58).

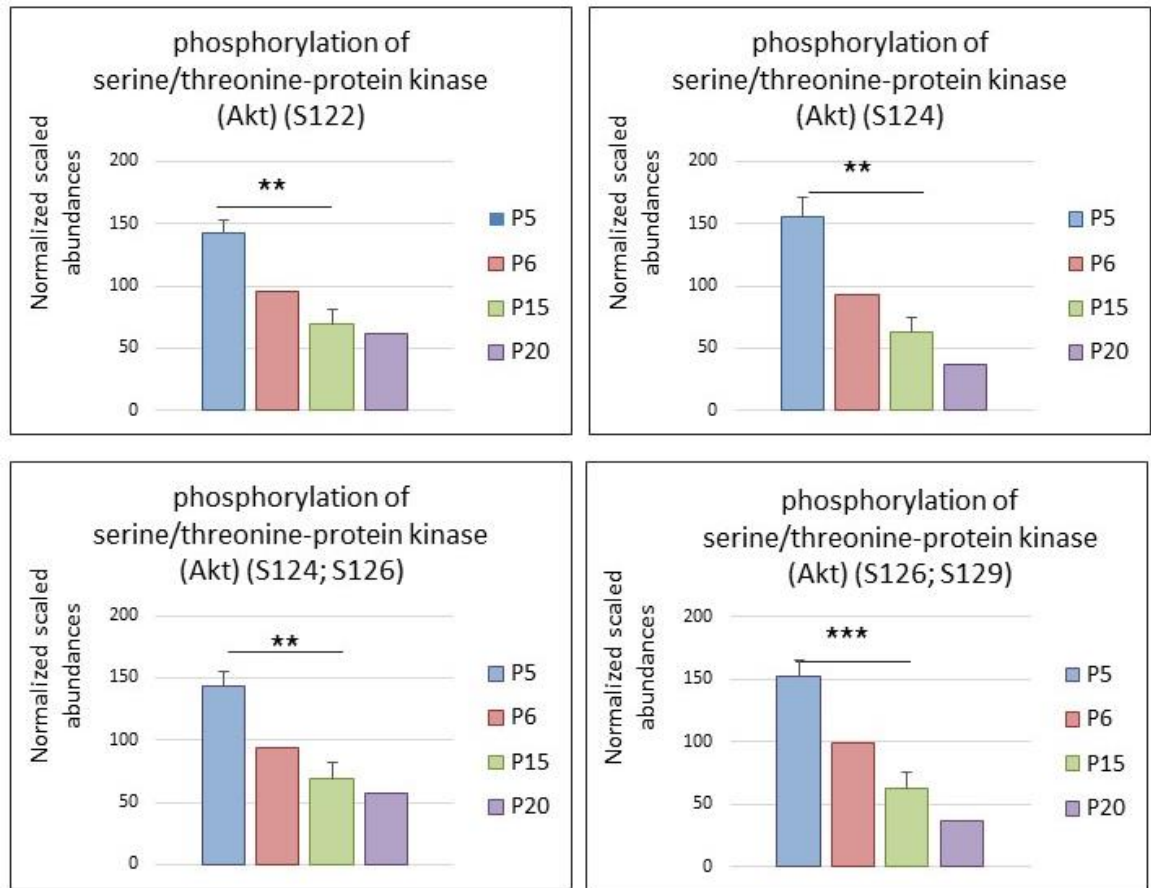


Figure 58. Changes in phosphorylation of Akt-1 in the retina between P5 – P20.

Interestingly, changes in phosphorylation were also found for Mitogen activated protein kinase (MAPK), however, the change was an increase in phosphorylation for MAPK1 (T183/Y185), MAPK3 (T203/Y205), MAPK8 (Y185/Y223) and a decrease in phosphorylation for MAPK6 at S189 (Figure 59). Interestingly UniProt database confirms that MAPK1 requires phosphorylation at T183/Y185 and MAPK3 T203 and Y205 for activity (Robbins, 1993, Zhang, 2012).

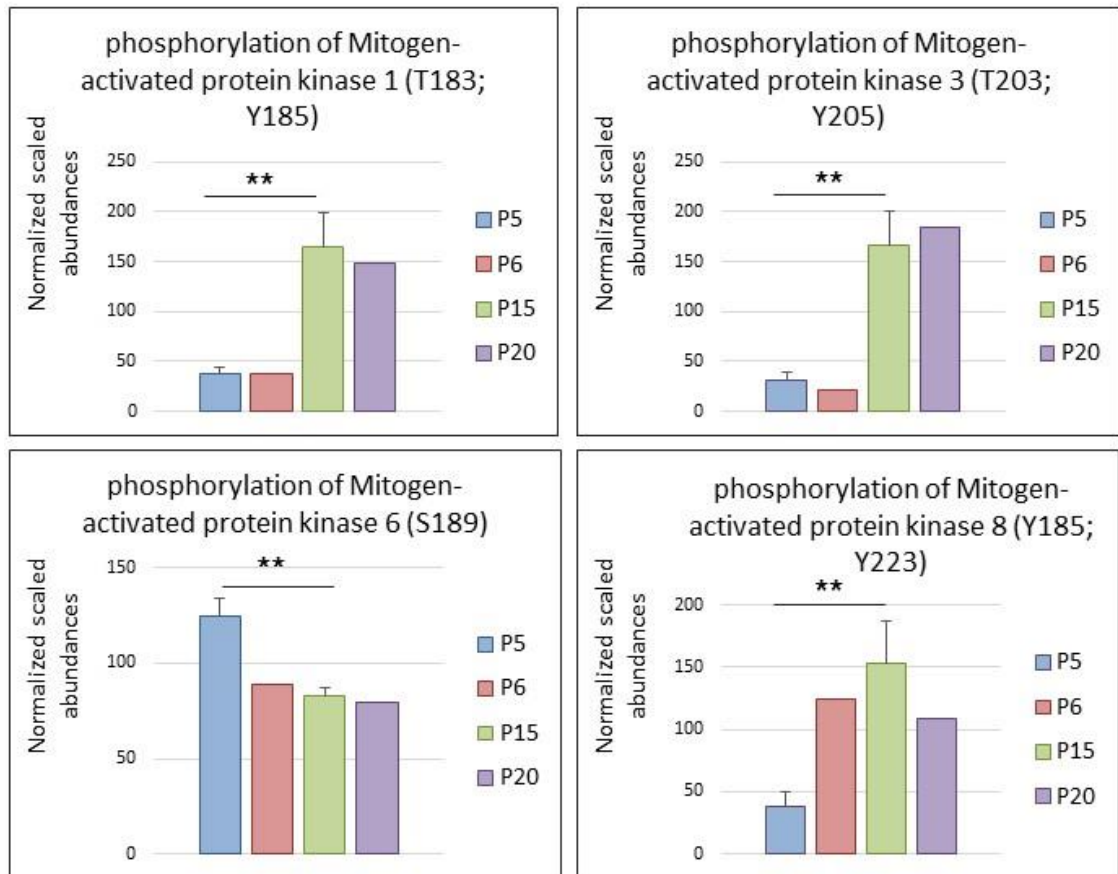


Figure 59. Changes in phosphorylation of MAPK in the retina between P5 – P20.

Protein kinase C (PKC) is a well-recognised effector of VEGF-A signalling. They belong to a family of phospholipid-dependent serine/threonine kinases that play key roles in many of the signalling pathways that control cellular growth, proliferation, differentiation and cell death. Phosphoproteomic analysis showed interesting changes in phosphorylation of various PKC isoforms in the retina, at different stages of post-natal retinal development. Increases were found for PKC- α at S319, and S321, PKC- β at T642, and PKC- ϵ S368, S388, S346/T349 (Figure 60).

Increased phosphorylation of various isoforms of PKC at later stage of retina development is a surprising and interesting finding. PKC is known for its involvements in VEGF-A regulated pathways, this is why we would expect to detect higher phosphorylations of PKCs at P5 compared to P15. For example PKC- β , which has been previously described by Murakami, is involved in

occludin phosphorylation downstream VEGF-A signalling, since PKC- β inhibitors blocked occludin phosphorylation (Murakami 2012).

The modulation of PKC activity via phosphorylation is highly complex. PKC undergoes phosphorylation at the A-loop, turn motif (TM) and hydrophobic motif (HM) sites, and these phosphorylations have been described as maturational or priming events that are processing of newly-transcribed PKC to the mature (but still inactive) form. However, PKCs can also undergo inducible phosphorylation at these sites following stimulation. Inducible phosphorylation of PKC is often interpreted as catalytic activation, which could be misleading for some isoforms. For example phosphorylation of PKC α or β II at the HM might not correlate with catalytic activation, but instead is more indicative of a stable enzyme conformation (Freeley, 2011, Bornancin, 1997, Edwards, 1997). Identification of PKCs role during vascular formation requires detail characterisation of specific phosphorylation sites of individual PKCs. For example, using phospho-specific antibodies to these sites might help us to localise phospho-PKC at different stages of vascular development and thus allow finding correlation between the changes in PKCs phosphor state, and concluding their involvement in retina vascular development.

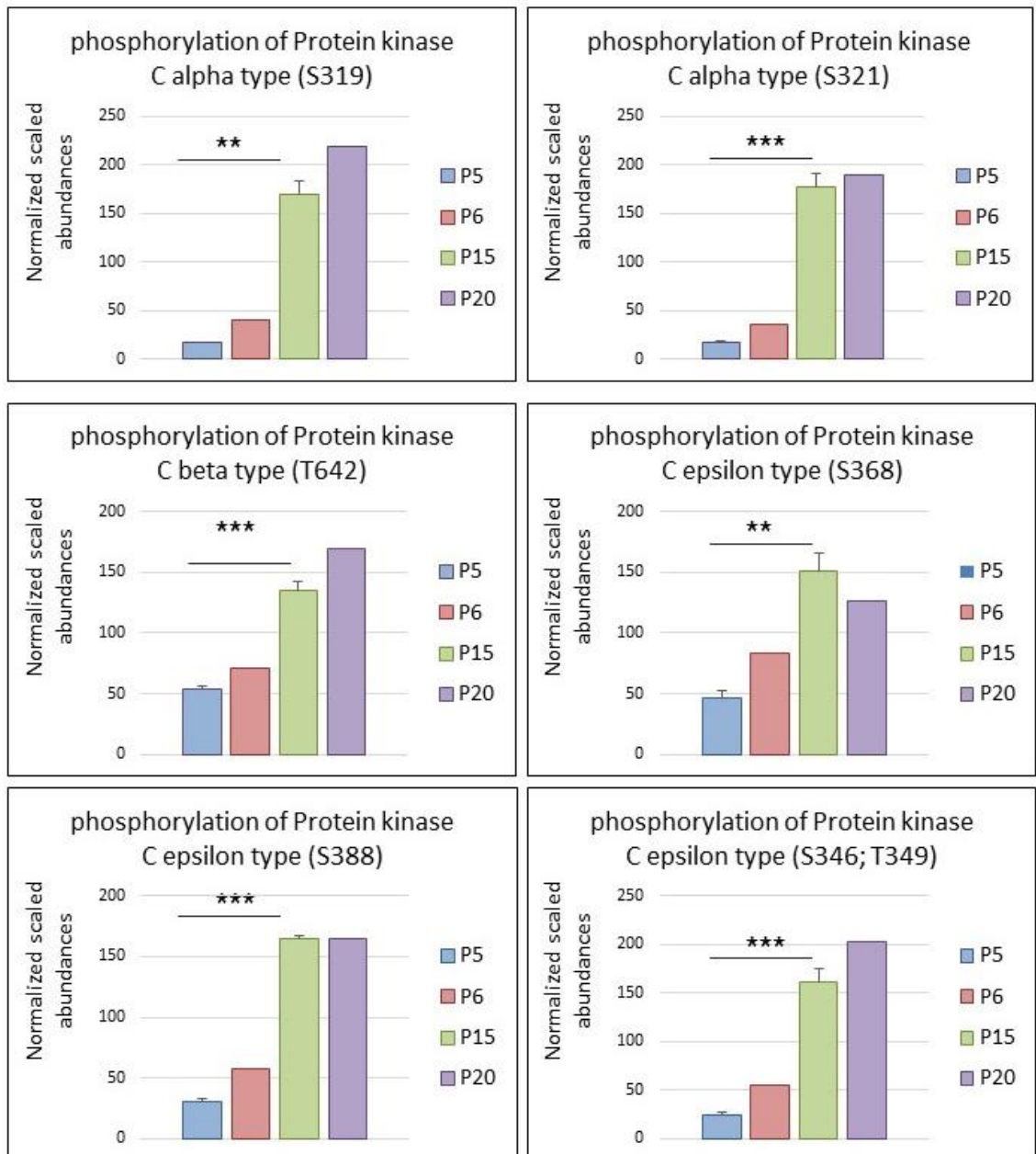


Figure 60. Changes in phosphorylation of PKC isoforms in the retina between P5 – P20.

Rho GTP-ases

The small Rho GTPases play an important role in regulation of cellular adherence, migration, and proliferation through control of actin-cytoskeletal assembly and cell contraction (Yao, 2010). Evidence suggests that Rho GTPases are essential for vascular endothelial growth factor (VEGF)-mediated angiogenesis (van der Meel, 2011). VEGF-A induces Rho GTP-ases which act as

molecular switches that promote EC migration and angiogenesis, accompanying growth factor-induced changes in the endothelial cytoskeleton (van Nieuw Amerongen, 2003).

The activity of Rho GTP-ases is regulated by Rho GTP-ase activating protein (GAP) and by Rho guanine nucleotide exchange factors (ARHGEF). GAPs inactivate Rho GTP-ase activity by enhancing their ability to hydrolyse bound GTP to GDP, and ARHGEFs catalyse the exchange of guanine diphosphate (GDP) for guanine triphosphate (GTP) (Figure 61).

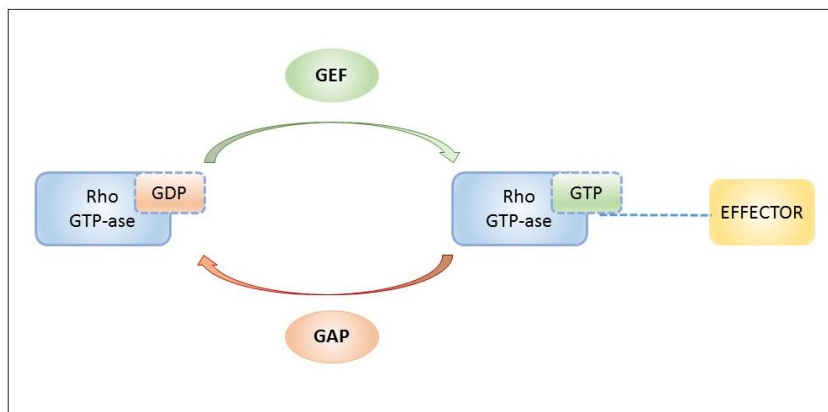


Figure 61. Schematic illustrating Rho GTP-ase activity.

The figure above has been adopted from *van der Meel 2011* and shows regulation of GTP-ase activity. Rho GTPase is activated by Rho guanine nucleotide exchange factors (ARHGEF), which catalyse the exchange of guanine diphosphate (GDP) for guanine triphosphate (GTP). GTP-ase activating protein (GAP) inactivates Rho GTP-ase activity by enhancing the ability to hydrolyse bound GTP to GDP.

Phosphoproteomic experiments revealed high up-/down-regulations of various GAP and ARHGEF proteins between different stages of retina development (Figure 62-65).

Changes in phosphorylation were found for GAP1, GAP5, GAP7, GAP12, GAP17, GAP20, GAP21, GAP23, GAP24, GAP26, GAP31, GAP32, GAP33, GAP35, GAP39, and GAP42 (Figure 62-63).

GAP converts Rho-GTP-ases to the inactive GDP-bound state; they are very specific for their substrates. Phosphoproteomic analysis showed numerous changes in phosphorylation of GAP proteins, however further research is required in order to identify their substrates and localisation in the retina.

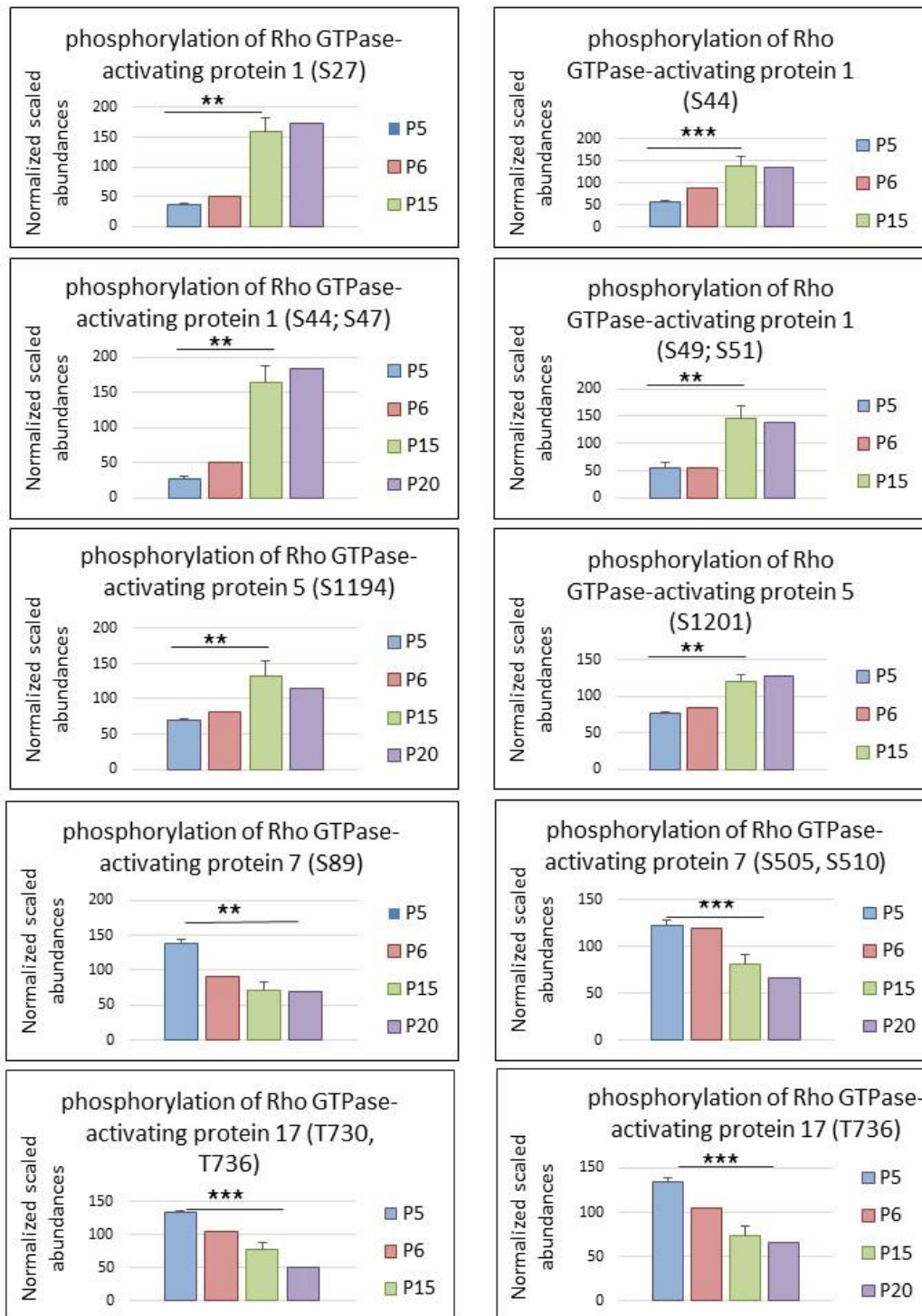


Figure 62. Changes in phosphorylation of selected GAPs in the retina between P5 – P20.

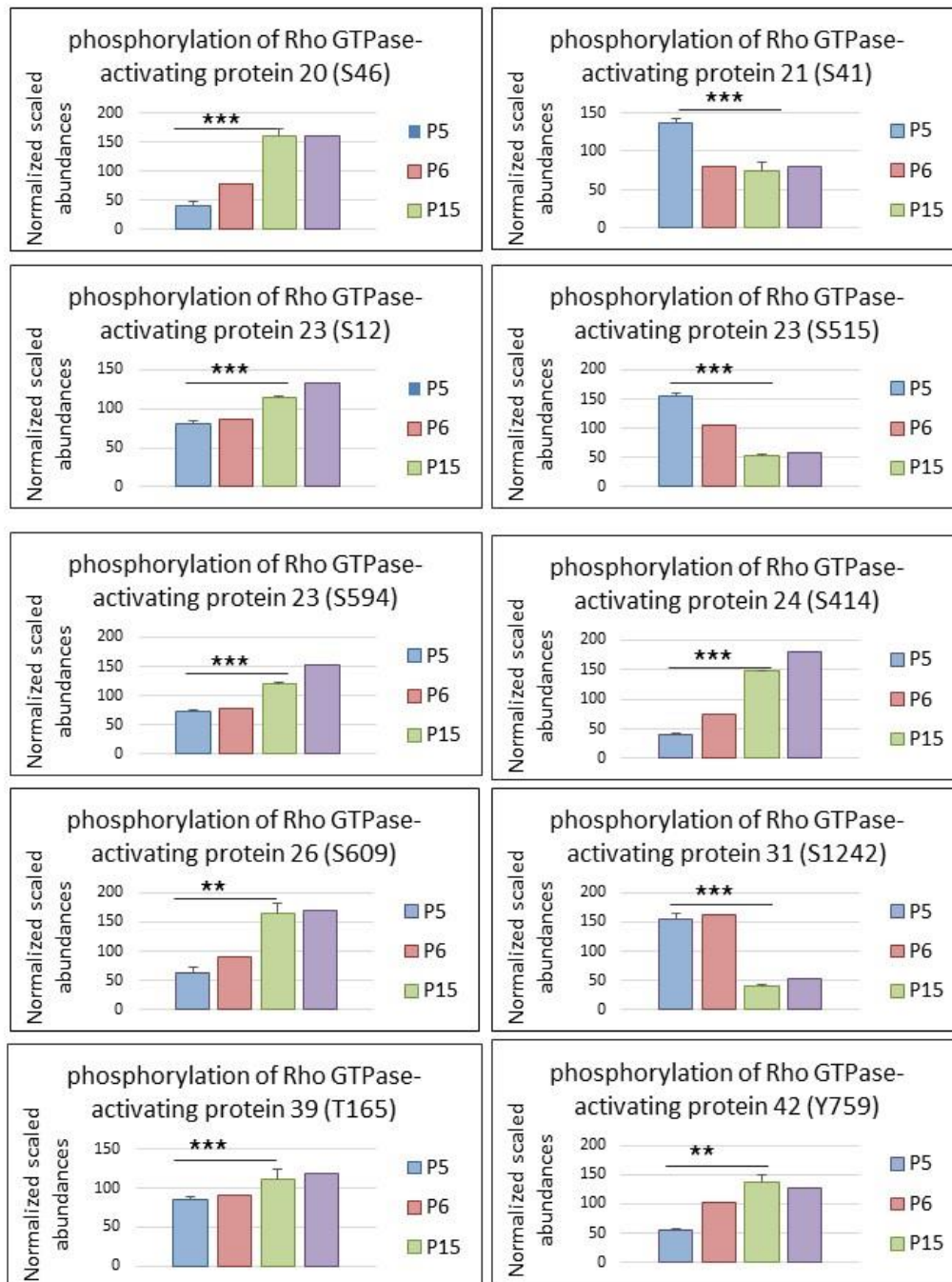


Figure 63. Changes in phosphorylation of selected GAPs in the retina between P5 – P20 (part2).

During retina development the following ARHGEFs were modified between P5 and P20: ARHGEF2, ARHGEF6, ARHGEF7, ARHGEF 10, ARHGEF 12, ARHGEF 18, and ARHGEF 40 (Figure 64-65).

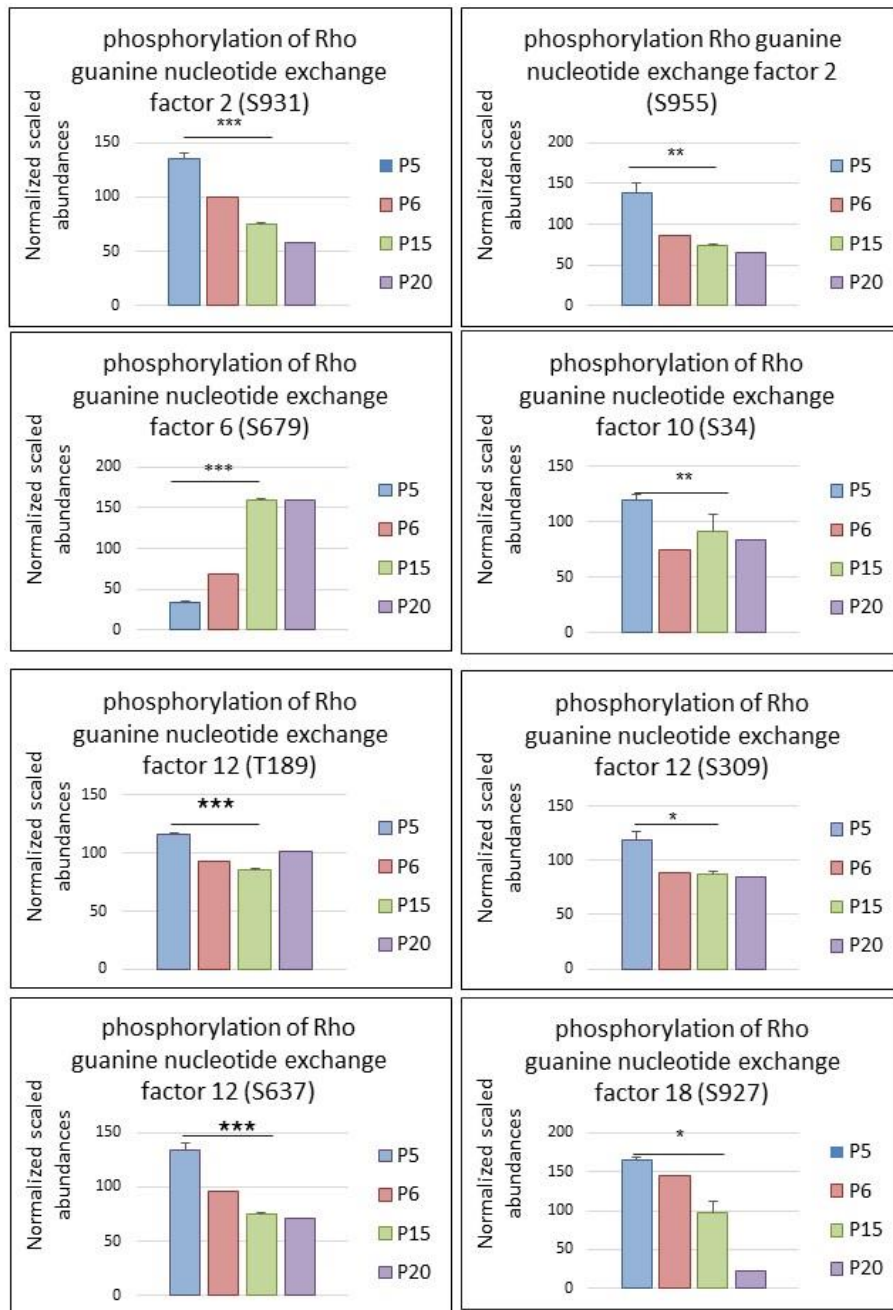


Figure 64. Changes in phosphorylation of ARHGEFs in the retina between P5 – P20.

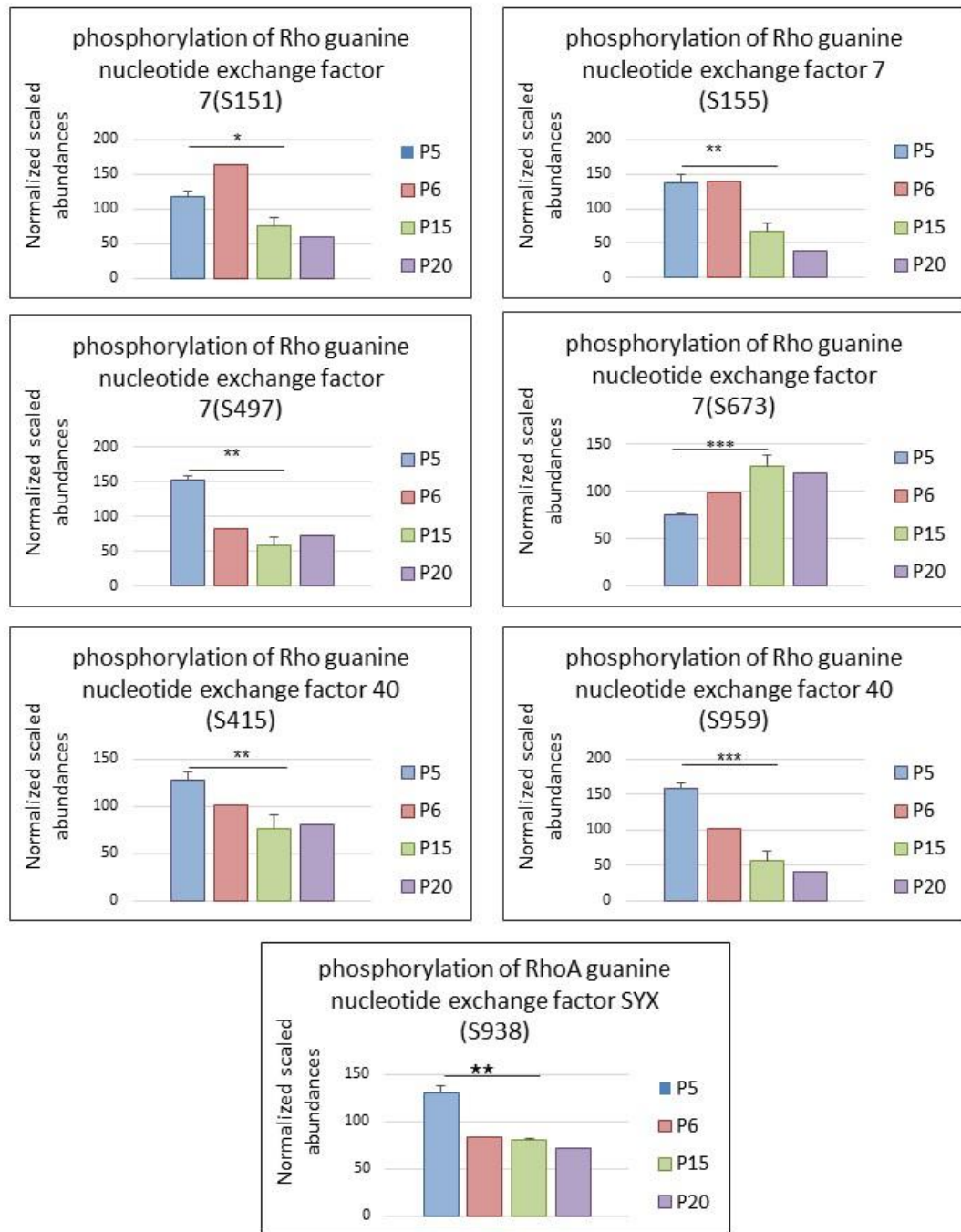


Figure 65. Changes in phosphorylation of ARHGEFs in the retina between P5 – P20 (part2)

There was a significant difference between P5 and P15 retina in the phosphorylation state of many GAPs and ARHGEFs.

Particularly interesting is the decrease in phosphorylation of RhoA guanine nucleotide exchange factor SYX at S938 at P15 (compared to the P5 retina), as it was published by Ngok and his colleagues, that VEGF-A induces

translocation of Syx from EC junctions, and via protein kinase D1 (PKD1) mediated serine phosphorylation of Syx. Syx phosphorylation reduces its association to junctions, and results in junction disassembly, increases in permeability and induces vascular leakages (Ngok, 2012). This is interesting as the phosphoproteomic assay showed higher serine phosphorylation of GEF Syx at P5, when we observe higher leakages in vascular retina, especially in the periphery where VEGF-A exposure is greater.

Rho GTP-ase activity is crucial for regulation of cytoskeleton reorganisation. It has also been suggested that acto-myosin contraction might be involved in regulation of VEGF-A induced increases in permeability of EC. One of the key players in regulation of acto-myosin reorganisation is myosin light chain (MLC). Interestingly, phosphoproteomic data indicates a higher phosphorylation state of MLC (S19) at P5, and this phosphorylation induces the activity of MLC (Figure 66).

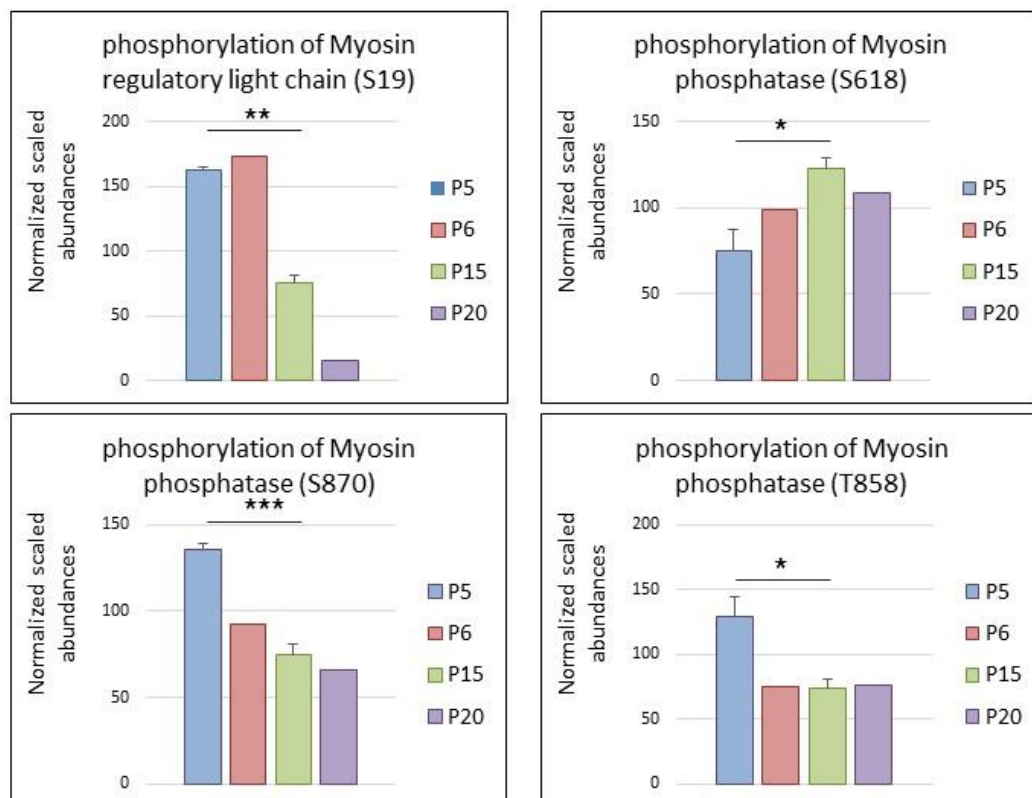


Figure 66. The phosphorylation of MLC at different stages of retina development.

MLC can be dephosphorylated by myosin phosphatase (MLCP). A phosphoproteomic study showed an increase in phosphorylation of MLCP at S618, and decrease in phosphorylation at S870 and at T858 between P5 and P15 stage of development. Particularly interesting is the decrease in phosphorylation at T858, as it was previously reported that phosphorylation of regulatory domain of MLCP at T696 or T853, inhibits the MLCP activity, via blocking its catalytic domain from accessibility to the substrate – myosin (Khromov 2009). This is an interesting finding that confirms the important role of MLC activity at early stages of vascular formation.

MLC phosphorylation is mediated via myosin light chain kinase (MLCK). The regulation of MLCK activity is highly complex, and can be regulated by many distinct signalling pathways, which in addition very often interact with each other. This complexity suggests that cells spatially and temporally compartmentalise their signals. In order to understand this complex pathways, Chew and colleagues adopted strategy to localise the MLCK in the active and inactive state and showed the recruitment of MLCK to various cytoskeletal structures during contraction, motility, and cytokinesis (Chew, 2002). MLCK activity can be modulated by PKA and PKC, however it is still under debate how phosphorylation affects MLCK activity, as many reports indicate, that MLCK gets activated upon MLCK phosphorylation at Y464 and Y47, others say, that MLCK phosphorylation reduces its ability to phosphorylate MLC (Shen, 2010, Giembycz, 2006).

Phosphoproteomic data from the retina study showed an increase in phosphorylation of MLCK at S355, S381, S802, S1795 at early stages – P5, compared to later P15 and P20 data points (Figure 67).

MLCK activity is increased by Ca^{2+} -calmodulin binding and phosphorylation by protein kinase C (PKC), however its activity can also be decreased in response to protein kinase A (PKA) activity (Rigor, 2012). These factors might mediate opposite outcomes in terms of regulation of acto-myosin contraction.

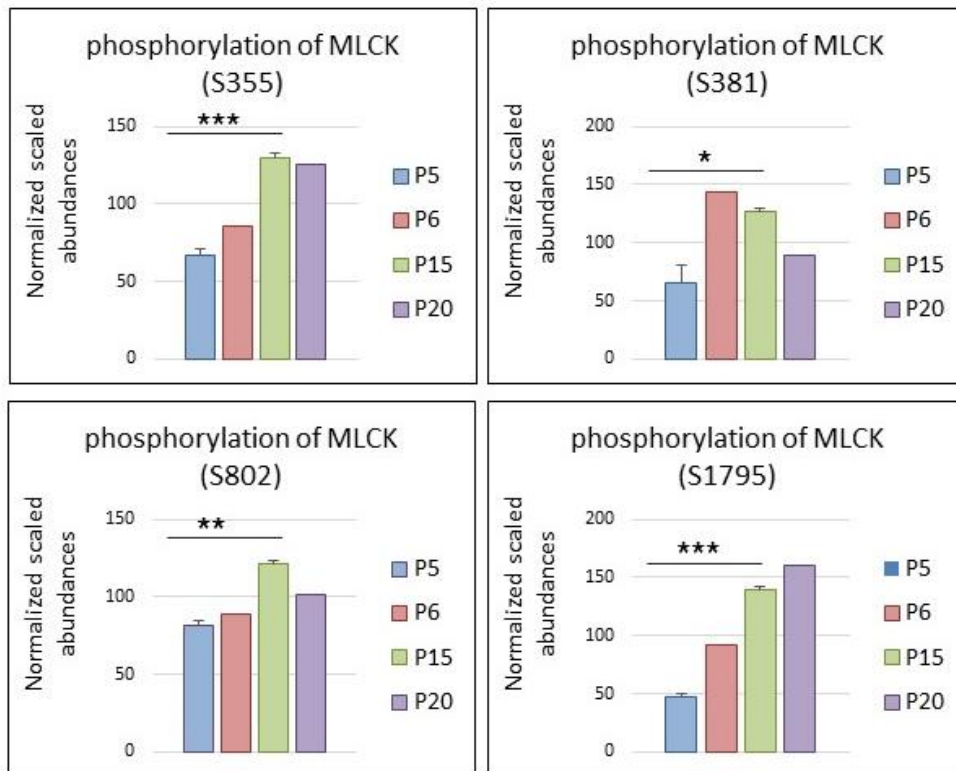


Figure 67. The phosphorylation of MLCK at different stages of retina development.

Another important effector for GTP-ase activity that links it with cytoskeleton reorganisation is p21 activated kinase (PAK). PAK is a serine/threonine protein kinase that plays a role in a variety of different signalling pathways including cytoskeletal rearrangement such as loss of focal adhesion, actin stress fibres formation. PAK is activated by the binding of active CDC42 and RAC1, and this results in a conformational change and a subsequent autophosphorylation on several serine and/or threonine residues (Chan, 2008).

Phosphoproteomic analysis showed higher phosphorylation of PAK2 at S141, and PAK4 at S181, during early retina development, in contrary PAK7 phosphorylation (S226, S561/S602) which increased at a later stage of retina development (Figure 68). It has been shown that RNAi-mediated suppression of PAK2 and PAK4 significantly blocks EC lumen and tube formation, additionally the process of lumen formation correlates with PAK2 and PAK4 phosphorylation (Koh, 2008). This is interesting given the fact that higher phosphorylation of both PAK2 and PAK4, was identified at early stages of retina development.

PAK7, also known as PAK5, in contrary to all other PAK family members, binds to the GTPases Cdc42 and Rac, but these GTPases do not regulate PAK7 kinase activity. PAK7 express constitutive and stronger than any other PAK kinase activity. PAK7 inhibits the apoptotic cascade that leads to apoptosis, via phosphorylation of BAD on S112, and prevents BAD localisation in mitochondria (Cotteret, 2003).

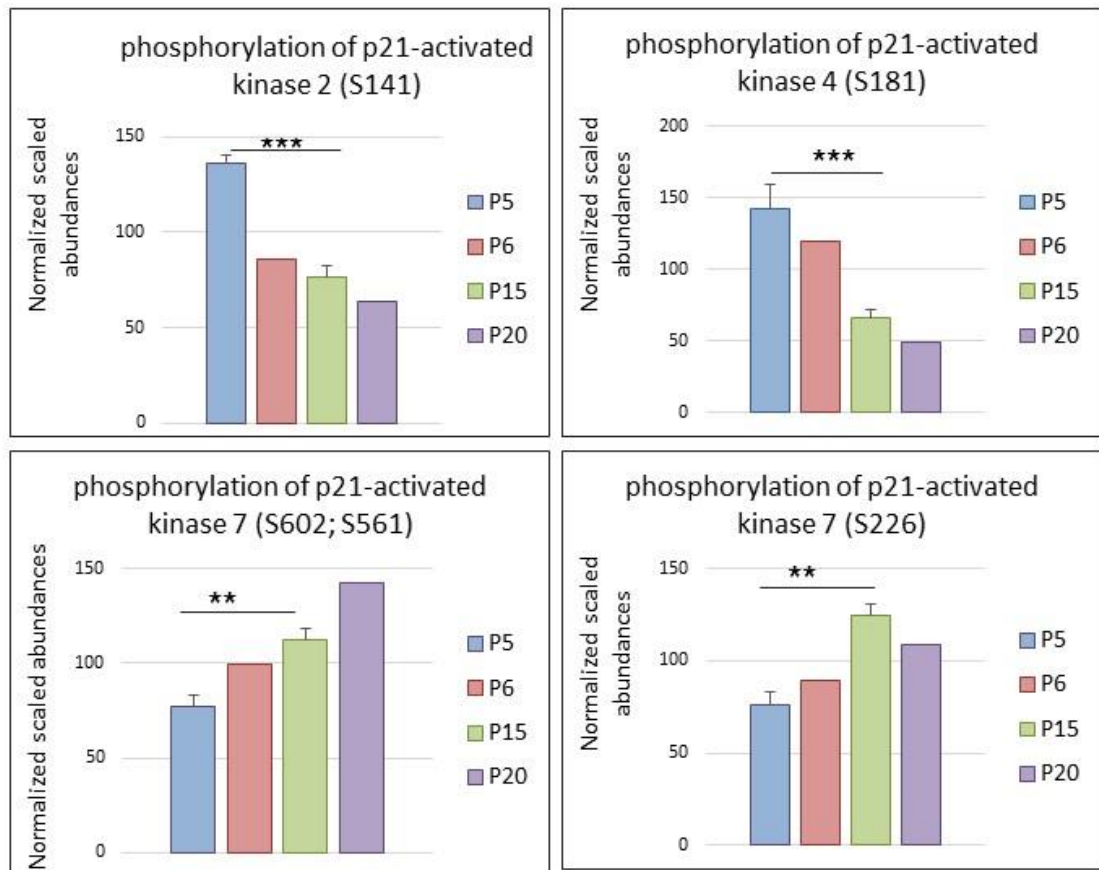


Figure 68. Changes in phosphorylation of p21-activated kinases (PAKs) at different stages of retina development.

Phosphoproteomic analysis of P5 and P15 retina - conclusion

Phosphoproteomic methods represent a rapid and effective method for comparative analysis of phospho-regulation and have allowed us to probe changes occurring during acquisition of the BRB.

The phosphoproteomic study was performed on the extract from the whole retina tissue, because the isolated capillaries would not provide us with

sufficient material for this method. However, the retina was carefully dissected in order to avoid RPE contamination.

The analysis of differences in phosphorylation of peptides between P5 and P15 retina allow us to identify numerous pathways that are activated or deactivated between P5 and P15. However, this extremely large datasets and complex results, will require further and more detail pathway analysis. In the future we also plan to compare the results from phosphoproteomic study on P5 and P15 retina with proteomic study also on P5 and P15 retina.

The phosphoproteomic results requires further verification and analysis in order to localise identified changes in proteins phosphorylation, and confirm its role in retinal vascular barrier formation.

In order to validate the data from the phosphoproteomic study, I will use commercially available antibodies that will help me localise identified changes in phosphorylations, and correlate their changes with the time point of BRB formation.

I will focus first on the proteins involved in the cytoskeletal changes and in the next chapter, I take steps to further probe the role of cytoskeletal regulation during changes to vascular barrier function.

Chapter 6.

The role of the cytoskeletal remodelling during BRB development

The data describing retina development underlines a high role of VEGF-A at early stages of BRB acquisition. Moreover, localisation of VEGF-A expression in the P5 retina overlay with the most leaky area of the vasculature. This leads us to believe that VEGF-A is responsible for the increased permeability of the EC. However, it is still not clear what mechanism it triggers. There are many reports that suggest that VEGF-A activates small Rho GTP-ases (Ngok, 2012, van Nieuw Amerongen, 2003). Rho GTP-ases plays a significant role in regulations of cytoskeletal organisation, but also in many diverse cellular events such as membrane trafficking transcriptional regulation, cell growth control, and development (Yalovsky, 2008). Very complex role of RhoGTPases confirms our phosphoproteomic data that shows many changes of phosphorylation stage of GAP and ARHGEF proteins that regulates RhoGTP-ases activity. This makes Rho GTP-ases very difficult to study.

Phosphoproteomic data also showed the changes in many junction proteins and MLC, MLCK and PAK phosphorylations. MLC is directly involved in cytoskeleton reorganisation, and it is controlled by MLCK and PAK. Cytoskeletal remodelling might play a significant role during barrier acquisition as it interacts with TJ and AJ molecules. The cytoskeleton is a dynamic set of structures that modulate cell motility, morphology, polarity and proliferation (Quiros, 2014).

Cytoskeletal reorganisation might be an interesting mechanism that leads to an increase of permeability of EC at early stages of vascular formation. One of

the hypothesised mechanism that this might happen, is via Myosin light chain kinase (MLCK) driven myosin regulatory light chain (MLC) phosphorylation.

MLC is a key player in cytoskeletal rearrangements and it has been demonstrated that phosphorylation of MLC is necessary for barrier disruption (Clayburgh, 2005, Zolotarevsky, 2002). Interestingly phosphoproteomic assay showed increased phosphorylation of MLC at P5, when EC do not maintain proper barrier function and allow for the dextran extravasation from the vasculature. Another important player in modulation of MLC activity is p21 activated protein (PAK). PAK is a direct effector Rho GTP-ases, Rac and CDC42. PAK is phosphorylated on S141, in response to VEGF-A, TNF α , histamine, and thrombin. PAK2 catalysis phosphorylation of MLC at S19 (Goeckeler, 2000, Stockton, 2004). Interestingly both of those phosphorylations decreased between P5 and P15 in phosphoproteomic study.

PAK/MLC-dependent stimulation of cytoskeleton appears to be an important concept in the study of barrier function. Activated PAK can directly phosphorylate MLC, and can also modulate the activity of MLCK.

This is why as a next step I decided to study the expression of proteins like MLC, PAK; that might be implicated in the pathway triggered by VEGF-A.

PAK, MLC and MLCK in the retina at different stages of postnatal retinal development

First we decided to look for differences in protein and/or phospho-protein between P5 and P15 retinas. Protein extracted from P5 and P15 were used for Western blot analysis in order to identify PAK, phospho-PAK, phospho-MLC. The protein extract was prepared using a Halt Protease and Phosphatase Inhibitor Cocktail that contains inhibitors for phosphatases in order to prevent loss of protein phosphorylation.

Table 13. Composition of the Halt Protease and Phosphatase Inhibitor Cocktail.
Adapted from Thermo Scientific.

Protease and phosphatase inhibitors included in the cocktail formulation and their targeted enzyme class.	
Inhibitor	Target
Sodium Fluoride	Ser/Thr and Acidic Phosphatases
Sodium Orthovanadate	Tyr and Alkaline Phosphatases
β -glycerophosphate	Ser/Thr Phosphatases
Sodium Pyrophosphate	Ser/Thr Phosphatases
Aprotinin	Ser Proteases
Bestatin	Amino-peptidases
E64	Cysteine Proteases
Leupeptin	Ser/Cys Proteases
EDTA	Metalloproteases

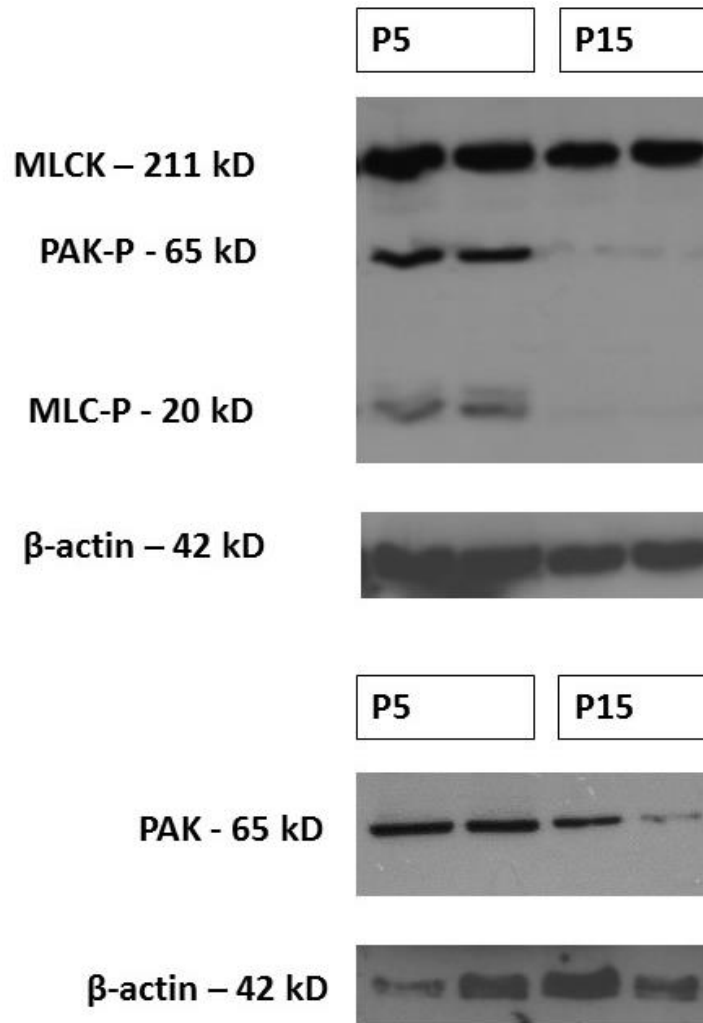


Figure 69. Western blotting data showing the differences in expression of MLCK, PAK-P, MLC-P and PAK at P5 and P15.

PAK-P (Anti-PAK1 (phospho S144) + PAK2 (phospho S141) + PAK3 (phospho S139))

MLC-P (Anti MLC Ser19-phospho)

The experiment was repeated twice, with at least two different samples of retina for each of the groups P5 and P15.

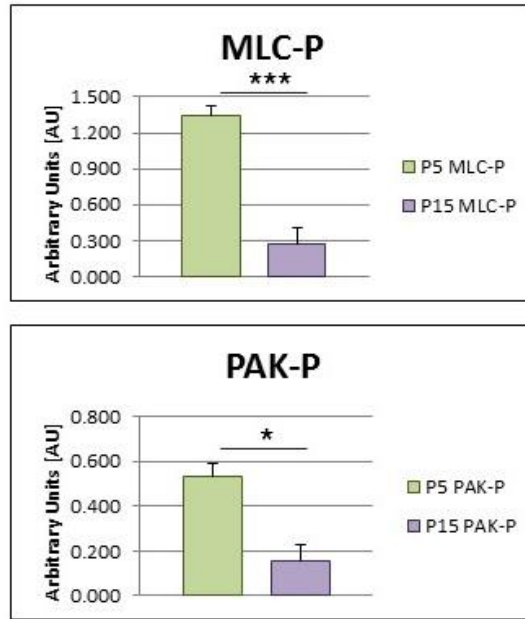


Figure 70. The differences in MLC-P and PAK-P expression between P5 and P15.

The difference in PAK-P (Anti-PAK1 (phospho S144) + PAK2 (phospho S141) + PAK3 (phospho S139)) and MLC-P (Anti MLC Ser19-phospho) expression based on western blotting results. The criterion for statistical significance was p-value < 0.05 (*), 0.01(**) or 0.001 (***)

The Western blot data demonstrated significant differences in the phosphorylation of MLC (Ser19-phospho) between P5 and P15. As a next step western blot for the total MLC is required. Phosphoanalysis has identified the differences in PAK2 at S141 phosphorylation, we decided to look at the differences in PAK phosphorylation using a western blot. Because of limitations in commercially available antibodies specific to the phospho PAK at S141 only, I used the antibody Anti-PAK1 (phospho S144) + PAK2 (phospho S141) + PAK3 (phospho S139). The phosphorylation of PAK also differs between early and late stages of development. Interestingly, we also noticed difference in total PAK between P5 and P15 samples. Further analysis of total PAK1, PAK2 and PAK3 is required in the future work (Figure 70).

Immunostaining and localisation of PAK-P and MLC-P in the retina

Western blotting data indicated differences in MLC-P and PAK-P in P5 and P15 retinas. Following Western blotting, I decided to localise MLC-P and PAK-P via immunostaining.

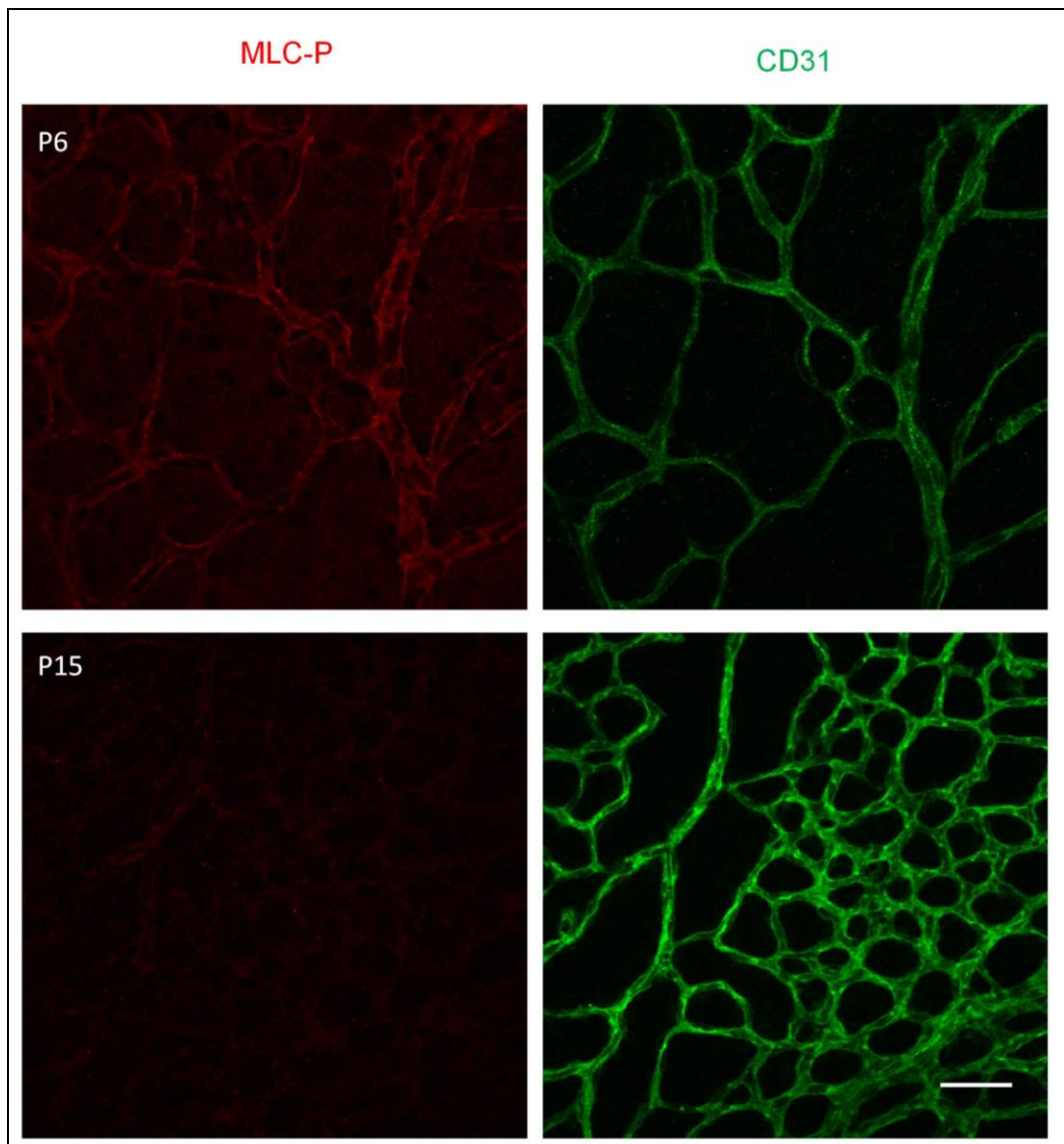


Figure 71. MLC-P immunostaining in the retina at P6 and P15.

MLC-P (Anti MLC Ser19-phospho) staining at P5 and P15 retina tissue, and CD31 co-staining. The scale bar indicates 50 μm for all pictures.

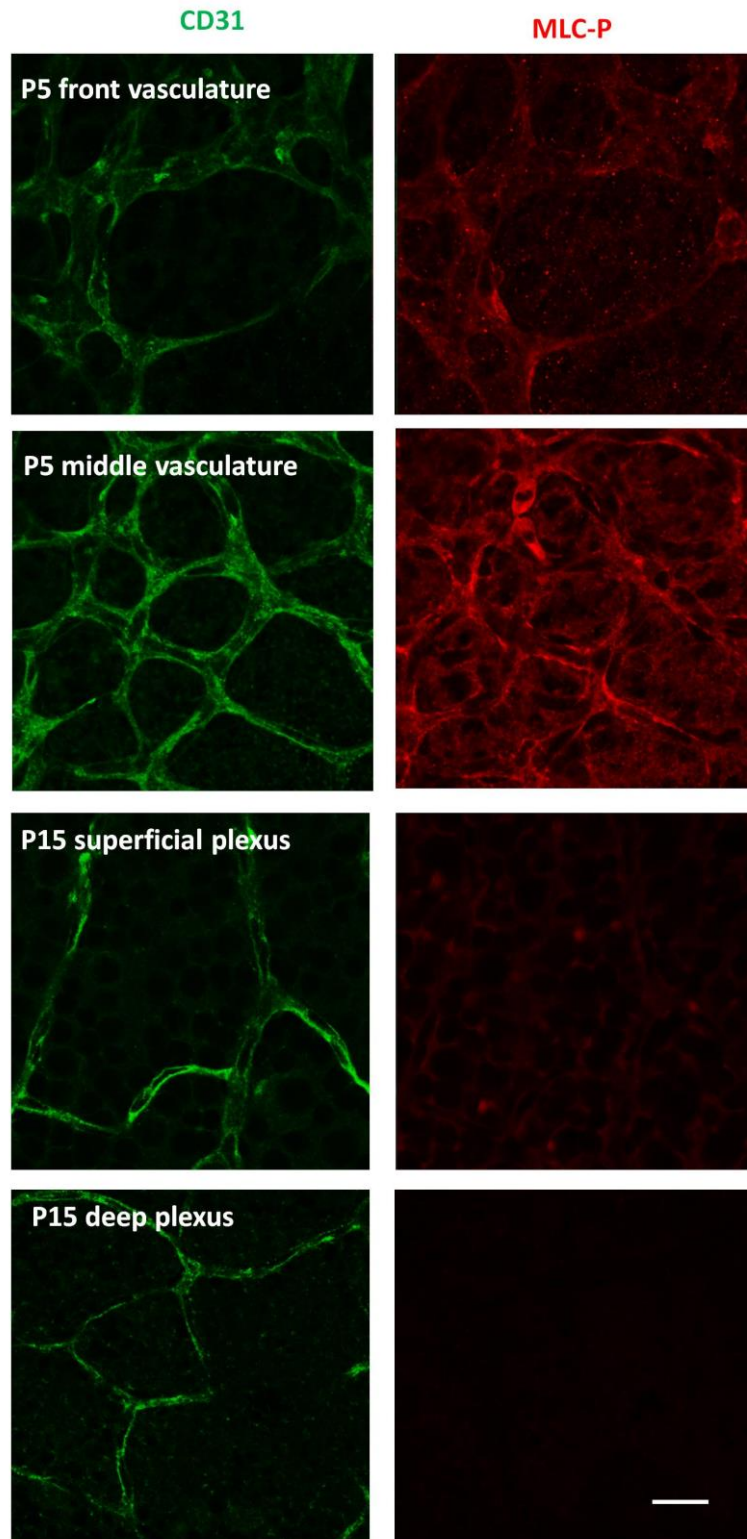


Figure 72. MLC-P staining in the P5 and P15 retina.

MLC-P (Anti MLC Ser19-phospho) staining at P5 and P15 retina and CD31 vascular costaining. The scale bar indicates 50 μ m for all pictures.

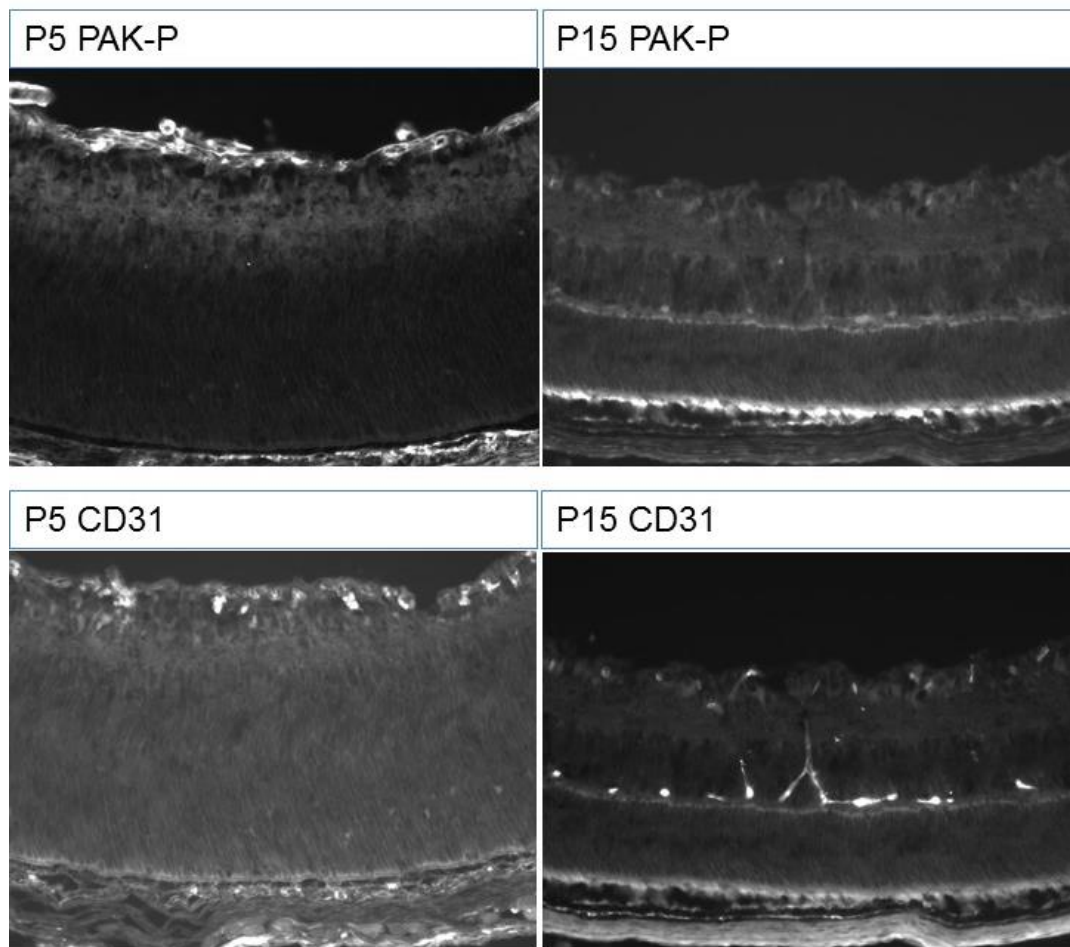


Figure 73. PAK-P localisation in the retina at P5 and P15 (retina section).

PAK-P (Anti-PAK1 (phospho S144) + PAK2 (phospho S141) + PAK3 (phospho S139)) immunostaining at P5 and P15 retina section and CD31 co-staining. The scale bar indicates 50 μ m for all pictures.

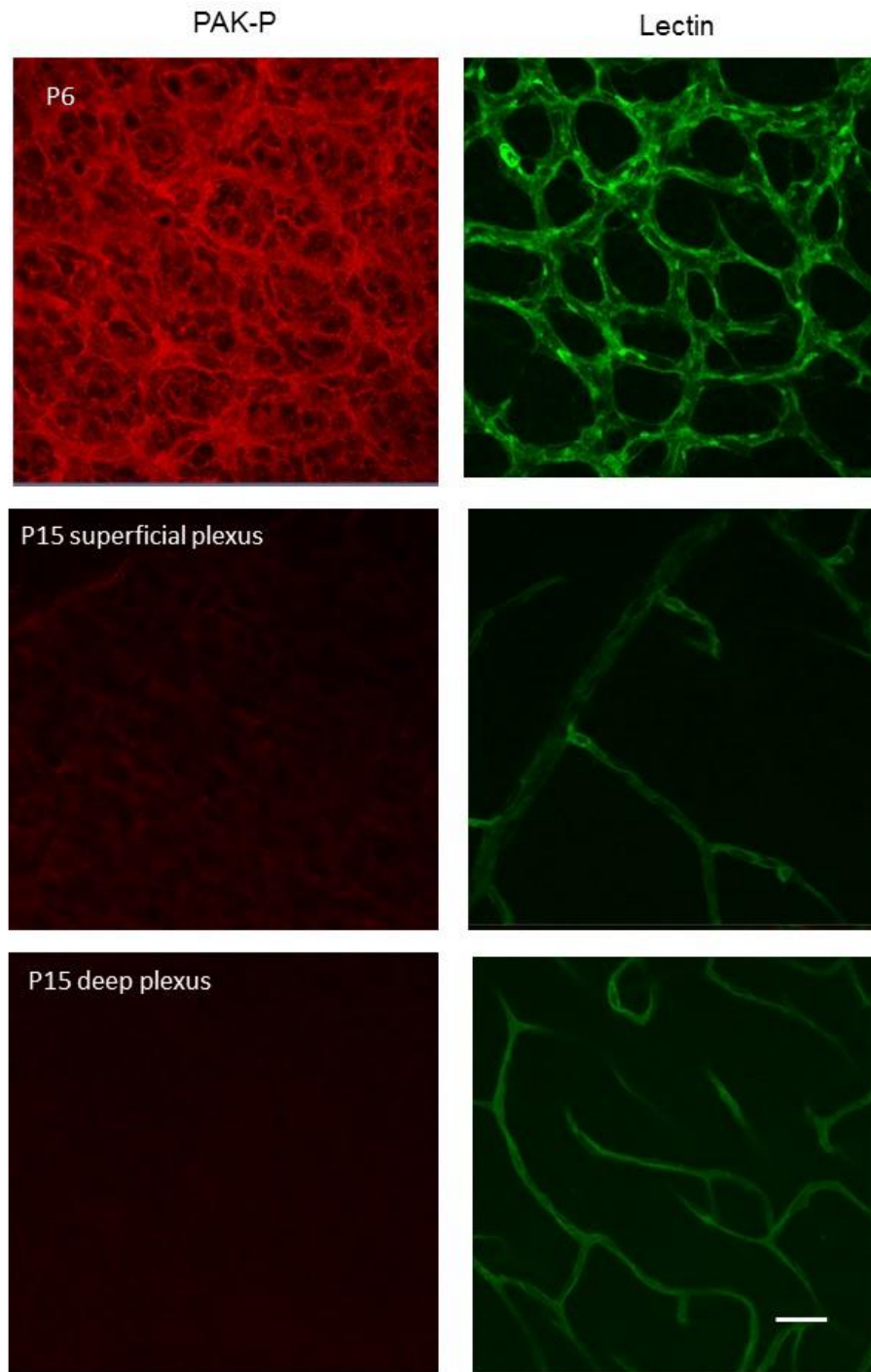


Figure 74. PAK-P localisation in the retina at P5 and P15 (retina flat mount).

PAK-P (Anti-PAK1 (phospho S144) + PAK2 (phospho S141) + PAK3 (phospho S139)) immunostaining at P5 and P15 (superficial and deep plexus) and Lectin co-staining. The scale bar indicates 50 μ m for all pictures.

Both MLC-P (Figure 71-73), and PAK-P (Figure 73-74) immunostainings confirmed previous Western blot findings that active forms of both MLC and PAK are dominant during early stages of vascular development. This might indicate that during vascular formation, VEGF-A, via Rho signalling and potentially followed via PAK phosphorylation, might activate MLC, and this might play an important role for vascular assembly.

Actin filament organisation in the vasculature

Previous data showed an increase in MLC and PAK phosphorylation at P5. This might imply that cytoskeleton remodelling in the retina vasculature is taking place at that stage.

In order to check if MLC and PAK activity influenced actin filament organisation, we localised F-actin with phalloidin. Firstly, we compared the periphery and central part of the vasculature of P5 retina (Figure 75). Secondly, we compared f-actin between P5 and P15 was done (Figure 76).

Phalloidin staining, especially at the periphery of P5 vasculature shows disorganisation of actin filaments. This makes sense considering new vessel growth in this area.

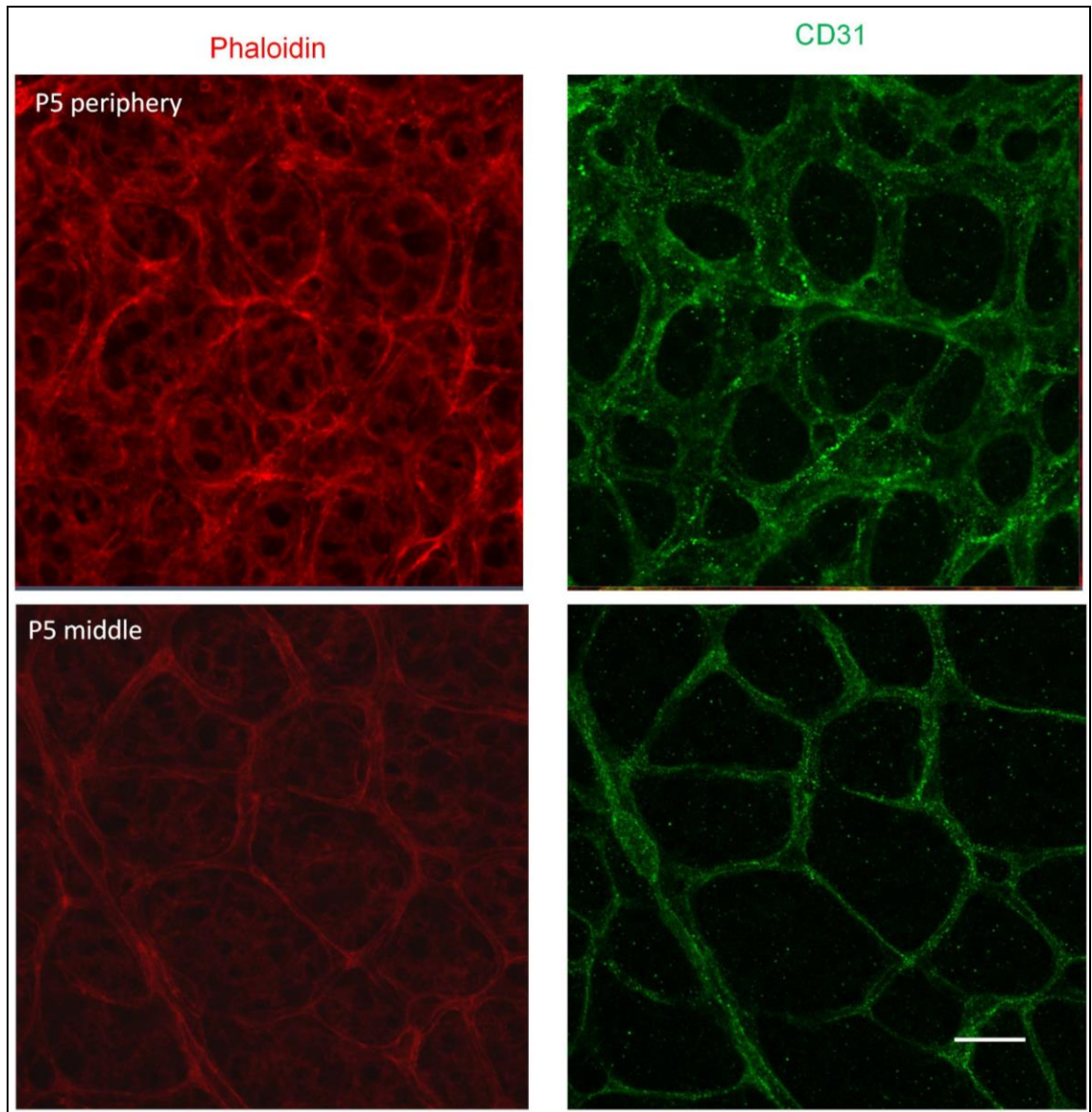


Figure 75. Phalloidin staining of P5 retina.

The differences in filament organisation between periphery and equator area of the retina at P5. The scale bar indicates 50 μm for all pictures.

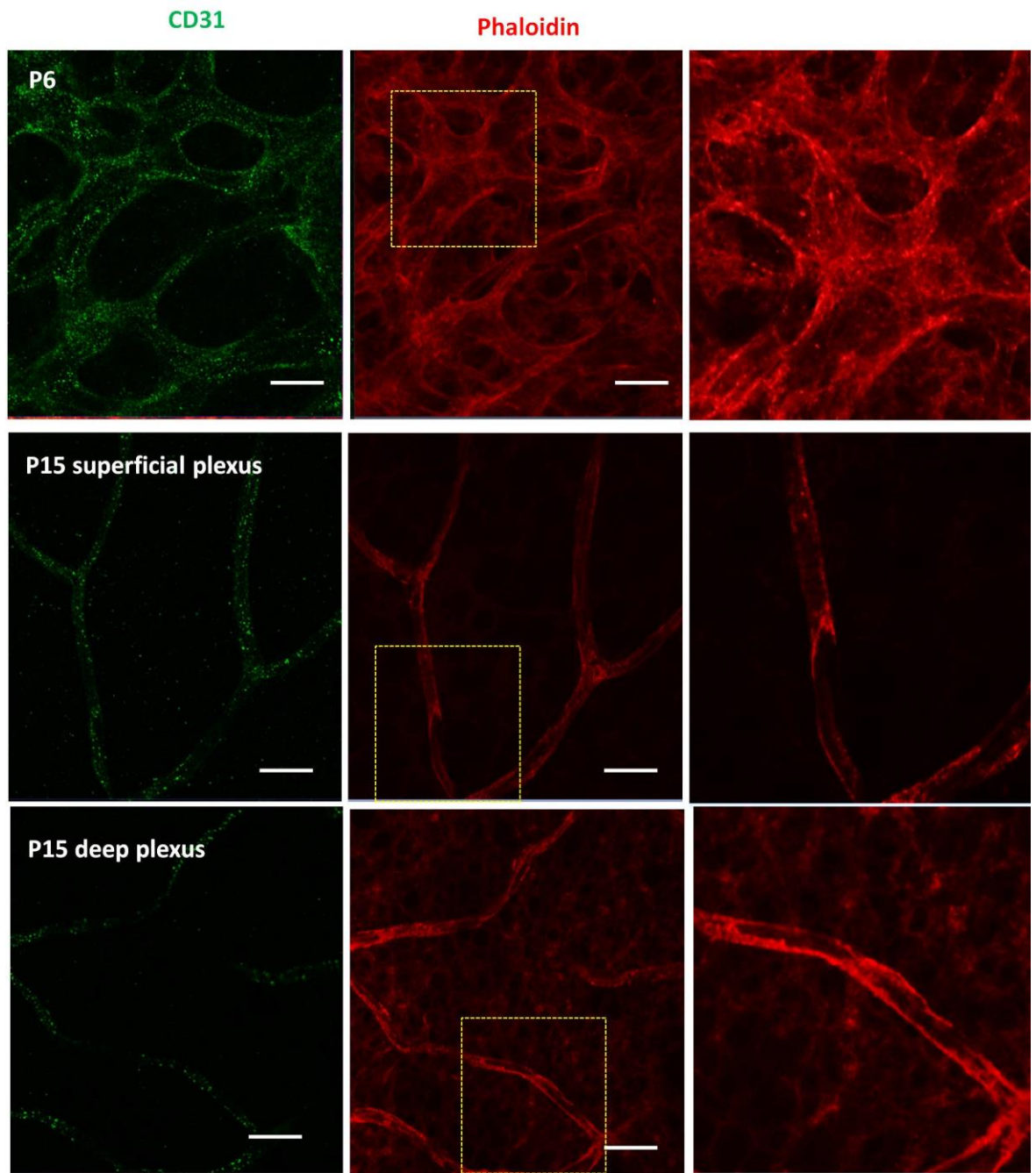


Figure 76. Phalloidin staining of P5 and P15 retina.

Phalloidin immunostaining at P5 and P15 (superficial and deep plexus) and CD-31 co-staining. The scale bar indicates 50 μm for all pictures.

BRB functions after blocking MLCK.

The phosphorylation of MLC appears to be associated with increased permeability of vascular endothelium prior to P10. MLC phosphorylation requires MLCK in an active state. We investigated if this was more than just a correlation by blocking MLCK activity. We evaluated barrier activity using the 3kD dextran tracer assay.

PIK peptide and its function.

MLCK activation is dependent on Ca²⁺ and calmodulin. Four calcium ions bind to calmodulin, which allows calmodulin to enter the binding pocket at the MLCK C-terminus, and this leads to the activation of MLCK via separation of the regulatory and catalytic domains. An active MLCK triggers MLC phosphorylation (Figure 77-B) (Shin, 2009).

An MLCK inhibitor termed PIK, is a membrane permeant nanopeptide (DLys-DArg-DArg-DTyr-DLys-DTyr-DLys-DLys-DArg-NH₂) which binds to the catalytic domain of MLCK and inactivates the enzyme, even in the presence of calmodulin (Figure 77-C) (Zolotarevsky, 2002). It has been shown in vivo that PIK prevents loss of barrier function in intestinal epithelium. PIK treatment reduced MLC phosphorylation and tight junction disruption (Clayburgh, 2005).

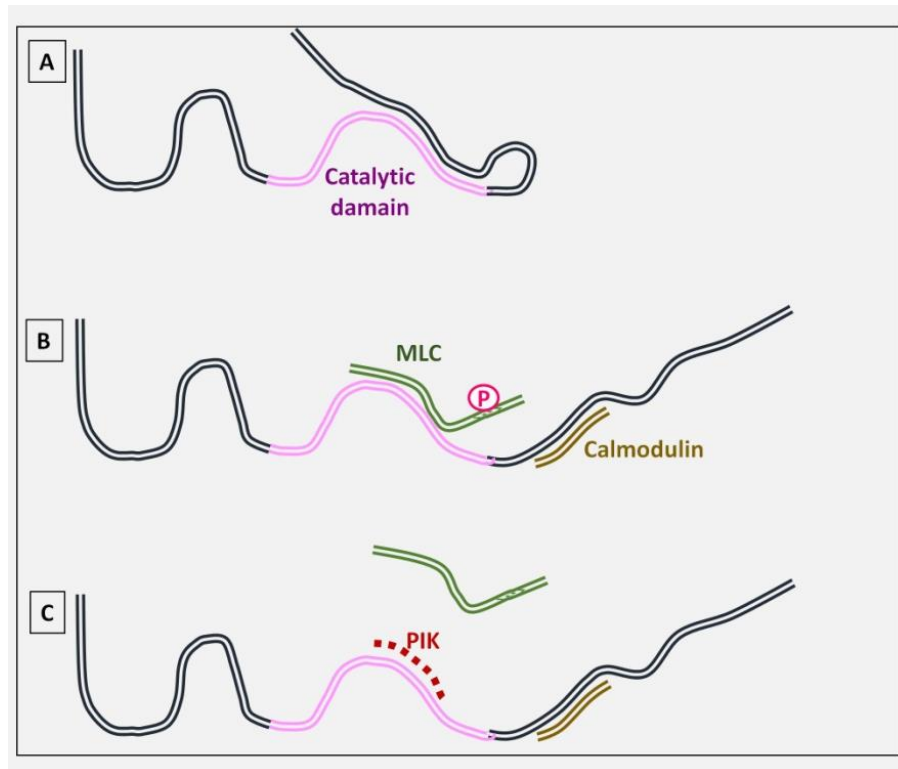


Figure 77 Schematic model of PIK action.

A- The inhibitory domain of MLCK interacts with the catalytic domain and inhibits the enzyme. B- Calmodulin binds to the inhibitory domain and activates MLCK by releasing the interaction between catalytic and inhibitory domains. Active MLCK mediates MLC phosphorylation. C- PIK binds to the MLCK catalytic domain and inactivates the enzyme, even in the presence of calmodulin.

The effect of PIK on permeability of P6 retinal vasculature

The hypothesis that we set out to test was that blocking MLCK, and thereby reducing acto-myosin dynamics, will lead to improvement in barrier function. Ideally we would intravitreally administer the PIK peptide. However, at P6, pup eyes are still closed and this type of injection is very difficult. Thus we decided to administer PIK intraperitoneally, where it has been previously shown to gain access to other organs and inhibit MLCK activity.

We intraperitoneally injected PIK into P6 animals at the dose of 20 mg/kg. One hour after the PIK injection we performed a 3kD dextran leakage assay in order to evaluate barrier function after MLCK inhibition.

As a control we used PBS for one group of animals, and PIK control peptide for a second control group. PIK control peptide is a version of PIK

peptide where the central triad of amino acids was changed to remove its activity (DLys-DArg-DArg- DAla-DAla-DAla- DLys-DLys-DArg-NH₂).

The PIK injection significantly improved barrier function in the retina. Leakage detected in the group of animals injected with MLCK inhibitory peptide was 60% lower than in the group injected with PBS, and 50% lower than the group injected with PIK control peptide (Figure 78). However, in order to confirm the hypothesis, that by blocking MLCK activity we improve barrier function via increased MLC and PAK phosphorylation, further experiments are required. As a next step we plan to perform Western blot and immunostaining on the retina treated with PIK and untreated tissue, in order to see the level of PAK and MLC phosphorylation.

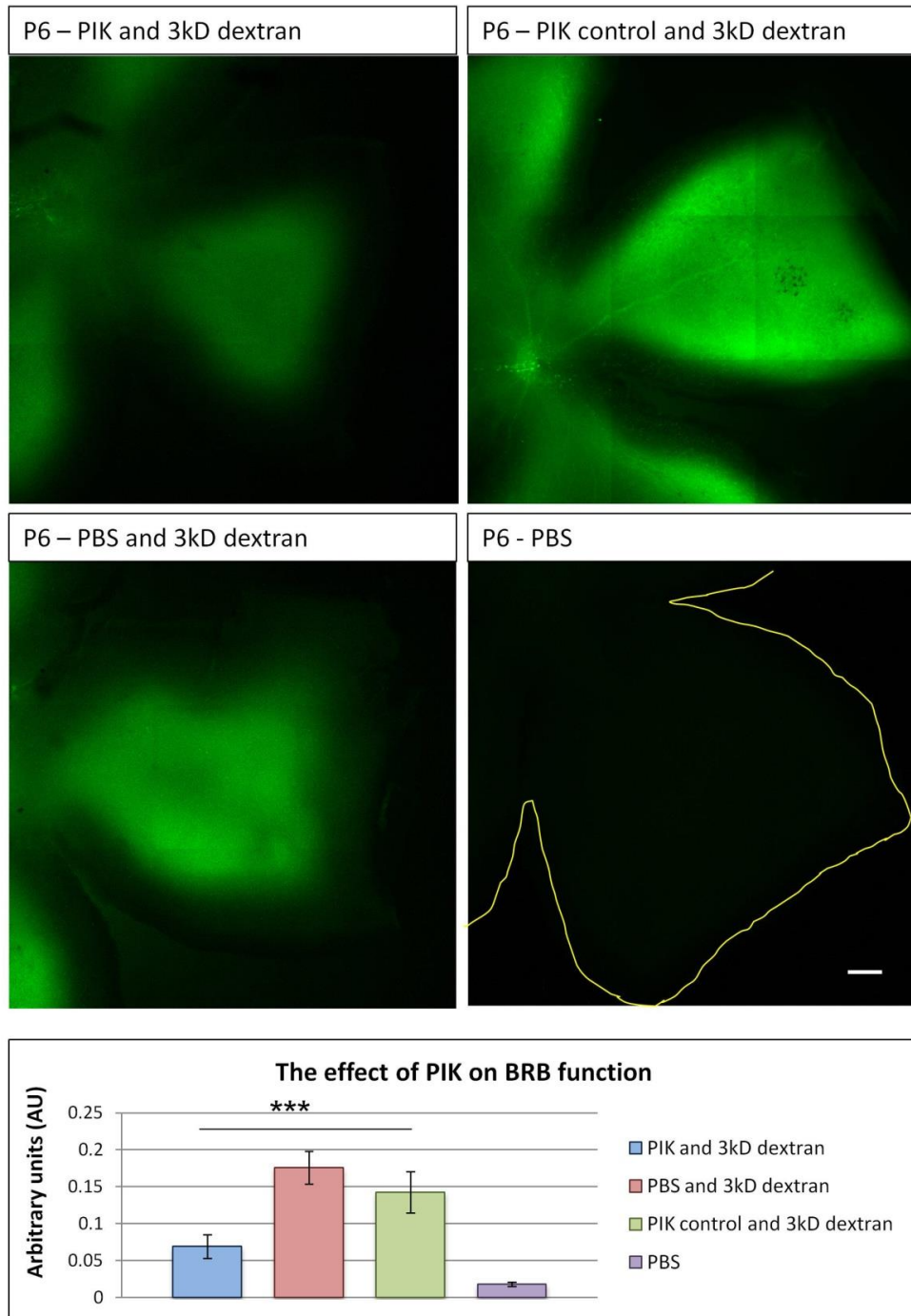


Figure 78. The effect of PIK on BRB function.

Pictures show 3kD dextran leakage assay at P6 retina after PIK injection, for the control PIK control peptide and PBS was used. Graph represents intensity of fluorescence of the retina; error bars indicates SEM value; $N \geq 8$. The scale bar indicates 200 μm for all pictures.

The role of cytoskeletal regulation during BRB development – discussion and summary

There are many recent reports demonstrating that Rho GTPases including Rac and Rho regulate transendothelial permeability barrier by controlling actin cytoskeletal reorganisation, contractile properties, cell-cell junctions and cell-ECM interactions in different cell types. Various growth factors including VEGF-A, mechanical stress and oxidative stress are also recognised to influence the activity of Rho GTPases and transendothelial permeability (Pattabiraman, 2014). Rho GTPases regulate the activity of kinases responsible for the phosphorylation of MLC, which is an output that triggers acto-myosin contractions.

MLC phosphorylations can be categorised into either inhibitory or activating. Phosphorylation of Ser-19 and Thr-18 stimulates myosin activity, whereas Ser-1, Ser-2, and Thr-9 phosphorylation lead to inhibition. Ser-19 can be phosphorylated by MLCK, Rho kinase, and PAK. Thr18-Ser19 diphosphorylation maximally activates myosin ATPase in vitro. On the other hand, phosphorylation of MLC at Ser-1, Ser-2, or Thr-9 by protein kinase C or Cdc2 kinase inhibits myosin activity. In addition, many of these pathways interact with each other. For example, cdc42-activated PAK phosphorylates MLC at Ser-19 and inhibits MLCK, preventing Thr-18 phosphorylation (Chew, 2002).

Terry *et al* showed that upon the blocking of RhoA signalling, by depletion of p114RhoGEF, which is an activator of RhoA, results in strong attenuation of the induction of double MLC phosphorylation at cell-cell contacts during wound repair in HCE cells (human corneal epithelial cells). Depletion of p114RhoGEF affected double MLC phosphorylation, but not single MLC phosphorylation (Terry, 2012).

This demonstrates the intriguing complexity of cytoskeletal regulatory signalling. Studying the mechanism of changes that accompany endothelial cell migration, growth, and wound repair requires meticulous attention to type and site of phosphorylation. In collaboration with Roche we continue to develop robust statistical analyses of protein phosphorylation changes in P5 and P15 retina.

In this chapter, using the Western blotting technique and immunostaining, we showed an increase in MLC-Ser19 phosphorylation, as well as an increase in active PAK prior to BRB acquisition. Blocking MLCK activity with PIK and improvement of barrier function at P6 provides supportive, functional evidence.

Currently, our data fit a model whereby VEGF-A signalling leads to PAK recruitment to junctions that lead to MLC activation. This event causes actin-myosin contraction, cell remodelling and reason to the increased permeability observed prior to BRB formation (Figure 79). However, this hypothesis requires further investigation, for example, immunostaining and Western blot analysis of active MLC and PAK, after intravitreal VEGF-A injection, and after VEGFR2 blocking antibody injection. The most suitable model that would help us to understand the mechanism that accompanies BRB formation would be an in-vitro endothelial cell model.

In the last results chapter I will try to develop a suitable in vitro system to more rigorously dissect the events surrounding barrier regulation.

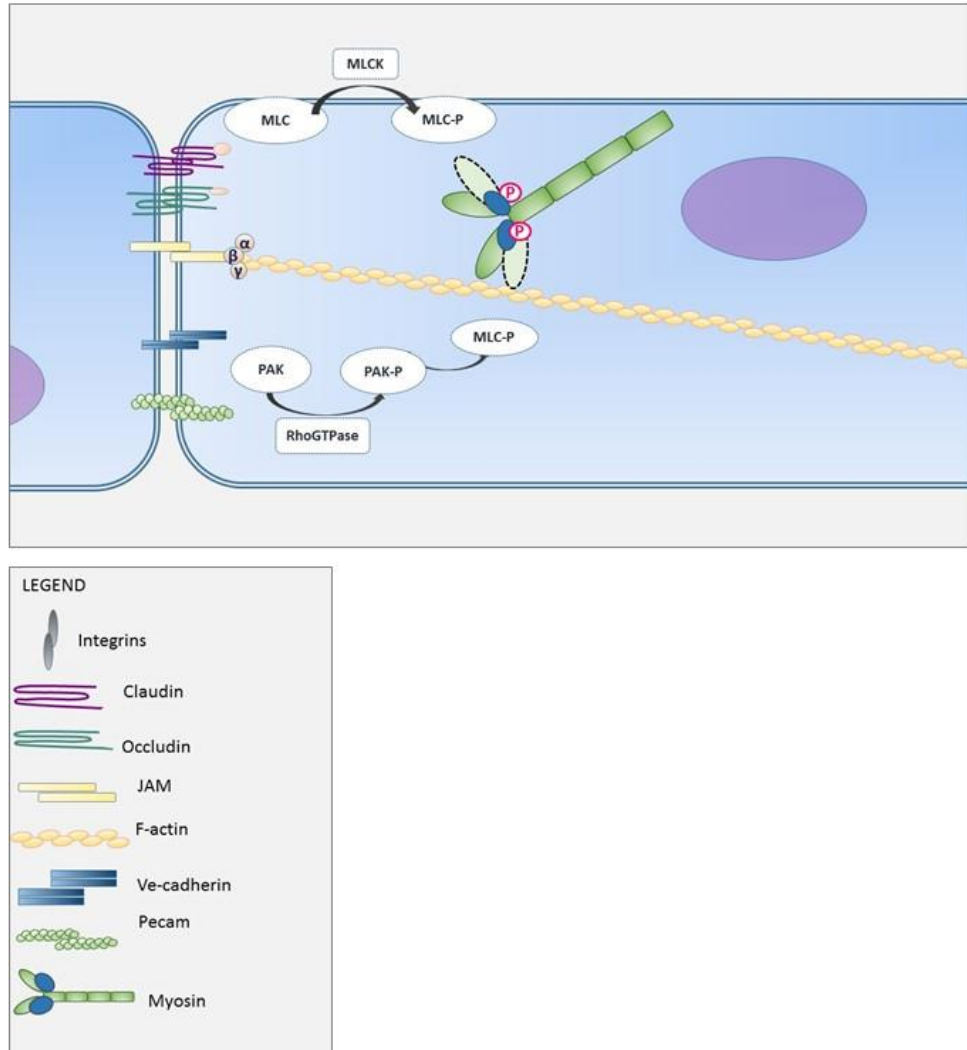


Figure 79. Potential mechanism involved in increased permeability at early stage of development.

MLCK mediates MLC phosphorylation, and it causes a change in conformation of myosin head and exposing its actin binding side. Activated PAK can also phosphorylate MLC in cause cytoskeleton rearrangement and changes in TJ and AJ molecules position.

Chapter 7

Developing an in vitro model for studying BRB

properties

In vivo studies examining BRB development helped us to understand and characterise the process of post-natal barrier function in the retina. However more resolved studies characterising the cellular mechanisms involved in the change from permeable vasculature to BRB are challenging. In order to deepen our understanding of changes in EC barrier function, we decided to develop a suitable in-vitro system.

A significant and very useful model for BBB and BRB study is primary EC culture. Under the appropriate isolation and culture conditions, isolated EC can maintain properties that facilitate BBB/BRB study, like preservation of cellular polarity and metabolism (Abbott, 1992). EC in tissue culture form a barrier that responds to different experimental manipulations, and by monitoring the changes in barrier function, one can investigate more mechanistic studies.

Characteristic of the primary rat brain endothelial cells

Considering the limitation of cell numbers available from isolation of retinal EC, we first focused on a well-established protocol for brain EC isolation (Abbott, 1992).

Cells were obtained from rat cortical grey matter, digested in collagenase/dispase digestion solution, BSA was added and then a Percoll density gradient centrifugation was performed. BSA's centrifugation role is to

separate the heavier capillary fragments from the lighter myelin, neurons, astrocytes and other single cell contaminants.

Purified vessels were then seeded onto collagen IV/fibronectin-coated tissue culture transwells, at high density. Cells were grown in EGM2-MV (Lonza) (with 5 $\mu\text{g/ml}$ puromycin during the first 4 days) for 2 to 3 weeks until their TEER reached a value above 200 Ωcm^2 (Figure 81).

In order to ensure that the cells maintained robust barrier function, a TEER (transendothelial electrical resistance) test was run on each transwell. TEER increased continuously from the first week after isolation and only the wells with the TEER above 200 Ωcm^2 were used for barrier function studies.

The TEER measurement on transwells usually gives values much lower to those measured in vivo – 1500-2000 Ωcm^2 . There are three main factors for that. The first is that the MVEC on the transwells model do not replicate all the biological and physiological conditions of the BBB and BRB. As a result, cell-cell junctional connections are not as effective in restricting paracellular transport. Another is incomplete monolayer formation by MVEC and poor adhesion to the transwell filters (Wong, 2013). Lastly, for maintaining the gate keeping role EC are mainly responsible, but other surrounding cells are implicated pericytes, smooth muscle cells, astrocytes and Müller cells. A possible solution for improving this model could be the co-culture of EC with cells such as astrocytes (Wisniewska-Kruk, 2012).

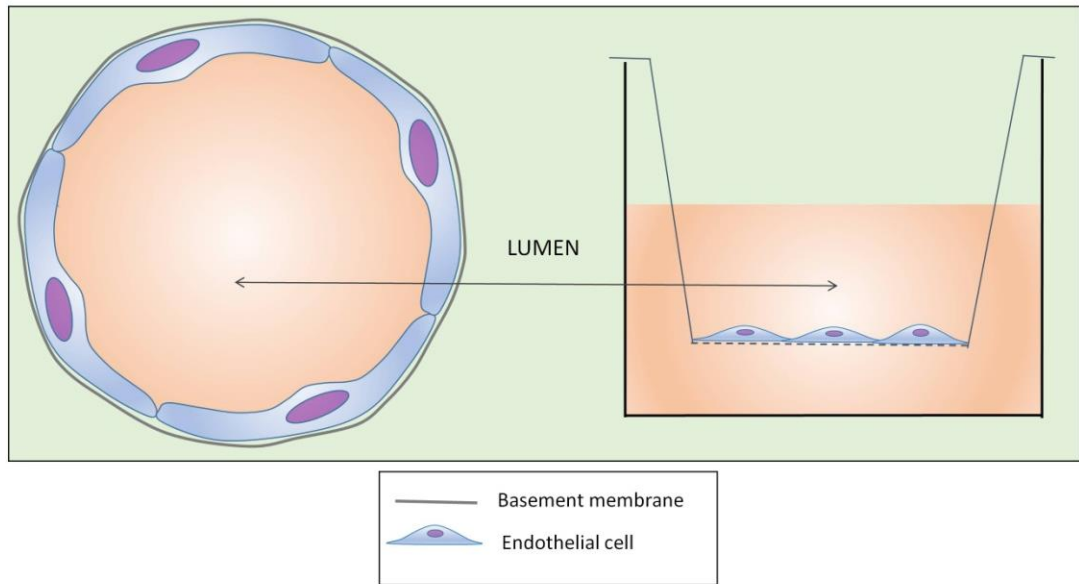


Figure 80. Schematic comparison of in-vivo microvessels and primary endothelial cells seeded on transwells.

We decided to focus on EC alone to start using Primary rat brain endothelial cells (PRBEC) grown on transwells, which mimics aspects of the in-vivo condition and allows for barrier function studies in-vitro. An additional advantage of this model is accessibility to the both sides of the cells: apical and basolateral, or luminal and abluminal, respectively (Figure 80).

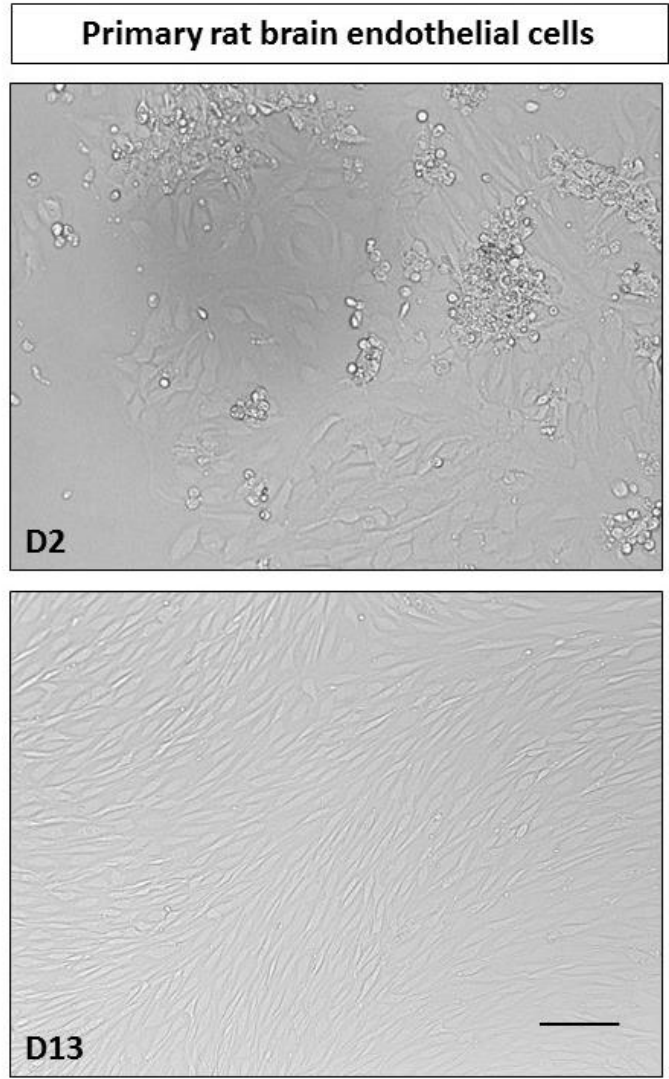


Figure 81. PRBEC on 2nd day after isolation and after 2 weeks in culture.

The scale bar indicates 100 μ m.

The purity of the cultures was checked by immunostaining for endothelial cell markers. Cells were stained with CD31, von Willebrand Factor, the tight junction protein Claudin 5 and adherens junction protein VE-cadherin. Junction proteins were mostly found in the contact area between neighbouring cells, and von Willebrand factor appeared to be more cytoplasmic, presumably in Weibel-Palade bodies (Figure 82).

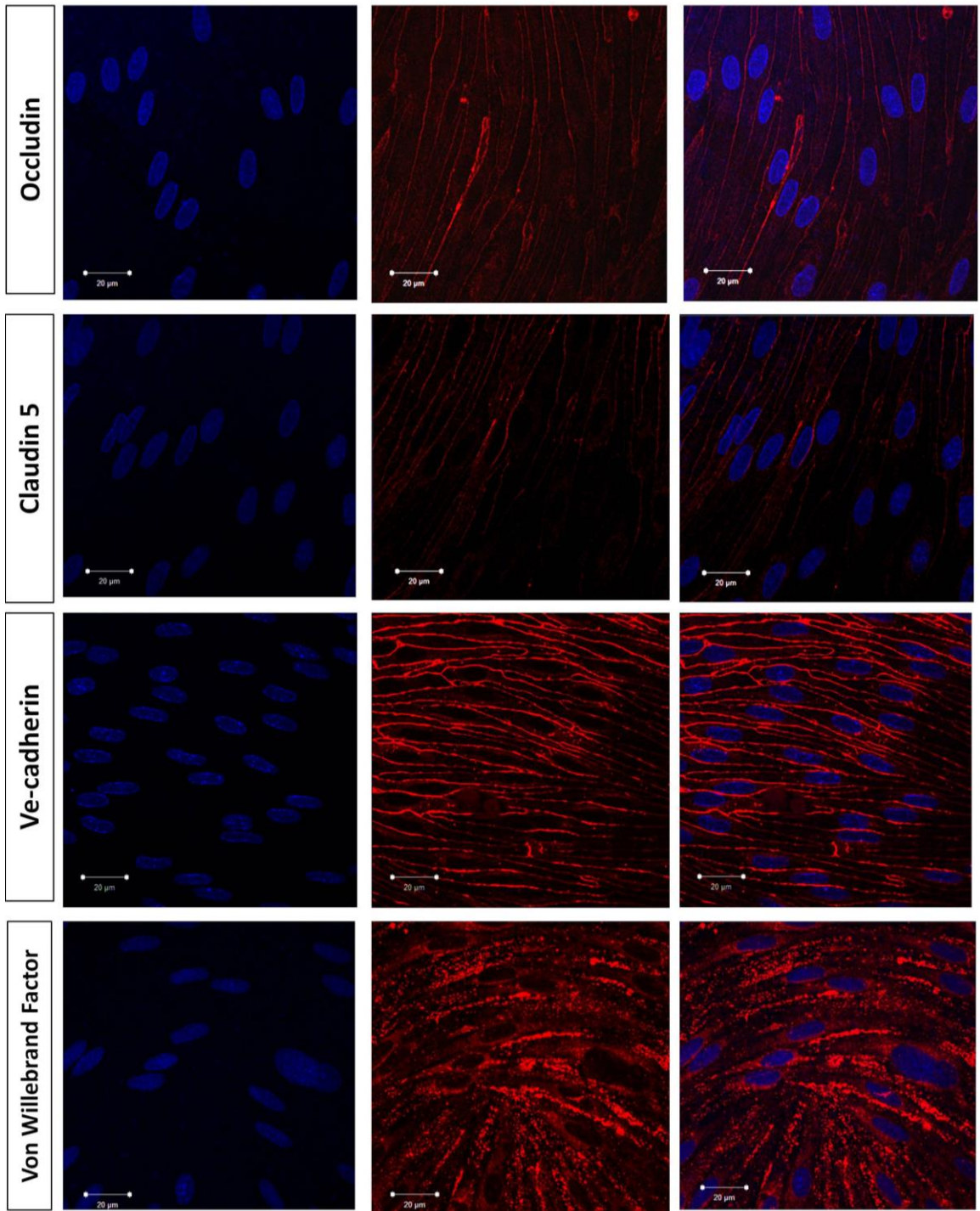


Figure 82. PRBEC stained with Occludin, VE-cadherin, VW-factor and CLaudin-5.

The scale bar represents 20 μ m.

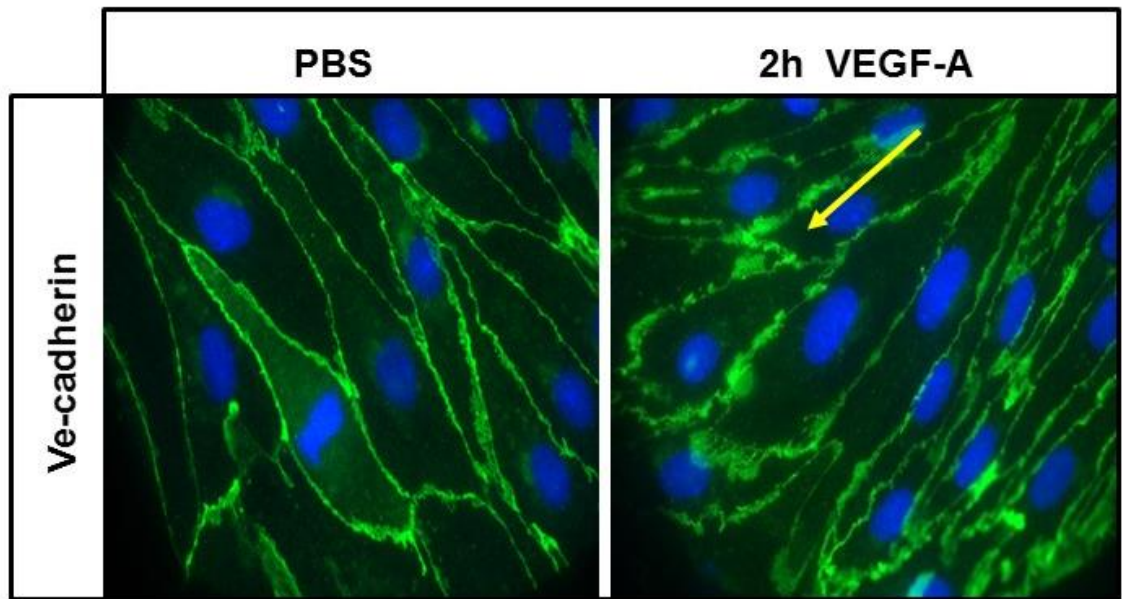


Figure 83. The effect of VEGF-A on VE-cadherin localization in PRBEC.

VE-cadherin localisation in the PRBEC 2h after VEGF-A (50ng/ml) treatment, PBS was used as a control.

We also noticed that junctional protein localisation was disrupted after 50 ng/ml of VEGF-A 2hour treatment (Figure 83). VE-cadherin is one of the main components of adherens junctions and interacts through its cytoplasmic domain with members of the catenin family of intracellular proteins, which in turn provide anchorage to the cytoskeleton (Dudek, 2001, Lampugnani, 2007). VEGF-A mediated VE-cadherin rearrangement might involve contraction of the cytoskeleton.

Flux assay – barrier properties of the PRBEC

Besides TEER, another functional test that monitors barrier properties of PRBEC is the tracer flux assay.

Following the introduction of 4kD fluorescent dextran to the luminal side of the transwells, we measured the intensity of fluorescence in the media on the basolateral side of the filter, as a function of time. Wells were divided into groups within different ranges of TEER values: group A included all wells with TEER values below 250 Ωcm^2 , group B wells with TEER value between 250-400 Ωcm^2 and group C wells with TEER above 400 Ωcm^2 . Curves represent the

intensity of fluorescence in the media on the basolateral side of the well, as a function of time. The higher slope of the curves, the more permeable the monolayer has become. Wells with a TEER value above $400 \Omega\text{cm}^2$, had a correspondingly good barrier function, as not much of the dextran passes through the filter to the basolateral side. Wells with the TEER between $250 - 400 \Omega\text{cm}^2$ were 3.4 higher permeability than wells above $400 \Omega\text{cm}^2$, and wells below $250 \Omega\text{cm}^2$ were 6.6 more permeable than wells above $400 \Omega\text{cm}^2$ (Figure 84). This experiment suggests that monolayers with a high TEER are more likely to mimic the in-vivo BRB and are most suitable for the flux assay.

We also measured the permeability of passaged PRBEC, to see if they maintained their barrier function. However, passaged PRBEC have 19 times higher permeability than primary isolated PRBEC (Figure 85). This indicates that PRBEC lose their gate keeping function after passaging. This might be explained by the fact that, the short term puromycin treatment of isolated PRBEC, which reduces cellular contaminants, such as pericytes, is not fully effective and therefore contaminating cells are able to expand their population upon splitting of cell cultures.

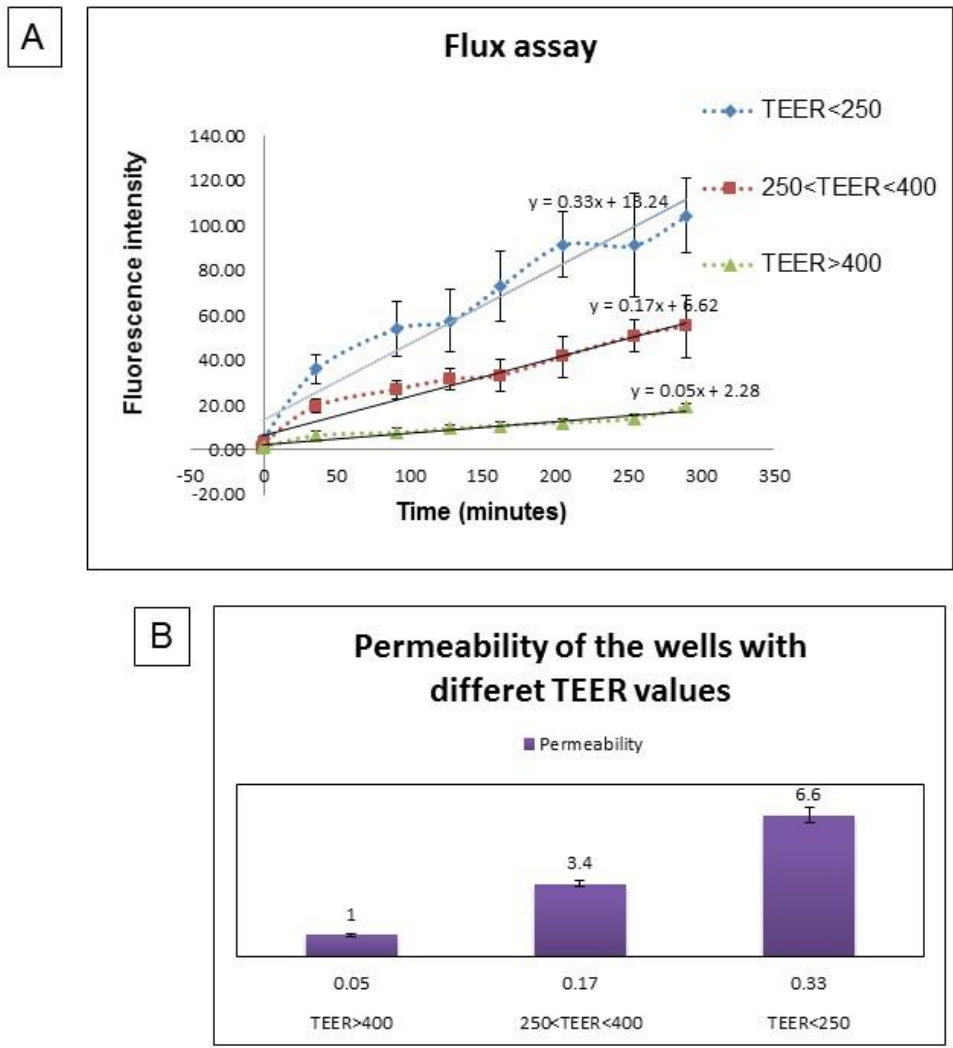


Figure 84. Flux assay on PRBEC of a different TEER values.

A - The curves represent the intensity of fluorescence of the media on the basolateral side of the filter, as a function of time, after introduction of 4 kD fluorescent dextran to the luminal side of the well. Experiment was repeated 3 times on at least 2 wells for each group.

B - The bar graph represents the differences in permeability of PRBEC of a different TEER value. The wells with TEER higher than 400 had the best barrier function and their permeability value was assigned as 1, the permeability value for the other groups of well was calculated as a ratio between the slope value from the curve.

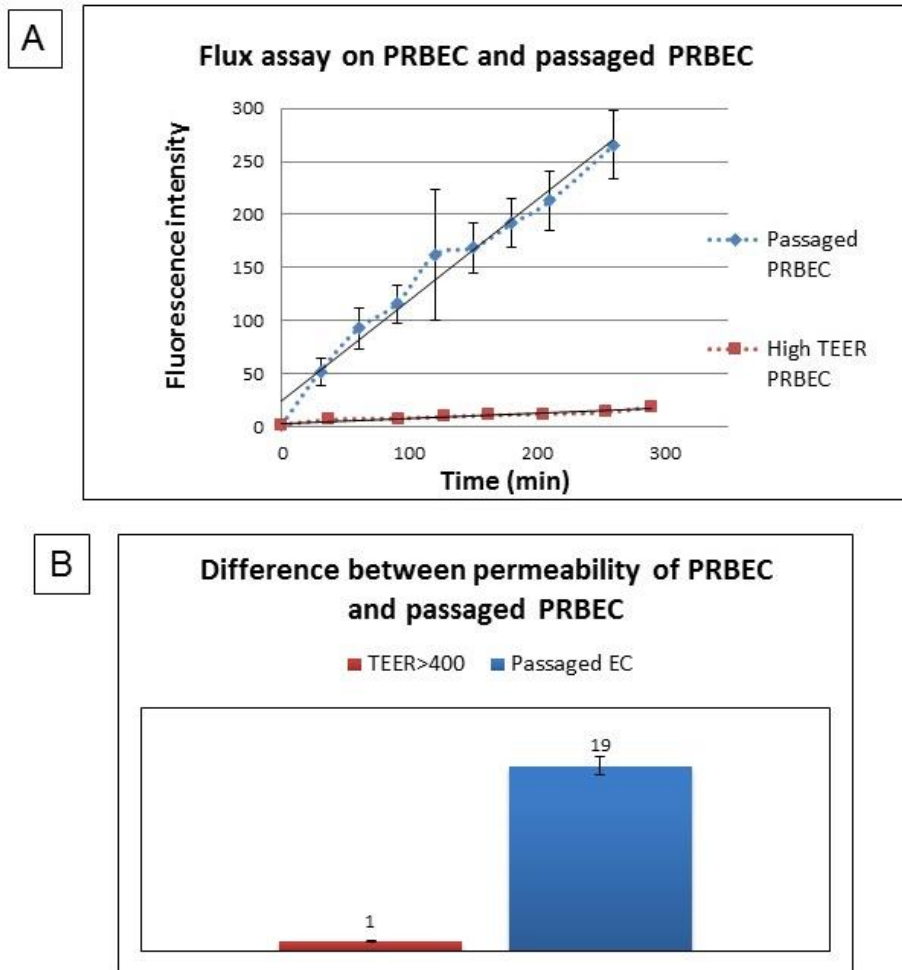


Figure 85. Flux assay on PRBEC and passaged PRBEC.

A - The curves represents the intensity of fluorescence of the media on the basolateral side of the filter, as a function of time, after introduction of 4 kD fluorescent dextran to the luminal side of the well.

B - The bar graph shows the slop value from the curves representing flux measurement on PRBEC and passaged PRBEC

Permeability of PRBEC after VEGF-A treatment

As a next step we wanted to check the permeability of PRBEC after VEGF-A treatment. We performed a flux experiment, as previously described, and after two hours we added VEGF-A (to a final concentration of 50 ng/ml) to the apical or basolateral side of the transwell. Afterwards, we continued to measure the intensity of the fluorescence in the media on the basolateral side of the filter (Figure 86). This method was previously described in the recent paper *Martins at al.* (Martins, 2013).

PRBEC exhibited a slight decrease in permeability both after apical and basolateral VEGF-A treatment. This was a very surprising finding. However, the PRBEC used for this assay exhibited TEER values between 200 and 250 Ωcm^2 . We reasoned it was possible that the 4kDa dextran may readily pass through the relatively low TEER monolayers. To probe this idea further, we decided to perform a similar experiment with 70 kD fluorescent dextran (Figure 87). When the flux assay was performed with the larger dextran, VEGF-A added to the basolateral side of the transwell increased permeability of PRBEC. There was no effect of VEGF-A when added to the apical side of the well.

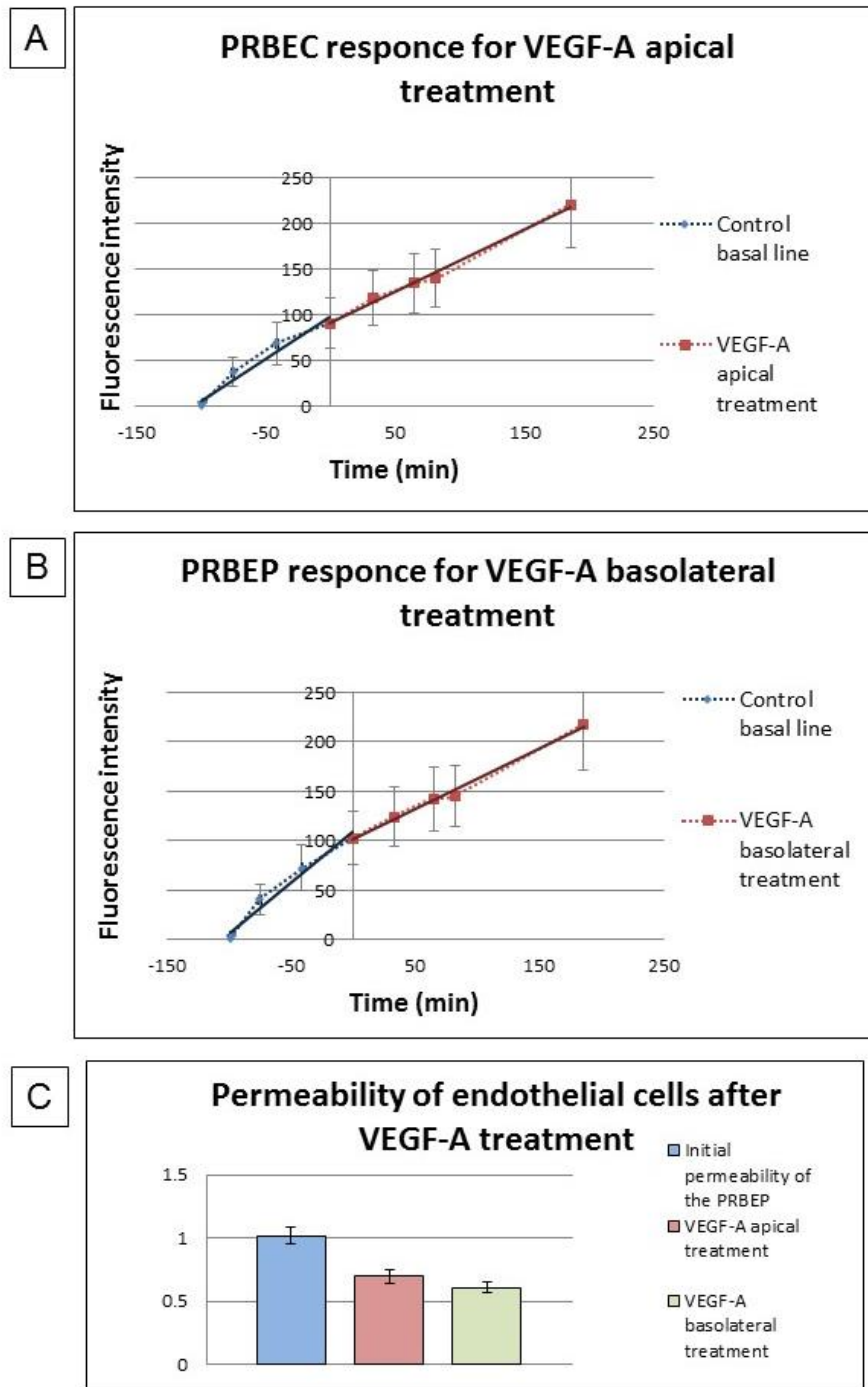


Figure 86. Permeability of the PRBEC after apical and basolateral VEGF-A treatment.

A and B - Flux assay on PRBEC using 3 kD dextran as a tracer. After 2 hours of initial flux measurement (control basal line) VEGF-A was introduced to the apical (A) or basolateral (B) side of the well and flux measurement was continued for another 3 hours.

C - Permeability of PRBEC was measured as a ratio of the slop of the curve before and after VEGF-A apical/basolateral treatment

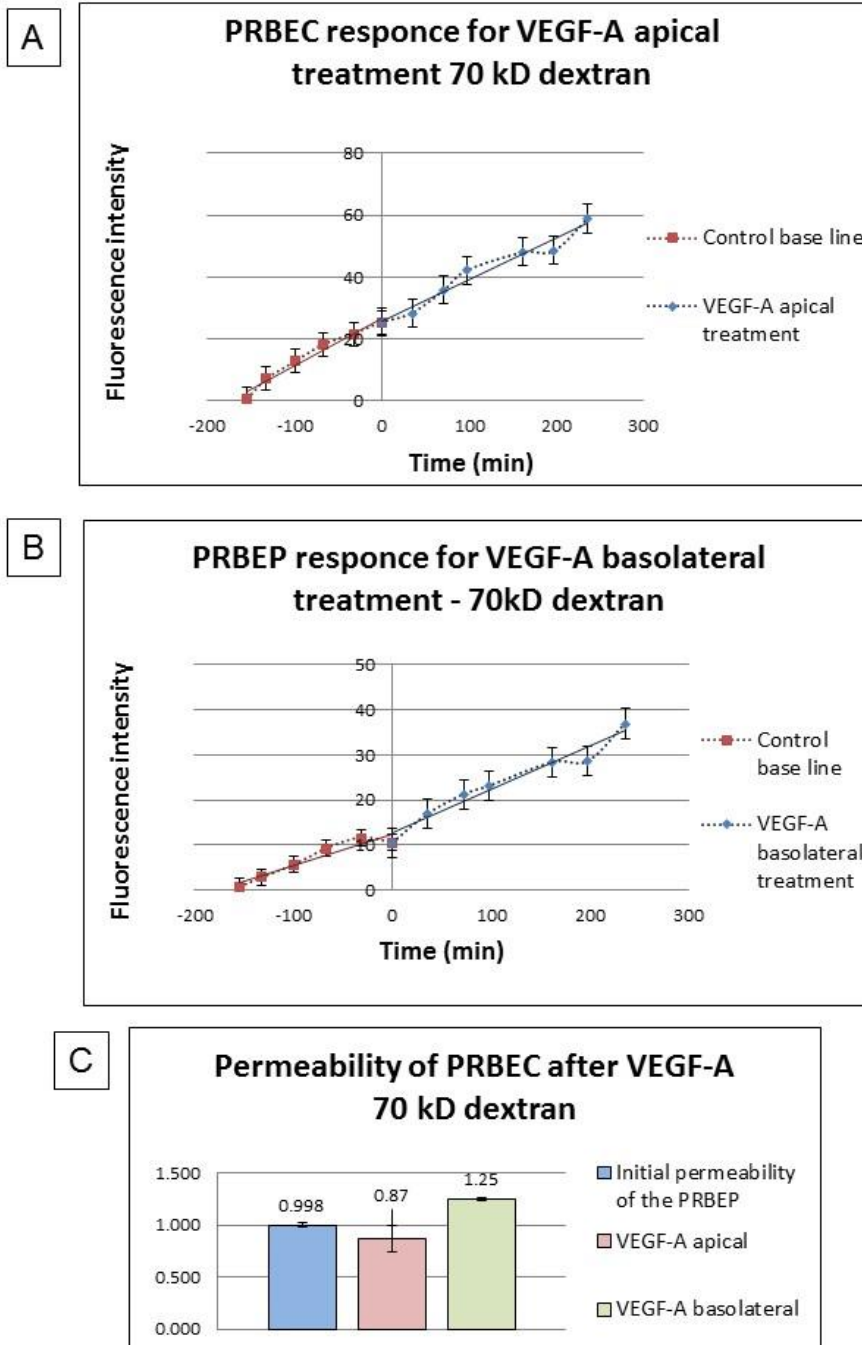


Figure 87. Permeability of the PRBEC after apical and basolateral VEGF-A treatment.

A and B - Flux assay on PRBEC using 70 kD dextran as a tracer. After 2 hours of initial flux measurement (control basal line) VEGF-A was introduced to the apical (A) or basolateral (B) side of the well and flux measurement was continued for another 3 hours.

C - Permeability of PRBEC was measured as a ratio of the slop of the curve before and after VEGF-A apical/basolateral treatment

Optimisation of the PRBEC isolation method

The initial experiments with PRBEC described above demonstrated the importance of obtaining reproducible, high TEER cultures. This observation was also made by Dr Patric Turowski and colleagues, who found that low TEER PRBEC cultures did not show reproducible cell polarity. Moreover, though initially obtaining high TEER cultures ($>400 \Omega\text{cm}^2$) with some success, cultures obtained over the course of approximately 1 year yielded very low TEER values, and we were unsure of the reason. Thus, I decided to optimise isolation conditions in order to improve the TEER quality of the primary cells.

Culture purity is crucial for receiving high TEER of PRBEC. I decided to increase the concentration of puromycin from $5 \mu\text{g}/\text{ml}$ to $10 \mu\text{g}/\text{ml}$. Puromycin is usually added to the culture on the second day after isolation - D1 (Day 1), and thus I also decided to add puromycin on the day of isolation - D0 (Day 0). TEER was measured and compared to the previous concentration and time of addition of puromycin. The change in puromycin concentration and day of exposure did not improve the TEER. However less variability in TEER was observed with puromycin added on D0, so we continued with that change in the protocol (Figure 88).

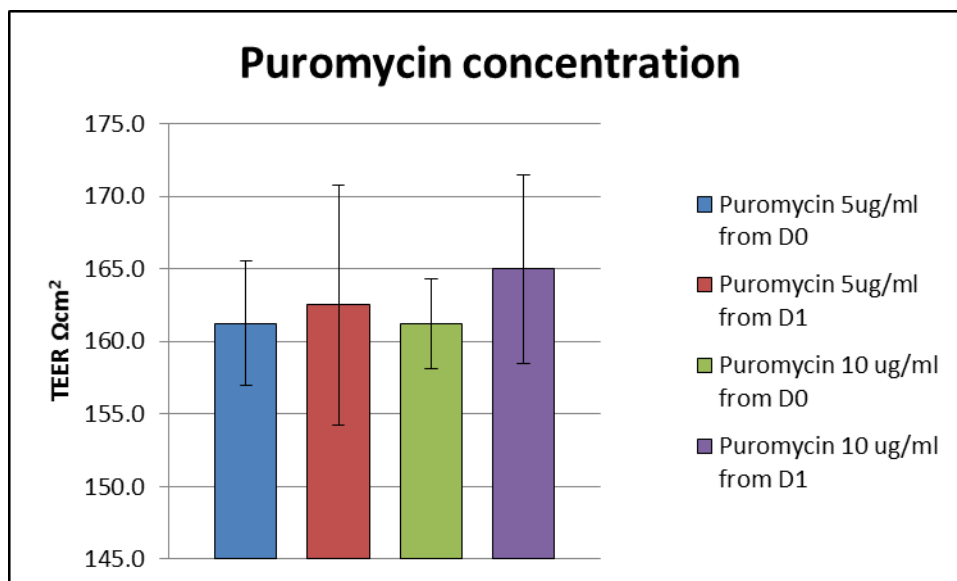


Figure 88. Optimisation of puromycin selection step.

PRBEC were treated with puromycin 5 or 10 $\mu\text{g/ml}$, on the day of the isolation and on the first day after the isolation. Charts represent average TEER values of at least 4 wells for each group. Error bars indicate SEM values.

We also tested, if the density of primary cells would influence TEER values (Figure 89). Cells were plated on transwells with the density described in the protocol (Methods), represented on the chart as a 100%, 1.5 times higher density - 150%, 2 times higher density 200%, and 0.5 times less dense - 50%. Variations in cell density had no significant effect on TEER values, with values still below 200 Ωcm^2 .

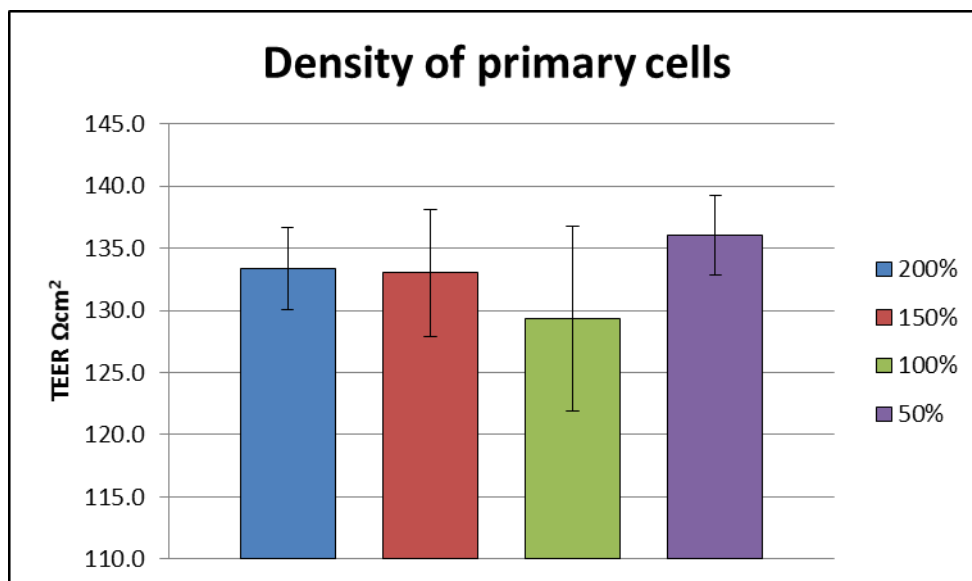


Figure 89. Optimisation of the plating density of PRBEC cells.

PRBEC were plated on transwells with different densities: chart – 200% corresponds to wells plated with a density 2 times higher than the density described in the initial protocol, 150% - 1.5 times higher, 100% normal density, 50% - 0.5 times less dense. Charts represent average TEER values of at least 3 wells for each group. Error bars indicate SEM values.

We continued to find steps in the protocol for optimisation. Microscopic examination of PRBEC immediately after isolation led to the observation that we were receiving an unusually high number of single cells and relatively short capillary fragments. This led us to compare digestion enzymes (Figure 90). The highest TEER values were obtained with collagenase/dispase digestion media from Roche. Their average TEER was $211 \pm 8 \Omega\text{cm}^2$, and we decided to use Roche enzyme for all further isolations. However we continued to obtain variability in PRBEC cultures in terms of TEER values, and were never able to obtain the $>400 \Omega\text{cm}^2$ cultures we used for initial studies.

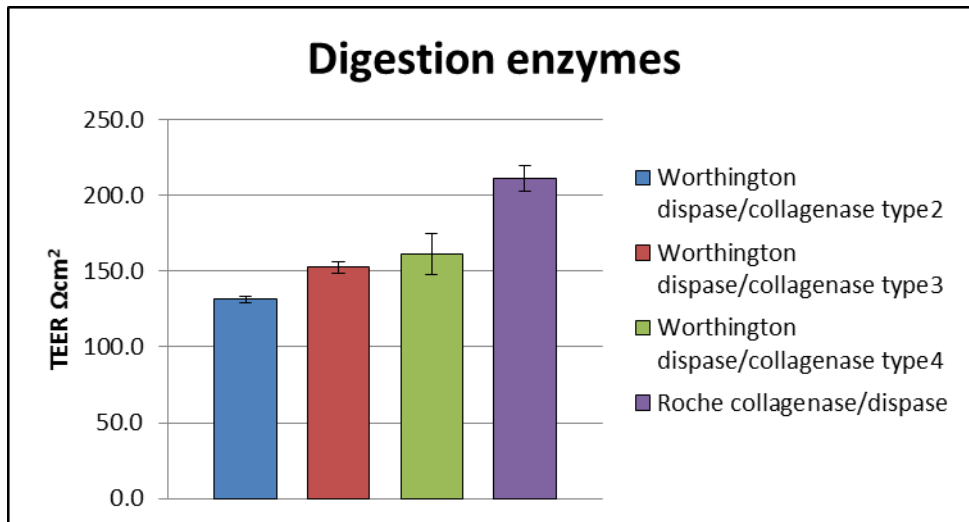


Figure 90. Optimisation of collagenase/dispase digestion step.

The chart represents the average TEER values of at least 12 wells for each group. Error bars indicate SEM values.

Primary rat brain endothelial cell isolation and experimentation - discussion and conclusion

PRBEC have proven to be a very valuable tool in studying barrier function, and have recently been used to demonstrate polarity of VEGF-A signalling (Hudson, 2014). However, we encountered increasing variability in the TEER of cultures, and low values, which were difficult to explain. We attempted to optimize isolation and culture conditions without success, and the next section of this chapter will describe initial steps to develop another method to study barrier function, using ex vivo culture of retinal capillary fragments.

However, it is important to note that a solution to the TEER problem was recently identified. The manufacturer of the transwell inserts, Costar, changed the composition of the membranes upon which the extracellular matrix and cells sit, without notifying customers on their website or catalogue. The new membranes were a poorer substrate for cell attachment, thus cells needed to be seeded significantly higher to obtain reproducible, high TEER cultures.

Capillary isolation

PRBEC isolation was labour intensive, barrier function studies were unreliable and the tissue of origin was not the retina. We decided to try to isolate capillary fragments from the retina.

Capillary fragments were enriched using a collagenase/dispase digestion step and 70 μm filters (see Methods). This method has been adapted from (Coisne, 2005) and was successfully used for capillary form cortex isolation (Figure 91) (Cristante, 2013).

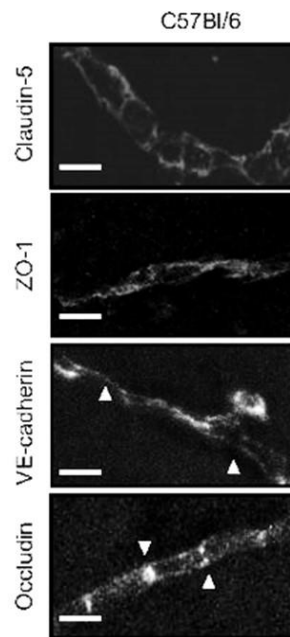


Figure 91. Cortical capillaries. Adapted from (Cristante, 2013).

Characteristics of obtained retina capillaries

In order to confirm the morphology of the retina capillary fragments, they were immunostained with anti-CI-5 antibody, anti-VE-cadherin antibody and with phalloidin (Figure 92-94).

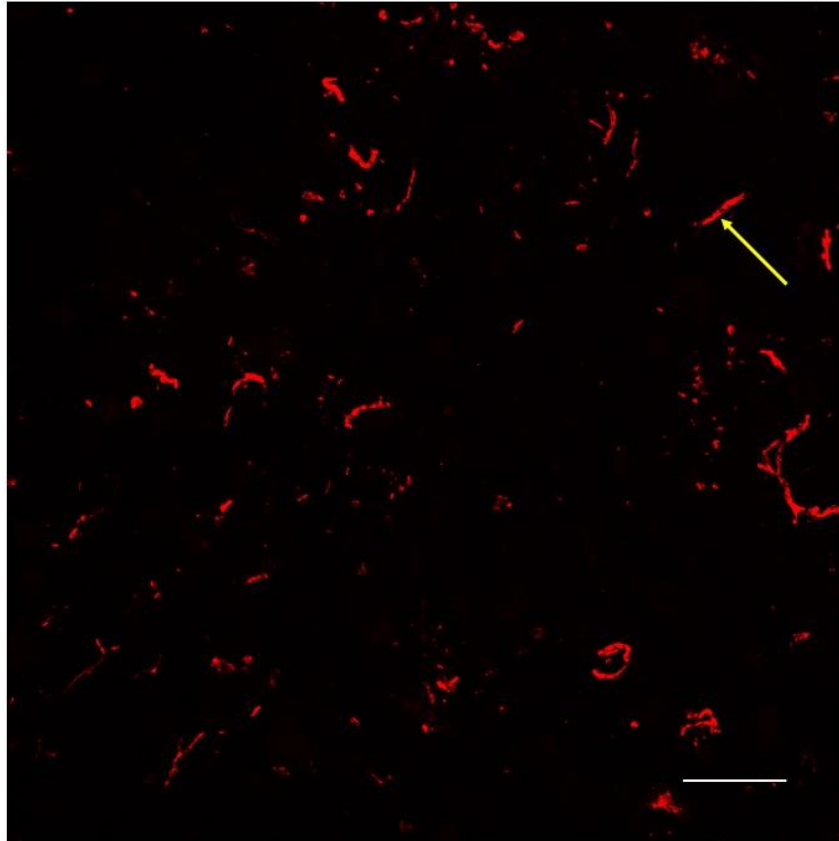


Figure 92. Topographic picture of the capillaries isolated from the retina.

Capillaries we stained with phalloidin. The scale bar indicates 100 μm for all pictures.

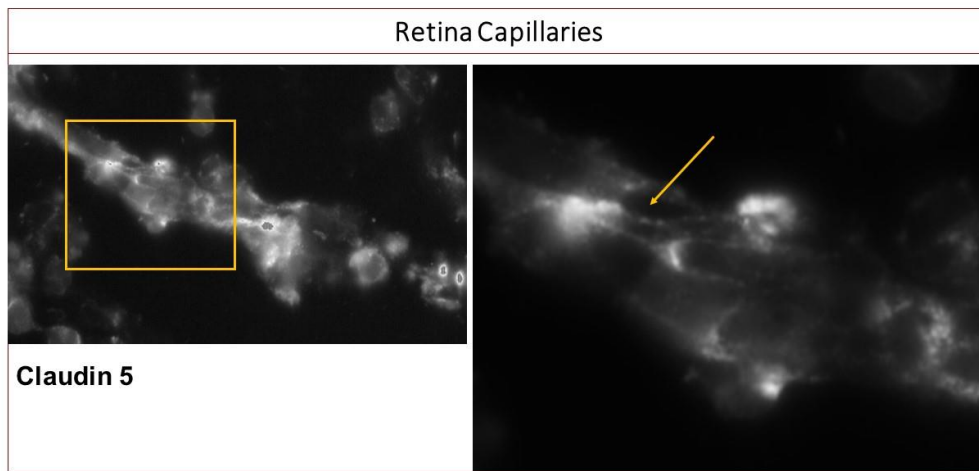


Figure 93. Capillaries from P15 retina, stained with anti Claudin5 antibody. The arrow points the junction localisation of the Claudin5.

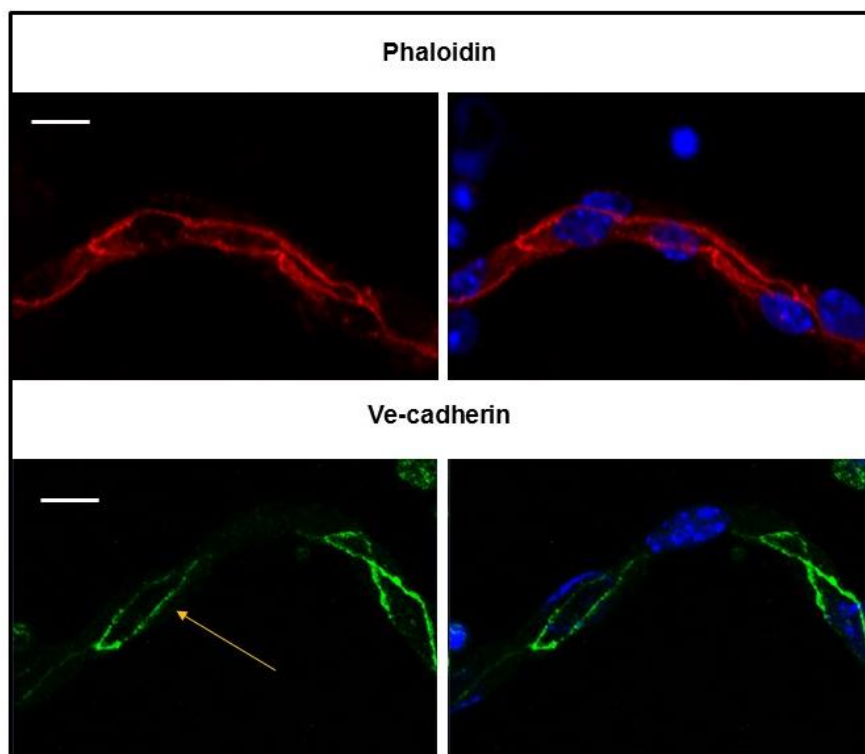


Figure 94 Capillaries from P15 retina stained with Phalloidin and anti VE-cadherin antibody.

Phalloidin and VE-cadherin were mostly localised in the cell junctions. The scale bar indicates 10 μm for all pictures.

Exploring PAK and MLC activity in the retinal capillary fragments at P5 and P15, and after VEGF-A treatment

Capillary fragment immunostaining confirmed that with the digestion and filtration method we can rapidly obtain fragments that maintain junctional protein localisation. Using this new approach we decided to explore previous in-vivo finding. We performed a Western blot on capillary fragments isolated from P5 and P15 retina. The Western blot experiment confirmed previous findings that MLC and PAK dominate in their phosphorylated state at early stages of development and suggest that the fragments may be a reliable source of tissue for mechanistic studies (Figure 95). The question that remained was if increases in MLC and PAK phosphorylation were a response to elevated VEGF-A, like that present at P5.

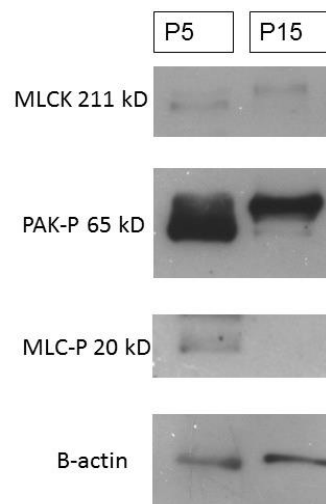


Figure 95. MLC-P, and PAK-P at P5 and P15 retina capillaries.

Western blotting data showing the differences in expression MLC-P (Anti MLC Ser19-phospho), and PAK-P (Anti-PAK1 (phospho S144) + PAK2 (phospho S141) + PAK3 (phospho S139) at P5 and P15 retina capillaries.

We decided to perform another experiment where we treated P15 capillaries with VEGF-A (25ng/ml, 50ng/ml, and 100ng/ml) and left them for incubation for 10 or 30 minutes (Figure 96). The preliminary experiment showed that after 30 min of 50ng/ml VEGF-A treatment and both 10 min and 30

min after 100ng/ml VEGF-A treatment we could see small increase in MLC (S19) phosphorylation. The data from PAK phosphorylation (Anti-PAK1 (phospho S144) + PAK2 (phospho S141) + PAK3 (phospho S139) was not clear, as after a small dose of VEGF-A treatment the level of PAK phosphorylation was slightly lower, whereas the higher dose of VEGF-A increased the phosphorylation of PAK.

These initial experiments require further investigation, and repetition as the experiments was performed only once. However, the retinal capillaries appear to be a good model for studying the molecular biology of BRB function.

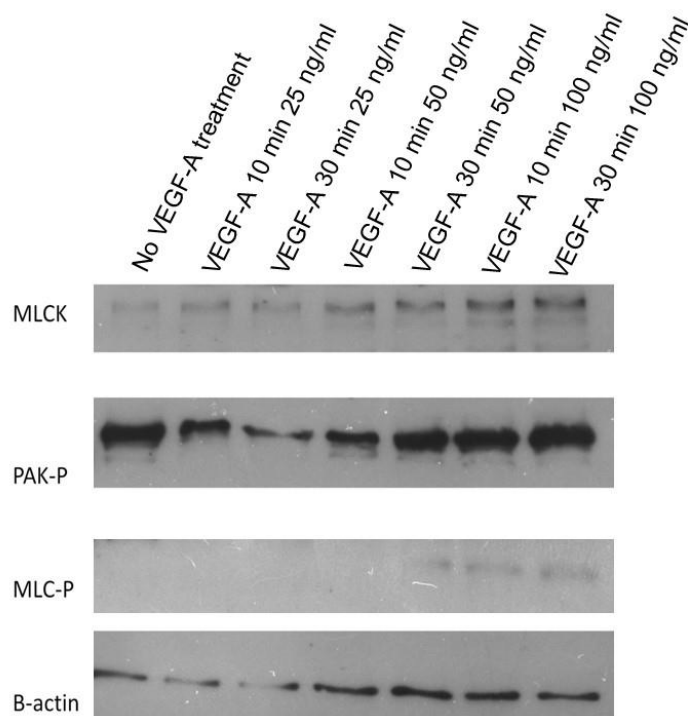


Figure 96. MLC-P and PAK-P level after VEGF-A treatment on capillaries.

Western blotting data showing the differences in level of MLC-P (Anti MLC Ser19-phospho), and PAK-P (Anti-PAK1 (phospho S144) + PAK2 (phospho S141) + PAK3 (phospho S139) at P15 retina capillaries after VEGF-A treatment.

Ex-vivo model for studying BRB properties - discussion and conclusion

There is a high demand to develop a valuable in vitro model that could well mimic the in vivo conditions. PRBEC plated on transwells is a very difficult

assay and it has been used for understanding the EC functions and polarity (Hudson, 2014). However, we found very difficult to optimise the assay and despite a lot of effort we could not successfully proceed with this assay. We attempted to use very simple and straight forward method to isolate retinal capillaries. These capillaries seems to be a very promising model that might allow us to study the BRB functions.

Final Discussion

Chapter 8.

Final discussion

There has been abundant research into the onset, molecular and cellular basis and the manipulation of the BBB, with the mapping of its onset in the rodent achieved nearly 30 years ago (Risau W, 1986). The BRB has been much less studied, despite the fact that loss of the barrier is a hallmark of sight threatening diseases such as neovascular AMD and diabetic retinopathy.

As a first step into developing a better understanding of the BRB, I initiated studies aimed at mapping the timing of BRB onset in the post-natal mouse retina, with hopes that this would provide a temporal focal point for mechanistic studies to understand the regulation of barrier formation. Tracer studies provided strong evidence that a vascular barrier to both large and small molecules was fully developed by P10, enabling a series of subsequent experiments comparing morphological and mechanistic features pre- and post BRB formation.

The tracer studies in the murine developmental model showed, that the most permeable part of the growing vasculature is the periphery. This was demonstrated using both NHS-biotin and 70 kD dextran. Interestingly no leakage was detected after P10, when the deep plexi is still developing. This interesting finding suggests that early vascular growth in the retina is accompanied by poor barrier function, but the proliferation, migration and remodelling that accompanies the formation of the deeper vascular beds occurs whilst maintaining the BRB. Just how the BRB is maintained during this period is completely unknown. This is a very interesting feature that requires further investigation and observation, for example by careful immunostaining with

various vascular markers, and attention to the area of the staining. This will help us better understand and map the differences between vascular layers. Another interesting and intriguing characteristic is the fact that retinal EC start displaying barrier function at the same time when all neuronal cells are established in the retina.

VEGF-A was first described as a Vascular permeability factor (VPF) in 1983 (Senger 1983). In 1989 Napoleone Ferrara and his colleagues were the first to isolate and clone VEGF-A at Genentech, which quickly became one of the best studied angiogenic factors (Ferrara, 2011, Leung, 1989). VEGF-A increases the permeability of the vasculature 50 000 times more than histamine (Shulman, 1996).

Our results underline the important role of VEGF-A during retina vascular development, as its level of expression is much higher at P5 compared to P15. Very interesting is also the pattern of VEGF-A expression at P5. Immunostaining of VEGF-A showed the highest expression at the periphery of vasculature. In the non-vascular part of the retina the pattern of VEGF-A localisation was a mesh-like network that tracked the astrocyte pattern in the retina. This makes sense as VEGF-A is expressed by astrocytes. In the future we are planning to do co-staining with VEGF-A and GFAP, which might assure us about this hypothesis. Interestingly the area of the highest expression of VEGF-A at P5 overlaps with the area of most permeable vasculature.

We also found that VEGF-A was responsible for BRB breakdown in the developed retina at P15, as we detected increased permeability of vasculature after intravitreal injection of VEGF-A. In contrast, by blocking VEGFR2 function at P6 we observed improvement in BRB function.

Knowing the important role of VEGF-A in vascular development we also localised the VEGFR1 and -2 and concluded that VEGFR1 is mainly localised in the vasculature whereas VEGFR-2 exhibits vascular and nonvascular – neuronal localisation in the retina. We also explored the polarity of the expression of VEGF-receptors in the retina by performing VEGF-receptor antibody tracer studies (to mimic luminal localisation of the receptors) and staining without permeabilisation (to mimic abluminal localisation of the receptors).

The VEGF-receptor polarity experiment suggested that, VEGFR2 is mainly localised on the abluminal side of the EC, whereas VEGFR1 expression is mainly luminal.

In future experiments we would like to expand the VEGFR1 and VEGFR2 in-vivo staining to see if there is any difference in luminal/abluminal localisation of these receptors at early stages of development. In order to do that we would like to do in-vivo VEGFR1 and VEGFR2 staining at P5 using similar assay, as described for P20. We would also like to perform staining for junctional proteins after VEGF-A intravitreal injection. This may give us interesting information, which would help to determine the role and function of junctional proteins in VEGF-A induced pathways that lead to increased permeability of the BRB.

Demonstration of the time point for BRB acquisition allowed us to investigate the pathways that might be implicated in increased permeability of the vasculature at the early stages of development. In order to screen changes in protein activities between P5 and P15 retina, in collaboration with Roche Innovation Center Basel we performed phosphoproteomic studies. This rapid and effective method allowed us to identify numerous pathways that are activated or deactivated between P5 and P15.

The phosphoproteomic experiments provided extremely large datasets and complex results, which will require further verification and study. Some of these changes are very interesting, for example a 23 times increase of phosphorylation of α -catenin 3 on S637 at P15 compared to P5. Change in α -catenin phosphorylation among many others might be an important feature for further investigation. It would be very interesting to localise in the retina, using for example immunostaining, the proteins that went thru the highest changes in phosphorylation among various stages of retina development.

Analysis of the phosphorylation pattern of proteins gave us very complex results. Some of the molecules upregulated between P5 and P15 were junction proteins, proteins implicated in VEGF-A signalling or cytoskeletal remodelling. This gave us a very interesting, however still an incomplete picture around all the changes that were taking place between P5 and P15 retina. We decided to focus on and study pathways implicated in cytoskeletal reorganisation, as this

appeared the most probable mechanism responsible for the changes in the permeability of vasculature during development.

Cytoskeletal dynamics are primarily modulated by actin–myosin interactions and are regulated by the phosphorylation of the regulatory MLC by MLCK (Sanders, 1999). Many studies have revealed that increased permeability of EC can be caused by actomyosin contractile activity in response to MLC phosphorylation (Rigor, 2012, Garcia, 1995).

It has been also demonstrated that MLCK mediated MLC phosphorylation might be implicated in controlling permeability in other tissue beds. Clayburgh and colleagues showed that epithelial barrier dysfunction is mediated by MLCK-dependent MLC phosphorylation. In addition in this model genetic and pharmacological MLCK inhibition prevented *in vivo* epithelial barrier dysfunction (Clayburgh, 2005).

It has been also recently shown that early BBB disruption is caused by the activation of MLC signalling, following actin polymerisation and disassembly of junctional proteins within EC (Shi, 2016). Interestingly phosphoproteomic data showed increased phosphorylation of MLC on S19 at P5, when BRB does not maintain proper gate keeping role.

Stockton and colleagues demonstrated the important role of PAK in the regulation of vascular permeability. PAK phosphorylated on S141, during activation downstream of Rac, translocates to the cell-cell junction. This event correlates with increased permeability and MLC phosphorylation (Stockton, 2004). Interestingly phosphoproteomic data showed increased phosphorylation of PAK on S141 at P5 compared to P15.

These findings led us to explore the expression and localisation of MLC and PAK in the retina at different stages of development. Using western blotting method and immunostaining we were able to confirm higher phosphorylation of MLC and PAK at P5, compare to later stages of retina development. We also tested the permeability of the vasculature at P6 after blocking MLCK activity. A small inhibitory peptide, termed PIK, which blocks the function of the catalytic domain of MLCK improved barrier function. As a next experiment we would like to look at the changes in MLC and PAK phosphorylation after PIK

administration, as this will help us better understand the changes in vascular permeability during BRB formation.

All of this work led us to believe that cytoskeletal remodelling caused by MLC activation could be responsible for poor barrier function of EC prior to P10. This might occur via endocytosis of junction proteins (Figure 97).

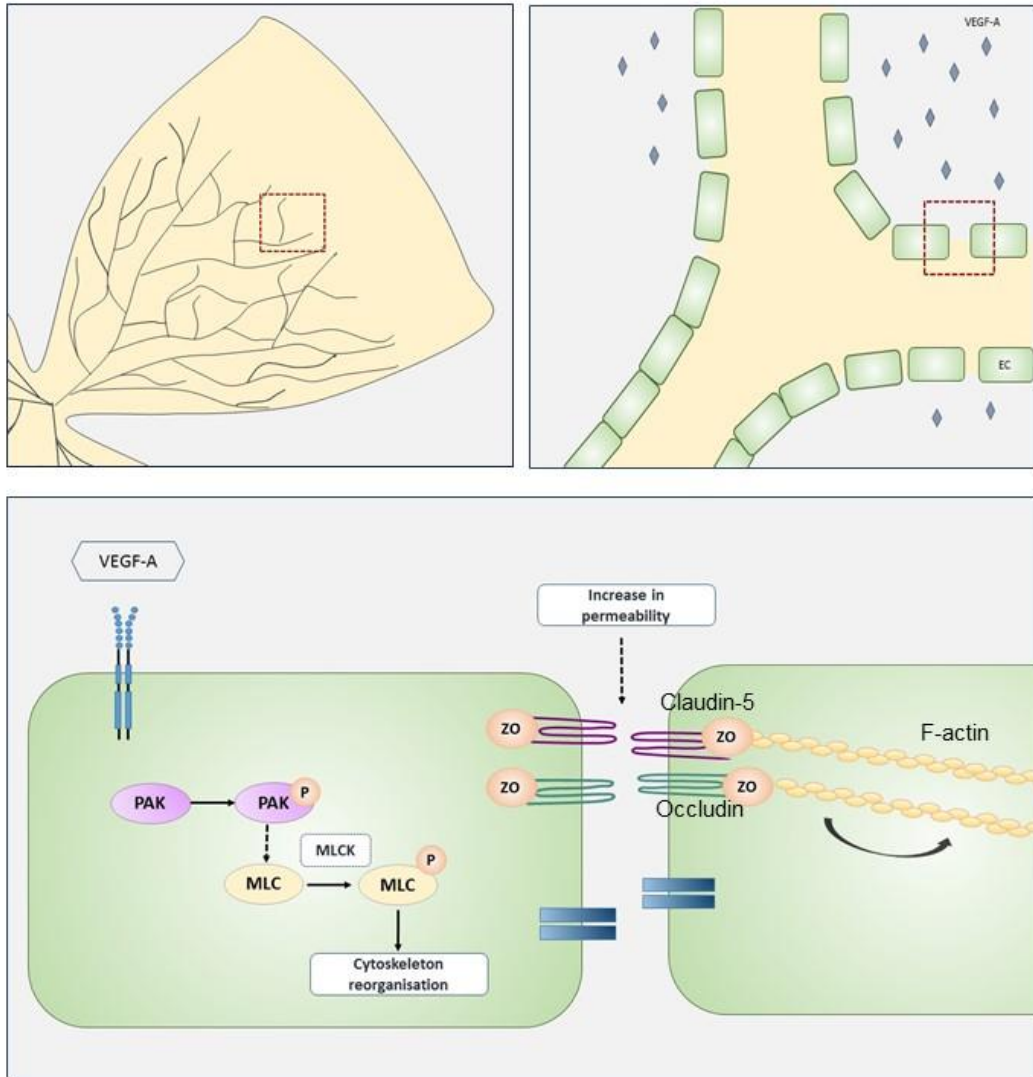


Figure 97. Proposed mechanism that is involved in increase permeability of EC prior to P10.

Endothelial cells at the peripheral vasculature, where the expression of VEGF-A is higher, does not maintain proper barrier function. VEGF-A might cause PAK phosphorylation, and MLCK mediated MLC phosphorylation. This causes cytoskeleton rearrangement and changes in TJ and AJ molecules position, and results in increased permeability.

The role of actomyosin cytoskeleton on assembly and function of junction molecules has been well described in epithelial cell models. Junction proteins are intimately linked to the cytoskeleton, and that is why they stay under the mechanism that regulates the dynamics of the cytoskeleton (Zihni, 2014, Quiros, 2014).

For this thesis, we have investigated an *in vivo* permeability model, checked EC function at the early stages of development, mapped BRB formation, localised JT and AJ proteins in the retina vasculature and tested the effect of VEGF-A on BRB function (by blocking VEGF-A activity at P6 and by injecting VEGF-A at P16). We screened all the differences in protein phosphorylations between P5 and P15 and saw that truly VEGF-A activity seems to be highly involved at early stages of development, we also detected very interesting phosphorylations at AJ and TJ proteins. All these results convinced us about the importance of further studies on these changes but using *in vivo* model.

In contrast, we encountered many difficulties in optimising PRBEC cell culture model in order to use it for our studies. The TEER values of cells plated on transwells was too low to study barrier function. We attempted efforts to optimise the culture, but unfortunately we could not overcome the variability in TEER values of the PRBEC.

We understood the high importance of developing *in vivo* model to study BRB functions and properties, especially in aspect of cytoskeletal remodelling as a potential mechanism involved in barrier regulations. We attempted to develop a new assay that allowed us to harvest capillary vessels from the retina at different stages of murine development. This model has been described previously and was used for the isolation of capillary vessels from cortex (Coisne, 2005 , Cristante, 2013).

This model allowed us to closely mimic *in vivo* condition and compare the phosphorylation of PAK and MLC in P5 and P15 capillaries. We also attempted to look at the PAK and MLC phosphorylation in capillaries after VEGF-A treatment. Interestingly we noticed an increase in MLC phosphorylation on S19 after 30min of VEGF-A treatment. This is a very encouraging result, however requires further investigation and testing.

This model might help us to better understand the changes in BRB during the process of its formation, and also the changes in BRB after VEGF-A treatment. This technique might also provide insight to explore the role in BRB function of different candidates identified in the phosphoproteomic assay.

Understanding the mechanism that controls BRB function is crucial from the clinical point of view. Breakdown of the inner BRB occurs in many eye

diseases: diabetic retinopathy, AMD, retinal vein occlusion, uveitis, and other chronic retinal diseases. Central mechanism that accompanies these diseases is a change in the permeability of retinal EC (Klaassen, 2013). Better understanding of the mechanism that lies behind increased permeability, would help us develop better treatments for those conditions.

Retinopathy of prematurity is a retina vascular disorder that affects prematurely-born babies under intensive neonatal care, which includes oxygen therapies. Up normal oxygen supply, cause extraretinal fibrovascular proliferation, which might result in retinal detachment. Current standard treatment for ROP is ablation of avascular retina using laser treatment or cryotherapy (German, 2016). However, these conventional treatments might cause complications, and does not prevent all vision loss. Recent studies shows that intravitreal injection of bevacizumab, anti-VEGF drug, could give us effective treatment (Mintz-Hittner, 2011). Nonetheless long term study is required in order to assure the safety and effectiveness of anti VEGF therapy in ROP, especially that some follow up studies report recurrence of ROP after initial ranibizumab treatment (Chan, 2016, Patel, 2012). In other eye conditions that involve increased vascular permeability and neovascularisation like diabetic retinopathy and AMD, main treatments - similarly to ROP, include laser therapy, anti-VEGF injections and in more severe cases vitrectomy. The main anti VEGF drugs used in clinics for DR is ranibizumab and for AMD aflibercept. These anti VEGF therapies require intravitreal injection that often needs to be repeated every month in a spectrum of 3-6 months period of time. Blocking VEGF in the eye diseases cause improvement, but the long term effect of these therapies is still unknown.

VEGF is a major player in course of retina development and proper vascular function. Over the past decades many research project grip the complexity of VEGF role in vascular and neuronal homeostasis. This is why we might be on a course of improvement anti VEGF treatments in eye diseases. Better understanding of the pathways triggered by VEGF might help us design better treatment for eye conditions. In this work I showed changes in the vasculature in the murine model, which are a very interesting target for further understanding of the mechanisms responsible for proper homeostatic function.

Cytoskeleton changes that might cause TJ and AJ proteins disorganisation, driven by VEGF-A, might be a potential target for designing new drugs, which for examples will block MLC and PAK phosphorylation.

In conclusion this work presents the time point for BRB acquisition, and shows that by P10, EC in the retina established the inner BRB. We also demonstrated the pattern of VEGF-A expression in the retina, which interestingly matches the area of the highest permeability of EC. In collaboration with Roche Innovation Centre Basel we performed phosphoproteomic assay that presented as many candidates that might be involved BRB formation. Many of these candidates require further validation and localisation in the retina, however the role of cytoskeletal dynamic in BRB function accrued to us as important mechanism for further investigation. We demonstrated that truly MLC and PAK are highly phosphorylated at the P5 retina, and phalloidin staining confirms the actin cytoskeleton disruption especially in the periphery at P5 retina. Interestingly CL-5 expression was also weaker and more diffused at the periphery of P5 retina vasculature. To dot point these are interesting and important findings that might help us better understand BRB function, however further investigation especially in in-vitro model is required in order to confirm the findings.

References

- ABBOTT, N. J., HUGHES, C.C., REVEST, P.A., GREENWOOD, J. 1992. Development and characterisation of a rat brain capillary endothelial culture: towards an in vitro blood-brain barrier. *Journal of Cell Science* 103, 23-37.
- ACKAH, E., YU, J., ZOELLNER, S., IWAKIRI, Y., SKURK, C., SHIBATA, R., OUCHI, N., EASTON, R.M., GALASSO, G., BIRNBAUM, M.J., WALSH, K., SESSA, W.C. 2005. Akt1/protein kinase B is critical for ischemic and VEGF-mediated angiogenesis. *Journal of Clinical Investigation*, 115, 2119-27.
- ALBERTS, B., JOHNSON, A., LEWIS, J., RAFF, M., ROBERTS, K., WALTER, P. 2007. Molecular Biology of the Cell, 5th Edition. *Garland Science*, 965-1010.
- ANDERSON, O. A., BAINBRIDGE, J.W.B., SHIMA, D.T.S. 2010. Delivery of anti-angiogenic molecular therapies for retinal disease. *Drug Discovery Today*, 15.
- ANTONETTI, D. A., BARBER, A. J., HOLLINGER, L. A., WOLPERT, E. B. & GARDNER, T. W. 1999. Vascular endothelial growth factor induces rapid phosphorylation of tight junction proteins occludin and zonula occludens 1. A potential mechanism for vascular permeability in diabetic retinopathy and tumors. *J Biol Chem*, 274, 23463-7.
- BASSETT, E. A., WALLACE, V.A. 2012. Cell fate determination in the vertebrate retina. *Trends in Neurosciences* 35, 565-573.
- BAZZONI, G., DEJANA, E. 2004. Endothelial Cell-to-Cell Junctions: Molecular Organization and Role in Vascular Homeostasis. *Physiological Reviews*, 84, 869-901.
- BEN-ZVI, A., LACOSTE, B., KUR, E., ANDREONE, B.J., MAYSHAR, Y., YAN, H., GU, C. 2014. Mfsd2a is critical for the formation and function of the blood-brain barrier. *Nature*, 507, 507-11.
- BERGERS, G., SONG, S. 2005. The role of pericytes in blood-vessel formation and maintenance. *Neuro Oncology*, 7, 452-464.
- BHATTACHARJEE, J., SANYAL, S. 1975. Journal of Anatomy. *Developmental origin and early differentiation of retinal Müller cells in mice.*, 120, 367-372.

- BORNANCIN, F. & PARKER, P. J. 1997. Phosphorylation of protein kinase C-alpha on serine 657 controls the accumulation of active enzyme and contributes to its phosphatase-resistant state. *J Biol Chem*, 272, 3544-9.
- BREKKEN, R. A., OVERHOLSER, J.P., STASTNY, V.A., WALTENBERGER, J., MINNA, J.D., THORPE, P.E. 2000. Selective Inhibition of Vascular Endothelial Growth Factor (VEGF) Receptor 2 (KDR/Flk-1) Activity by a Monoclonal Anti-VEGF Antibody Blocks Tumor Growth in Mice. . *Cancer Research* 60, 5117-5124.
- BROWN, M. V., BURNETT, P.E., DENNING, M.F., REYNOLDS, A.B. 2009. PDGF receptor activation induces p120-catenin phosphorylation at serine 879 via a PKCalpha-dependent pathway. *Experimental Cell Research*, 315, 39-49.
- CARMELIET, P., FERREIRA, V., BREIER, G., POLLEFEYT, S., KIECKENS, L., GERTSENSTEIN, M., FAHRIG, M., VANDENHOECK, A., HARPAL, K., EBERHARDT, C., DECLERCQ, C., PAWLING, J., MOONS, L., COLLEN, D., RISAU, W., NAGY, A. 1996. Abnormal blood vessel development and lethality in embryos lacking a single VEGF allele. *Nature*, 380, 435-9.
- CARVEY, P. M., HENDEY, B., MONAHAN, A.J. 2009. The Blood Brain Barrier in Neurodegenerative Disease: A Rhetorical Perspective. *Journal of Neurochemistry*, 111, 291-314.
- CERMAN, E., OZARSLAN OZCAN, D., CELIKER, H., ERASLAN, M., SAHIN, O. & KAZOKOGLU, H. 2016. Late clinical characteristics of infants with retinopathy of prematurity and treated with cryotherapy. *Int J Ophthalmol*, 9, 567-71.
- CHAN, J. J., LAM, C. P., KWOK, M. K., WONG, R. L., LEE, G. K., LAU, W. W. & YAM, J. C. 2016. Risk of recurrence of retinopathy of prematurity after initial intravitreal ranibizumab therapy. *Sci Rep*, 6, 27082.
- CHAN, P. M., LIM, L., MANSER, E. 2008. PAK is regulated by PI3K, PIX, CDC42, and PP2Calpha and mediates focal adhesion turnover in the hyperosmotic stress-induced p38 pathway. *Journal of Biological Chemistry*, 283, 24949-61.
- CHEW, T. L., WOLF, W.A., GALLAGHER, P.J., MATSUMURA, F., CHISHOLM, R.L. 2002. A fluorescent resonant energy transfer-based biosensor reveals transient and regional myosin light chain kinase activation in lamella and cleavage furrows. *Journal of Cell Biology*, 156, 543-53.

- CHLENSKI, A., KETELS, K.V., KOROVAITSEVA, G.I., TALAMONTI, M.S., OYASU, R., SCARPELLI, D.G. 2000. Organization and expression of the human zo-2 gene (*tjp-2*) in normal and neoplastic tissues. *Biochimica et Biophysica Acta* 1493, 1493 319-324.
- CINES, D., POLLAK, E., BUCK, C., LOSCALZO, J., ZIMMERMAN, G., MCEVER, R., POBER, J., WICK, T., KONKLE, B., SCHWARTZ, B., BARNATHAN, E., MCCRAE, K., HUG, B., SCHMIDT, A., STERN, D. 1998. Endothelial Cells in Physiology and in the Pathophysiology of Vascular Disorders. *Blood*, 91.
- CLAYBURGH, D. R., BARRETT, T.A., TANG, Y., MEDDINGS, J.B., VAN ELDIK, L.J., WATTERSON, D.M., CLARKE, L.L., MRSNY, R.J., TURNER, J.R. 2005. Epithelial myosin light chain kinase-dependent barrier dysfunction mediates T cell activation-induced diarrhea in vivo. *The Journal of Clinical Investigation*, 115, 2702-2715.
- COISNE, C., DEHOUCQ, L., FAVEEUW, C., DELPLACE, Y., MILLER, F., LANDRY, C., MORISSETTE, C., FENART, L., CECHELLI, R., TREMBLAY, P., DEHOUCQ, B. 2005 Mouse syngenic in vitro blood-brain barrier model: a new tool to examine inflammatory events in cerebral endothelium. *Laboratory Investigation - Nature*, 85, 734-46.
- COOPER, G. M. 2000. The Cell: A Molecular Approach. 2nd edition. *Sinauer Associates*.
- COTTERET, S., JAFFER, Z. M., BEESER, A. & CHERNOFF, J. 2003. p21-Activated kinase 5 (Pak5) localizes to mitochondria and inhibits apoptosis by phosphorylating BAD. *Mol Cell Biol*, 23, 5526-39.
- CRAWFORD, Y., FERRARA, N. 2009. VEGF inhibition: insights from preclinical and clinical studies. *Cell and Tissue Research*, 335, 261-9.
- CRISTANTE, E., MCARTHUR, S., MAURO, C., MAGGIOLI, E., ROMERO, I.A., WYLEZINSKA-ARRIDGE, M., COURAUD, P.O., LOPEZ-TREMOLEDA, J., CHRISTIAN, H.C., WEKSLER, B.B., MALASPINA, A., SOLITO, E. 2013. Identification of an essential endogenous regulator of blood-brain barrier integrity, and its pathological and therapeutic implications. *Proceedings of the National Academy of Sciences*, 110, 832-41.
- CUNHA-VAZ, J., BERNARDES, R., LOBO, C. 2011. Blood-retinal barrier. *European Journal of Ophthalmology*, 21.

- CUNHA-VAZ, J. G., SHAKIB, M., ASHTON, N. 1965. Studies on the permeability of the blood-retinal barrier. I. On the existence, development, and site of a blood-retinal barrier. *British Journal of Ophthalmology* 80, 441–453.
- DEJANA, E. 2004. Endothelial cell-cell junction: happy together *Cell biology*, 5, 261-70.
- DERYCKE, L. D., BRACKE, M.E. 2004. N-cadherin in the spotlight of cell-cell adhesion, differentiation, embryogenesis, invasion and signalling. *International Journal of Developmental Biology*, 48, 463-76.
- DORRELL, M. I., AGUILAR, E., FRIEDLANDER, M. 2002 Retinal vascular development is mediated by endothelial filopodia, a preexisting astrocytic template and specific R-cadherin adhesion. *Investigative ophthalmology & visual science* 43, 3500-10.
- DORRELL, M. I., FRIEDLANDER, M. 2006. Mechanisms of endothelial cell guidance and vascular patterning in the developing mouse retina. *Progress in Retinal and Eye Research*, 25, 277-95.
- DUDEK, S. M., GARCIA, J.G. 2001. Cytoskeletal regulation of pulmonary vascular permeability. *Journal of Applied Physiology*, 91, 1487-1500.
- EDWARDS, A. S. & NEWTON, A. C. 1997. Phosphorylation at conserved carboxyl-terminal hydrophobic motif regulates the catalytic and regulatory domains of protein kinase C. *J Biol Chem*, 272, 18382-90.
- ELICEIRI, B. P., PUENTE, X.S., HOOD, J.D., STUPACK, D.G., SCHLAEPFER, D.D., HUANG, X.Z., SHEPPARD, D., CHERESH, D.A. 2002. Src-mediated coupling of focal adhesion kinase to integrin $\alpha\beta 5$ in vascular endothelial growth factor signaling. *Journal of Cell Biology*, 157, 149–160.
- ERICKSON, B. K., JEDRYCHOWSKI, M. P., MCALISTER, G. C., EVERLEY, R. A., KUNZ, R. & GYGI, S. P. 2015. Evaluating multiplexed quantitative phosphopeptide analysis on a hybrid quadrupole mass filter/linear ion trap/orbitrap mass spectrometer. *Anal Chem*, 87, 1241-9.
- ESCOBAR, D. J., DESAI, R., ISHIYAMA, N., FOLMSBEE, S.S., NOVAK, M.N., FLOZAK, A.S., DAUGHERTY, R.L., MO, R., NANAVATI, D., SARPAL, R., LECKBAND, D., IKURA, M., TEPASS, U., GOTTARDI, C.J. 2015. α -Catenin phosphorylation promotes intercellular adhesion through a dual-kinase mechanism. *Journal of Cell Science: Home*, 128, 1150-65.

- FAMIGLIETTI, E. V., STOPA, E.G., MCGOOKIN, E.D., SONG, P., LEBLANC, V., STREETEN, B.W. 2003. Immunocytochemical localization of vascular endothelial growth factor in neurons and glial cells of human retina. *Brain Research*, 18, 195-204.
- FANTIN, A., VIEIRA, J.M., GESTRI, G., DENTI, L., SCHWARZ, Q., PRYKHOZHIIJ, S., PERI, F., WILSON, S.W., RUHRBERG, C. 2010. Tissue macrophages act as cellular chaperones for vascular anastomosis downstream of VEGF-mediated endothelial tip cell induction. *Blood*, 116 829-40.
- FERRARA, N. 2011. From the discovery of vascular endothelial growth factor to the introduction of avastin in clinical trials - an interview with Napoleone Ferrara by Domenico Ribatti. *The International Journal of Developmental Biology*, 55, 383-8.
- FERRARA, N., CARVER-MOORE, K., CHEN, H., DOWD, M., LU, L., O'SHEA, K.S., POWELL-BRAXTON, L., HILLAN, K.J., MOORE, M.W. 1996. Heterozygous embryonic lethality induced by targeted inactivation of the VEGF gene. *Nature*, 380, 439-42.
- FERRARA, N., GERBER, H.P., LECOATER, J. 2003. The biology of VEGF and its receptors. *Nature Medicine*, 9, 669-76.
- FONG, G. H., ROSSANT, J., GERTSENSTEIN, M., BREITMAN, M.L. 1995. Role of the Flt-1 receptor tyrosine kinase in regulating the assembly of vascular endothelium. *Nature*, 376, 66-70.
- FONG, G. H., ZHANG, L., BRYCE, D.M., PENG, J. 1999. Increased hemangioblast commitment, not vascular disorganization, is the primary defect in flt-1 knock-out mice. *Development*, 126, 3015-25.
- FOXTON, R. H., FINKELSTEIN, A., VIJAY, S., DAHLMANN-NOOR, A., KHAW, P.T., MORGAN, J.E., SHIMA, D.T., NG, Y.S. 2013. VEGF-A is necessary and sufficient for retinal neuroprotection in models of experimental glaucoma. *American Journal of Pathology*, 182, 1379-90.
- FREELEY, M., KELLEHER, D. & LONG, A. 2011. Regulation of Protein Kinase C function by phosphorylation on conserved and non-conserved sites. *Cell Signal*, 23, 753-62.

- FRUTTIGER, M. 2002. Development of the mouse retinal vasculature: angiogenesis versus vasculogenesis. *Investigative Ophthalmology & Visual Science*, 43, 522-7.
- FRUTTIGER, M. 2007. Development of the retinal vasculature. *Angiogenesis*, 10, 77-88.
- FUJITA, K., KATAHIRA, J., HORIGUCHI, Y., SONODA, N., FURUSE, M., TSUKITA, S. 2000. Clostridium perfringens enterotoxin binds to the second extracellular loop of claudin-3, a tight junction integral membrane protein. *FEBS Letters*, 7, 258-61.
- FURUSE, M. 2010. Molecular basis of the core structure of tight junctions. *Cold Spring Harbor Perspectives Biology*, 2.
- GARCIA, J. G., DAVIS, H.W., PATTERSON, C.E. 1995 Regulation of endothelial cell gap formation and barrier dysfunction: role of myosin light chain phosphorylation. *Journal of Cellular Physiology*, 163 510-22.
- GAVARD, J., GUTKIND, J.S. 2006. VEGF controls endothelial-cell permeability by promoting the beta-arrestin-dependent endocytosis of VE-cadherin. *Nature Cell Biology*, 8, 1223-34.
- GAVARD, J., GUTKIND, J.S. 2008. VE-cadherin and claudin-5: it takes two to tango. *Nature Cell Biology*, 10, 883-5.
- GERHARDT, H., GOLDING, M., FRUTTIGER, M., RUHRBERG, C., LUNDKVIST, A., ABRAMSSON, A., JELTSCH, M., MITCHELL, C., ALITALO, K., SHIMA, D., BETSHOLTZ, C. 2003. VEGF guides angiogenic sprouting utilizing endothelial tip cell filopodia. *The Journal of Cell Biology*, 161, 1163-77.
- GIEMBYCZ, M. A., NEWTON, R. 2006. Beyond the dogma: novel beta2-adrenoceptor signalling in the airways. *European Respiratory Society*, 27, 1286-306.
- GOECKELER, Z. M., MASARACCHIA, R.A., ZENG, Q., CHEW, T.L., GALLAGHER, P., WYSOLMERSKI, R.B. 2000. Phosphorylation of myosin light chain kinase by p21-activated kinase PAK2. *Journal of Biological Chemistry* 275, 18366-74.
- GOLDMAN, D. 2014. Müller glial cell reprogramming and retina regeneration. *Nature Reviews Neuroscience*, 15, 431-442.

- HARTSOCK, A., NELSON, W.J. 2008. Adherens and tight junctions: structure, function and connections to the actin cytoskeleton. *Biochimica et Biophysica Acta* 1778, 660-9.
- HE, H., XU, J., WARREN, C.M., DUAN, D., LI, X., WU, L., IRUELA-ARISPE, M.L. 2012. Endothelial cells provide an instructive niche for the differentiation and functional polarization of M2-like macrophages. *Blood*, 120, 3152-62.
- HOELZLE, M. K. & SVITKINA, T. 2012. The cytoskeletal mechanisms of cell-cell junction formation in endothelial cells. *Mol Biol Cell*, 23, 310-23.
- HUBER, D., BALDA, M.S., MATTER, K. 2000. Occludin modulates transepithelial migration of neutrophils. *The Journal of Biological Chemistry*, 275, 5773-8.
- HUDSON, N., POWNER, M.B., SARKER, M.H., BURGOYNE, T., CAMPBELL, M., OCKRIM, Z.K., MARTINELLI, R., FUTTER, C.E., GRANT, M.B., FRASER, P.A., SHIMA, D.T., GREENWOOD, J., TUROWSKI, P.. 2014. Differential apicobasal VEGF signaling at vascular blood-neural barriers. *Developmental Cell*, 8, 541-52.
- HURLEY, T. D., YANG, J., ZHANG, L., GOODWIN, K. D., ZOU, Q., CORTESE, M., DUNKER, A. K. & DEPAOLI-ROACH, A. A. 2007. Structural basis for regulation of protein phosphatase 1 by inhibitor-2. *J Biol Chem*, 282, 28874-83.
- INGE, L. J., RAJASEKARAN, S.A., WOLLE, D., BARWE, S.P., RYAZANTSEV, S., EWING, C.M., ISAACS, W.B., RAJASEKARAN, A.K. 2008. alpha-Catenin overrides Src-dependent activation of beta-catenin oncogenic signaling. *Molecular Cancer Therapeutics*, 7, 1386-97.
- JOUSSEN, A. M., POULAKI, V., LE, M.L., KOIZUMI, K., ESSER, C., JANICKI, H., SCHRAERMEYER, U., KOCIOK, N., FAUSER, S., KIRCHHOF, B., KERN, T.S., ADAMIS, A.P. 2004. A central role for inflammation in the pathogenesis of diabetic retinopathy. *The FASEB Journal*, 18, 1450-2.
- JU, M. 2013. Role of membrane cytoskeleton in fenestra biogenesis. . *Doctoral thesis, UCL (University College London)*, 22.
- KATSUNO, T., UMEDA, K., MATSUI, T., HATA, M., TAMURA, A., ITOH, M., TAKEUCHI, K., FUJIMORI, T., NABESHIMA, Y., NODA, T., TSUKITA, S., TSUKITA, S. 2008. Deficiency of Zonula Occludens-1 Causes Embryonic

Lethal Phenotype Associated with Defected Yolk Sac Angiogenesis and Apoptosis of Embryonic Cells. *Molecular Biology of the Cell*, 19, 2465–2475.

KERNS, E. H. 2015. Blood-Brain Barrier in Drug Discovery: Optimizing Brain Exposure of CNS Drugs and Minimizing Brain Side Effects for Peripheral Drugs. *Wiley*, 229-300.

KETTENBACH, A. N. & GERBER, S. A. 2011. Rapid and reproducible single-stage phosphopeptide enrichment of complex peptide mixtures: application to general and phosphotyrosine-specific phosphoproteomics experiments. *Anal Chem*, 83, 7635-44.

KHROMOV, A., CHOUDHURY, N., STEVENSON, A. S., SOMLYO, A. V. & ETO, M. 2009. Phosphorylation-dependent autoinhibition of myosin light chain phosphatase accounts for Ca²⁺ sensitization force of smooth muscle contraction. *J Biol Chem*, 284, 21569-79.

KLAASSEN, I., VAN NOORDENB, C.J.F., SCHLINGEMANNA, R. 2013. Molecular basis of the inner blood-retinal barrier and its breakdown in diabetic macular edema and other pathological conditions. *Progress in Retinal and Eye Research*, 34, 19-48.

KOH, W., MAHAN, R. D. & DAVIS, G. E. 2008. Cdc42- and Rac1-mediated endothelial lumen formation requires Pak2, Pak4 and Par3, and PKC-dependent signaling. *J Cell Sci*, 121, 989-1001.

KUR, J., NEWMAN, E.A., CHAN-LING, T. 2012 Cellular and physiological mechanisms underlying blood flow regulation in the retina choroid in health disease. *Progress in Retinal and Eye Research*, 31, 377-406.

LAMALICE, L., HOULE, F., HUOT, J. 2006 Phosphorylation of Tyr¹²¹⁴ within VEGFR-2 triggers the recruitment of Nck and activation of Fyn leading to SAPK2/p38 activation and endothelial cell migration in response to VEGF. *Journal of Biological Chemistry*, 281, 34009-20.

LAMPUGNANI, M. G., DEJANA, E. 2007. Adherens junctions in endothelial cells regulate vessel maintenance and angiogenesis. *Thrombosis Research*, 120, S1–S6.

- LEUNG, D. W., CACHIANES, G., KUANG, W.J., GOEDEL, D.V., FERRARA, N. 1989. Vascular endothelial growth factor is a secreted angiogenic mitogen. *Science*, 246, 1306-9.
- LODISH, H., BERK, A., ZIPURSKY, S.L., MATSUDAIRA, P., BALTIMORE, D., DARNELL, J. 2000. *Molecular Cell Biology*, 4th edition. *New York: W. H. Freeman*.
- MACKENZIE, F., RUHRBERG, C. 2012. Diverse roles for VEGF-A in the nervous system. *Development*, 139, 1371-80.
- MARNEROS, A., FAN, J., YOKOYAMA, Y., GERBER, H., FERRARA, N., CROUCH, R., OLSEN, B. 2005. Vascular endothelial growth factor expression in the retinal pigment epithelium is essential for choriocapillaris development and visual function. *American Journal of Pathology*, 167, 1451-9
- MARTINS, T., BURGOYNE, T., KENNY, B.A., HUDSON, N., FUTTER, C.E., AMBRÓSIO, A.F., SILVA, A.P., GREENWOOD, J., TUROWSKI, P. 2013. Methamphetamine-induced nitric oxide promotes vesicular transport in blood-brain barrier endothelial cells. *Neuropharmacology*, 65, 74-82.
- MCALISTER, G. C., NUSINOW, D. P., JEDRYCHOWSKI, M. P., WUHR, M., HUTTLIN, E. L., ERICKSON, B. K., RAD, R., HAAS, W. & GYGI, S. P. 2014. MultiNotch MS3 enables accurate, sensitive, and multiplexed detection of differential expression across cancer cell line proteomes. *Anal Chem*, 86, 7150-8.
- MCNEIL, E., CAPALDO, C.T., MACARA, I.G. 2006. Zonula Occludens-1 Function in the Assembly of Tight Junctions in Madin-Darby Canine Kidney Epithelial Cells. *Molecular Biology of the Cell*, 17, 1922-1932.
- MESTAS, J., LEY, K. 2008. Monocyte-endothelial cell interactions in the development of atherosclerosis. *Trends in Cardiovascular Medicine*, 18, 228-32.
- MILDE, F., LAUW, S., KOUMOUTSAKOSZ, P., IRUELA-ARISPE, M.L. 2013. The mouse retina in 3D: quantification of vascular growth and remodeling. *Integrative Biology*, 5, 1419-1510.
- MINETA, K., YAMAMOTO, Y., YAMAZAKI, Y., TANAKA, H., TADA, Y., SAITO, K., TAMURA, A., IGARASHI, M., ENDO, T., TAKEUCHI, K., TSUKITA, S. 2011.

Predicted expansion of the claudin multigene family. *FEBS Letters*, 18, 606-12.

MINTZ-HITTNER, H. A., KENNEDY, K. A. & CHUANG, A. Z. 2011. Efficacy of intravitreal bevacizumab for stage 3+ retinopathy of prematurity. *N Engl J Med*, 364, 603-15.

MORGAN, J., WONG, R. 2007. Development of Cell Types and Synaptic Connections in the Retina. *Webvision: The Organization of the Retina and Visual System*

MURAKAMI, T., FREY, T., LIN, C. & ANTONETTI, D. A. 2012. Protein kinase c beta phosphorylates occludin regulating tight junction trafficking in vascular endothelial growth factor-induced permeability in vivo. *Diabetes*, 61, 1573-83.

NAG, S. 2011. The Blood-Brain and Other Neural Barriers. *Humana Press*.

NAGAI, N., JU, M., IZUMI-NAGAI, K., ROBBIE, S.J., BAINBRIDGE, J.W., GALE, D.C., PIERRE, E., KRAUSS, A.H., ADAMSON, P., SHIMA, D.T., NG, Y.S. 2015. Novel CCR3 Antagonists Are Effective Mono- and Combination Inhibitors of Choroidal Neovascular Growth and Vascular Permeability. *The American Journal of Pathology*, 185, 2534-49.

NGOK, S. P., GEYER, R., LIU, M., KOURTIDIS, A., AGRAWAL, S., WU, C., SEERAPU, H.R., LEWIS-TUFFIN, L.J., MOODIE, K.L., HUVELDT, D., MARX, R., BARABAN, J.M., STORZ, P., HOROWITZ, A., ANASTASIADIS, P.Z. 2012. VEGF and Angiopoietin-1 exert opposing effects on cell junctions by regulating the Rho GEF Syx. *Journal of Cell Biology*, 199, 1103-15.

NITTA, T., HATA, M., GOTOH, S., SEO, Y., SASAKI, H., HASHIMOTO, N., FURUSE, M., TSUKITA, S. 2003. Size-selective loosening of the blood-brain barrier in claudin-5-deficient mice. , 2003. 161: p. . *The Journal of Cell Biology*, 653-660.

OAS, R. G., NANES, B. A., ESIMAI, C. C., VINCENT, P. A., GARCIA, A. J. & KOWALCZYK, A. P. 2013. p120-catenin and beta-catenin differentially regulate cadherin adhesive function. *Mol Biol Cell*, 24, 704-14.

OLSSON, A. K., DIMBERG, A., KREUGER, J., CLAESSION-WELSH, L. 2006. VEGF receptor signalling? in control of vascular function. *Nature Reviews Molecular Cell Biology*, 7, 359-371.

- PATEL, R. D., BLAIR, M. P., SHAPIRO, M. J. & LICHTENSTEIN, S. J. 2012. Significant treatment failure with intravitreal bevacizumab for retinopathy of prematurity. *Arch Ophthalmol*, 130, 801-2.
- PATTABIRAMAN, P. P., EPSTEIN, D.L., RAO, P.V. 2014. Regulation of Adherens Junctions in Trabecular Meshwork Cells by Rac GTPase and their influence on Intraocular Pressure. *Journal of Ocular Biology* 1.
- PAULO, J. A., MCALLISTER, F. E., EVERLEY, R. A., BEAUSOLEIL, S. A., BANKS, A. S. & GYGI, S. P. 2015. Effects of MEK inhibitors GSK1120212 and PD0325901 in vivo using 10-plex quantitative proteomics and phosphoproteomics. *Proteomics*, 15, 462-73.
- PENN, J. S. 2008. *Retinal and Choroid Angiogenesis*, Springer.
- POOR, S., MAILHOS, C., BRADLEY, J., MULLIN, L., ROBINSON, G., SHIMA, D.T. 2006. PV-1 Gene Expression Correlates With Retinal Vascular Leakage Of The Blood Retinal Barrier In Development And Disease. *ARVO poster*.
- QAUM, T., XU, Q., JOUSSEN, A., CLEMENS, M., WENYING QIN, K., MIYAMOTO, K., HASSESIAN, H., WIEGAND, S., RUDGE, J., YANCOPOULOS, G., ADAMIS, A. 2001. VEGF-initiated Blood–Retinal Barrier Breakdown in Early Diabetes. *Investigative Ophthalmology & Visual Science*, 42, 2408-2413.
- QUAGGIN, S. E. 2012. Turning a blind eye to anti-VEGF toxicities. *Journal of Clinical Investigation*, 122.
- QUIROS, M., NUSRAT, A. 2014 RhoGTPases, actomyosin signaling and regulation of the epithelial Apical Junctional Complex. *Seminars in Cell & Developmental Biology*, 36, 194-203.
- RADHIKA, B., BALOJU, S., VEMULA, C., RAMYA, C., SWAPNA, K., THATI, M. 2011. Blood-Brain Barrier - Its Implication in Drug Transport. Novel Strategies in Drug Delivery to the Brain *International Journal of Pharmacy and Biological Sciences*, 1, 265-278.
- RAHIMI, N. 2006. VEGFR-1 and VEGFR-2: two non-identical twins with a unique physiognomy. *Frontiers in Bioscience*, 11, 818-29.
- RAPPSILBER, J., ISHIHAMA, Y. & MANN, M. 2003. Stop and go extraction tips for matrix-assisted laser desorption/ionization, nanoelectrospray, and LC/MS sample pretreatment in proteomics. *Anal. Chem.*, 75, 663-70.

- RAYMOND, S. M., JACKSON, I.J. 1995. The retinal pigmented epithelium is required for development and maintenance of the mouse neural retina. *Current Biology*, 5, 1286-95.
- RHEE, J., MAHFOOZ, N.S., ARREGUI, C., LILIEN, J., BALSAMO, J., VANBERKUM, M.F. 2002. Activation of the repulsive receptor Roundabout inhibits N-cadherin-mediated cell adhesion. *Nature Cell Biology*, 4, 798-805.
- RIGOR, R. R., SHEN, Q., PIVETTI, C.D., WU, M.H., YUAN, S.Y. 2012. Myosin light chain kinase signaling in endothelial barrier dysfunction. *Medicinal Research Reviews*, 33, 911-933.
- RINCON-CHOLES, H., VASYLYEVA, T. L., PERGOLA, P. E., BHANDARI, B., BHANDARI, K., ZHANG, J. H., WANG, W., GORIN, Y., BARNES, J. L. & ABOUD, H. E. 2006. ZO-1 expression and phosphorylation in diabetic nephropathy. *Diabetes*, 55, 894-900.
- RISAU, W., HALLMANN, R., ALBRECHT, U. 1986. Differentiation-dependent expression of proteins in brain endothelium during development of the blood-brain barrier. *Developmental Biology*, 117, 537-45.
- RISAU W, H. R., ALBRECHT U. 1986. Differentiation-Dependent Expression of Proteins in Brain Endothelium during Development of the Blood-Brain Barrier *Developmental Biology*, 117, 537-45.
- ROBBINS, D. J., ZHEN, E., OWAKI, H., VANDERBILT, C. A., EBERT, D., GEPPERT, T. D. & COBB, M. H. 1993. Regulation and properties of extracellular signal-regulated protein kinases 1 and 2 in vitro. *J Biol Chem*, 268, 5097-106.
- RUHRBERG, C. 2003. Growing and shaping the vascular tree: multiple roles for VEGF. *BioEssays*, 25, 1052-1060,.
- SANDERS, L. C., MATSUMURA, F., BOKOCH, G.M., DE LANEROLLE, P. 1999. Inhibition of Myosin Light Chain Kinase by p21-Activated Kinase. *Science* 283, 2083-2085
- SAPIEHA, P. 2012. Eyeing central neurons in vascular growth and reparative angiogenesis. *Blood*, 120, 2182-2194.
- SARPAL, R., PELLIKKA, M., PATEL, R.R., HUI, F.Y., GODT, D., TEPASS, U. 2012. Mutational analysis supports a core role for Drosophila α -catenin in adherens junction function. *Journal of Cell Science*, 125, 233-45.

- SCOTT, A., POWNER, M.B., GANDHI, P., CLARKIN, C., GUTMANN, D.H., JOHNSON, R.S., FERRARA, N., FRUTTIGER, M. 2010. Astrocyte-Derived Vascular Endothelial Growth Factor Stabilizes Vessels in the Developing Retinal Vasculature. *PLoS ONE*, 5.
- SENGER, D. R., GALLI, S. J., DVORAK, A. M., PERRUZZI, C. A., HARVEY, V. S. & DVORAK, H. F. 1983. Tumor cells secrete a vascular permeability factor that promotes accumulation of ascites fluid. *Science*, 219, 983-5.
- SHALABY, F., HO, J., STANFORD, W.L., FISCHER, K.D., SCHUH, A.C., SCHWARTZ, L., BERNSTEIN, A., ROSSANT, J. 1997. A requirement for Flk1 in primitive and definitive hematopoiesis and vasculogenesis. *Cell Biology*, 89, 981-90.
- SHALABY, F., ROSSANT, J., YAMAGUCHI, T.P., GERTSENSTEIN, M., WU, X.F., BREITMAN, M.L., SCHUH, A.C. 1995. Failure of blood-island formation and vasculogenesis in Flk-1-deficient mice. *Nature*, 376, 62-6.
- SHEN, L., WEBER, C.R., RALEIGH, D.R., YU, D., TURNER, J.R. 2011a. Tight junction pore and leak pathways: a dynamic duo. *Annual Review of Physiology*, 73, 283-309.
- SHEN, Q., RIGOR, R., PIVETTI, C., WU, M., YUAN, S. 2010. Myosin light chain kinase in microvascular endothelial barrier function. *Cardiovascular Research*, 87, 272-280.
- SHEN, W., LI, S., CHUNG, S.H., ZHU, L., STAYT, J., SU, T., COURAUD, P.O., ROMERO, I.A., WEKSLER, B., GILLIES, M.C. 2011b. Tyrosine phosphorylation of VE-cadherin and claudin-5 is associated with TGF- β 1-induced permeability of centrally derived vascular endothelium. *European Journal of Cell Biology*, 90, 323-32.
- SHI, Y., ZHANG, L., PU, H., MAO, L., HU, X. & JIANG, X. 2016. Rapid endothelial cytoskeletal reorganization enables early blood-brain barrier disruption and long-term ischaemic reperfusion brain injury. 7, 10523.
- SHIN, D. H., CHUN, Y.S., LEE, K.H., SHIN, H.W., PARK, J.W. 2009. Arrest Defective-1 Controls Tumor Cell Behavior by Acetylating Myosin Light Chain Kinase. *PLoS ONE*, 4, 7451.
- SHULMAN, K., ROSEN, S., TOGNAZZI, K., MANSEAU, E.J., BROWN, L.F. 1996. Expression of vascular permeability factor (VPF/VEGF) is altered in

many glomerular diseases. *Journal of the American Society of Nephrology*, 7, 661-6.

SMITH, L. E., WESOLOWSKI, E., MCLELLAN, A., KOSTYK, S.K., D'AMATO, R., SULLIVAN, R., D'AMORE, P.A. 1994 Oxygen-induced retinopathy in the mouse. *Investigative Ophthalmology & Visual Science*, 35, 101-11.

STAMATOVIC, S., KEEP, R., ANDJELKOVIC, A. 2008. Brain Endothelial Cell-Cell Junctions: How to "Open" the Blood Brain Barrier. *Current Neuropharmacology*, 6, 179-192.

STEWART, M. W. 2012. The Expanding Role of Vascular Endothelial Growth Factor Inhibitors in Ophthalmology. *Mayo Clinic Proceedings*, 87, 77-88.

STEWART, P. A., TUOR, U.I. 1994. Blood-eye barriers in the rat: correlation of ultrastructure with function. *Journal of Comparative Neurology*, 340, 566-76.

STOCKTON, R., SCHAEFER, E., SCHWARTZ, M.A. 2004. p21-activated kinase regulates endothelial permeability through modulation of contractility. *The Journal of Biological Chemistry*, 279, 46621-46630.

STONE, J., ITIN, A., ALON, T., PE'ER, J., GNESSIN, H., CHAN-LING, T., KESHET, E. 1995. Development of retinal vasculature is mediated by hypoxia-induced vascular endothelial growth factor (VEGF) expression by neuroglia. *The Journal of Neuroscience*, 15, 4738-47.

STUTTFELD, E., BALLMER-HOFER, K. 2009. Structure and Function of VEGF Receptors. *IUBMB Life*, 61, 915-922.

TAKAHASHI, M., KITAGAWA, S., MASUYAMA, J.I., IKEDA, U., KASAHARA, T., TAKAHASHI, Y.I., FURUKAWA, Y., KANO, S., SHIMADA, K. 1996. Human monocyte-endothelial cell interaction induces synthesis of granulocyte-macrophage colony-stimulating factor. *Circulation*, 93, 1185-93.

TATA, M., RUHRBERG, C., FANTIN, A. 2015 Vascularisation of the central nervous system. *Mechanisms of Development*, ahead of print.

TERRAK, M., KERFF, F., LANGSETMO, K., TAO, T. & DOMINGUEZ, R. 2004. Structural basis of protein phosphatase 1 regulation. *Nature*, 429, 780-4.

- TERRY, S. J., ELBEDIWY, A., ZIHNI, C., HARRIS, A.R., BAILLY, M., CHARRAS, G.T., BALDA, M.S., MATTER, K. 2012. Stimulation of cortical myosin phosphorylation by p114RhoGEF drives cell migration and tumor cell invasion. *PLoS One*, 7.
- TERVONEN, A., VAINIO, I., NYMARK, S., HYTTINEN, J. 2014. Prediction of Passive Drug Permeability Across the Blood-Retinal Barrier. *Pharmaceutical Research*.
- TODA, R., KAWAZU, K., OYABU, M., MIYAZAKI, T., KIUCHI, Y. 2011. Comparison of drug permeabilities across the blood-retinal barrier, blood-aqueous humor barrier, and blood-brain barrier. *Journal of Pharmaceutical Sciences* 100, 3904-11.
- TOMINAGA, J., FUKUNAGA, Y., ABELARDO, E., NAGAFUCHI, A. 2008. Defining the function of beta-catenin tyrosine phosphorylation in cadherin-mediated cell-cell adhesion. *Genes Cells*, 13, 67-77.
- TRABALZINI, L., RETTA, S.F. 2014. Ras Signaling Methods and Protocols. *Humana Press*, 1-14.
- VAN DER MEEL, R., SYMONS, M.H., KUDERNATSCH, R., KOK, R.J., SCHIFFELERS, R.M., STORM, G., GALLAGHER, W.M., BYRNE, A.T. 2011. The VEGF/Rho GTPase signalling pathway: a promising target for anti-angiogenic/anti-invasion therapy. *Drug Discovery Today*, 16, 219-28.
- VAN NIEUW AMERONGEN, G. P., KOOLWIJK, P., VERSTEILEN, A., VAN HINSBERGH, V.W. 2003 Involvement of RhoA/Rho Kinase Signaling in VEGF-Induced Endothelial Cell Migration and Angiogenesis In Vitro. *Arteriosclerosis, Thrombosis, and Vascular Biology*, 23, 211-7.
- VANDENBROUCKE ST AMANT, E., TAUSEEF, M., VOGEL, S. M., GAO, X. P., MEHTA, D., KOMAROVA, Y. A. & MALIK, A. B. 2012. PKC α activation of p120-catenin serine 879 phospho-switch disassembles VE-cadherin junctions and disrupts vascular integrity. *Circ Res*, 111, 739-49.
- VAUGHAN, D., ASBURY, T., RIODAN-EVA, P. 1995. General Ophthalmology. *Appleton & Lange; 14 edition*.
- WABNITZ, G. H., NESSMANN, A., KIRCHGESSNER, H., SAMSTAG, Y. 2015 InFlow microscopy of human leukocytes: A tool for quantitative analysis of actin

rearrangements in the immune synapse. *Journal of Immunological Methods*.

WALLEZ, Y., HUBER, P. 2008. Endothelial adherens and tight junctions in vascular homeostasis, inflammation and angiogenesis. *Biochimica et Biophysica Acta* 1778, 794-809.

WEIS, S. M. 2008. *Methods in Enzymology* Elsevier.

WENNERBERG, K., ROSSMAN, K.L., DER, C.J. 2005. The Ras superfamily at a glance. *Journal of Cell Science*, 118, 843-6.

WILLIAMS, M. J., LOWRIE, M.B., BENNETT, J.P., FIRTH, J.A., CLARK, P. 2005. Cadherin-10 is a novel blood-brain barrier adhesion molecule in human and mouse. *Brain Research*, 1058, 62-72.

WISNIEWSKA-KRUK, J., HOEBEN, K.A., VOGELS, I.M., GAILLARD, P.J., VAN NOORDEN, C.J., SCHLINGEMANN, R.O., KLAASSEN, I. 2012. A novel co-culture model of the blood-retinal barrier based on primary retinal endothelial cells, pericytes and astrocytes. *Experimental Eye Research* 96, 181-90.

WONG-RILEY, M. T. 2010. Energy metabolism of the visual system. *Eye Brain*, 2, 99-116.

WONG, A. D., YE, M., LEVY, A.F., ROTHSTEIN, J.D., BERGLES, D.E., SEARSON, P.C. 2013. The blood-brain barrier: an engineering perspective. *Frontiers in Neuroengineering* 6.

WOOLLARD, J., WANG, W.Y., BEVAN, H.S., QIU, Y., MORBIDELLI, L., PRITCHARD-JONES, R.O., CUI, T.G., SUGIONO, M., WAINE, E., PERRIN, R., FOSTER, R., DIGBY-BELL, J., SHIELDS, J.D., WHITTLES, C.E., MUSHENS, R.E., GILLATT, D.A., ZICHE, M., HARPER, S.J., BATES, D.O. 2004. VEGF165b, an Inhibitory Vascular Endothelial Growth Factor Splice Variant Mechanism of Action, In vivo Effect On Angiogenesis and Endogenous Protein Expression. *Cancer Research* 64, 7822-35.

WOOLLARD, K. J., GEISSMANN, F. 2010. Monocytes in atherosclerosis: subsets and functions. *Nature Reviews Cardiology*, 7, 77-86.

- YALOVSKY, S., BLOCH, D., SOREK, N. & KOST, B. 2008. Regulation of membrane trafficking, cytoskeleton dynamics, and cell polarity by ROP/RAC GTPases. *Plant Physiol*, 147, 1527-43.
- YAO, L., ROMERO, M.J., TOQUE, H.A., YANG, G., CALDWELL, R.B., CALDWELL, R.W. 2010. The role of RhoA/Rho kinase pathway in endothelial dysfunction. *Journal of Cardiovascular Disease Research*, 1, 165-170.
- YUAN, S. Y., RIGOR, R.R. 2010. *Regulation of Endothelial Barrier Function*, Morgan & Claypool Life Sciences.
- ZHANG, X., HOJLUND, K., LUO, M., MEYER, C., GEETHA, T. & YI, Z. 2012. Novel tyrosine phosphorylation sites in rat skeletal muscle revealed by phosphopeptide enrichment and HPLC-ESI-MS/MS. *J Proteomics*, 75, 4017-26.
- ZIHNI, C., BALDA, B., MATTER, K. 2014. Signalling at tight junctions during epithelial differentiation and microbial pathogenesis. *Journal of Cell Science* 127, 3401-3413.
- ZOLOTAREVSKY, Y., HECHT, G., KOUTSOURIS, A., GONZALEZ, D.E., QUAN, C., TOM, J., MRSNY, R.J., TURNER, J.R. 2002. A membrane-permeant peptide that inhibits MLC kinase restores barrier function in in vitro models of intestinal disease. *Gastroenterology* 123, 163-72.